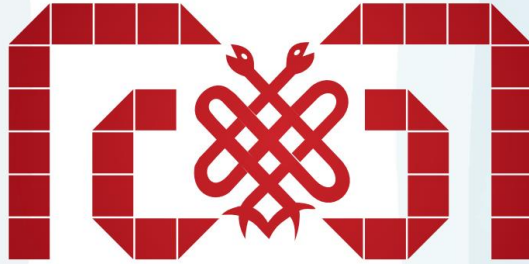


Year: 2024 December

Vol: 25

Issue: 4

E-ISSN: 2149-9063



MEANDROS

MEDICAL AND DENTAL JOURNAL



MEANDROS MEDICAL AND DENTAL JOURNAL

THE OFFICIAL JOURNAL OF ADNAN MENDERES UNIVERSITY
FACULTY OF MEDICINE AND DENTISTRY

Citation Abbreviation: *Meandros Med and Dental J*
(Formerly Adnan Menderes Üniversitesi Tıp Fakültesi Dergisi)



www.meandrosmedicaljournal.org

EDITORIAL BOARD

Editor in Chief

Seda ÖRENAY BOYACIOĞLU

Aydın Adnan Menderes University Faculty of Medicine, Department of Medical Genetics, Aydın, Türkiye
ORCID: 0000-0003-1651-1940

Associate Editors

Sultan KELEŞ

Aydın Adnan Menderes University Faculty of Dentistry, Department of Pedodontics, Aydın, Türkiye
ORCID: 0000-0001-7978-8715

Esra TALAY ÇEVLİK

Aydın Adnan Menderes University Faculty of Dentistry, Department of Prosthodontics, Aydın, Türkiye
ORCID: 0000-0002-8898-6710

Mahmut Alp KILIÇ

Aydın Adnan Menderes University Faculty of Medicine, Department of Biophysics, Aydın, Türkiye
ORCID: 0000-0003-2645-1988

Secretary & Layout Editors

Umut Kerem KOLAÇ

Aydın Adnan Menderes University Faculty of Medicine, Department of Medical Biology, Aydın, Türkiye
ORCID: 0000-0003-0266-9069

Bakiye GÖKER BAĞÇA

Aydın Adnan Menderes University Faculty of Medicine, Department of Medical Biology, Aydın, Türkiye
ORCID: 0000-0002-5714-7455

İlkim Pınar SARAL

Aydın Adnan Menderes University Faculty of Dentistry, Department of Endodontics, Aydın, Türkiye
ORCID: 0000-0003-1278-7464

Hüseyin ŞEKER

Aydın Adnan Menderes University Faculty of Dentistry, Department of Prosthodontics, Aydın, Türkiye
ORCID: 0000-0002-6690-3267

Issue Editors

Seda ÖRENAY BOYACIOĞLU

Aydın Adnan Menderes University Faculty of Medicine, Department of Medical Genetics, Aydın, Türkiye
ORCID: 0000-0003-1651-1940

Sultan KELEŞ

Aydın Adnan Menderes University Faculty of Dentistry, Department of Pedodontics, Aydın, Türkiye
ORCID: 0000-0001-7978-8715

Esra TALAY ÇEVLİK

Aydın Adnan Menderes University Faculty of Dentistry, Department of Prosthodontics, Aydın, Türkiye
ORCID: 0000-0002-8898-6710

Yazgı AY ÜNÜVAR

Aydın Adnan Menderes University Faculty of Dentistry, Department of Orthodontics, Aydın, Türkiye
ORCID: 0000-0002-1455-9855

Kadriye ULU GÜZEL

Aydın Adnan Menderes University Faculty of Dentistry, Department of Pedodontics, Aydın, Türkiye
ORCID: 0000-0002-3129-8490

Mahmut Alp KILIÇ

Aydın Adnan Menderes University Faculty of Medicine, Department of Biophysics, Aydın, Türkiye
ORCID: 0000-0003-2645-1988

Bakiye GÖKER BAĞÇA

Aydın Adnan Menderes University Faculty of Medicine, Department of Medical Biology, Aydın, Türkiye
ORCID: 0000-0002-5714-7455

Umut Kerem KOLAÇ

Aydın Adnan Menderes University Faculty of Medicine, Department of Medical Biology, Aydın, Türkiye
ORCID: 0000-0003-0266-9069

Çağatay BİLEN

Aydın Adnan Menderes University Faculty of Medicine, Department of Pediatric Cardiovascular Surgery, Aydın, Türkiye
ORCID: 0000-0002-9158-5627

Hicran DÖNMEZ ÖZKAN

Aydın Adnan Menderes University Faculty of Dentistry, Department of Endodontics, Aydın, Türkiye
ORCID: 0000-0002-4495-2746

CONTENT

- 337** Shear Bond Strength of Different Calcium Silicate Based Cements to Composite and Compomer
Fatih Öznurhan , Fatma Kübra Atınay
- 351** DNase I Impact on Breast Cells Co-Cultured with Ovarian Cancer Cells: A Study of Cellular Interactions and Viability
Didem Turgut Coşan, İbrahim Uğur Çalış
- 365** Examining the Role of Supar and hs-CRP Levels in Predicting Coronary Artery Disease Severity in Acute Myocardial Infarction: an Age-Stratified Analysis Incorporating Syntax Score
Muhammet Salih Ateş, Abdullah Tunçez, Muhammed Ulvi Yalçın, Kenan Demir, Nazif Aygül, Bülent Behlül Altunkeser, Hüseyin Tezcan, Onur Can Polat, Aslıhan Merve Toprak, Bahadır Öztürk
- 379** Finite Element Analysis of 3D Transient Linear Temperature Changes in the Periodontal Ligament During Thermoplasticized Gutta-Percha Obturation Techniques
Emir Esim, Özgür Er, Tuğrul Aslan, Ayşe Tuğba Eminsoy Avcı, Yakup Üstün
- 396** Differentially Regulated miRNAs by Twist1 in Triple Negative Breast Cancer Cells
Bahadır Öztürk, Akın Kol, Suray Pehlivanoğlu, Fatma Şengül Bağ
- 412** Comparative Assessment of Auditory and Vestibular Functions in Multiple Sclerosis Patients Using Audiological Diagnostic Tools
Serap Uçar, Özgür Sürmelioğlu, Halime Dana
- 424** The Utility of Hematological Indices at the Initial Admission to the Neurosurgery Clinic in Cervical Disc Herniation
Havva Yasemin Çinpolat, Ali Akar, Ümit Ali Malçok, Sevil Alkan
- 436** High Prevalence of Transferable Integron-Associated Drug Resistance In Escherichia Coli Strains Isolated From Blood Cultures In A University Hospital In Trabzon, Türkiye
Ahu Reis, Osman Birol Özgümüş, Erva Rakıcı, İnci Durukan, Kurtuluş Buruk, Gülçin Bayramoğlu, Ali Osman Kılıç
- 451** Thiol/Disulphide Homeostasis and Vascular Endothelial Growth Factor Levels in Saliva of Type 1 Diabetic Children with Gingivitis
Sultan Keleş, Burçin İrem Abas, Ahmet Anık , Ayşe Anık , Özge Çevik
- 466** Evaluation of Fractal Analyses of the Trabecular Bone Region In Lesioned and Healthy Mandibular First Permanent Molars According to Age and Gender on Panoramic Radiographs
Elif Bilgin, Emin Caner Tümen

CONTENT

- 481** **How Reliable Is The Amount Of Interproximal Reduction Clincheck Software Recommends?**
Yasemin Tunca, Nihal Fahrzadeh, Murat Tunca
- 492** **Factors That Are Determinant in the Preparation of Effective and Reliable Colonoscopy: A Prospective Clinical Study From a Single Center**
Sümeyra Işık, Altay Kandemir, Yaşar Barış Turgut, Mehmet Hadi Yaşa, İsmail Taşkıran
- 506** **Unveiling Preoperative Clinical Profiles in Pediatric Aortic Coarctation: Insights Into Surgical Interventions and Institutional Anesthesia Practices**
Canan Salman Önemli, Kübra Evren Şahin, Ömer Faruk Gülaştı, Mustafa Karaçelik, Çağatay Bilen

Research Article

SHEAR BOND STRENGTH OF DIFFERENT CALCIUM SILICATE BASED CEMENTS TO COMPOSITE AND COMPOMER

 Fatih ÖZNRHAN ^{1*} and  Fatma Kübra ALTINAY ²

¹ Department of Pediatric Dentistry, Faculty of Dentistry, Sivas Cumhuriyet University, Sivas/TURKIYE

² Kütahya Oral and Dental Health Training and Research Hospital, Kütahya/TURKIYE

*Correspondence: fatihozn@hotmail.com

ABSTRACT

Objective: Shear bond strength (SBS) of different calcium silicate cements (CSC) with different adhesive systems and restoratives was evaluated.,

Materials and methods: NeoMTA2, NeoPutty and TheraCalPT were used as CSC.120 acrylic blocks with a hole in the middle were prepared and divided into three groups (n=40) depending on the CSC used. CSCs were placed in the prepared cavities. All groups were divided into two subgroups and adhesives (Prime&BondNT) and Universal adhesive (Scotchbond) were applied. Then, composite (n=10) and compomer (n=10) were applied and polymerized. The prepared samples were kept at 37°C in a 100% humid environment for 24 hours and SBS tests was performed with an universal testing device. Fracture types were evaluated with SEM and stereomicroscope.

Results: TheraCalPT had statistically significant increased SBS values when compared to other materials (p<0.05). On the other hand, SBS values of NeoMTA and NeoPutty were insignificant (p>0.05). The difference between the adhesive systems and the restorative materials themselves was not significant (p>0.05).

Conclusion: The ease of use of TheraCal PT and its strong bonding ability with resin restorative materials may provide support for the idea that it is suitable for pulp therapies. However, since in vitro environmental conditions do not reflect intraoral conditions, it must be supported by clinical studies to understand the actual performance and clinical usability.

Keywords: NeoMTA, NeoPutty, TheraCal PT, composite, compomer, shear bond strength

Received: 11 November 2024
Revised: 25 November 2024
Accepted: 28 November 2024
Published: 22 December 2024



Copyright: © 2024 by the authors. Published Aydın Adnan Menderes University, Faculty of Medicine and Faculty of Dentistry. This is an open access article under the Creative Commons Attribution Non Commercial 4.0 International (CC BY-NC 4.0) License.

INTRODUCTION

Vital pulp treatment aims to eliminate microbial irritation by placing a impermeable dental biomaterial to protect the exposed dentin and pulp from external stimuli, through appropriate caries management, and thus prevent any new bacterial damage that may occur. The material to be placed on the pulp must be a biocompatible material that can maintain the vitality of the pulp, prevent bacterial leakage, be resistant to forces during restoration placement and function, and ensure the formation of a dentin bridge. In this way, it is aimed for the pulp to heal itself and maintain its vitality and function (1).

The search for an ideal pulp capping agent for vital pulp treatments has continued for many years, and in this process, calcium hydroxide, dental bonding agents, formocresol, ferric sulfate, mineral trioxide aggregate (MTA) and MTA-like biomaterials such as calcium silicate, calcium phosphate and calcium aluminate-based cements have been suggested (2).

Calcium hydroxide ($\text{Ca}(\text{OH})_2$) has been the first preferred material in vital pulp treatment for many years. The advantages of calcium hydroxide are its antibacterial properties, its effect on pulp healing and repair, its stimulation of dentin formation, its ability to activate alkaline phosphatase by neutralizing acid products, its low cost and ease of use (3). However, calcium hydroxide has some disadvantages such as high solubility, water absorption and dissolution in the presence of moisture, low modulus of elasticity, low compressive strength and low thermal conductivity, poor adhesion to dental structures, restorative materials and dentin, superficial pulp necrosis, tunnel defects in the dentin bridge and degradation after acid etching. Due to the inadequate physical properties of calcium hydroxides, it has brought about the need to investigate new materials that have better sealing properties, are easier to use, and can stimulate the complete dentinal bridge formation. For this reason, biomaterials have been developed as alternatives for direct pulp capping in the last two decades (4).

Calcium silicate-based materials have been considered the most suitable material for pulp capping as a surface-active hard tissue substitute due to its excellent bioactivity and biocompatibility. Calcium silicate-based materials began their development with Portland cement (PC) in 1878, and their use became widespread with the invention of MTA in the 1990s. Portland cement, which constitutes the main component of MTA,

contains tetracalcium aluminoferrite, dicalcium silicate, tricalcium aluminate, tricalcium silicate, and gypsum and bismuth oxide as a radiopaque substance. MTA is accepted as the gold standard material in vital pulp treatments due to its properties such as biocompatibility, bioactivity/biomineralization, low solubility and desirable biological properties such as hydrophilicity. Its antibacterial activity thanks to its high pH value, stimulation of reparative dentin formation, low solubility, high sealability, non-mutagenic, genotoxic, carcinogenic, biocompatible and bioactive material have made MTA an attractive material. In addition to these advantages, different MTA formulations have been developed due to the disadvantages of MTA such as long hardening time, difficulty of use, coloration and high cost (5).

NeoMTA 2 (NuSmile Avalon Biomed, Bradenton, FL, USA) is a bioactive material that stimulates hard tissue formation by releasing Ca^{+2} and OH^- ions, like calcium hydroxide and other calcium silicate-containing cements, and provides antibacterial activity at alkaline pH. It triggers the healing process by stimulating hydroxyapatite in dentin (5, 6).

To reduce the effect of hand mixing on the setting reaction and to simplify clinical application, premixed calcium silicate cements have been developed as an alternative to traditional powder-liquid cements. Premixed tricalcium silicate and dicalcium-based NeoPUTTY is used as a retrograde filling material in vital pulp procedures, apexification, root resorption and perforation repair (6). NeoPUTTY, which is easy to use and has high bioactivity, is a resin-free bioceramic. The material stimulates the formation of hydroxyapatite by releasing Ca^{+2} and OH^- ions from the surface. It has an alkaline pH when applied, thus providing antibacterial activity (7).

Because MTA and similar hydraulic calcium silicate-based materials exhibit a water-based chemical structure and therefore create insufficient micromechanical adhesion to the overlying resin restoration, new light-curing resin-modified tricalcium silicate materials are being formulated for pulp treatment procedures. For this purpose, TheraCal PT (ThPT; Bisco Inc., Schaumburg, IL, USA), a new dual-cured resin modified calcium silicate material designed for pulpotomy, has recently been introduced into clinical use with its biocompatibility, radiopacity, ease of use and calcium release feature (8).

Versatile universal adhesive (UA) systems introduced to the market are designed to provide bonding to tooth structures with both etch-and-rinse (ER) and self-etch (SE) techniques.

Glass ionomer cements and resin modified glass ionomers are frequently used for permanent restorations to be applied after vital pulp treatment, especially in pediatric dentistry, due to their chemical adhesion to dental tissues, fluoride release properties and the fact that they do not require much sensitivity in their application. However, in cases where chewing forces are intense or aesthetics are important, composite and compomer resins are the first choice (9).

Our research; It aims to comparatively evaluate the shear bond strength (SBS) of three different calcium silicate containing vital pulp treatment materials, with two different adhesive systems, to composite and compomer restorative materials frequently used in the clinic.

The null hypotheses of this research are (a) the bond strength of TheraCal PT, a resin-containing material, is significantly higher than the other two materials, (b) there is no significant difference in bond strength between NeoMTA 2 and NeoPUTTY, (c) the bond strength of groups using the ER adhesive system is significantly different from groups using the universal adhesive system, (d) there is no significant difference between the bond strength of the materials to the composite and the bond strength to the compomer.

MATERIALS AND METHODS

Materials Used

In our research, 3 different biomaterials (Group 1: NeoMTA 2, Group 2: NeoPUTTY, Group 3: TheraCal PT), 2 different restorative materials (compomer and composite resin) and one self-etch and one universal adhesive material were used.

Table 1. Materials used in the study

Material	Content	Type / Application Method	Manufacturer
NeoMTA 2	Di and Tricalcium silicate / Tantalum oxide / tricalcium aluminate	Powder-liquid gel	NuSmile, Houston, TX, USA
NeoPutty	Di and Tricalcium silicate / calcium aluminate / Tantalum oxide / Tricalcium aluminate / calcium sulfate / proprietary organic liquid and stabilizers	Premixed paste	NuSmile, Houston, TX, USA
TheraCal PT	Base: Silicate glass mixed cement / polyethylene glycol / dimethacrylate / BisGMA / barium zirconate Catalyst: Barium zirconate / ytterbium fluoride / initiator	Syringe	Bisco Inc., Schaumburg, IL, USA
Prime&Bond NT	Di and Trimethacrylate Resins / PENTA /Bis-GMA/ Nanofillers - Amorphous Silicon Dioxide / Photoinitiators / Stabilizer / Cetylamine Hydrofluoride / Acetone	Etch&Rinse Adhesive	Dentsply, Caulk, Germany
Scotchbond Universal	10-MDP monomer / dimethacrylate resins / HEMA / Methacrylate modified polyalkenoic acid copolymer / Filler / Ethanol,Water / Initiators / Silane	Universal Adhesive	3M ESPE Dental Products, St. Paul, MN, USA
Compoglass F Compomer	UDMA / Polyethylene glycoldimethacrylate / CADCADMA / Silanized mix oxide / Ytterbium trifluoride / Ba-Al-Fluorosilicatecam / (silanized) Catalysts / Stabilizers / Pigments	Refill compomer/ gun application	Ivoclar Vivadent, Schaan, Liechtenstein
3M ESPE Filtek Z550 composite	Bis-GMA, UDMA, Bis-EMA / PEGDMA / TEGDMA / Zirconia and Silica fillers	Nanohybrid composite	3M ESPE, St. Paul, MN, USA

Preparation of Samples

For the SBS test, 120 acrylic blocks with cylindrical cavities (depth: 2 mm, diameter:4 mm) were prepared. NeoMTA 2 was prepared according to the manufacturer's instructions and placed in the space in the middle of the acrylic molds. NeoPUTTY was placed into the molds with appropriate hand tools. In order for the hardening reaction to occur, the molds where these two materials were applied were covered with moist cotton pellets. In accordance with the manufacturer's recommendations, it was kept at 37°C, 100% humidity for 48 hours. TheraCal PT was applied to the molds and hardened by irradiation with the Elipar™ Deepcure-L Light Device for 20 seconds. Before the adhesive application, the biomaterials were left for at least 5 days without any force to complete their hardening.

Each biomaterial group was divided into 2 subgroups for adhesive application. After acid application, Prime&Bond NT adhesive agent was applied to 20 of them according to the manufacturer's instructions. 3M Scotchbond universal adhesive agent was applied and polymerized to the other 20 according to the manufacturer's instructions.

A cylindrical polyethylene mold (diameter: 2 mm, height:2 mm) was used to place the restorative materials to be applied on the biomaterials. Each biomaterial sample was divided into 2 groups, with 10 samples in each group, according to the restorative material to be applied; Ivoclar Compoglass F compomer was placed in one group and 3M Filtek Z550 composite was placed in the other group and polymerized by irradiating with a LED light device for 20 seconds.

Evaluation of Shear Bond Strength

To measure SBS values, the samples were fixed on the universal testing device (LF Plus, LLOYD Instruments, Amatek Inc, UK). An approach speed of 1 mm/min was applied and waited until rupture occurred. Later; The test was stopped automatically and the results were calculated by the computer in Newtons. The values obtained on the test device were converted to MPa after being saved to the computer. After fracture, the fracture surfaces of all samples were examined with a stereomicroscope (SMZ 800, Nikon, Tokio, Japan) under 25x magnification. After examination, the fracture types of the samples were determined and recorded. Five of the broken samples from each biomaterial group were examined at various magnifications on the Tescan Mira3 SEM device.

Statistical Evaluation

To analyze data SPSS22.0 (SPSS, Inc., Chicago, IL, America) program was used. Since parametric test assumptions could not be fulfilled in the evaluation of the data (Shapiro-Wilk Test), Kruskal-Wallis Test was used when comparing measurements obtained from more than two independent groups. When the significance decision was made as a result of the analysis, the Mann-Whitney U Test was used to indicate which group the difference originated from, and the Mann-Whitney U Test was used when comparing the measurements obtained from two independent groups. Our data were stated in the tables as arithmetic mean, median, standard deviation, minimum value, maximum value, and the error level was taken as 0.05.

RESULTS

The mean SBS values of the groups are shown in Table 2. According to these results, TheraCal PT showed significantly higher values than the NeoMTA 2 and NeoPUTTY groups ($p < 0.05$). No statistically significant difference was detected between NeoMTA 2 and NeoPutty groups ($p > 0.05$).

Table 2. Mean and std. dev of shear bond strength of the groups without subdividing them

Groups	Mean±Std. Deflection
Group 1 (NeoMTA2)	13.51±4.88
Group 2 (NeoPUTTY)	11.58±6.93
Group 3 (TheraCalPT)*	31.90±9.57*

Among all groups, the highest average SBS value was in the TheraCal PT-UA-compomer group (34.93 ± 8.53 MPa), and the lowest average SBS value was in the NeoPUTTY-UA-compomer group (8.00 ± 6.30 MPa) was observed (Table 3).

When all groups were compared in terms of bonding strength to the composite and compomer, the difference between the groups was found to be insignificant ($p > 0.05$). When all groups were compared in terms of bond strength of UA and SE adhesive systems, the difference between the groups was found to be insignificant ($p > 0.05$) (Table 3).

Table 3. Mean and std. dev. values of shear bond strength for subgroups

Groups		Mean±Std. Dev	
		Composite	Compomer
NeoMTA2	ER	14.59±4.75	15.16± 3.93
	UA	12.80 ± 5.69	11.48 ± 4.86
NeoPUTTY	ER	12.92±7.03	13.63± 6.25
	UA	11.76 ± 7.68	8.00 ± 6.30
TheraCalPT*	ER	31.63±7.58*	29.02± 12.83*
	UA	32.03 ± 9.11*	34.93 ± 8.53*

When the types of ruptures between the biomaterial and the restorative material were evaluated, it was seen that all (100%) of the fractures were cohesive ruptures within the biomaterial. In the SEM analysis

performed on randomly selected broken sample surfaces from biomaterial groups, only the material surface could be examined because all the breaks were cohesive within the material. It was observed that TheraCal PT (Figure 3) had a more homogeneous structure and its surface was more regular and less porous than the surface of NeoPUTTY (Figure 2) and NeoMTA 2 (Figure 1). The structure of NeoMTA 2 was seen to be more hollow and heterogeneous than NeoPUTTY.

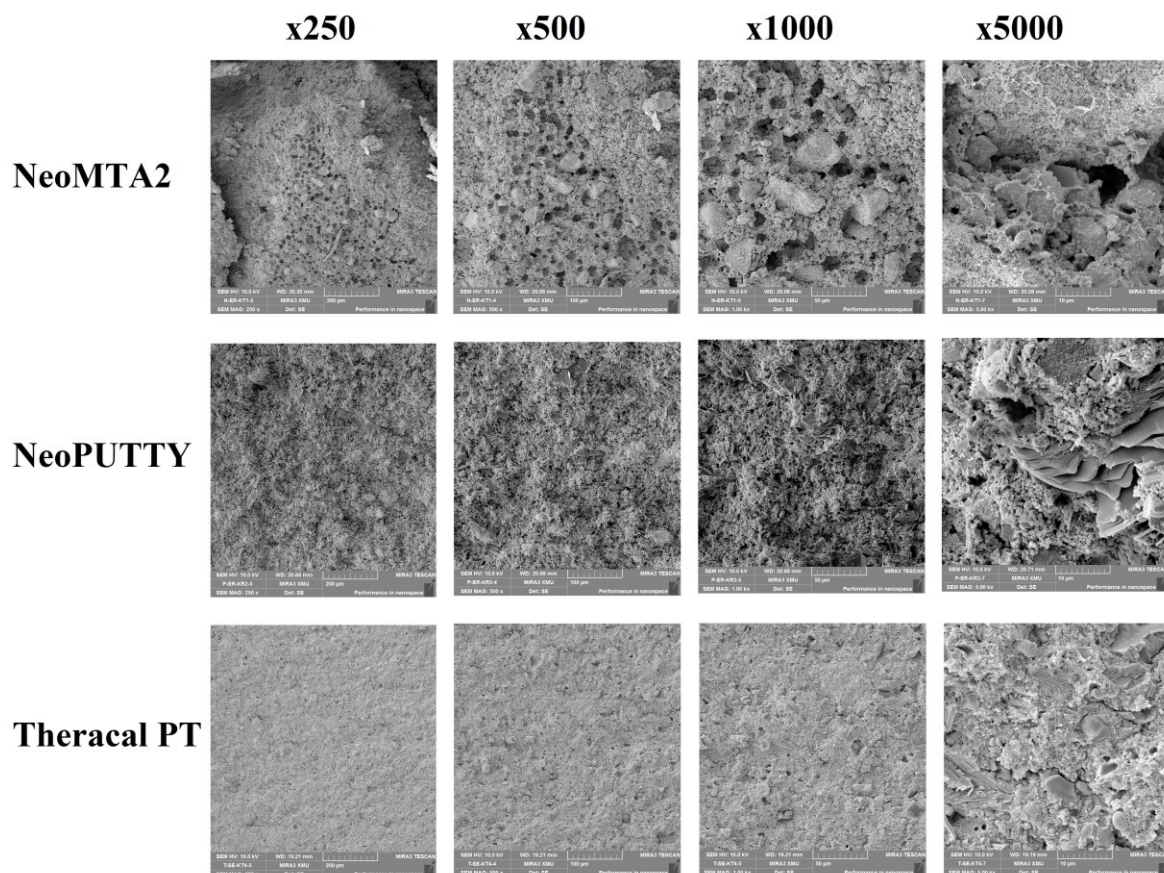


Figure 1. SEM images of NeoMTA 2, NeoPUTTY and TheraCal PT (250x, 500x, 1000x, 5000x)

DISCUSSION

Vital pulp therapy (VPT) procedure is a treatment performed by removing carious and infected tissue and placing a protective, healing, biocompatible and good covering material on the healthy and vital pulp. For the success of the treatment, a permanent restoration must be placed immediately after the treatment to

ensure and maintain good coverage. In addition, in reducing bacterial microleakage and in the long-term success of vital pulp treatment, the bond strength between the pulp material and the restorative material must be high (10).

Biomaterials containing calcium silicate have come to the fore with their advantages such as better physical properties and higher clinical success, and with the discovery of MTA, their use for many treatments and VPT has become widespread (11). The good covering ability of MTA, which is a biocompatible material with its high impermeability, low solubility, high alkaline structure, antibacterial activity and dentinogenesis properties, has a significant impact on the success of VPT. However, MTA has disadvantages such as long hardening time, difficult manipulation, and high cost. In addition to these disadvantages, problems such as being difficult to remove after hardening and the negative effect of etching on the bonding of MTA to increase the adhesion of resin-containing filling materials have led to the development of different MTA formulations (12).

NeoMTA 2, one of these developed materials, has a structure that is resistant to washing, unlike MTA, it is more radiopaque and contains tantalum oxide instead of bismuth oxide for radiopacity. The fine particle structure of the powder and the gel form of the liquid facilitate the manipulation of the material and provide comfortable working (13).

Pre-prepared calcium silicate cements have been developed as an alternative to traditional powder liquid cements in order to eliminate the mixing process of powder liquid materials, reduce their effect on the hardening reaction, facilitate their use and provide a homogeneous structure (14). Since NeoPUTTY, a premixed cement, is formulated with an organic liquid that does not contain water, its manufacturer reports that it is minimally affected by air humidity and has a longer shelf life than its counterparts (15). NeoPUTTY, which has a non-sticky, firm consistency, is resistant to washing, which creates an advantage in that there is no problem in contact with water after it is applied to the cavity (16).

Resin modified calcium silicate cements have been developed to eliminate the disadvantages of MTA and similar hydraulic cements, such as their inability to provide adequate adhesion with the placed resin restoration and the delay of the permanent restoration to complete the hardening of some MTA derivatives.

TheraCal PT, which the manufacturer states that it is designed for pulpotomy, is a resin-modified calcium silicate material and thanks to its dual cure nature, it prevents the problem of insufficient polymerization due to application thickness. The fact that this material contains resin provides better adhesion with resin restorations and has a positive effect on sealing (8).

The long-term success of VPT depends on many features of pulp capping agents, as well as providing good sealing, strong adhesion with the permanent restoration, and thus high sealing. This adhesion strength is routinely determined by shear bond tests (12).

When the literature information on the SBS of calcium silicate-based biomaterials was examined, it was seen that there were few studies (15, 17) on TheraCal PT, NeoMTA 2, NeoPUTTY. In our study, TheraCal PT showed high bond strength in both adhesive systems and restorative materials. NeoPUTTY exhibited the lowest average shear bond value in all groups.

Yavuz et al. (17) evaluated the SBS of three different calcium silicate cements (TheraCal PT, NeoPUTTY, Biodentine) with three different universal adhesive systems and reported that TheraCal PT showed the highest values and NeoPUTTY showed the lowest values. Özata et al. (15) in their study with TheraCal LC, NeoMTA 2 and NeoPUTTY; They reported the average bond strengths as TheraCal LC (23.32 Mpa), NeoMTA 2 (12.17 Mpa) and NeoPUTTY (11.37 Mpa), respectively. Ipek et al. (18) evaluated the bond strength of Biodentine, MTA Repair HP and NeoPUTTY to root dentin and stated that NeoPUTTY showed low bond values. Ipek et al. (19), in another study, evaluated the bond strength of NeoPUTTY, Biodentine and MTA Cem LC to two different bulk fill composites with and without fiber content and reported that NeoPUTTY showed the lowest bond values in both composite groups. Alqahtani et al. (20) evaluated the immediate and delayed (7 days) bonding of 4 different biomaterials (NeoPUTTY, NeoMTA 2, TotalFill BC RRM™ and ProRoot MTA) to resin-modified glass ionomer cement and flowable composite. They reported that ProRoot MTA (14.65 MPa) showed the highest average bond strength in delayed bonding in flowable composite groups, and NeoPUTTY (8.03 MPa) showed the lowest average bond strength. Şişmanoğlu et al. (21) in their study investigating the bond strength of five calcium silicate cements (MTA Angelus, Biodentine, NeoMTA, TheraCal LC, Well Root ST) to the composite with ER and SE adhesive systems, reported that the highest bond strength values

belonged to TheraCal LC, which is a resin-containing material. Akbıyık et al. (22) reported that resin-containing coating agents (Calcimol LC, ApaCal ART, TheraCal LC) showed higher bond strength than others in the shear bond test they conducted with different pulp capping materials (TheraCal LC, Dycal, ProRoot MTA, Calcimol LC, Biodentine, ApaCal ART) and different adhesive systems. It was found that the resin-containing biomaterials exhibited the highest bond strengths in these studies and that TheraCal PT, a resin-containing dual cure material, showed the highest bond strengths in our study. Thus, our first hypothesis regarding TheraCal PT was accepted. The success of TheraCal PT in the SBS test is thought to be due to the resin monomer in its forming a strong adhesion by establishing a chemical bond with the adhesive resin (17).

When the bond strength studies in the literature about the NeoPUTTY group, which showed the lowest SBS values in our research, were examined, it was reported that the NeoPUTTY material showed low bond strength, consistent with our study (17-19). When applied clinically, NeoPUTTY is a material that hardens by absorbing moisture and water from the dentinal tubules and surrounding tissues. The low binding values of NeoPUTTY in in vitro studies can be considered as the inability to achieve ideal hardening because it cannot find sufficient moisture and water when placed in acrylic molds (17). Further in vitro and in vivo studies are necessary which tests the binding success of NeoPUTTY.

When studies evaluating the bonding of biomaterials with adhesive systems were examined, different results were found. While there are studies reporting that MTA shows more successful results with ER adhesive systems (23-25), there are also studies reporting that the etching process weakens the physical properties of MTA and reduces its bonding strength (26-28). In our research, the bond strength averages of NeoMTA 2 and NeoPUTTY's ER adhesive applied samples were higher than the bond strength averages of UA applied samples; It was observed that the average of UA values of TheraCal PT groups was higher than the average of ER adhesive values.

There are a few studies comparing the bond strength of calcium silicate-containing materials to compomer and composite (25, 29, 30). Keleş et al. (29) reported in their study that composite resin showed significantly higher bond strength than compomer, while Tunç et al. (25) and Tulumbacı et al. (30) reported that there was no significant difference between the two restorative materials in their studies. In our study,

when composite resin and compomer were compared in all NeoMTA 2, NeoPUTTY and TheraCal PT groups, no statistically significant difference was seen between the two restorative materials ($p>0.05$). Therefore, our hypothesis regarding composite and component materials was accepted.

In our research, cohesive type rupture was observed in the biomaterial in all materials. For this reason, when classifying our rupture types, we classified them as deep cohesive rupture and superficial cohesive rupture. We think that another reason for the cohesive rupture in this biomaterial is the non-homogeneous stress distribution. The majority of the ruptures observed in the NeoPUTTY material were observed as superficial cohesive ruptures. We attribute the cause of superficial cohesive ruptures to the low bonding values of the material itself and the inability to complete the hardening reaction. In addition, the fact that NeoMTA 2 and NeoPUTTY materials exhibit lower values and more superficial ruptures compared to TheraCal PT may be due to the fact that MTA is water-based and has a particulate, granular and brittle structure. We think that the reason why deep cohesive breaks are mostly observed in TheraCal PT samples and SBS values are higher than previous studies may be due to the difference in surface preparation and environmental conditions. Deep breaks suggest that the bonds within the material are also strong.

When the SEM images were examined, it was seen that the surfaces of TheraCal PT and NeoPUTTY were more regular and homogeneous than the surface of NeoMTA 2. It is thought that this is because manual mixing cannot provide sufficient homogeneous mixing.

One of the limitation of this study is that in vitro environmental conditions do not reflect intraoral conditions and in vivo studies are necessary to see these effects on bonding strength values. Another limitation of this study was that one of the tested material "TheraCal PT" is a light cured material, but there is no other material that can be light cured in order to compare as calcium silicate based material.

CONCLUSION

According to the findings of our research, it is thought that TheraCal PT, a resin-containing material, can prevent treatment failure due to microleakage thanks to its high bond strength to resin restorations, and its use can be recommended. However, since our study only tests the mechanical and physical properties of

the material, more biological and histological in vitro and in vivo studies are needed for this material to be placed on the pulp. Although the average SBS values of NeoPUTTY and NeoMTA 2 materials are below the clinically accepted SBS value of 17-20 MPa (31, 32), since in vitro environmental conditions do not reflect intraoral conditions, they need to be supported by in vivo studies to understand the real performance and clinical usability of the materials.

Acknowledgments

None

Authorship contributions

Contributed to conception FO and FKA, design FO and FKA, collecting data FKA, statistical analysis FKA, data acquisition and interpretation FO, SEM analysis FKA, writing some parts of manuscript FKA, writing and editing of the manuscript FO.

Data availability statement

The data that support the findings of this study are available from the corresponding author, [FO], upon reasonable request.

Declaration of competing interest

The authors deny any conflicts of interest related to this study.

Ethics

Cumhuriyet University Clinical Research Ethic Committee (2021-11/10).

Funding

This study was supported by the Scientific Research Project Fund Cumhuriyet University (Grant number DİŞ-2022-286).

REFERENCES

1. Tziafas D, Smith A, Lesot H. Designing new treatment strategies in vital pulp therapy. *Journal of dentistry* 28 (2000) 77-92.
2. da Rosa WL, Cocco AR, Silva Tmd, Mesquita LC, Galarca AD, Silva AFd, et al. Current trends and future perspectives of dental pulp capping materials: A systematic review. *Journal of Biomedical Materials Research Part B: Applied Biomaterials* 106 (2018) 1358-68.
3. Ba-Hattab R, Al-Jamie M, Aldreib H, Alessa L, Alonazi M. Calcium hydroxide in endodontics: An overview. *Open Journal of Stomatology* 6 (2016) 274-89.
4. Luo Z, Li D, Kohli MR, Yu Q, Kim S, He W-x. Effect of biodentine™ on the proliferation, migration and adhesion of human dental pulp stem cells. *Journal of Dentistry* 42 (2014) 490-97.
5. Rodríguez-Lozano F, Lozano A, López-García S, García-Bernal D, Sanz J, Guerrero-Gironés J, et al. Biom mineralization potential and biological properties of a new tantalum oxide (ta 2 o 5)-containing calcium silicate cement. *Clinical Oral Investigations* 26(2022)1-15.

6. Sun Q, Meng M, Steed JN, Sidow SJ, Bergeron BE, Niu L-n, et al. Manoevrability and biocompatibility of endodontic tricalcium silicate-based putties. *Journal of dentistry* 104 (2021) 103530.
7. Primus C, Gutmann JL, Tay FR, Fuks AB. Calcium silicate and calcium aluminate cements for dentistry reviewed. *Journal of the American Ceramic Society* 105 (2022) 1841-63.
8. Küden C, Karakaş SN, Batmaz SG. Comparative chemical properties, bioactivity, and cytotoxicity of resin-modified calcium silicate-based pulp capping materials on human dental pulp stem cells. *Clinical Oral Investigations* 26 (2022) 6839-53.
9. Çapan BŞ, Akyüz S. Current fluoride-releasing restorative materials used in pediatric dentistry. *Clinical and Experimental Health Sciences* 6 (2016) 129-34.
10. Oskoee SS, Bahari M, Kimyai S, Motahhari P, Eghbal MJ, Asgary S. Shear bond strength of calcium enriched mixture cement and mineral trioxide aggregate to composite resin with two different adhesive systems. *Journal of Dentistry (Tehran, Iran)* 11 (2014) 665-71.
11. Nie E, Yu J, Jiang R, Liu X, Li X, Islam R, et al. Effectiveness of direct pulp capping bioactive materials in dentin regeneration: A systematic review. *Materials* 14 (2021) 6811.
12. Biçer H, Bayrak Ş. Vital pulpa tedavisinde kullanılan kalsiyum silikat içerikli biyomateryallerin restoratif materyallere bağlanma dayanımının değerlendirilmesi. *Selcuk Dental Journal* 6 (2019) 271-79.
13. NuSmile. Available from: <https://tp-dc.Com.Au/products/nusmile-neomta-2-starter-kit-1-0gm>. Accessed on 29 January 2023.
14. Persson C, Engqvist H. Premixed calcium silicate cement for endodontic applications: Injectability, setting time and radiopacity. *Biomatter* 1 (2011) 76-80.
15. Yeniçeri Özata M, Falakaloğlu S, Plotino G, Adıgüzel Ö. The micro-shear bond strength of new endodontic tricalcium silicate-based putty: An in vitro study. *Aust Endod J* 49 (2022) 124-129.
16. NuSmile. Available from: <https://nusmile.Com/pages/nusmile-neoputty2>. 2020 Accessed on 29 January 2023.
17. Yavuz Y. Biomateryallerin universal adeziv sistemlere bağlanma dayanımının karşılaştırılması: İn vitro çalışma. *Selçuk Dental Journal* 9 (2022) 513-19.
18. İpek İ, Ünal M, Güner A, Candan M. Push-out bond strength of biodentine, mta repair hp, and a new pre-mixed neoputty bioactive cement: Scanning electron microscopy energy dispersive x-ray spectroscopy analysis. *Journal of the Australian Ceramic Society* 58 (2022) 1-9.
19. İpek İ, BK E, Yıldız Ş, Ataş O, Ünal M. Evaluation of the shear bond strength of biodentine, pre-mixed neoputty and new resin modified calcium silicate cement with bulk fill composites; scanning electron microscopy-energy distributed x-ray spectroscopy analysis. (2023)
20. Alqahtani AS, Sulimany AM, Alayad AS, Alqahtani AS, Bawazir OA. Evaluation of the shear bond strength of four bioceramic materials with different restorative materials and timings. *Materials* 15 (2022) 4668.
21. Sismanoglu S, Yildirim-Bilmez Z, Gurcan A, Gumustas B. Influence of application mode of universal adhesive on the surface morphology, elemental composition and bond strength of calcium silicate-based cements to composite resin: A sem-edx microanalysis study. *Journal of Adhesion Science and Technology* 36 (2022) 1833-46.
22. Akbiyik SY, Bakir EP, Bakir Se. Evaluation of the bond strength of different pulp capping materials to dental adhesive systems: An in vitro study. *Journal of Advanced Oral Research* 12 (2021) 286-95.
23. Bayrak S, Tunc ES, Saroglu I, Egilmez T. Shear bond strengths of different adhesive systems to white mineral trioxide aggregate. *Dental materials journal* 28 (2009) 62-67.
24. Atabek D, Sililelioğlu H, Ölmez A. Bond strength of adhesive systems to mineral trioxide aggregate with different time intervals. *Journal of endodontics* 38 (2012) 1288-92.
25. Tunç EŞ, Bayrak Ş, Egilmez T. The evaluation of bond strength of a composite and a compomer to white mineral trioxide aggregate with two different bonding systems. *Journal of Endodontics* 34 (2008) 603-05.
26. Kayahan M, Nekoofar MH, Kazandağ M, Canpolat C, Malkondu O, Kaptan F, et al. Effect of acid-etching procedure on selected physical properties of mineral trioxide aggregate. *International endodontic journal* 42 (2009) 1004-14.
27. Namazikhah M, Nekoofar MH, Sheykhrezae M, Salariyeh S, Hayes SJ, Bryant ST, et al. The effect of ph on surface hardness and microstructure of mineral trioxide aggregate. *International Endodontic Journal* 41 (2008) 108-16.
28. Lee Y-L, Lee B-S, Lin F-H, Lin AY, Lan W-H, Lin C-P. Effects of physiological environments on the hydration behavior of mineral trioxide aggregate. *Biomaterials* 25 (2004) 787-93.
29. Keleş S, Derelioğlu SŞ. Shear bond strength of composite and compomer to biodentine® applied with various bonding agents: An in-vitro study. *Atatürk Üniversitesi Diş Hekimliği Fakültesi Dergisi* 29 (2019) 49-54.
30. Tulumbaci F, Almaz ME, Arikan V, Mutluay MS. Shear bond strength of different restorative materials to mineral trioxide aggregate and biodentine. *Journal of conservative dentistry: JCD* 20 (2017) 292.
31. Al-Sarheed MA. Evaluation of shear bond strength and sem observation of all-in-one self-etching primer used for bonding of fissure sealants. *The Journal of Contemporary Dental Practice* 7 (2007) 9-16.
32. Davidson C, De Gee A, Feilzer A. The competition between the composite-dentin bond strength and the polymerization contraction stress. *Journal of dental research* 63 (1984) 1396-99.

Research Article

DNASE I IMPACT ON BREAST CELLS CO-CULTURED WITH OVARIAN CANCER CELLS: A STUDY OF CELLULAR INTERACTIONS AND VIABILITY

 Didem TURGUT COŞAN ^{1*} and  İbrahim Uğur ÇALIŞ ²

¹ Department of Medical Biology, Faculty of Medicine, Eskişehir Osmangazi University, Eskişehir, TÜRKİYE

² Department of Medical Biology, Faculty of Medicine Muğla Sıtkı Koçman University, Muğla, TÜRKİYE

*Correspondence: dcosan@gmail.com

ABSTRACT

Objective: Cell-free DNAs (cf-DNAs) are released into the bloodstream through cell apoptosis, necrosis, or active secretion, often originating from cancer cells. These cf-DNAs have been associated with cancer development and metastasis, although their precise role remains under debate. DNase I, an enzyme that degrades extracellular DNA, has shown potential to impact cf-DNAs and influence cancer progression. This study investigates the effects of ovarian cancer cells on the proliferation and viability of non-tumorigenic breast cells, with a focus on DNase I's role.

Materials and Methods: Human ovarian cancer cells (OVCAR-3) and normal human breast cells (MCF-10A) were cultured under standard conditions (37°C, 5% CO₂). Co-culture experiments were conducted by incubating cells separately in plates and inserts, with or without DNase I, for 72 hours. Cell viability was assessed using the trypan blue exclusion test, while proliferation and adhesion were measured with an XTT assay.

Results: DNase I significantly reduced OVCAR-3 proliferation ($p < 0.001$) and adhesion ($p < 0.01$) without affecting MCF-10A cells. DNase I also decreased OVCAR-3 cell viability but did not significantly impact MCF-10A viability. Genetic analysis identified p53 exon 7 mutations and methylation of APC1A, APC1B, and RASSF1A genes in OVCAR-3 cells, which were unaffected by DNase I. No mutations or methylation were detected in MCF-10A cells.

Conclusion: The results suggest that the impact of DNase I on the proliferation and viability of cancer cells is significant and warrants further investigation. The potential effects of prolonged exposure between different cell types could yield even more compelling findings.

Keywords: cf-DNA, OVCAR-3, MCF-10A, Cancer, DNase I

Received: 24 August 2024
Revised: 13 October 2024
Accepted: 14 October 2024
Published: 22 December 2024



Copyright: © 2024 by the authors. Published Aydın Adnan Menderes University, Faculty of Medicine and Faculty of Dentistry. This is an open access article under the Creative Commons Attribution Non Commercial 4.0 International (CC BY-NC 4.0) License.

INTRODUCTION

DNA fragments, known as cell-free DNAs (cf-DNAs), can be released into the bloodstream through processes such as apoptosis, cell death, or active secretion by living cells, including those from cancerous tumors. Research has suggested that cf-DNAs shed by tumor cells into the bloodstream may contribute to cancer spread(1). It has long been recognized that cancer cells can disseminate throughout the body via metastatic processes. Free DNAs, discovered in 1948, have been shown in various in vivo studies to integrate into the genome of certain cells through horizontal gene transfer (2-4). Data from 1982 suggested that dominant oncogenes found in tumor cells could be transferred to normal cells (5). This led to the hypothesis that "cancer metastasis might occur through the transfection of cell-free DNAs containing dominant genes from the primary tumor into susceptible cells in the target organ"(3). The finding that cell-free DNAs can reflect the invasive and prognostic characteristics of the original cancer spurred laboratory research into their clinical potential. Studies have shown that DNA fragment levels, which are usually low, increase as malignancy progresses(5). These observations underscore the role of cell-free DNA in cancer development and metastasis. Research focusing on the relationship between tumor-specific DNA changes in primary tumors and blood samples has emphasized alterations in methylation, microsatellites, oncogenes, and tumor suppressor genes(6-8) .

Point mutations or changes in chromosomal integrity within various genomic regions of tumor cells can influence oncogenes, tumor suppressor genes, and genes related to metastasis, such as HIF-1 (Hypoxia-Inducible Factor-1) (9). It is reported that over 50% of human cancers carry gene mutations (10). Mutations in exons 5-8 of the p53 gene are commonly found in primary tumors and are frequently detected in plasma as well (2). Mutant p53 plays a crucial role in the development of metastasis by either blocking or activating downstream target genes, leading to DNA damage and the activation of multiple oncogenes. For example, OVCAR-3 cells exhibit a specific mutation (743G>A) in exon 7 of the p53 gene (11, 12).

Mutations in cancer-related genes are typically not due to regulatory abnormalities alone. Metastasis is also facilitated by epigenetic modifications, such as chromatin remodeling in CpG islands and gene silencing errors related to hyper-methylation (13). DNA methylation-induced gene silencing leads to gene inactivation

at the transcriptional level (14, 15). While CpG islands in the promoter regions of approximately 50% of genes remain unmethylated in normal cells, CpG dinucleotides in repetitive sequences are methylated. In cancer cells, widespread hypo-methylation across the genome is often observed, along with hyper-methylation of CpG islands in promoter regions, resulting in gene silencing crucial for the inactivation of tumor suppressor genes (16). The inactivation of these genes, such as the RASSF1A gene, is vital for cancer progression. One significant epigenetic mechanism implicated in the development of ovarian cancer is the methylation of tumor suppressor genes. Research has shown that patients with primary or metastatic breast cancer exhibit RASSF1A methylation in their plasma and serum (16).

In normal cells, CpG islands in the promoter regions of about half of all genes remain unmethylated, while CpG dinucleotides in repetitive sequences are methylated. Cancer cells frequently display widespread genome-wide hypo-methylation along with hyper-methylation of CpG islands in promoter regions, leading to gene silencing and the inactivation of tumor suppressor genes, which is crucial for cancer development (16). The inactivation of tumor suppressor genes like RASSF1A is essential for cancer progression. Epigenetic mechanisms, such as RASSF1A methylation, have been identified in the plasma and serum of patients with primary or metastatic breast cancer, underscoring their role in cancer development.

Studies have indicated that promoter hyper-methylation and the reduced expression of the tumor suppressor gene adenomatous polyposis coli (APC) play significant roles in cancer development. The association between ovarian cancer and APC promoter hyper-methylation has been well-established. Research has shown that APC promoter hyper-methylation is more prevalent in ovarian cancer patients than in healthy and benign controls, suggesting that this could increase the risk of developing ovarian cancer (17). It has been proposed that RASSF1A and APC genes could serve as epidemiological biomarkers in individuals at risk for breast cancer due to the high incidence of promoter hyper-methylation in cancers (18).

DNase I, a member of the endonuclease enzyme class, breaks down phosphodiester bonds between srch has shown that metastases can form due to the leakage of free DNA from tumor cells into the circulation. Numerous studies have investigated the role of DNase I in metastasis formation. This study aimed to determine whether certain genes and structural features of OVCAR-3 tumor cells can be transferred to healthy

MCF-10A cells via free DNA. Additionally, the differences between the presence and absence of DNase I in these two cell types (cancerous and non-cancerous) were explored for the first time in the literature.

MATERIALS AND METHODS

Cell Culture

The human ovarian cancer cell line OVCAR-3 (ATCC, HTB-16, Washington D.C., USA) was cultured in 25 cm² and 75 cm² flasks (Thermo Fisher Scientific, USA) using RPMI-1640 medium (ATCC, Washington, USA) supplemented with 20% FBS (Gibco, UK) and 0.01 mg/ml bovine insulin (Sigma, USA), and maintained in a humidified incubator at 37°C with 5% CO₂ (Sanyo, Japan). The human normal breast cell line MCF-10A (ATCC, CRL-10317, Washington D.C., USA) was cultured in Dulbecco's Modified Eagle's Medium (DMEM; Gibco, UK), which was supplemented with 10% Fetal Bovine Serum (Gibco, UK) and 2 mM L-Glutamine, in 25 cm² and 75 cm² flasks (Thermo Fisher Scientific, USA). These cells were incubated under the same conditions at 37°C with 5% CO₂ (Sanyo, Japan).

Table 1. Experimental Groups

Group no	Groups
1	OVCAR-3
2	OVCAR-3 DNase I
3	MCF10A
4	MCF10A DNase I
5	Co-culture OVCAR-3
6	Co-culture MCF10A
7	Co-culture OVCAR-3 DNse I
8	Co-culture MCF10A DNase I

DNase I Treatment

A DNase I stock solution (10 mg/ml) was prepared by dissolving 10 mg of powdered DNase I (Sigma-Aldrich, Germany) in 1 ml of the appropriate medium. Cells were then treated with DNase I at a final

concentration of 0.1 mg/ml for 72 hours. For co-culture experiments, sterile inserts (Thermo Scientific, USA) with a 6.5 mm diameter and a pore size of 0.4 μm were placed in a 24-well plate.

Proliferation Assay

Cell proliferation was assessed using the XTT assay (Biological Industries, Israel). A 5 ml reaction solution, containing 100 μl of activation solution, was prepared, and 50 μl of this mixture was added to each well containing the cell samples. After a 2-hour incubation at 37°C, absorbance was measured at 450 nm using a Multiskan GO spectrophotometer (Thermo Scientific, USA). The proliferation rates were determined using raw data and standard curves. Each experiment was conducted at least three times for consistency.

Adhesion Assay

The cells were detached from the flask surface using trypsin, counted, and 7×10^3 cells were transferred to 7 separate wells of 96-well plates for each group. The cells were incubated for 24 hours to allow adhesion to the flask surface. After performing the appropriate procedures for each group in the wells designated for adhesion, the cells were washed three times with PBS, and 100 μl of fresh medium was added. Then, the XTT assay was applied. The adhesion of the cells was determined by substituting the results into the formula. $[1 - (\text{absorbance of unwashed well} - \text{absorbance of washed well}) / \text{absorbance of unwashed well}]$

Cell Viability Assay

Cell viability was assessed using the trypan blue exclusion method. After trypsinization, a portion of the cell suspension was mixed with 10 μl of trypan blue dye (Biological Industries, Israel), placed on slides, and analyzed using a cell counter (JuLI™ Br, Nanoentek Inc., Seoul, Korea), with results expressed as the percentage of viable cells.

DNA Extraction

DNA extraction was performed using the Direct PCR kit (Thermo Fisher Scientific, USA), following the manufacturer's instructions. Dilution buffer and DNA release solution were added to the cells and media,

followed by vortexing. The mixture was incubated at room temperature for 5 minutes, then heated to 98°C. A PCR mixture was prepared using the supernatant, and DNA concentrations were measured with a Multiskan GO spectrophotometer (Thermo Scientific, USA). Samples were stored at -20°C until further analysis.

Primer Design and PCR Protocols

APC1A and APC1B Methylation Analysis: Methylated and unmethylated primers were designed for the APC1A and APC1B gene regions. The forward primer sequences for APC1A were 5'-TATTGCGGAGTGCGGGTC-3' (methylated) and 5'-GTGTTTTATTGTGGAGTGTGGGTT-3' (unmethylated), while the reverse primer sequences were 5'-TCGACGAACTCCCGACGA-3' (methylated) and 5'-CCAATCAACAAACTCCCAACAA-3' (unmethylated). For APC1B, the forward primer sequences were 5'-TAGAATAGCGAACGAGTGTTTC-3' (methylated) and 5'-GATAGAATAGTGAATGAGTGTTC-3' (unmethylated), and the reverse primer sequences were 5'-TCCGACGACCACACCCCG-3' (methylated) and 5'-CTTCCAACAACCACACCCCA-3' (unmethylated). A 25 µl reaction mixture was prepared using 12.5 µl of One Taq Quick-Load 2x Master Mix (BioLabs, UK), 2 µl of forward primer, 2 µl of reverse primer, 2 µl of bisulfite-converted DNA, and dH₂O to reach the final volume. The PCR conditions included an initial denaturation at 95°C for 15 minutes, followed by 35 cycles of denaturation at 95°C for 15 seconds, annealing at 60°C for 45 seconds, and extension at 72°C for 30 seconds. A final extension step was performed at 72°C for 10 minutes.

RASSF1A Methylation Analysis: For the RASSF1A gene, methylated and unmethylated primers were designed. The forward primer sequences were 5'-CGAGAGCGCGTTTAGTTTCGTT-3' (methylated) and 5'-GGGGGTTTTGTGAGAGTGTGTTT-3' (unmethylated), while the reverse primer sequences were 5'-CGATTAAACCCGTACTIONTCGCTAA-3' (methylated) and 5'-CCCAATTAAACCCATACTIONTCACTAA-3' (unmethylated). The PCR reaction setup and cycling conditions were identical to those used for APC1A and APC1B analysis. PCR products were separated on a 2% agarose gel at 120V for 30 minutes and visualized using a SynGene UV imaging system.

p53 Exon 7 Mutation Analysis: Primers targeting p53 exon 7 were used, with the forward primer sequence 5'-TCCTAGGTTGGCTCTGACTGT-3' and the reverse primer sequence 5'-AGTGGCCCTGACCTGGAGTCT-3'. The reaction mixture consisted of 12.5 µl of One Taq Quick-Load 2x Master Mix, 2 µl of forward primer, 2 µl of reverse primer, 2 µl of the DNA sample, and dH₂O to complete a 25 µl volume. The PCR protocol included an initial denaturation at 95°C for 5 minutes, followed by 40 cycles of denaturation at 94°C for 1 minute, annealing at 62°C for 1 minute, and extension at 72°C for 1 minute. A final extension step was performed at 72°C for 10 minutes. After PCR amplification, samples were mixed with 95% formamide, heated at 80°C for 10 minutes, and chilled on ice. A 30% polyacrylamide gel electrophoresis was performed at 120V for 4 hours at 4°C, and the bands were visualized using a silver staining method.

Statistical Analysis

The normality of the quantitative data was evaluated using the Shapiro-Wilk test. For groups that exhibited a normal distribution, one-way analysis of variance (ANOVA) was used, followed by Tukey HSD test for multiple comparisons. Statistical significance was determined for p-values less than 0.05. The results were reported as mean ± standard deviation in tables and graphs. All statistical analyses were performed using IBM SPSS Statistics 21.0 software.

RESULTS

Proliferation Analysis

A statistical difference was observed between the groups ($p < 0.001$). DNase I significantly reduces the proliferation of OVCAR-3. The untreated OVCAR-3 cells had a proliferation rate of $(32,581 \pm 4,784)$, while DNase I-treated OVCAR-3 cells (OVCAR-3 DNase I) showed a reduced proliferation rate of $(22,714 \pm 4,059)$ ($p < 0.05$). This demonstrates that DNase I effectively decreases cancer cell proliferation. In contrast, the MCF-10A cells (non-cancerous breast cells) showed minimal impact from DNase I, with MCF10A having a proliferation rate of $(31,445 \pm 3,469)$ and MCF10A DNase I exhibiting $(32,909 \pm 3,969)$ ($p > 0.05$). (Table 2).

Table 2.Determination of Proliferation in Cells

Groups	Mean ± standard deviation	p value	Multiple Comparison
1	32581 ± 4784	p<0.001	1-2: p<0.05 6-8: p<0.05
2	22714 ± 4059		
3	31445 ± 3469		
4	32909 ± 3969		
5	27090 ± 5199		
6	26571 ± 6618		
7	26895 ± 5736		
8	35152 ± 4499		

Adhesion Analysis

A statistically significant difference was observed between the groups ($p<0.01$). DNase I had a strong effect on the adhesion of OVCAR-3 cells. Untreated OVCAR-3 cells had an adhesion value of $(69,126 \pm 8,500)$, while DNase I-treated OVCAR-3 cells (OVCAR-3 DNase I) showed a significantly lower adhesion value of $(47,925 \pm 10,028)$ ($p<0.01$) (Table 3).

Table 3.Determination of Adhesion in Cells

Groups	Mean ± standard deviation	p value	Multiple Comparison
1	69126±8500	p<0.01	1-2: p<0.01
2	47925±10028		
3	63291±3584		
4	57132±6195		
5	60443±6556		
6	65229±6443		
7	56471±10549		
8	63639±4683		

Cell Viability

Cell viability analysis shows that DNase I selectively impacts cancer cells. Untreated OVCAR-3 cells had a viability rate of 87.2%, which significantly dropped to 68.1% after DNase I treatment. In contrast, MCF-

10A cells (non-cancerous breast cells) remained largely unaffected by DNase I, with untreated cells showing 81.3% viability and DNase I-treated cells at 77.5%. This indicates that DNase I effectively targets cancer cells while preserving the viability of non-cancerous cells (Table 4).

Table 4. Determination of Viability in Cells

Groups	Viability %
1	% 87,2
2	% 68,1
3	% 81,3
4	% 77,5
5	% 80,4
6	%83,3
7	%71,6
8	%82,2

Gene Mutation and Methylation Analysis

Gene mutation analysis showed that p53 exon 7 mutations were present in OVCAR-3 cells, confirming their cancerous nature, while no mutations were found in MCF-10A cells. Additionally, APC1A, APC1B, and RASSF1A gene methylation was detected in both untreated and DNase I-treated OVCAR-3 cells, indicating DNase I may degrade hyper-methylated cfDNA in cancer cells. In contrast, no methylation was observed in MCF-10A cells, showing that DNase I selectively affects cancer cells without impacting non-cancerous cells (Table 5).

Table 5. Gene Mutation and Methylation Analysis

Condition	p53 Exon 7	APC1A Methylated	APC1A Unmethylated	APC1B Methylated	APC1B Unmethylated	RASSF1A Methylated	RASSF1A Unmethylated
OVCAR-3 Untreated	+	+	-	+	-	+	-
OVCAR-3 DNase I Treated	+	+	-	+	-	+	-
MCF-10A Untreated	-	-	-	-	-	-	-
MCF-10A DNase I Treated	-	-	-	-	-	-	-
Co-culture OVCAR-3 Untreated	+	+	-	+	-	+	-
Co-culture OVCAR-3 DNase I Treated	+	+	-	+	-	+	-
Co-culture MCF-10A Untreated	-	-	-	-	-	-	-
Co-culture MCF-10A DNase I Treated	-	-	-	-	-	-	-

DISCUSSION

Molecular diagnostic markers have become indispensable tools for detecting cancer metastasis and tumor formation, significantly contributing to personalized cancer treatments. These markers provide detailed insights into the tumor's genetic profile, essential for selecting appropriate therapies such as chemotherapy or surgery. Circulating free DNA (cfDNA) is a promising non-invasive biomarker that reflects cancer's invasive and prognostic characteristics. Studies have emphasized its importance in understanding cancer progression and metastasis, highlighting its potential in clinical research and tailored treatment approaches (20-23).

cfDNA is released from tumor cells primarily through apoptosis and necrosis, carrying mutations and epigenetic modifications that may drive metastasis. A pivotal study using a rat model of colon cancer demonstrated that oncogenic material from tumor cells could be transferred to normal cells, contributing to metastatic processes. The transfer of the CAT marker gene to lung tissues after injecting plasma from cancer-bearing rats was one of the first experimental validations of cfDNA-mediated metastasis, often referred to as

"genometastasis" (2, 4). These findings have been supported by more recent studies, confirming that cfDNA can promote the dissemination of oncogenic DNA, leading to cancer spread in distant organs (20, 22).

DNase I, an enzyme traditionally associated with nucleic acid metabolism, has gained attention for its potential therapeutic role in cancer treatment due to its ability to degrade cfDNA. Early studies presented conflicting evidence regarding its effectiveness, but recent research confirms DNase I's capacity to reduce cancer progression by breaking down hyper-methylated cfDNA, a feature of cancer cells. This enzymatic degradation prevents the transfer of oncogenic material to healthy cells, limiting metastasis. Our study focused on the selective targeting of hyper-methylated cfDNA fragments by DNase I, revealing its potential as a cancer treatment tool (24). The enzyme's ability to degrade cfDNA makes it a promising candidate for future cancer therapies aimed at reducing tumor metastasis (25).

DNA methylation is a key epigenetic process involved in cancer development, as it often silences tumor suppressor genes. CpG dinucleotides, which constitute over 70% of vertebrate DNA, are frequently methylated in cancer cells, leading to the inactivation of critical genes such as APC and RASSF1A (26). These genes play essential roles in controlling cell proliferation and apoptosis, and their silencing contributes significantly to cancer progression (27). DNase I's ability to degrade hyper-methylated cfDNA fragments suggests it may reverse gene silencing, reactivating tumor suppressor genes and inhibiting tumor growth (25). This therapeutic potential offers a promising avenue for epigenetic cancer therapies, particularly when combined with other targeted treatments.

One key finding in DNase I research is its selective action on cancer cells. Previous studies demonstrated that DNase I effectively reduced the viability of MDA-MB-231 breast cancer cells without harming healthy bone cells. This specificity is linked to the hyper-methylation of APC1A, APC1B, and RASSF1A genes in cancer cells, while healthy cells remain unaffected (28). Our study expanded on this, showing that DNase I's effectiveness may vary depending on the cellular environment. For example, no significant differences in gene methylation were observed between MCF-10A and OVCAR-3, suggesting that the enzyme's activity may be cell-type specific. These findings indicate DNase I could be developed as a targeted therapy for specific cancer types.

Despite DNase I's promising results in degrading cfDNA and selectively targeting cancer cells, further research is needed to fully understand its potential as a cancer therapy. In particular, studies should explore its long-term effects, especially when combined with other epigenetic therapies, to determine its efficacy across different cancer types and genetic profiles (24). Additionally, interactions between cancer and healthy cells, particularly how cancer cells influence normal cell proliferation and viability, remain critical areas for future research (26). DNase I's ability to reverse gene silencing by degrading hyper-methylated cfDNA fragments could pave the way for novel cancer treatments, but more comprehensive studies are required to confirm these findings.

CONCLUSION

In conclusion, molecular diagnostic markers like cfDNA have proven essential in understanding cancer metastasis and guiding personalized treatment plans. DNase I has emerged as a promising therapeutic tool for targeting hyper-methylated cfDNA, potentially reactivating silenced tumor suppressor genes and inhibiting cancer progression. While further research is required to validate DNase I's long-term efficacy, its selective action on cancer cells offers hope for developing more effective cancer therapies in the future.

Acknowledgments

The authors express their gratitude to the Research Foundation of Eskisehir Osmangazi University for the valuable support provided throughout this study.

Authorship contributions

All authors have contributed equally to the work

Data availability statement

The authors state that the data supporting the study's results can be found in the article. Additionally, the raw data can be obtained from the corresponding author upon a reasonable request.

Declaration of competing interest

The Authors declare no conflict of interest pertaining to the current work

Ethics

Since the study was conducted on commercially purchased cell cultures, an ethics committee approval document is not required.

Funding

This study was supported by a Grant from the Research Foundation of Eskisehir Osmangazi University, Turkey (Project no: 201811066).

REFERENCES

1. Weinberg RA, Weinberg RA. *The Biology of Cancer*: W.W. Norton; 2013.
2. Garcia-Olmo D, Garcia-Olmo D, Ontanon J, Martinez E, Vallejo M. Tumor DNA circulating in the plasma might play a role in metastasis. The hypothesis of the genomestasis. *Histology and histopathology*. 1999;14(4):1159-64.
3. Garcia-Olmo D, Ontanon J, Garcia-Olmo D, Atienzar M, Vallejo M. Detection of genomically-tagged cancer cells in different tissues at different stages of tumor development: lack of correlation with the formation of metastasis. *Cancer letters*. 1999;140(1-2):11-20.
4. Garcia-Olmo Dn, Garcia-Olmo DC, Ontañón Js, Martinez E. Horizontal transfer of DNA and the “genomestasis hypothesis”. *Blood, The Journal of the American Society of Hematology*. 2000;95(2):724-5.
5. Chen Z, Fadiel A, Naftolin F, Eichenbaum K, Xia Y. Circulation DNA: biological implications for cancer metastasis and immunology. *Medical hypotheses*. 2005;65(5):956-61.
6. Silva JM, Dominguez G, Garcia JM, Gonzalez R, Villanueva MJ, Navarro F, et al. Presence of tumor DNA in plasma of breast cancer patients: clinicopathological correlations. *Cancer research*. 1999;59(13):3251-6.
7. Silva JM, Silva J, Sanchez A, Garcia JM, Dominguez G, Provencio M, et al. Tumor DNA in plasma at diagnosis of breast cancer patients is a valuable predictor of disease-free survival. *Clinical Cancer Research*. 2002;8(12):3761-6.
8. Garcia JM, Garcia V, Silva J, Pena C, Dominguez G, Sanchez A, et al. Extracellular tumor DNA in plasma and overall survival in breast cancer patients. *Genes, Chromosomes and Cancer*. 2006;45(7):692-701.
9. Lujambio A, Esteller M. How epigenetics can explain human metastasis: a new role for microRNAs. *Cell cycle*. 2009;8(3):377-82.
10. Krypuy M, Ahmed AA, Etemadmoghadam D, Hyland SJ, org AOCSGntp, deFazio A, et al. High resolution melting for mutation scanning of TP53 exons 5–8. *BMC cancer*. 2007;7:1-
11. Gasco M, Shami S, Crook T. The p53 pathway in breast cancer. *Breast cancer research*. 2002;4:1-7.
12. Petitjean A, Mathe E, Kato S, Ishioka C, Tavtigian SV, Hainaut P, Olivier M. Impact of mutant p53 functional properties on TP53 mutation patterns and tumor phenotype: lessons from recent developments in the IARC TP53 database. *Human mutation*. 2007;28(6):622-9.
13. Esteller M. Epigenetics in cancer. *New England Journal of Medicine*. 2008;358(11):1148-59.
14. Rishi V, Bhattacharya P, Chatterjee R, Rozenberg J, Zhao J, Glass K, et al. CpG methylation of half-CRE sequences creates C/EBP α binding sites that activate some tissue-specific genes. *Proceedings of the National Academy of Sciences*. 2010;107(47):20311-6.
15. Rozenberg JM, Shlyakhtenko A, Glass K, Rishi V, Myakishev MV, FitzGerald PC, Vinson C. All and only CpG containing sequences are enriched in promoters abundantly bound by RNA polymerase II in multiple tissues. *BMC genomics*. 2008;9:1-13.
16. Zhu J, Yao X. Use of DNA methylation for cancer detection and molecular classification. *BMB Reports*. 2007;40(2):135-41.
17. Shen C, Sheng Q, Zhang X, Fu Y, Zhu K. Hypermethylated APC in serous carcinoma based on a meta-analysis of ovarian cancer. *Journal of Ovarian Research*. 2016;9:1-8.
18. Lewis CM, Cler LR, Bu D-W, Zöchbauer-Müller S, Milchgrub S, Naftalis EZ, et al. Promoter hypermethylation in benign breast epithelium in relation to predicted breast cancer risk. *Clinical Cancer Research*. 2005;11(1):166-72.
19. Powell E, Piwnica-Worms D, Piwnica-Worms H. Contribution of p53 to metastasis. *Cancer discovery*. 2014;4(4):405-14.
20. Wan JC, Massie C, Garcia-Corbacho J, Mouliere F, Brenton JD, Caldas C, et al. Liquid biopsies come of age: towards implementation of circulating tumour DNA. *Nature Reviews Cancer*. 2017;17(4):223-38.
21. Diaz Jr LA, Bardelli A. Liquid biopsies: genotyping circulating tumor DNA. *Journal of clinical oncology*. 2014;32(6):579-86.
22. Thierry AR, El Messaoudi S, Gahan P, Anker P, Stroun M. Origins, structures, and functions of circulating DNA in oncology. *Cancer and metastasis reviews*. 2016;35:347-76.
23. Jahr S, Hentze H, Englisch S, Hardt D, Fackelmayer FO, Hesch R-D, Knippers R. DNA fragments in the blood plasma of cancer patients: quantitations and evidence for their origin from apoptotic and necrotic cells. *Cancer research*. 2001;61(4):1659-65.

-
24. Alekseeva L, Mironova N. Role of cell-free DNA and deoxyribonucleases in tumor progression. *International Journal of Molecular Sciences*. 2021;22(22):12246.
25. Trejo-Becerril C, Pérez-Cardenas E, Gutiérrez-Díaz B, De La Cruz-Sigüenza D, Taja-Chayeb L, González-Ballesteros M, et al. Antitumor effects of systemic DNase I and proteases in an in vivo model. *Integrative cancer therapies*. 2016;15(4):NP35-NP43.
26. Baylin SB, Jones PA. Epigenetic determinants of cancer. *Cold Spring Harbor perspectives in biology*. 2016;8(9):a019505.
27. Esteller M. Cancer epigenomics: DNA methylomes and histone-modification maps. *Nature reviews genetics*. 2007;8(4):286-98.
28. Dal A, Coşan DT. The effect of DNase I on free DNAs and its relationship with metastasis: A preliminary results. *Biological Diversity and Conservation*. 2020;13(2):153-9.

Research Article

EXAMINING THE ROLE OF SUPAR AND HS-CRP LEVELS IN PREDICTING CORONARY ARTERY DISEASE SEVERITY IN ACUTE MYOCARDIAL INFARCTION: AN AGE-STRATIFIED ANALYSIS INCORPORATING SYNTAX SCORE

 Muhammet Salih ATEŞ *¹,  Abdullah TUNÇEZ ²,  Muhammed Ulvi YALÇIN ²,  Kenan DEMİR ²,  Nazif AYGÜL ²,  Bülent Behlül ALTUNKESER ²,  Hüseyin TEZCAN ³,  Onur Can POLAT ⁴,  Aslıhan Merve TOPRAK ⁵,  Bahadır ÖZTÜRK ⁶

¹Department of Cardiology, Ahi Evran University, Kırşehir, TURKIYE,

²Department of Cardiology, Selcuk University Medical Faculty, Konya, TURKIYE,

³Department of Cardiology, Konya City Hospital, Konya, TURKIYE,

⁴Department of Cardiology, Sandıklı State Hospital, Afyonkarahisar, TURKIYE,

⁵Department of Cardiology, Kayseri State Hospital, Kayseri, TURKIYE,

⁶Department of Biochemistry, Selcuk University Medical Faculty, Konya, TURKIYE

*Correspondence: m.salih.ates@gmail.com

ABSTRACT

Objective: This study examines the association between traditional inflammatory biomarkers, soluble urokinase plasminogen activator receptor (suPAR) levels in elderly and young myocardial infarction patients, and coronary artery disease severity.

Materials and Methods: In this study, 332 participants, including 227 acute myocardial infarction (AMI) patients and 107 controls, underwent evaluation through Syntax Score analysis, suPAR, and high-sensitivity C-reactive protein (hs-CRP) level assessments. AMI patients were divided into young and elderly groups based on age. Syntax Score was utilized to ascertain the severity of coronary artery disease.

Results: suPAR plasma concentrations were significantly higher in AMI patients compared to controls, with values of 2.76 (2.32-3.56) in the young MI group and 3.33 (2.43-4.41) in the elderly MI group, versus 2.33 (1.94-3.11) in the control group ($p<0.001$). Additionally, hs-CRP levels were notably elevated in the elderly MI groups ($p<0.001$). The ROC analysis identified threshold values for suPAR at 3.10 pg/mL and hs-CRP at 6.5 mg/dL to predict a Syntax Score of 23 or higher, with suPAR showing 74.7% sensitivity, 69.9% specificity, and an area under the curve (AUC) of 0.811 ($p<0.001$). The sensitivity of hs-CRP was 65.8%, the specificity was 60.2%, and the AUC was 0.700 ($p<0.001$).

Conclusion: Our study reveals a pivotal relationship between inflammatory markers, particularly suPAR, and Syntax Score in MI patients, suggesting its potential in refining cardiovascular risk assessment and informing future diagnostic and therapeutic approaches for coronary artery disease management.

Keywords: suPAR, hs-CRP, Young myocardial infarction, Elderly myocardial infarction

Received: 09 August 2024
Revised: 17 October 2024
Accepted: 22 October 2024
Published: 22 December 2024



Copyright: © 2024 by the authors. Published Aydın Adnan Menderes University, Faculty of Medicine and Faculty of Dentistry. This is an open access article under the Creative Commons Attribution Non Commercial 4.0 International (CC BY-NC 4.0) License.

INTRODUCTION

The complex pathophysiology of acute myocardial infarction (AMI); includes inflammation, myocardial structural change, and myocardial injury as a result of myocardial stress (1). Biomarkers involved in this complex process help infarct size, myocardial dysfunction, identification of risky patients, treatment and follow-up (2).

In particular, traditional biomarkers reflecting inflammatory processes, such as high-sensitivity C-reactive protein (hs-CRP) and erythrocyte sedimentation rate (ESR), have been associated with an increased risk of cardiovascular disease and AMI (3). Known to be involved in the inflammatory process, soluble urokinase plasminogen activator receptor (suPAR) has been associated with newly discovered cardiovascular disease risk and all-cause mortality (4,5).

SuPAR can be found in a variety of cell types, including monocytes, endothelial cells, activated T lymphocytes, macrophages, fibroblasts, megakaryocytes, smooth muscle cells, keratinocytes, and some tumor cells (6,7). uPAR consists of three sites and is involved in immune system activation. The release of suPAR occurs when the membrane-bound uPAR is cleaved, leading to its presence in various bodily fluids such as plasma, cerebrospinal fluid, serum, blood, and urine. The concentration of suPAR in bodily fluids can vary depending on the level of immune system activation (8).

Recent studies have revealed that patients with AMI have significantly higher suPAR levels which can be used as a predictor of cardiac events (9-11). It is also known that the suPAR level increases with age (12). The risk of AMI also increases with age. However, it is still unknown about suPAR values based on the age of the patients who have AMI.

The main objective of this study was to compare the traditional inflammatory biomarkers and suPAR levels in elderly and young myocardial infarction (MI) patients with those in patients who had been determined not to have coronary artery disease (CHD). Furthermore, this research aimed to investigate the correlation between suPAR concentrations and the extent of CHD severity.

MATERIALS AND METHODS

This study encompassed 243 patients admitted to the intensive care unit with an initial diagnosis of AMI, who were scheduled for coronary angiography between April 2019 and January 2020. Of these, 14 patients, initially diagnosed and set to partake in the study, declined to undergo coronary angiography, leading to their exclusion. Furthermore, two individuals from the control group were also excluded on account of rheumatological diseases. The study further categorized patients based on age: those 55 years and younger were classified as the 'young' group, while those older than 55 years were designated as the 'elderly' group. The control group consisted of patients who underwent coronary angiography for indications other than AMI and had less than 50% coronary artery stenosis.

The study excluded patients presenting with active infections, malignancies, autoimmune disorders, hyperthyroidism, or those on immunosuppressive medication. Additionally, individuals with chronic kidney disease, rheumatological conditions, those who had undergone revascularization with fibrinolytic therapy, or had a history of pulmonary embolism were also excluded.

The study's intended participants were given information about the study and given the option to volunteer for it after receiving their consent. Ethical clearance was granted by Selçuk University's Ethics Committee (Decision No: 2019/92, Date: 08.05.2019). The study received funding support from the Selçuk University Scientific Research Projects Coordinatorship, under the project identifier 19102049.

Blood samples

At the time of hospitalization, 5 ml of blood were drawn from the patients upon admission to the intensive care unit with the diagnosis of AMI, and from the control group after coronary angiography. Then, those blood samples were placed in eppendorf tubes to study the suPAR level and stored at -80°C after centrifugation at 4000 rpm for 5 minutes.

In the biochemistry laboratory, blood samples such as creatinine, HDL cholesterol, triglyceride, LDL cholesterol, sodium, potassium, and hs-CRP in the BECKMAN COULTER AU5800 autoanalyzer, complete

blood count (hemoglobin, platelet, leukocyte) in the COULTER DXH 800 blood count device. Sedimentation was measured in the ALIFAX device, and the results were recorded separately for each patient.

Plasma suPAR levels were measured on an automated BMG LABTECH CLARIOSTAR instrument utilizing the suPARnostic AUTO Flex ELISA kit for determination, based on the instructions provided by the manufacturer (ViroGates A/S, Birkerød, Denmark).

Syntax score analysis

Catheterization images were evaluated using the Syntax Score system. All lesions causing a reduction in luminal diameter of 50% or more in coronary vessels with a diameter equal to or greater than 1.5 mm were accounted for in the Syntax Score computation. For this calculation, we utilized the dedicated software available at <http://www.syntaxscore.com> (13). The evaluation of the Syntax Score was independently conducted by two interventional cardiologists who were not informed of the study protocol or the patient demographics. Intermediate-high risk was determined as 23 and above.

Statistical analysis

Statistical analyses were conducted using SPSS version 29.0 (SPSS Inc., Chicago, IL, USA). The normality of distribution for numerical variables was verified through the Kolmogorov-Smirnov test. These variables were presented as mean \pm standard deviation and median (with interquartile range from the 25th to 75th percentile). Categorical variables were expressed in terms of frequencies and percentages. The comparison of numerical variables among the three study groups was performed using either one-way ANOVA or the Kruskal-Wallis test, depending on the suitability for parametric analysis. The chi-square test was applied for the assessment of categorical variables. For the analysis of bivariate relationships among continuous variables, Spearman's rank correlation coefficient was employed. The efficacy of the Syntax Score in predicting the severity of coronary artery disease was evaluated using Receiver Operating Characteristic (ROC) curve

analysis, with a particular focus on establishing a diagnostic threshold for a Syntax Score greater than 23 and above. Two-sided p values less than 0.05 were considered statistically significant.

RESULTS

Basic characteristics of patients

This investigation included a total of 332 participants, who were allocated into three groups: a young myocardial infarction (MI) group with 100 patients, an elderly MI group encompassing 127 patients, and a control group consisting of 105 individuals, as outlined in Table 1.

The median age in the group of young patients with MI was 49 years (44.2–53), in the group of elderly patients with MI the median age was 66 years (62–74), and in the control group the median age was 59 years (53–66), showing a statistically significant difference ($p < 0.001$). Compared to the control group, both groups of AMI patients had a higher proportion of men (88% in the young MI group, 65.4% in the older MI group, 45.7% in the control group, $p < 0.001$). However, there was no statistically significant difference in body mass index (BMI) between the groups ($p = 0.77$).

Diabetes Mellitus (DM) appears to be homogeneously distributed in all three groups ($p = 0.07$). Among the young MI group, 52% presented with ST-segment elevation MI (STEMI), and in the elderly MI group, 41.7% had STEMI. In the AMI population compared to the control group, left ventricular ejection fraction as determined by Simpson's formula in echocardiography was significantly lower (49.68 ± 9.84 for the young MI group, 44.84 ± 9.58 for the elderly MI group, 54.27 ± 7.35 for the control group, $p < 0.001$).

Laboratory findings

The laboratory test results of patients participating in this study are presented in Table 1. The suPAR plasma concentration value was 2.76 (2.32–3.56) for the young MI group, 3.33 (2.43–4.41) for the elderly MI group, and 2.33 (1.94–3.11) for the control group. In comparison to the control group, a significant increase was seen in the AMI population ($p < 0.001$). In the elderly MI group, hs-CRP and ESR were

significantly higher ($p < 0.001$). In comparison to the control group, the AMI population had significantly higher levels of syntax score, white blood cell, triglycerides, and LDL-C ($p < 0.001$).

Table 1. Patient characteristics and serum parameters

Variable	Young MI n=100	Elderly MI n=127	Control n=105	p value
Age, year	49(44.2~53)	66(62~74)	59(53~66)	<0.001
Sex (male), n (%)	88/88	83/65.4	48/45.7	<0.001
Body Mass Index (kg/m ²)	27.6(26.1~29.4)	27.5(25.4~29.8)	28.4(24.9~31.2)	=0.774
DM n (%)	19/19	41/32.3	31/29.5	=0.07
STEMI n (%)	52/52	53/41.7		<0.001
LVEF %	52(45~58)	46(38~54)	58(54.25~58)	<0.001
suPAR	2.76(2.32~3.56)	3.33(2.43~4.41)	2.33(1.94~3.11)	<0.001
Hs-CRP	5(2.6~9.2)	8.7(3.6~21)	3.66(1.57~6.94)	<0.001
ESR	8(4~12.7)	13(7.5~23.5)	9(4.5~15)	<0.001
Syntax Score	12(8~18.75)	22(19~28)		<0.001
Hgb, g/dl	14.7(13.7~15.5)	12.7(11.1~14.2)	13.6(12.3~15)	<0.001
White Blood Cell, 10 ³ /μl	10.8(9.2~12.9)	10.4(7.7~11.5)	7.3(6~8.4)	<0.001
Platelet, 10 ³ /μl	227(185~262)	213(163~253)	239(207~286)	=0.001
Creatinine, mg/dl	0.74(0.67~0.86)	0.81(0.67~0.99)	0.72(0.63~0.84)	=0.003
HDL, mg/dl	38(31.2~43)	38(33~44)	43(38~51)	=0.015
LDL, mg/dl	130±39.2	119.70±39.15	112.56±32.80	<0.001

The values are presented as n (%), mean ± standard deviation, or median (25th and 75th percentiles). LDL: low-density lipoprotein, HDL: high-density lipoprotein, Hgb: hemoglobin, Na⁺: sodium, K⁺: potassium, suPAR: soluble urokinase plasminogen activator receptor, Hs-CRP: high-sensitivity C-reactive protein, ESR: erythrocyte sedimentation rate, LVEF: left ventricular ejection fraction, STEMI: ST-segment elevation myocardial infarction, DM: diabetes mellitus

The assessment of all three groups within the analyzed patient cohort is summarized in Table 2. Significantly higher suPAR plasma concentrations were observed in the elderly MI group compared to the young MI group ($p = 0.002$). Additionally, in the elderly MI group, both hs-CRP and ESR values were significantly elevated when compared to the young MI group ($p = 0.003$, $p < 0.001$, respectively). In contrast, the young MI group exhibited significantly higher suPAR plasma concentrations than the control group ($p = 0.008$). However, no significant differences were observed in the concentration of Hs-CRP and ESR between the group with young MI and the control group ($p = 0.725$, $p = 0.658$, respectively).

When the elderly MI group was compared to the control groups, in the elderly MI group, the suPAR plasma concentration was significantly higher ($p < 0.001$). In the elderly MI group, Hs-CRP and sedimentation values were significantly higher when both groups were compared ($p < 0.001$ for both).

Table 2. Comparison of groups

	Young MI n=100	Elderly MI n=127	Control n=105	p value ^a	p value ^b	p value ^c
suPAR	2.76(2.32~3.56)	3.33(2.43~4.41)	2.33(1.94~3.11)	0.002	0.008	<0.001
Hs-CRP	5(2.6~9.2)	8.7(3.6~21)	3.66(1.57~6.94)	0.003	0.725	<0.001
ESR	8(4~12.7)	13(7.5~23.5)	9(4.5~15)	<0.001	0.658	<0.001

The values are presented as medians (25th and 75th percentiles). suPAR: soluble urokinase plasminogen activator receptor, Hs-CRP: high-sensitivity C-reactive protein, ESR: erythrocyte sedimentation rate, ^a p value for comparison of young MI and elderly MI, ^b p value for comparison of young MI and control groups, ^c p value for comparison of elderly MI and control groups

Table 3. Correlations of suPAR with other parameters

	suPAR	
	Coefficient(r)	p value
Hs-CRP	0.291	<0.001
ESR	0.234	<0.001
Syntax Score	0.533	<0.001
Age	0.157	=0.004
LV EF %	-0.336	<0.001
Hgb, g/dl	-0.127	0.023
White Blood Cell, 10 ³ /μl	0.338	<0.001
Creatinine, mg/dl	0.209	<0.001
HDL, mg/dl	-0.262	<0.001
LDL, mg/dl	-0.087	0.118

LDL: low-density lipoprotein, HDL: high-density lipoprotein, Hgb: hemoglobin, suPAR: soluble urokinase plasminogen activator receptor, Hs-CRP: high-sensitivity C-reactive protein, ESR: erythrocyte sedimentation rate, LVEF: left ventricular ejection fraction

Table 3 summarizes the correlation analysis between suPAR and commonly used clinical biomarkers. The results revealed several important relationships. Notably, suPAR was significantly correlated with hs-CRP ($r=0.291$, $p < 0.001$), grammar score ($r=0.533$, $p < 0.001$), white blood cell count ($r=0.338$, $p < 0.001$) and ESR ($r=0.234$, $p < 0.001$), age ($r=0.157$, $p=0.004$) and creatinine ($r=0.209$, $p < 0.001$). On the other hand, negative correlations were observed between suPAR and hemoglobin ($r=-0.127$, $p=0.023$), left ventricular ejection fraction (LVEF) ($r=-0.336$, $p < 0.001$) and high-density lipoprotein (HDL) . ($r=-0.262$, $p < 0.001$).

In the logistic regression model assessing age, SuPAR, and Hs-CRP as predictors of intermediate-high Syntax Scores (≥ 23), all three variables showed a significant association in the univariate analysis with a p-value of <0.001 . In the multivariate analysis, age remained significant with a p-value of 0.002, Hs-CRP with a p-value of 0.003, and SuPAR with a p-value of <0.001 . ESR had a significant association in univariate analysis ($p < 0.001$), but it had no significant association in multivariate analysis ($p = 0.424$). WBC had a significant univariate effect ($p = 0.038$), but it had no significant impact on the multivariate analysis ($p = 0.146$). The association between DM, gender and obesity was considered, but this did not have a significant impact on the statistics (Table 4).

Table 4. Binary logistic regression analysis aiming to determine independent variables associated with intermediate-high SYNTAX score (≥ 23)

Variable	Univariate Analysis			Multivariate Analysis		
	OR	95% CI	P	OR	95% CI	P
SuPAR	3.134	2.219-4.428	<0.001	2.436	1.508-3.937	<0.001
Hs-CRP	1.067	1.036-1.099	<0.001	1.025	1.025-1.122	0.003
ESR	1.043	1.018-1.069	0.001	1.007	0.972-1.040	0.424
Age	1.107	1.048-1.170	<0.001	1.160	1.057-1.273	=0.002
DM status	0.952	0.447-2.028	0.899			
Gender	1.679	0.900-3.130	0.103			
BMI	1.070	0.994-1.153	0.073			
WBC	1.104	1.005-1.213	0.038	1.146	0.953-1.378	0.146
HDL	0.961	0.929-0.994	0.023	0.978	0.921-1.037	0.454
LDL	1.002	0.995-1.009	0.552			

LDL: low-density lipoprotein, HDL: high-density lipoprotein, suPAR: soluble urokinase plasminogen activator receptor, Hs-CRP: high-sensitivity C-reactive protein, ESR: erythrocyte sedimentation rate, DM: Diabetes mellitus

Table 5: Assessing the predictive value of SuPAR and Hs-CRP in determining the severity of coronary artery disease: An evaluation of intermediate-high syntax scores (≥ 23)

	p	AUC	Cutoff	Sensitivity	Specificity
suPAR	<0.001	0.811	3.10	74.7%	69.9%
Hs-CRP	<0.001	0.700	6.5	65.8%	60.2%

suPAR: soluble urokinase plasminogen activator receptor, Hs-CRP: high-sensitivity C-reactive protein,

In the ROC analysis, the established threshold values for suPAR and hs-CRP for forecasting a Syntax Score of 23 or higher were identified as 3.10 pg/mL and 6.5 mg/dL, respectively. These thresholds exhibited sensitivities of 74.7% for suPAR and 69.9% for hs-CRP, and specificities of 65.8% and 60.2%, respectively.

The respective area under the curve (AUC) metrics were calculated as 0.811 ($p < 0.001$) for suPAR and 0.700 ($p < 0.001$) for hs-CRP, as depicted in Figure 1 and Table 5.

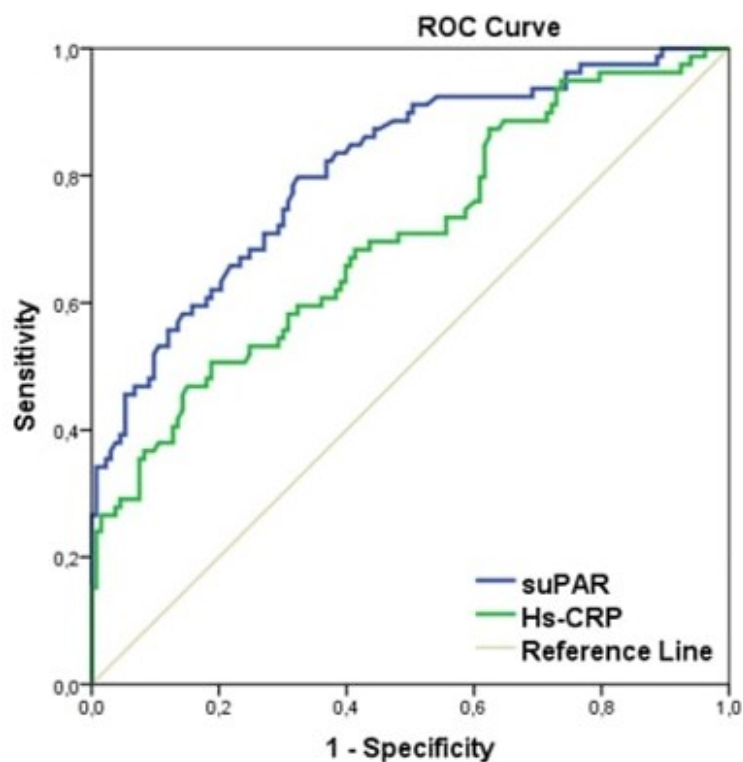


Figure 1. Assessing the predictive value of SuPAR and Hs-CRP in determining the severity of coronary artery disease: An evaluation of intermediate-high syntax scores (≥ 23)

DISCUSSION

Our main findings from this study indicate that suPAR levels were significantly higher in patients with MI compared to healthy controls. Additionally, it was observed that suPAR concentrations were notably higher in the elderly MI group in comparison to the younger MI group. In a similar vein, Hs-CRP levels demonstrated an increase in the elderly MI group. However, the comparison between the young MI group and the control group did not reveal any statistically significant rise in Hs-CRP levels. A strong positive

correlation was observed with the suPAR syntax score. Levels of suPAR and hs-CRP have been associated with predicting intermediate and high Syntax scores. In this context, ROC analysis revealed that new threshold values of suPAR and Hs-CRP could be useful in predicting an intermediate-high syntax score (≥ 23), suggesting their potential as simple and repeatable diagnostic tools for assessing the severity of coronary artery disease. Therefore, our findings contribute further to the existing literature on the relationship between suPAR, syntax score, and AMI patients. To our knowledge, this is the first study examining the relationship between suPAR levels and syntax scores in patients with AMI.

An increased syntax score is a globally applied and well-established scoring system that indicates the severity of coronary artery disease. Previous studies have shown that an elevated syntax score is associated with increased cardiovascular mortality and morbidity (14,15). Chronic inflammatory processes have also been shown to contribute to the increase in Syntax Score (16). Chronic inflammation is linked to endothelial dysfunction, vasculopathy, and atherosclerosis (17). In a study by Corban et al., a relationship between suPAR and endothelial dysfunction was established (18). Another study by Hindy et al. demonstrated that suPAR triggers monocyte modulation, thereby inducing atherosclerosis (19). In research conducted by Goodchild et al., suPAR plays a key role in the pathophysiology of atherosclerosis by stimulating pro-inflammatory cytokines and activating neutrophils, monocytes, and endothelial cells (20).

Similarly, previous studies involving hs-CRP have also established its association with endothelial dysfunction, vasculopathy, and atherosclerosis. Research conducted by Zaghloul et al and Mario et al demonstrated the relationship between endothelial dysfunction and hs-CRP (21,22). Additionally, studies by Niknezhad et al, Yu et al, and Swastini et al have linked hs-CRP with the development of atherosclerosis (23-25).

Previous studies have examined the relationship between hs-CRP and the syntax score. In the studies by Rezk et al. and Karadeniz et al., increased hs-CRP levels have been associated with an elevated syntax score in patients with ACS (26,27). Karadeniz et al. found that in patients with ACS, hs-CRP at a cut-off value of 5.77 mg/dL predicted an intermediate-high risk syntax score (≥ 23) with 75% sensitivity and 69% specificity (27). In our study, similarly, hs-CRP at 6.5 mg/dL was found to predict an intermediate-high syntax score,

demonstrating 65.8% sensitivity and 60.2% specificity ($p < 0.001$). However, SuPAR levels were superior to Hs-CRP in both regression and ROC analyses for predicting moderate-to-high Syntax Scores.

In contrast to hs-CRP, it has been demonstrated that the level of suPAR in plasma is not influenced by circadian rhythms and remains more stable under acute stress conditions (8,28). Additionally, suPAR has been shown to be superior to hs-CRP in predicting in-hospital mortality in patients with severe sepsis and septic shock (29).

Numerous studies involving coronary artery disease have emphasized the significance of suPAR. Persson et al.'s research found that elevated plasma suPAR levels are linked to a higher incidence of cardiovascular disease (30). Lyngbæk et al. demonstrated that in patients with AMI, plasma suPAR levels are predictive of all-cause mortality and recurrent MI (28). Furthermore, Eapen et al. revealed that plasma suPAR levels are indicative of the presence of Coronary Artery Disease and can predict future adverse events (31). Importantly, this study also established that in predicting MI and mortality, suPAR operates independently of hs-CRP.

Botha et al. observed a significant increase in suPAR levels over a five-year follow-up in South African black individuals who developed hypertension, indicating an independent association of baseline suPAR levels with the hypertensive group (32). Tahhan et al. found that individuals with peripheral artery disease have higher plasma suPAR levels compared to those with only coronary artery disease, correlating the prevalence of the disease with increased suPAR levels (33). Persson et al. also noted an increase in plasma suPAR levels in patients with carotid plaque, significantly elevating the risk of ischemic stroke and coronary artery disease (34).

In our study, we examined the relationship between suPAR and SYNTAX score. Although it has been shown that suPAR triggers endothelial dysfunction, stimulates pro-inflammatory cytokines, and ultimately leads to atherosclerosis, to our knowledge, there are no studies demonstrating a relationship between suPAR levels and the SYNTAX score, which is used to indicate the severity of coronary artery disease. In this study, suPAR was found to be a strongly independent predictor of an intermediate-high syntax score (≥ 23). The cut-off for suPAR was identified at 3.10 pg/dl, demonstrating a sensitivity of 74.7% and specificity of 69.9%.

Our study has several limitations. Firstly, its cross-sectional design suggests a need for larger, more comprehensive studies in the future to expand upon our results. Secondly, the age cutoff of 55 years used for grouping patients, while not a definitive boundary, has been utilized in some studies (35-38). The median age in the young MI group was 49, and in the elderly MI group, it was 66, indicating a significant age difference between the two groups. Thirdly, we recognize a major limitation in the gender distribution within the groups, particularly the predominance of male patients in the young MI group. This imbalance is a concern, though it is well-known that the incidence of AMI in younger ages is much higher in males (39,40).

The principal strength of our research, likely to be of significant interest to clinical practitioners, lies in its provision of novel evidence concerning the pronounced impact of suPAR on the syntax score in predicting intermediate-high risk scenarios. This finding introduces a critical line of inquiry in the realm of cardiovascular risk assessment and management.

CONCLUSION

Our study contributes valuable insights into the relationship between inflammatory markers and the syntax score in MI patients. The strong correlation of suPAR with intermediate-high syntax scores offers a novel perspective in cardiovascular risk assessment. Despite its limitations, this research paves the way for future investigations, emphasizing the need for larger, more diverse cohorts to fully elucidate these relationships. Ultimately, these findings could have significant implications for the development of more nuanced diagnostic tools and targeted therapeutic strategies in the management of coronary artery disease.

Acknowledgments

The study does not take any financial support.

Authorship contributions

Concept: M.S.A, A.T. Design: M.S.A, A.T., B.B.A, Data Collection or Processing: M.S.A., A.T., M.U.Y., K.D. N.A., B.B.A., H.T., O.C.P., A.M.T., Analysis or Interpretation: M.S.A., A.T., M.U.Y., K.D., H.T., O.C.P., A.M.T., B.Ö., Literature Search: M.S.A., A.T., N.A., B.B.A. B.Ö., Writing: M.S.A, A.T., B.B.A.

Declaration of competing interest

No conflict of interest was declared by the authors.

Ethics

Ethical clearance was granted by Selçuk University's Ethics Committee (Decision No: 2019/92, Date: 08.05.2019).

Funding

The study received funding support from the Selçuk University Scientific Research Projects Coordinatorship, under the project identifier 19102049.

REFERENCES

1. Ong S-B, Hernández-Reséndiz S, Crespo-Avilan GE, Mukhametshina RT, Kwek X-Y, Cabrera-Fuentes HA, et al. Inflammation following acute myocardial infarction: multiple players, dynamic roles, and novel therapeutic opportunities. *Pharmacol Ther* 2018; 186: 73-87.
2. Arbel Y, Strauss BH. suPAR: A cardiac biomarker with a future? *Can J Cardiol* 2015; 31: 1223-4.
3. Baghai TC, Varallo-Bedarida G, Born C, Häfner S, Schüle C, Eser D, et al. Classical risk factors and inflammatory biomarkers: one of the missing biological links between cardiovascular disease and major depressive disorder. *Int J Mol Sci* 2018; 19: 1740.
4. Li Y, Ding Y, Zhao Y, Gui Y, Shen Y, Xiang Q. Prognostic value of soluble urokinase-type plasminogen activator receptor in coronary artery disease: A meta-analysis. *Eur J Clin Invest* 2022; 52: e13867.
5. Torino C, Pizzini P, Cutrupi S, Postorino M, Tripepi G, Mallamaci F, et al. Soluble urokinase plasminogen activator receptor (suPAR) and all-cause and cardiovascular mortality in diverse hemodialysis patients. *Kidney international reports* 2018; 3: 1100-9.
6. Rasmussen LJH, Petersen JEV, Eugen-Olsen J. Soluble urokinase plasminogen activator receptor (suPAR) as a biomarker of systemic chronic inflammation. *Front Immunol* 2021; 12: 780641.
7. Estreicher A, Mühlhauser J, Carpentier J-L, Orci L, Vassalli J-D. The receptor for urokinase type plasminogen activator polarizes expression of the protease to the leading edge of migrating monocytes and promotes degradation of enzyme inhibitor complexes. *The Journal of cell biology* 1990; 111: 783-92.
8. Thunø M, Macho B, Eugen-Olsen J. suPAR: the molecular crystal ball. *Dis Markers* 2009; 27: 157-72.
9. Wang X-Y, Zhang F, Zhang C, Zheng L-R, Yang J. The biomarkers for acute myocardial infarction and heart failure. *BioMed research international* 2020; 2020.
10. Sörensen NA, Nikorowitsch J, Neumann JT, Rübsamen N, Goßling A, Hartikainen TS, et al. Predictive value of soluble urokinase-type plasminogen activator receptor for mortality in patients with suspected myocardial infarction. *Clin Res Cardiol* 2019; 108: 1386-93.
11. Pan Y, Wang L, Xie Y, Tan Y, Chang C, Qiu X, et al. Characterization of differentially expressed plasma proteins in patients with acute myocardial infarction. *J Proteomics* 2020; 227: 103923.
12. Wlazel RN, Szwabe K, Guligowska A, Kostka T. Soluble urokinase plasminogen activator receptor level in individuals of advanced age. *Sci Rep* 2020; 10: 15462.
13. Serruys PW, Onuma Y, Garg S, Sarno G, van den Brand M, Kappetein A-P, et al. Assessment of the SYNTAX score in the Syntax study. *EuroIntervention* 2009; 5: 50-6.
14. Kul S, Akgul O, Uyarel H, Ergelen M, Kucukdagli OT, Tasal A, et al. High SYNTAX score predicts worse in-hospital clinical outcomes in patients undergoing primary angioplasty for acute myocardial infarction. *Coron Artery Dis* 2012; 23: 542-8.
15. Girasis C, Garg S, Räber L, Sarno G, Morel M-A, Garcia-Garcia HM, et al. SYNTAX score and Clinical SYNTAX score as predictors of very long-term clinical outcomes in patients undergoing percutaneous coronary interventions: a substudy of SIRolimus-eluting stent compared with pacliTAXel-eluting stent for coronary revascularization (SIRTAX) trial. *Eur Heart J* 2011; 32: 3115-27.
16. Altunova M, Karakayalı M, Kahraman S, Avcı Y, Demirci G, Sevinç S, et al. Systemic Immune-inflammatory index is associated with residual SYNTAX score in patients with st-segment elevation myocardial infarction. *Anatolian Journal of Cardiology* 2023; 27: 472.
17. Castellon X, Bogdanova V. Chronic inflammatory diseases and endothelial dysfunction. *Aging Dis* 2016; 7: 81.

18. Corban MT, Prasad A, Nesbitt L, Loeffler D, Herrmann J, Lerman LO, et al. Local production of soluble urokinase plasminogen activator receptor and plasminogen activator inhibitor-1 in the coronary circulation is associated with coronary endothelial dysfunction in humans. *Journal of the American Heart Association* 2018; 7: e009881.
19. Hindy G, Tyrrell DJ, Vasbinder A, Wei C, Presswalla F, Wang H, et al. Increased soluble urokinase plasminogen activator levels modulate monocyte function to promote atherosclerosis. *The Journal of clinical investigation* 2022; 132.
20. Goodchild TT, Li Z, Lefer DJ. Soluble urokinase plasminogen activator receptor: From biomarker to active participant in atherosclerosis and cardiovascular disease. *The Journal of Clinical Investigation* 2022; 132.
21. Zaghoul A, Al-Bukhari TA, Al-Pakistani HA, Shalaby M, Halawani SH, Bajuaifer N, et al. Soluble endothelial protein C receptor and high sensitivity C reactive protein levels as markers of endothelial dysfunction in patients with type 1 and type 2 diabetes mellitus: their role in the prediction of vascular complications. *Diabetes Res Clin Pract* 2014; 106: 597-604.
22. Maio R, Perticone M, Suraci E, Sciacqua A, Sesti G, Perticone F. Endothelial dysfunction and C-reactive protein predict the incidence of heart failure in hypertensive patients. *ESC Heart Failure* 2021; 8: 399-407.
23. Niknezhad N, Haghighatkah HR, Zargari O, Ghalamkarpour F, Younespour S, Niknejad N, et al. High-sensitivity C-reactive protein as a biomarker in detecting subclinical atherosclerosis in psoriasis. *Dermatol Ther* 2020; 33: e13628.
24. Swastini DA, Wiryantini IAD, Ariastuti NLP, Muliantara A. Atherosclerosis prediction with high sensitivity C-reactive protein (hs-CRP) and related risk factor in patient with dyslipidemia. *Open access Macedonian journal of medical sciences* 2019; 7: 3887.
25. Yu H, Rifai N. High-sensitivity C-reactive protein and atherosclerosis: from theory to therapy. *Clin Biochem* 2000; 33: 601-10.
26. Rezk A, Sarhan M, Elmoghl A. Highly-Sensitive C-reactive Protein Level and its Association with Intermediate and High Syntax Score in cases of Acute Coronary Syndrome. *The Egyptian Journal of Hospital Medicine* 2019; 75: 2064-70.
27. Karadeniz M, Duran M, Akyel A, Yarlıoğlu M, Öcek AH, Çelik İE, et al. High sensitive CRP level is associated with intermediate and high syntax score in patients with acute coronary syndrome. *Int Heart J* 2015; 56: 377-80.
28. Lyngbæk S, Marott JL, Møller DV, Christiansen M, Iversen KK, Clemmensen PM, et al. Usefulness of soluble urokinase plasminogen activator receptor to predict repeat myocardial infarction and mortality in patients with ST-segment elevation myocardial infarction undergoing primary percutaneous intervention. *The American journal of cardiology* 2012; 110: 1756-63.
29. Suberviola B, Castellanos-Ortega A, Ruiz Ruiz A, Lopez-Hoyos M, Santibañez M. Hospital mortality prognostication in sepsis using the new biomarkers suPAR and proADM in a single determination on ICU admission. *Intensive Care Med* 2013; 39: 1945-52.
30. Persson M, Engström G, Björkbacka H, Hedblad B. Soluble urokinase plasminogen activator receptor in plasma is associated with incidence of CVD. Results from the Malmö Diet and Cancer Study. *Atherosclerosis* 2012; 220: 502-5.
31. Eapen DJ, Manocha P, Ghasemzadeh N, Patel RS, Al Kassem H, Hammadah M, et al. Soluble urokinase plasminogen activator receptor level is an independent predictor of the presence and severity of coronary artery disease and of future adverse events. *Journal of the American heart association* 2014; 3: e001118.
32. Botha S, Fourie CM, Schutte R, Eugen-Olsen J, Schutte AE. Soluble urokinase plasminogen activator receptor and hypertension among black South Africans after 5 years. *Hypertens Res* 2015; 38: 439-44.
33. Tahhan AS, Hayek SS, Sandesara P, Hajjari J, Hammadah M, O'Neal WT, et al. Circulating soluble urokinase plasminogen activator receptor levels and peripheral arterial disease outcomes. *Atherosclerosis* 2017; 264: 108-14.
34. Persson M, Östling G, Smith G, Hamrefors V, Melander O, Hedblad B, et al. Soluble urokinase plasminogen activator receptor: a risk factor for carotid plaque, stroke, and coronary artery disease. *Stroke* 2014; 45: 18-23.
35. Yusuf S, Hawken S, Öunpuu S, Dans T, Avezum A, Lanas F, et al. Effect of potentially modifiable risk factors associated with myocardial infarction in 52 countries (the INTERHEART study): case-control study. *The lancet* 2004; 364: 937-52.
36. Pilote L, Karp I. GENESIS-PRAXY (GENdEr and Sex determinantS of cardiovascular disease: From bench to beyond-Premature Acute Coronary SYndrome). *Am Heart J* 2012; 163: 741-6. e2.
37. Spatz ES, Curry LA, Masoudi FA, Zhou S, Strait KM, Gross CP, et al. The variation in recovery: role of gender on outcomes of young AMI patients (VIRGO) classification system: a taxonomy for young women with acute myocardial infarction. *Circulation* 2015; 132: 1710-8.
38. Lichtman JH, Lorenze NP, D'Onofrio G, Spertus JA, Lindau ST, Morgan TM, et al. Variation in recovery: role of gender on outcomes of young AMI patients (VIRGO) study design. *Circ Cardiovasc Qual Outcomes* 2010; 3: 684-93.
39. Gao H, Wang Y, Shen A, Chen H, Li H. Acute myocardial infarction in young men under 50 years of age: clinical characteristics, treatment, and long-term prognosis. *Int J Gen Med* 2021: 9321-31.
40. Peters SA, Muntner P, Woodward M. Sex differences in the prevalence of, and trends in, cardiovascular risk factors, treatment, and control in the United States, 2001 to 2016. *Circulation* 2019; 139: 1025-35.

Research Article

FINITE ELEMENT ANALYSIS OF 3D TRANSIENT LINEAR TEMPERATURE CHANGES IN THE PERIODONTAL LIGAMENT DURING THERMOPLASTICIZED GUTTA-PERCHA OBTURATION TECHNIQUES

Emir ESİM¹, Özgür ER², Tuğrul ASLAN³, Ayşe Tuğba EMİNSOY AVCI^{3*},
Yakup ÜSTÜN³

¹Department of Mechatronics Engineering, Faculty of Engineering, Erciyes University, Kayseri, TURKIYE

²Department of Endodontics, Faculty of Dentistry, Dokuz Eylül University, Izmir, TURKIYE

³Department of Endodontics, Faculty of Dentistry, Erciyes University, Kayseri, TURKIYE

*Correspondence: dtaysetugbaeminsoy@gmail.com

ABSTRACT

Objective: This study used finite element analysis to evaluate temperature changes in the periodontal ligament due to various thermoplasticized gutta-percha obturation techniques.

Materials and Methods: Mandibular premolar models were created in SolidWorks software, simulating carrier-based obturation (CBO) and continuous wave of condensation with backfill obturation (CWC+BFO).

Results: Upon analyzing seven models, the study revealed that the CWC+BFO models with the highest temperature settings (Models 4 and 7) recorded the highest maximum temperatures, nearing 127°C. In contrast, the CBO model (Model 1) exhibited the lowest maximum temperature at 47.835°C. These temperatures were primarily measured at the apical region. The duration exceeding 10°C above body temperature was highest in Models 4 and 7. CBO caused a brief 10.835°C rise for 0.43 s, deemed safe, while all CWC+BFO techniques exceeded 10°C above body temperature, lasting up to 14.40 s. Lower temperature settings, particularly during CWC, are recommended for safer CWC+BFO application.

Conclusion: The CBO technique caused minimal temperature increase and appears safe. However, the CWC technique with BFO resulted in significantly higher temperatures, potentially harming the periodontal ligament. The authors recommend using lower temperatures with both techniques, especially with the CWC technique, and applying the BFO technique in multiple layers to minimize risks.

Keywords: Backfill obturation, carrier-based obturation, continuous wave of condensation, periodontal ligament, Ttemperature rise

Received: 01 September 2024
Revised: 19 October 2024
Accepted: 12 November 2024
Published: 22 December 2024



Copyright: © 2024 by the authors. Published Aydın Adnan Menderes University, Faculty of Medicine and Faculty of Dentistry. This is an open access article under the Creative Commons Attribution Non Commercial 4.0 International (CC BY-NC 4.0) License.

INTRODUCTION

Thermoplasticized filling techniques employ heat to plasticize the gutta-percha, achieving greater homogeneity and enhanced canal adaptation (1). However, warm gutta-percha obturation techniques have the disadvantage of causing high temperatures on the external root surface (2). Dental treatments that raise the temperature of the outer root surface beyond the established critical threshold of 10°C have the potential to cause damage to the periodontal tissues, as demonstrated in a classic study of implant dentistry conducted by Eriksson and Albrektsson. Their research, involving rabbit tibia exposed to temperatures exceeding 47°C, revealed fat cell replacement and irreversible bone resorption (3,4). According to another source, the upper limit of acceptable temperature is suggested to be 53°C (16°C increase) and surpassing this limit has been proposed to lead to bone necrosis potentially (5,6). Some previous studies mentioned that an increase of 10°C above body temperature for 1 minute is considered the safety threshold for periodontal tissues (7-9). It is widely accepted that limiting any temperature increase on the root surface to within 10°C is essential to prevent periodontal ligament and bone injury (4).

Carrier-based obturation (CBO) aims to reduce working time and ensure predictable thermoplasticization and gutta-percha flow using a specialized oven with precise temperature control. CBO simplifies the procedure by eliminating the need for instruments like spreaders, pluggers, heaters, and compactors in complex root canals (10). In the continuous wave of condensation (CWC) technique, a single master cone and a heat source are used to obturate the root canal by applying pressure from a heated plugger (11). When the CWC method is chosen as a canal filling technique, the limitations of the technique are usually overcome by using the backfill obturation (BFO) technique.

Various precise methodologies, including thermistor (12), infrared cameras (13), finite element analysis (FEA) (4,14,15), and thermocouples (13,16), have been used to quantify the heat produced within the root canal and its dispersion to the periodontium and bone. In the present investigation, FEA has been utilized to evaluate the alterations in temperature on the external root surface. FEA is a well-established technique for evaluating stress and temperature distribution in teeth under *in vitro* conditions (4,15). It is a faster and more reliable alternative to physical measurement devices for measuring temperature (14). The finite element

method offers significant advantages, as complex structures that are either difficult or costly to investigate experimentally can be readily modeled (15).

To the best of our knowledge, although there are a few studies in the existing literature (4,14,15) that evaluate the effect of warm gutta-percha obturation techniques on the tooth and surrounding tissues using finite element analysis, there is currently no study that compares CBO and CWC+BFO techniques using FEA. Therefore, this FEA study aimed to assess the temperature increases in the PDL generated by two different thermoplasticized gutta-percha obturation techniques (CBO and CWC+BFO) on a simulated mandibular premolar tooth model.

MATERIALS AND METHODS

Creation of the FEA models

A mandibular second premolar tooth with supporting tissues was created, and the geometric and anatomical dimensions of the models were established based on the existing literature (17). The surrounding tissues and bones were also included, and the enamel, dentin, periodontal ligament (PDL), cancellous bone, and cortical bone regions were identified. The assumed width of the periodontal ligament was 0.3 mm, while the alveolar bone was created 2 mm below the cemento-enamel junction. The thin cementum layer was neglected, and the hard tissue of the roots was assumed to be dentin only. The root canal's working length was supposed to be 12 mm. It had undergone root canal instrumentation before the filling procedure (taper: 6%, master apical file size: 40). All the mentioned processes and thermoplasticized gutta-percha (GP) canal fillings were performed using the SolidWorks software program (SolidWorks Corp, Waltham, MA, USA). The heating process applied to the GP layers was performed using ANSYS software (version 18.1; ANSYS, Canonsburg, PA).

Thermoplasticized GP techniques

Carrier-based obturation (CBO) technique (soft-core)

In this technique, it was assumed that a well-fitted Soft-Core (Kerr, Romulus, MI, USA) carrier-based gutta-percha obturator (Size #40) was heated in a Soft-Core oven (Kerr Endodontics) to a temperature of 110°C (18). The obturator cone was inserted into the root canal with apical pressure until reaching the apical stop, and this insertion process took one second. When the obturator cone had cooled, it was assumed that the handle and insertion pin were removed, and the gutta-percha was compacted vertically by hand plugger (Figure 1).

Continuous wave of condensation (CWC) technique followed by backfill obturation (BFO) (elements IC) technique (CWC+BFO)

In this study, the CWC technique is evaluated with two different BFO layering approaches, each with three different temperature settings. First, it was assumed that a well-fitted master gutta-percha cone (size: #40, taper: 6%) was placed into the root canal at the working length, and a heat plugger was advanced towards the apex by approximately 4 mm with CWC technique at 140°C, 200°C or 400°C using down pack unit of the Elements IC device (Kerr, Culver City, CA, USA), according to the description by Buchanan (11). It was assumed that this process took 3 seconds. Subsequently, the heat was turned off, and a 10-second wait was allowed for cooling. After this waiting period, an additional 1 second of heat was applied to the heating plugger to retrieve the cooled gutta-percha (at the temperature at which the down pack procedure was performed). The time elapsed while removing the heat plugger from the canal (1 second) and the condensation of apical GP into the canal using the appropriate Buchanan's hand plugger (5 seconds) was considered a total of 6 seconds. Then, the BFO procedure was initiated.

The first approach performed BFO in a single layer (SL). For this purpose, the remaining 8 mm portion of the canal was filled with flowable GP using the backfill unit of the Elements IC Device (Kerr) at 100°C, 170°C, or 230°C, and it was assumed that this process took 3 seconds. BFO was performed in two layers (TL) in the second approach. The 4 mm portion in the middle third of the canal was filled with flowable GP (1.5 seconds)

at 100°C, 170°C or 230°C. It was assumed that 4 seconds were required for condensing GP into the canal using hand pluggers. Subsequently, the 4 mm portion in the coronal third of the canal was filled with flowable GP (1.5 seconds) (at the temperature at which the first layer of BFO was performed) (Figure 1).

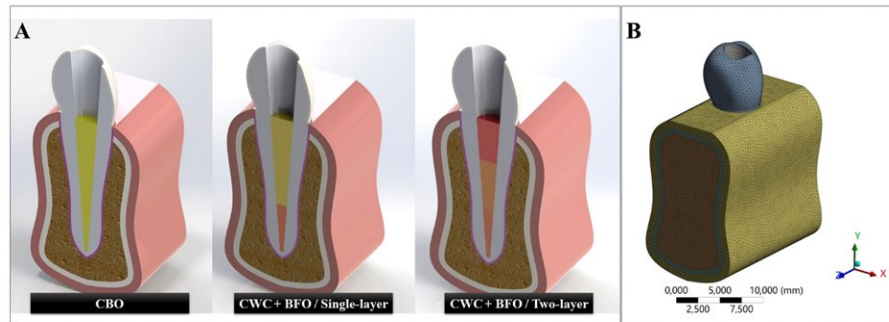


Figure 1. A) Finite element models of carrier-based obturation (CBO) and continuous wave of condensation technique followed by backfill obturation (CWC + BFO) techniques. **B)** A meshed model containing elements and nodes.

The preferred temperature settings were determined considering the default temperature setting (DefTS) (200°C/170°C) provided by the Elements IC device (Kerr) and the minimum and maximum down pack and backfill temperature settings (MinTS and MaxTS) (140°C/100°C, 400°C/230°C) that the device can offer (19).

Consequently, a total of seven models were assessed in this study:

Model 1 (M1): CBO at 110°C.

Model 2 (M2): CWC followed by single-layer BFO with minimum temperature settings (140°C-100°C).

Model 3 (M3): CWC followed by single-layer BFO with default temperature settings (200°C-170°C).

Model 4 (M4): CWC followed by single-layer BFO with maximum temperature settings (400°C-230°C).

Model 5 (M5): CWC followed by two-layer BFO with minimum temperature settings (140°C-100°C-100°C).

Model 6 (M6): CWC followed by two-layer BFO with default temperature settings (200°C-170°C-170°C).

Model 7 (M7): CWC followed by two-layer BFO with maximum temperature settings (400°C-230°C-230°C).

Root canal sealer was not used for obturation due to its negligible thickness and to minimize the number of variables, as in the study by Zhou et al (14). In all FEA models, temperature changes were monitored from the start of heat application until 13 seconds after the procedures were completed.

Geometric models were meshed with 10-node tetrahedral elements with quadratic displacement shape functions and 3 degrees of freedom per node, with an average size of 0.2 mm (Figure 1). The preferred

modeling type between different tissues/materials was the "bonded" interface. Additionally, the accuracy of the FEA models was validated through a convergence test. The CBO, CWC+BFO/SL, and CWC+BFO/TL finite element models were created using nodes and tetrahedral solid elements, with approximately 429,226 nodes and 242,906 elements, 455,795 nodes, and 247,999 elements, and 454,051 nodes and 247,406 elements, respectively. It was assumed that the materials under consideration were homogeneous and isotropic.

Table 1. The thermal properties of dental materials.

	Specific heat [J / (g . °C)]	Thermal Conductivity [J/(mm . s . °C)]	Density [g/mm ³]
Enamel	0.75366	9.2114E-04	2.9E-03
Dentin	1.17236	6.2805E-04	4E-03
Cancellous bone	1.84228	5.8618E-04	1.3E-03
Cortical bone	1.84228	5.8618E-04	1.3E-03
Periodontal ligament	4.817	5.8618E-04	1E-03
Gutta-percha	1.828	1.53E-04	0.97E-03

The thermal properties of the elements utilized in FEA were sourced from the existing literature (Table 1) (14,20,21). All dental components within the tooth model were assumed to have a standard body temperature of 37°C and the ambient air was set at a constant 22°C (14). Additionally, the process assumed transient heat conduction throughout the tooth elements. Furthermore, free heat convection from the tooth crown to the surrounding ambient air occurred during the process. For this purpose, a heat convection coefficient of $h = 6E - 06$ [J/(mm². s . °C)] was used (22). Temperature measurements started at the moment of applying the heat source. The temperature changes in the dentine and surrounding tissues were analyzed and recorded using ANSYS v.18.1 software (Canonsburg, PA, USA).

RESULTS

The durations from the initiation of root canal obturation to the onset of post-procedural cooling were 14, 37, and 41 seconds for the CBO, CWC+BFO/SL, and CWC+BFO/TL techniques, respectively. The time-dependent temperature changes in all tested FEA models are illustrated in Figure 2.

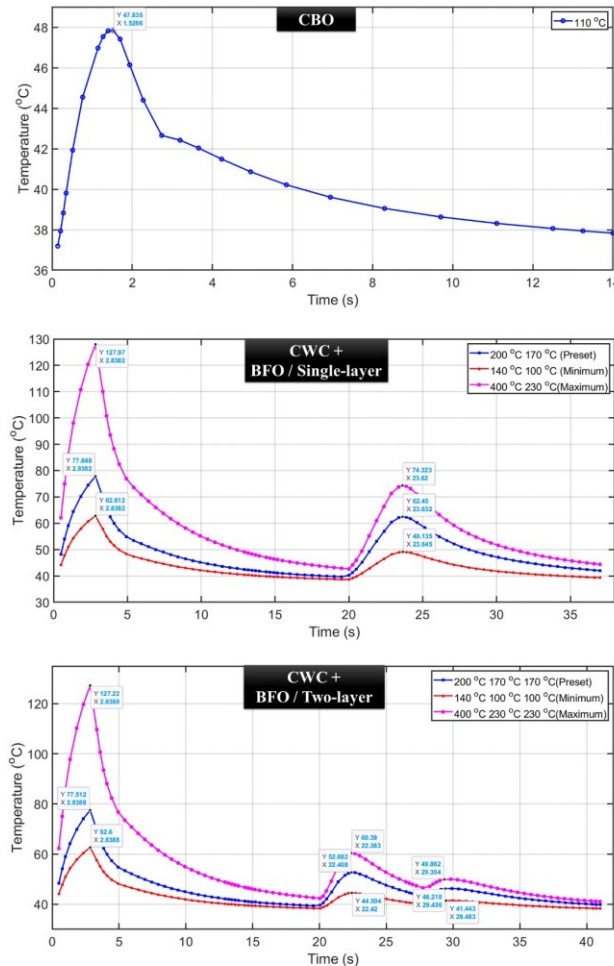


Figure 2. Time-dependent temperature changes in periodontal ligament tissue in each FEA model. The initial peaks in temperature represent the application of CWC and CBO techniques, while the second and third peaks indicate the application of the BFO technique for CWC + BFO models, respectively.

During the CWC technique (down pack), the highest maximum temperatures in the PDL were recorded in the apical regions of the M4 and M7 models (~127°C). For approximately 14 seconds, the temperature levels remained above 10°C higher than the body temperature. The M1 model exhibited the lowest maximum temperature of 47.835°C in the apical region of the PDL, surpassing a 10°C difference from the body temperature in less than 1 second (0.43 seconds). In the BFO application, the highest PDL temperature was observed in the M4 model (74.323°C), lasting 12.24 seconds, while the lowest maximum temperature was detected in the M5 model (44.504°C), which never exceeded 10°C above the body temperature; and these

changes were observed in the middle thirds of the roots. The distributions of maximum temperatures induced by various stages of the tested warm gutta-percha obturation techniques in the PDL are illustrated in Figures 3 and 4.

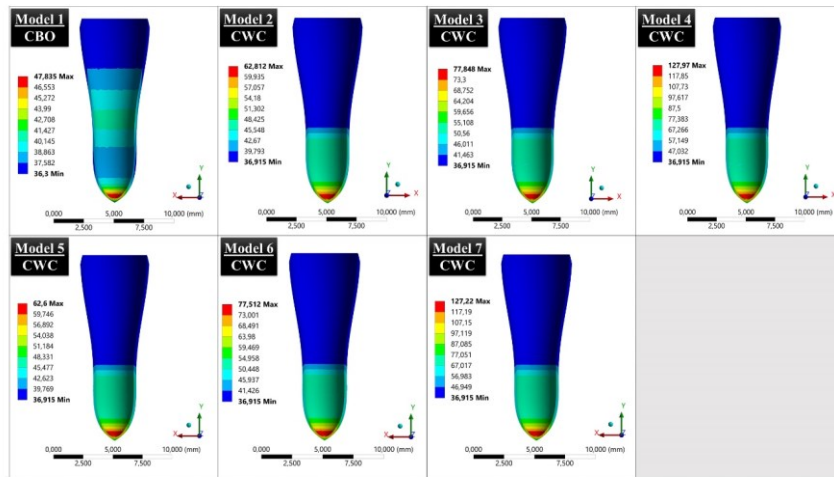


Figure 3. The maximum temperatures observed in periodontal ligament tissue in the FEA models.

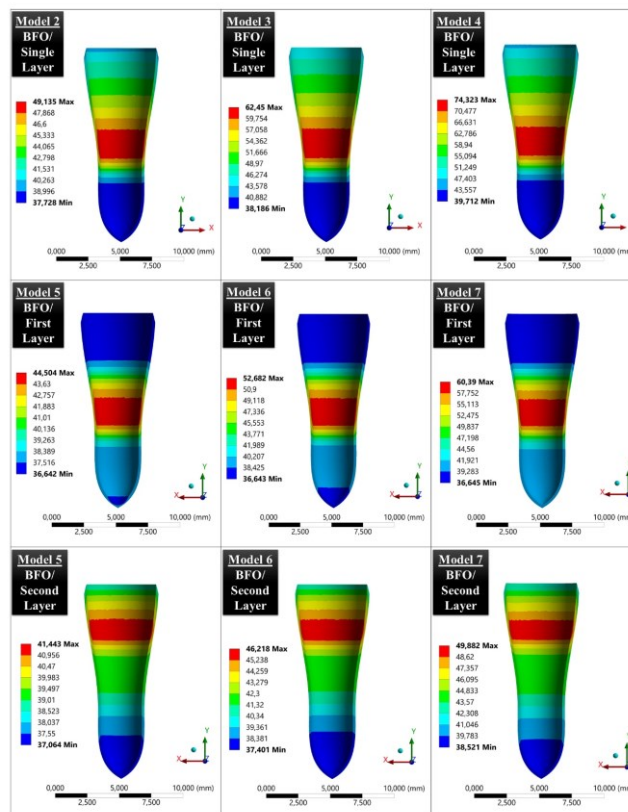


Figure 4. Maximum temperatures observed in BFO applications in the FEA models from Model 2 to Model 7.

In addition, temperature distributions 13 seconds after the completion of the obturation process in all models are shown in Figure 5.

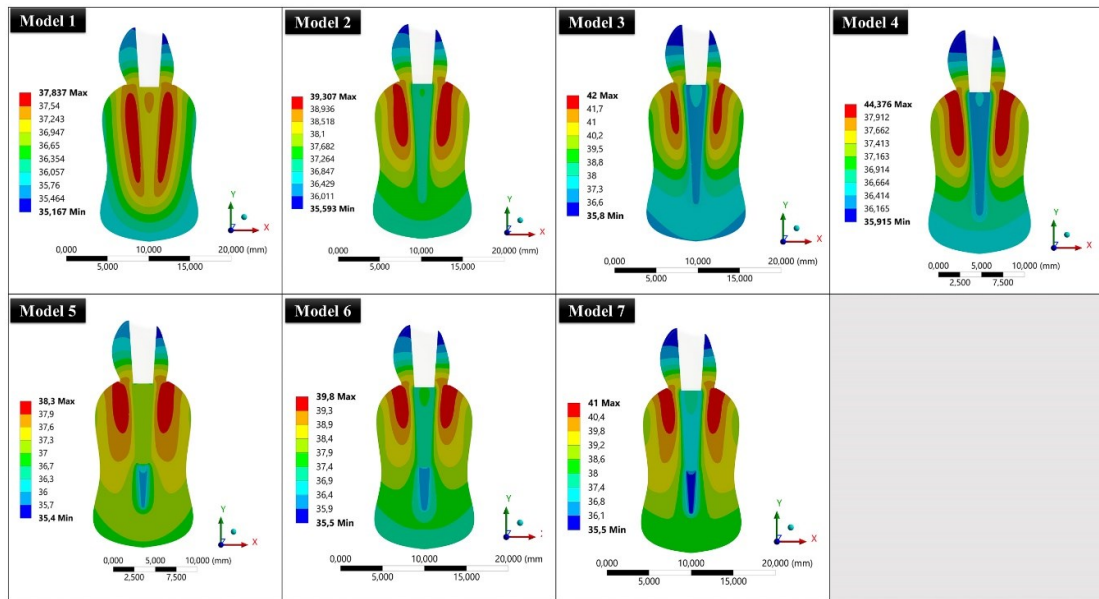


Figure 5. The maximum temperatures detected 13 s after the completion of thermoplasticized gutta-percha obturation procedures in the FEA models.

After a cooling period of 13 seconds, no temperature levels capable of causing damage to the PDL were observed in any model. Data regarding temperature changes and time parameters for all experimental models are provided in Tables 2 and 3.

Table 2. The maximum temperatures detected in the periodontal ligament, the maximum temperature increase in the periodontal ligament relative to body temperature, and the maximum temperature after cooling for 13 s in the tested FEA models.

	Maximum temperatures (°C)	Maximum temperature increase according to body temperature (°C)	Maximum temperatures after cooling (°C)
Model 1	47.835	10.835	37.837
Model 2	62.812	25.812	39.307
Model 3	77.79	40.79	42
Model 4	127.97	90.97	44.376
Model 5	62.6	25.6	38.3
Model 6	77.512	40.512	39.8
Model 7	127.22	90.22	41

Table 3. The durations (seconds) above the increase of 10°C.

	<i>Obturation Phase</i>			
	Carrier-Based Obturation (s)	Continuous wave of Condensation (s)	Backfill Obturation (First Layer) (s)	Backfill Obturation (Second Layer) (s)
Model 1	0.43	-	-	-
Model 2	-	4.68	2.24	-
Model 3	-	8.43	8.74	-
Model 4	-	14.40	12.24	-
Model 5	-	4.68	-	-
Model 6	-	8.44	3.58	-
Model 7	-	13.94	6.37	4.80

DISCUSSION

Premolars were selected to ensure compatibility with other studies in the literature, facilitating result comparison (2). Additionally, mandibular premolars offer several advantages, such as a more rounded root morphology, consistent dentin thickness throughout most of the root, and generally curvature-free roots. In our study, the Soft-Core (Kerr) system was used as a reference to replicate the CBO technique. Following the manufacturer's instructions, the Soft-Core (Kerr) system operates at 110°C (18), thus, our simulation for this model was conducted at 110°C. For the CWC+BFO technique, the wireless Elements IC device (Kerr), currently widely used in clinical practice, was chosen as a reference. This device is being evaluated because it allows a broad range of temperature adjustments in the CWC and BFO stages. In this regard, the minimum temperatures provided by the device (140°C for CWC, 100°C for BFO), the preset temperatures that come with the device (200°C for CWC, 170°C for BFO), and the maximum temperatures it can achieve (400°C for CWC, 230°C for BFO) were included in this study. Notably, the maximum temperatures offered by this device align with a temperature range that has not been previously explored in the literature.

According to the findings of our study, the highest temperatures in the PDL were detected at the apical third of the roots in all tested models (Figure 3). As the distance from the apex of the root to the coronal third of the root increased, the maximum temperatures in the PDL decreased gradually (Figure 4). One of the reasons for this is that the root narrows. The remaining dentin thickness decreases as the apex of the root is approached (23). Thus, the applied heat can more readily be emitted to the PDL, inducing undesirable temperature increases in these regions. Lipski et al. reported that the temperature rise on the root surface

depends on the remaining radicular dentin, and they mentioned that the temperature elevation was three times higher on mandibular incisors with thin root walls compared to maxillary incisors (24). McCullagh et al. stated that the most elevated temperatures recorded on the external root surface are associated with the final position reached by the tip of the heat carrier in the root canal (13). The findings of these studies are consistent with our findings. In accordance with the laws of thermodynamics, all systems in nature strive to reach equilibrium, leading to the occurrence of heat transfer (25). When there is a temperature difference, heat transfer takes place from the warmer environment to the cooler one to achieve thermal equilibrium. In this study, based on these laws, cooling begins from the outermost layer and progresses toward the warmer environment.

When Figure 3 is examined, the most noticeable observation is that CWC application causes higher temperature increases in the PDL than CBO and BFO applications. Among the CWC applications, the most elevated maximum temperatures were observed in models M4 (127.97°C) and M7 (127.22°C), while the lowest maximum temperatures were obtained in models M2 (62.812°C) and M5 (62.6°C). The default settings determined by the device manufacturer resulted in a temperature increase between the temperature increases caused by these minimum and maximum temperature settings (77.79°C for M3, 77.512°C for M6). Consequently, the heat intensity applied during the CWC phase appears to be a determining factor in the temperature increase in the PDL. The CBO technique, on the other hand, caused a maximum temperature of 47.835°C, which is approximately at the threshold of potential harm to the PDL. The reason CBO causes lower temperature increases than CWC applications may be due to the lower applied temperature (110°C) and the shorter application time (1 second) compared to the 3-second application time of CWC. Ulusoy et al. examined temperature changes during root canal filling, comparing techniques with and without simulated internal resorption. They assessed injectable gutta-percha (Obtura II, 160°C), carrier-based (Soft-Core, 110°C), and continuous wave of condensation (System B, 200°C). High-temperature methods (System B and Obtura II) exceeded the critical 10°C threshold with internal resorption, while the carrier-based (Soft-Core) technique remained within safe limits regardless of resorption (2). Our study findings were also consistent with their study.

When reviewing relevant literature, Venturi et al. used thermocouples to examine temperature variations within gutta-percha during vertical compaction using a System-B Heat Source heated to 250°C. Their findings indicated that the System-B Heat Source could be safely employed for vertical compaction, as it did not substantially elevate gutta-percha temperature and posed no risk to periradicular tissues (16). However, in our study, particularly in CWC techniques with higher temperature settings, we observed potentially harmful temperature increases in the periodontal ligament. These discrepancies may be attributed to differences in experimental conditions, such as the types of teeth used, dentin thickness, and methodological variations. Er et al. assessed the temperature variations in a maxillary canine using finite element analysis on the adjacent periodontal tissues and bones during the continuous wave of condensation technique (System-B). The maximum temperature observed in the periodontal ligament was 43.5°C. The continuous wave of condensation technique did not generate temperature levels considered potentially harmful (15). While our study identified higher temperatures, especially in the apical region, when the CWC+BFO technique was used. These discrepancies may result from differences in tooth morphology and the thermal properties of tissues modeled in the studies. On the other hand, McCullagh et al. discovered an average temperature increase of 13.9°C on the root surface when employing the continuous wave of condensation technique with the System-B heat carrier system for root canal obturation (13). Which is consistent with our findings of elevated temperatures in the CWC models. Using finite element analysis, Cen et al. compared two dental filling techniques (System-B and Obtura II). They found that without blood flow, both techniques could reach potentially elevated temperatures (50-52°C) in a molar tooth. However, with simulated blood flow, peak temperatures dropped below 47°C, suggesting blood effectively cools the tooth during both procedures (4). While our study did not simulate blood flow, the observed temperature increases align with their findings.

BFO applications also led to harmful temperature levels (up to 74.323°C), mainly when used at higher temperatures. The difference of BFO applications from CBO and CWC applications lies in their impact on the middle and coronal thirds of the root rather than the apical third. Before initiating the BFO application, there is some cooling opportunity for the apical PDL, and the newly applied backfill layers mainly affect the PDL, corresponding to the regions where they are used. All CWC+BFO/SL models exhibited temperatures higher

than the maximum observed in CBO during the BFO phases. In the two-layer backfill models, relatively lower maximum temperatures were observed in both backfill layers of CWC+BFO/TL MinTS and the second backfill layer of CWC+BFO/TL DefTS compared to those detected in CBO. Our findings regarding the BFO technique are consistent with the results reported by Ulusoy et al., who compared the injectable Obtura II system with Soft-Core and System-B and said that this system could lead to elevated temperatures in the PDL (2).

Additionally, it is observed that the maximum temperature values in models with a two-layer backfill are lower than those in models with a single-layer. The reason for this could be the application of hot GP for shorter durations and smaller masses, allowing for a cooling period by being exposed to room temperature between the two layers. Zhou et al. used finite element analysis to measure temperature increases in the periodontal ligament and apical gutta-percha in a mandibular molar tooth model. The apical thirds of the canals were filled using a continuous wave of condensation. The remainder was backfilled with injected gutta-percha in 2 segments (using Obtura II), and during the obturation procedure using Obtura II, the temperature at the periodontal ligament remained below 47°C (14). Another aspect related to BFO is the observation of maximum temperatures being lower in BFO applications in each model compared to CWC. Possible reasons for this situation include the application of less heat in BFO than in CWC and a thicker dentin layer in the teeth's middle and coronal root thirds compared to the apical third.

The carrier-based obturation technique caused a maximum temperature rise (10.835°C) near the threshold of potential harm for 0.43 seconds. Additionally, all CWC applications resulted in excessive temperature increases (up to 90.97°C), surpassing 10°C above body temperature, lasting up to 14.40 seconds. Among the BFO applications, the CWC+BFO/SL MaxTS model caused a temperature rise of 37.323°C above body temperature, lasting 12.24 seconds. In the CWC+BFO/TL MinTS model, hazardous temperatures were never reached during the BFO stage. In all other CWC+BFO models except the CWC+BFO/TL MaxTS model, dangerous temperatures did not occur during the second layer backfill process. It is essential to avoid prolonged exposure to temperatures above 47°C, which can harm teeth. Previous studies have suggested that an increase of 10°C above body temperature for 1 minute is considered the safety threshold for periodontal tissues (7–9). In light of these data, among all tested models, only the M1 model (CBO) appears to have the

potential to be safe for the periodontal ligament (PDL), as it marginally and briefly exceeded the harmful temperature limit. This finding is per the study of Ulusoy et al., further supporting the safety profile of the carrier-based obturation technique (2).

In thermoplasticized obturation techniques, as the duration of heat application increases, the temperature also rises in the root and surrounding tissues. Lipski and Wozniak used the thermoplasticized core techniques (Thermafil system) for root canal obturation and employed the continuous wave of condensation with System B heat source for 5- and 8-seconds during retreatment procedures. They observed temperatures ranging from 26.7°C to 46.0°C, potentially causing harm to the periodontal tissues (26). Zhou et al. investigated continuous wave of condensation filling in mandibular molars for 3 and 4 seconds. They found that, when filling for 3 seconds, the periodontal ligament temperature reached 46.9°C, and extending the activation time to 4 seconds caused a temperature increase of more than 10°C. In conclusion, they advised against exceeding the 3-second activation time (14). Therefore, the duration of heat application did not exceed 3 seconds in this study.

A monitoring period of 13 seconds was established following the completion of root canal filling procedures in the tested finite element models, as the models exhibited a trend of returning to non-harmful temperatures after 10 seconds. Temperature changes in the models were tracked until the end of this monitoring period. After this cooling period, maximum temperatures in the PDL were measured, and no destructive elevated temperatures were observed in the PDL and bone in any of the models (Figure 5).

Finally, the maximum temperature values observed in our study are generally higher than other studies in the literature (4,14,15). This may be attributed to methodological differences such as the teeth used in the studies, differences in dentin thickness, and variations in operator application.

One of the limitations of this study is the standardization of the working length of the teeth to 12 mm for the finite element analysis (FEA). This was done to ensure consistency across the models and to minimize variability in temperature distribution due to root length differences. However, in clinical practice, root lengths vary, and this variation may influence the heat transmission to the periodontal ligament (PDL) and surrounding tissues. In teeth with shorter roots, the proximity of the heat source to the apical region and

surrounding tissues may lead to faster heat transmission, potentially increasing the risk of thermal injury. Conversely, in teeth with longer roots, the greater distance between the heat source and the PDL may act as an insulator, reducing the amount of heat transmitted to the surrounding tissues. These factors could impact the safety thresholds of the tested thermoplasticized obturation techniques. Future studies should consider evaluating the effects of these techniques on teeth with varying root lengths to provide a more comprehensive understanding of temperature dynamics in clinical conditions.

The cementum layer was omitted in our study to simplify the model and reduce computational complexity, focusing primarily on the heat transfer within the root and surrounding tissues. Given the thinness and low thermal conductivity of the cementum, we believed its impact on temperature distribution in the periodontal ligament (PDL) would be minimal. Cement layer had not been modeled in previous studies in the literature (4,14,27). However, we recognize that in clinical settings, the cementum may act as an insulator, slightly affecting heat dissipation.

CONCLUSION

This study compared two warm gutta-percha obturation techniques using FEA method. The CBO technique remained within safe temperature limits, with only a brief and minimal temperature rise of 10.835°C above body temperature, making it a safer option. In the CWC+BFO technique, models with higher temperature settings (200°C-400°C for CWC and 170°C-230°C for BFO) exceeded the critical 10°C temperature rise, lasting up to 14.40 seconds, which could pose a risk to the PDL. The two-layer backfill (TL) approach at minimum temperature settings (140°C/100°C for CWC+BFO) was found to be the safest variant of the CWC+BFO technique, with temperatures staying within safer limits. The authors recommend using lower temperatures with both techniques, especially with the continuous wave technique, and applying the backfilling technique in multiple layers to minimize risks.

Acknowledgments

The authors thank Professor Eugene Steele (Erciyes University, Kayseri, TURKIYE) for his valuable assistance in editing this paper's English. His insights and suggestions helped improve the manuscript's clarity and accuracy.

Authorship contributions

Conceptualization: Özgür Er; Tuğrul Aslan; Methodology: Tuğrul Aslan, Emir Esim; Validation: Emir Esim; Formal analysis: Emir Esim; Data curation: Emir Esim; Writing—original draft preparation: Tuğrul Aslan; Ayşe Tuğba Eminsoy Avcı; Yakup Üstün Writing—review and editing: Tuğrul Aslan; Yakup Üstün; Ayşe Tuğba Eminsoy Avcı

Declaration of competing interest

The authors declare no competing interests.

Data availability statement

The datasets used and/or analyzed during the current study are available from the corresponding author upon reasonable request.

Ethics

This finite element analysis study did not involve the use of human or animal subjects. Therefore, no ethical approval was required

Funding

This research did not receive any specific grant from funding agencies in the public, commercial, or not-for-profit sectors.

REFERENCES

1. Buchanan LS. The continuous wave of condensation technique: a convergence of conceptual and procedural advances in obturation. *Dent today*. 1994;13(10):80, 82, 84–5.
2. Ulusoy Ö, Yılmazoğlu MZ, Görgül G. Effect of several thermoplastic canal filling techniques on surface temperature rise on roots with simulated internal resorption cavities: an infrared thermographic analysis. *International Endodontic Journal*. 2015;48(2):171–6.
3. Eriksson AR, Albrektsson T. Temperature threshold levels for heat-induced bone tissue injury: A vital-microscopic study in the rabbit. *J Prosthet Dent*. 1983;50(1):101–7.
4. Cen R, Wang R, Cheung GSP. Periodontal Blood Flow Protects the Alveolar Bone from Thermal Injury during Thermoplasticized Obturation: A Finite Element Analysis Study. *J Endod*. 2018;44(1):139–44.
5. Kim S, Trowbridge H, Soda H (2002) Pulpul reaction to caries and dental procedures. In: Cohen S, Burns RC (eds) *Pathways of the pulp*. Mosby, Missouri, p 590.
6. Spangberg L (2002) Instruments, materials and devices. In: Cohen S, Burns RC (eds) *Pathways of the pulp*. Mosby, Missouri, p 565.
7. Ramsköld LO, Fong CD, Strömberg T. Thermal effects and antibacterial properties of energy levels required to sterilize stained root canals with an Nd:YAG laser. *J Endod*. 1997;23(2):96–100.

8. ANIĆ I, TACHIBANA H, MASUMOTO K, QI P. Permeability, morphologic and temperature changes of canal dentine walls induced by Nd: YAG, CO₂ and argon lasers. *Int Endod J.* 1996;29(1):13–22.
9. Gutknecht N, Franzen R, Meister J, Vanweersch L, Mir M. Temperature evolution on human teeth root surface after diode laser assisted endodontic treatment. *Lasers Méd Sci.* 2005;20(2):99–103.
10. Gambarini G, Piasecki L, Schianchi G, Nardo D, Miccoli G, Sudani D, et al. In vitro evaluation of carrier based obturation technique: a CBCT study. *Annali di stomatologia.* 2016;7(1–2):11–5.
11. Buchanan LS. The continuous wave of obturation technique: “centered” condensation of warm gutta percha in 12 seconds. *Dent today.* 1996;15(1):60–2, 64–7.
12. Gutmann JL, Rakusin H, Powe R, Bowles WH. Evaluation of heat transfer during root canal obturation with thermoplasticized gutta-percha. Part II. In vivo response to heat levels generated. *J Endod.* 1987;13(9):441–8.
13. Cullagh JJPM, Setchell DJ, Gulabivala K, Hussey DL, Biagioni P, Lamey P -J., et al. A comparison of thermocouple and infrared thermographic analysis of temperature rise on the root surface during the continuous wave of condensation technique. *Int Endod J.* 2000;33(4):326–32.
14. Zhou X, Chen Y, Wei X, Liu L, Zhang F, Shi Y, et al. Heat transfers to periodontal tissues and gutta-percha during thermoplasticized root canal obturation in a finite element analysis model. *Oral Surgery, Oral Medicine, Oral Pathology, Oral Radiology, and Endodontology.* 2010;110(2):257–63.
15. Er Ö, Yaman SD, Hasan M. Finite element analysis of the effects of thermal obturation in maxillary canine teeth. *Oral Surgery, Oral Medicine, Oral Pathology, Oral Radiology, and Endodontology.* 2007;104(2):277–86.
16. Venturi M, Pasquantonio G, Falconi M, Breschi L. Temperature change within gutta-percha induced by the System-B Heat Source. *Int Endod J.* 2002;35(9):740–6.
17. Jr. MMA, Nelson S. *Wheeler’s dental anatomy, physiology, and occlusion.* 8th ed. St Louis, MO: Elsevier Saunders, St. Louis, Missouri; 2003. 154 p.
18. User Manual: Soft-Core® Endodontic Heater and Obturators [Internet]. [cited 2023 Sep 11]. Available from: <https://kavokerr.widen.net/content/cc2nsyq8gw/original/softcore-ifu-eng.pdf?u=18sth1&download=true>
19. Instructions For Use: Elements™ IC Obturation System [Internet]. [cited 2023 Sep 11]. Available from: <https://embed.widencdn.net/download/kavokerr/h6dfxqdx5/elements-IC-IFU.pdf?u=18sth1>
20. Moroi HH, Okimoto K, Moroi R, Terada Y. Numeric approach to the biomechanical analysis of thermal effects in coated implants. *Int J Prosthodont.* 1993;6(6):564–72.
21. Brandrup J, Immergut EH, editors. *Polymer handbook.* 3rd ed. New York: Wiley; 1989.
22. Holman JP, editor. *Heat transfer.* 4th ed. New York: McGrawHill; 1976. p. 253.
23. Lipski M. Root surface temperature rises during root canal obturation, in vitro, by the continuous wave of condensation technique using System B HeatSource. *Oral Surgery, Oral Medicine, Oral Pathology, Oral Radiology, and Endodontology.* 2005;99(4):505–10.
24. Lipski M. In Vitro Infrared Thermographic Assessment of Root Surface Temperatures Generated by High-Temperature Thermoplasticized Injectable Gutta-Percha Obturation Technique. *Journal of Endodontics.* 2006;32(5):438–41.
25. Niu, L., Dong, S. J., Kong, T. T., Wang, R., Zou, R., & Liu, Q. D. Heat Transfer Behavior Across The Dentino-Enamel Junction In The Human Tooth. *PloS one.* 2016. 11(9), e0158233.
26. Lipski M, Woźniak K. In Vitro Infrared Thermographic Assessment of Root Surface Temperature Rises During Thermafil Retreatment Using System B. *J Endod.* 2003;29(6):413–5.
27. Oskui, I. Z., Ashtiani, M. N., Hashemi, A., & Jafarzadeh, H. Thermal analysis of the intact mandibular premolar: a finite element analysis. *International Endodontic Journal,* 2013; 46(9), 841-846.

Research Article

DIFFERENTIALLY REGULATED MIRNAS BY TWIST1 IN TRIPLE NEGATIVE BREAST CANCER CELLS

 Bahadır ÖZTÜRK¹,  Akın KOL¹,  Suray PEHLIVANOĞLU²,  Fatma ŞENGÜL BAĞ^{3*}

¹ Department of Medical Biochemistry, Faculty of Medicine, Selçuk University, Konya, TURKIYE

² Department of Molecular Biology and Genetics, Faculty of Science, Necmettin Erbakan University, Konya, TURKIYE

³ Department of Biochemistry, Faculty of Pharmacy, Adiyaman University, Adiyaman TURKIYE

*Correspondence: fsengul@adiyaman.edu.tr

ABSTRACT

Objective: Breast cancer (BC) is the most common cancer in women and the second leading cause of cancer-related deaths. MicroRNAs (miRNAs) are short, non-coding RNA molecules that regulate gene expression post-transcriptionally and play a central role in the dysregulation of gene expression associated with carcinogenesis, cancer cell proliferation and metastasis. Twist1 is a transcription factor that binds to E-box motifs and controls the transcriptional activity of genes as a positive or negative regulator decisive in the cellular mechanisms. Accordingly, Twist1 also regulates the expression of miRNAs that are associated with cancer progression. In the present study, we aimed to investigate the expression changes of possible miRNAs directly regulated by Twist1 in triple negative breast cancer (TNBC) MDA-MB-231 cells.

Materials and Methods: In this study, a total of 43 miRNA genes were evaluated that predicted might be associated with TNBC. To determine the Twist1-targeted miRNA genes, endogenous high-level Twist1 expression was suppressed through the antisense oligonucleotides in MDA-MB-231 TNBC cells. Differential miRNA expression levels were analyzed using quantitative real-time PCR (qRT-PCR) in Twist1-suppressed cells compared to the control group.

Results: Twist1 suppression resulted in increased expression of miR-1-1 and miR-210-3p, while the expression of miR-193b-3p, miR-181b-5p, and miR-148a-3p decreased.

Conclusion: This study shows that the expression levels of certain miRNAs linked to invasion, metastasis, and apoptosis are controlled by Twist1 in TNBC cells.

Keywords: Breast cancer, MDA-MB-231, microRNA, Twist1

Received: 13 October 2024
Revised: 15 November 2024
Accepted: 19 November 2024
Published: 22 December 2024



Copyright: © 2024 by the authors. Published Aydın Adnan Menderes University, Faculty of Medicine and Faculty of Dentistry. This is an open access article under the Creative Commons Attribution Non Commercial 4.0 International (CC BY-NC 4.0) License.

INTRODUCTION

According to global statistics, breast cancer (BC) is identified as the most frequently detected cancer worldwide, affecting individuals across all genders (1). Clinically, this type of cancer is divided into different subtypes based on the status of specific receptors: the human epidermal growth factor receptor 2 (HER2), which promotes aggressive tumor growth; the progesterone receptor (PR), associated with hormone-driven tumor development; and the estrogen receptor (ER), a key factor in hormone-dependent BC (2). The major subtypes include luminal A, which is generally hormone receptor-positive with a slower growth rate, luminal B, known for its higher proliferation rate and possible HER2 positivity, and triple-negative breast cancer (TNBC), which lacks hormone receptor expression. TNBC constitutes approximately 15-20% of total BC diagnoses and is marked by its aggressive behavior and poor prognosis (3). MDA-MB-231, which is derived from human breast adenocarcinoma, is an epithelial cell type that is classified as TNBC because of the absence of HER2, PR and PR expression on its cell membrane (4). The identification of breast cancer-specific miRNAs and the determination of their mechanisms of action in cellular signaling pathways are important for cancer diagnosis and treatment. The effects on miRNA profile in cancer cells are being studied and their importance is increasing day by day (5, 6).

MicroRNAs (miRNAs) are short, non-coding RNA sequences that exert pivotal functions in post-transcriptional gene regulation by modulating the degradation and translational efficiency of specific target messenger RNAs (7). These miRNAs participate in numerous biological functions, including development, cell differentiation, growth, and programmed cell death, acting as crucial modulators of gene activity (8). In healthy cells, miRNAs are tightly controlled to maintain homeostasis (9), while dysregulation of miRNAs occurs in many diseases, including cancer (10). Studies indicate that miRNA dysregulation contributes to cancer development and progression, with miRNAs acting either as oncogenes or tumor suppressors, influencing different stages of tumorigenesis. In the field of cancer gene therapy, focusing on particular miRNAs has demonstrated potential as an effective approach in the management, detection, and prediction of disease outcomes (11).

Twist1, a transcription factor, has a significant function in several molecular pathways, especially contributing to cancer advancement. Twist1 participates in tumor formation, development, spread, and epithelial-mesenchymal transition (EMT) across different cancer types, including lung, breast, gastric, and prostate cancer (12). In addition, Twist1 has been identified as a master regulator in BC progression by controlling multiple genes in different metabolic pathways (13).

Previous research has examined how miRNAs contribute to controlling both metastasis and angiogenesis via the Twist1 gene in MDA-MB-231 TNBC cells. Nevertheless, the miRNA profile related to the antisense inhibition of Twist1 gene expression remains unexplored. This study seeks to analyze the alterations in miRNA expression levels in MDA-MB-231 TNBC cells after Twist1 gene activity is suppressed using an antisense approach.

MATERIALS AND METHODS

Cell culture and transfection

The TNBC cell line derived from humans, MDA-MB-231 (American Type Culture Collection, HTB-26), was preserved in Dulbecco's Modified Eagle Medium (DMEM) (Gibco™, catalog #11965092) supplemented with 10% fetal bovine serum (FBS), 1% penicillin-streptomycin, and L-glutamine. The cell line was cultivated at 37 °C in a humidified environment with 5% carbon dioxide. Before cell transfection, cells were plated one day earlier to achieve approximately 70% confluence.

A transfection reagent (Lipofectamine 2000, catalog no. 11668-027, purchased from Thermo Fisher Scientific, USA) was used for transfection of Twist1AS-pcDNA3.1 vector cloned with Twist1 anti-sense complementary DNA (cDNA), and pcDNA3.1 empty vector as a control into MDA-MB 231 TNBC cells. Following 72 hours post-transfection, cell selection was carried out using G-418 at a concentration of 0.4 mg/mL (Invitrogen #10131) until the wells reached 80-90% confluency. Then, the RNA samples of each well were obtained and quantified by Nanodrop.

miRNA Isolation

Total RNA, including miRNAs, was extracted and purified from control and Twist1-silenced cells using the RTA Total miRNA Isolation Kit (lot: AR2264118) according to the manufacturer's instructions. Briefly, 350 µl of lysis solution and 20 µl of proteinase K were added to each cell sample, followed by incubation in an IKA dry block heater at 60°C for 30 minutes. Afterward, 350 µl of binding solution was added, and the mixture was transferred to spin columns and centrifuged at 11,000 rpm for 1 minute. The washing step involved adding 500 µl of wash solution, followed by centrifugation at 10,000 rpm for 1 minute.

For elution, 40 µl of pre-warmed elution solution (65°C) was applied to the center of the miRNA spin column and incubated at room temperature (20-25°C) for 1-3 minutes. Eluted miRNA was collected by centrifugation at 8,000 rpm for 1 minute and stored at -20°C. Relative miRNA expression was evaluated using the comparative CT (Δ CT) method, with SNORD44 as a reference gene.

Quantitative Real-Time PCR (qRT-PCR)

qRT-PCR assays were conducted using a BrightGreen 2X Qrt-PCR Master Mix on a LightCycler® 96 real-time PCR system. Each reaction mixture (20 µl) contained 5 µl of 2X Master Mix, 0.5 µl of forward and reverse primers (300 nM), 1.75 µl of cDNA, and 2.25 µl of nuclease-free water.

The qRT-PCR program included an initial denaturation at 95°C for 10 minutes, followed by 40 cycles of denaturation at 95°C for 10 seconds, annealing at 60°C for 15 seconds, and elongation at 72°C for 30 seconds. A melting curve analysis was performed to ensure the specificity of the amplification, increasing the temperature from 50°C to 95°C in 0.5°C increments every 30 seconds. The primers for Twist1 were; Forward: CGA CGA CAG CCT GAG CAA CA, Reverse: TGC AGC TCC TCG TAC GAC TG. The aim of this study was to compare miRNA expression levels between control cells and cells transfected with the Twist1 antisense clone (Twist1AS-pcDNA3.1 vector). miRNA analysis was performed in duplicate for both groups, with SNORD68 as the internal control for the 43 miRNAs analyzed.

Bioinformatics Analysis Using DIANA Tools

To identify the miRNAs potentially regulated by Twist1, bioinformatics analyses were performed using the DIANA Tools platform (<http://diana.imis.athena-innovation.gr>). Specifically, the DIANA-microT-CDS tool was used to predict the interactions between miRNAs and their potential target genes, focusing on regulatory elements such as E-box motifs within the 3' UTR regions. Additionally, the DIANA-miRPath v3.0 tool was employed to evaluate the impact of these miRNAs on biological pathways, using KEGG (Kyoto Encyclopedia of Genes and Genomes) pathway analysis. These analyses facilitated the identification of 43 miRNAs that may play significant roles in TNBC biology.

Statistical Analysis

Data are expressed as means \pm standard errors. Statistical analysis was performed using Student's t-test in GraphPad Prism 8 software. The significance of the results was determined at a probability level of $p < 0.05$. Each experiment was conducted in triplicate across three independent experiments.

RESULTS

To investigate whether Twist1 drives miRNA expression under normal physiological conditions, a cloned Twist1 antisense oligonucleotide was utilized. Initially, an empty vector (pcDNA3.1) was used as a control, and the Twist1-AS vector was transfected into cells known to express high levels of endogenous Twist1. The transfected cells were then selected using G-418-containing medium. Subsequently, the cells were analyzed for endogenous Twist1 expression, and their morphology was examined using an inverted microscope.

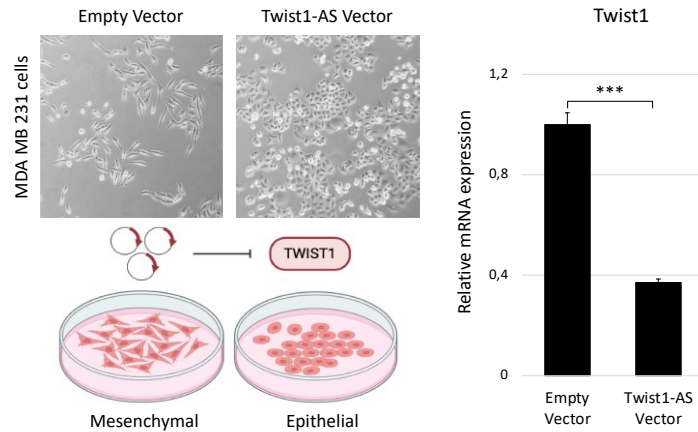


Figure 1 The Twist1 suppression level of Twist1-AS vector transfected cells compared to control cells (empty vector) resulted in the loss of their original mesenchymal morphology and transformation into epithelial morphology. (** $p < 0.001$)

Cells with decreased Twist1 expression (a 2.7-fold reduction) due to antisense oligonucleotides lost their mesenchymal appearance and adopted an epithelial morphology. This finding aligns with the widely recognized role of Twist1 as a crucial regulator of epithelial-mesenchymal transition (EMT).

Table 1. CT values of up-regulated or down-regulated miRNAs in Twist1-silenced cells compared to the control, with a statistically significant difference ($p < 0.05$).

	CT average (control group)	CT reference average (control group)	Δ CT average (control group)	CT average (transfection group)	CT reference average (transfection group)	Δ CT average (transfection group)	$-\Delta\Delta$ CT
hsa-miR-1-1	33,7	24,02	9,67	29,28	24,08	5,2	4,47*
hsa-miR-193b-3p	25,19	24,02	1,17	26,77	24,08	2,69	-1,52*
hsa-miR-181b-5p	23,65	24,02	-0,37	25,7	24,08	1,62	-1,99*
hsa-miR-148a-3p	29,55	24,02	5,525	31,3	24,08	7,22	-1,69*
hsa-miR-210-3p	23,96	24,02	-0,06	22,11	24,08	-1,96	1,9*

hsa, homo sapiens, * $p < 0.05$

These results suggest that efficient downregulation of Twist1 promotes the mesenchymal-epithelial transition (MET) process in cells (as shown in Figure 1). In this study, 43 miRNAs were analyzed (Supplement 1). Among them, 2 miRNAs (miR-1-1 and miR-210-3p) were upregulated, while 3 miRNAs (miR-193b-3p, miR-181b-5p, and miR-148a-3p) were downregulated. The cycle threshold (CT) was determined using the following formula (Table 1):

$$[\Delta\Delta CT = \Delta CT (\text{target sample}) - \Delta CT (\text{reference sample})] (14).$$

DISCUSSION

In this study, changes in the expression levels of 43 miRNAs, previously characterized as either oncogenic or tumor suppressive, were investigated following Twist1 gene knockdown. These miRNAs were identified through in silico analyses and a comprehensive literature review, focusing on their potential roles in TNBC biology. Among these, miR-193b-3p, miR-1-1, miR-210-3p, miR-181b-5p, and miR-148a-3p were selected for further analysis due to their significant expression changes following Twist1 inhibition. These miRNAs play crucial roles in key biological processes associated with TNBC, including metastasis, angiogenesis, and apoptosis. Notably, miR-210-3p and miR-1-1 are linked to adaptation to hypoxia and cellular energy metabolism, with miR-1-1 generally exhibiting tumor-suppressive effects by reducing proliferation and metastasis in cancer cells (15, 16). Similarly, miR-193b-3p has been reported to suppress metastatic processes (17), while miR-181b-5p exhibits either oncogenic or tumor-suppressive roles in BC (15, 16). miR-148a-3p acts as a tumor suppressor in various cancers, including BC, where its low expression levels are associated with cancer progression (17).

Given their significant expression changes and established roles in TNBC, this study focuses on these five miRNAs to investigate the biological impact of Twist1 suppression on their regulatory pathways. Ongoing research underscores the potential of miRNAs as biomarkers for early BC detection and prognosis determination, highlighting the importance of identifying specific miRNAs and understanding their mechanistic roles in cellular signaling pathways (18).

Twist1 is an essential regulator of cancer progression and spread (19). It plays a key role in the promotion of EMT, cellular invasion, metastatic spread, and maintenance of cancer stem cell properties (20, 21). The importance of Twist1 has been highlighted in several cancers, including BC, prostate cancer and lung cancer (22-24). Additionally, Twist1 is associated with drug resistance in cancer cells (25). Twist1 promotes cancer cell invasion and metastasis by suppressing genes such as *Foxa1*, with its downregulation contributing to EMT, invasiveness, and metastasis in BC (13).

Twist1 functions as a regulatory factor in highly aggressive cells, including TNBC cells like the MDA-MB-231 line. Its interactions with specific DNA recognition sites can either upregulate or downregulate miRNAs. Twist1 activity influences the expression of miRNAs such as miR-34a, miR-373, miR-424, miR-129-5p, miR-20a, miR-448, miR-10, and miR-200, all of which are linked to invasion and metastasis. Research shows that Twist1 suppression reduces oncogenic miRNA expression while enhancing tumor-suppressive miRNA levels (26-29).

Li et al. found that inhibition of Twist1 affects apoptosis through nuclear factor kappa B (NF- κ B)-dependent p53 activation by impairing the expression of miR-10a (26). Similarly, Yu et al. demonstrated that increased miR-129-5p levels suppress EMT, while its downregulation enhances EMT in BC cells. They showed that Twist1 directly represses miR-129-5p expression, with low miR-129-5p levels linked to poor clinical outcomes. Yeh et al. identified miR-151-3p, which targets Twist1 to limit BC cell motility, modulating Twist1 via its interaction with the 3' untranslated region (3'UTR). This regulation inhibits motility and infiltration by promoting E-cadherin production (30). These investigations have shown that suppression of the Twist1 gene leads to a reduction in oncogenic miRNAs and an elevation in tumor-suppressive miRNAs.

miRNAs like miR-145a-5p, miR-300, miR-337-3p, miR-720, miR-151-5p have also been studied in relation to Twist1 inhibition (28, 29, 31). u et al. demonstrated that miR-300 directly targets Twist1 at its 3' UTR, with elevated miR-300 levels inhibiting cell invasion in vitro and reducing experimental metastasis in vivo. An inverse relationship between miR-300 and Twist1 expression was observed in clinical samples, where reduced miR-300 levels correlated with higher metastatic potential (31). Activation of miR-720 significantly reduced BC cell migration both in vitro and in vivo. miR-720 directly targets Twist1, inhibiting metastasis by

suppressing its activity, with a negative correlation observed in human BC tissues (32). Nairismagi et al. reported that Twist1's 3' UTR is highly conserved, with miR-151-5p significantly inhibiting Twist1 expression, particularly when paired with miR-337-3p or miR-145a-5p (29).

However, previous studies have not comprehensively investigated the full miRNA expression panel following Twist1 knockdown. This study addresses this gap by selecting 43 miRNAs not previously associated with Twist1 in BC to provide new insights for future research. The data revealed that Twist1 inhibition in MDA-MB-231 cells led to increased expression of miR-1-1 and miR-210-3p, while the expression of miR-193b-3p, miR-181b-5p, and miR-148a-3p decreased.

Yamasaki et al. identified miR-1-1 as a member of the miR-1 family and demonstrated that in carcinomas of epithelial origin, such as bladder cancer, the expression of miR-1 family members is significantly downregulated. They showed that protmosin- α and purine nucleoside phosphorylase are directly regulated by miR-1 family members. Silencing these two genes led to a marked inhibition of cell proliferation and invasion while significantly promoting apoptosis in cancer cells (33). Liu et al. reported decreased expression of miR-1 family members in BC tissues, which inhibited proliferation and impaired apoptosis in BC cells. miR-1 family members were shown to function as tumor suppressors by targeting K-ras and metastasis-associated lung adenocarcinoma transcript 1. Patients with low miR-1 family expression levels were found to have shorter survival times compared to those with high expression levels (34).

In a study analyzing miRNA expression profiles in metastatic BC cases, miR-1 was identified as a miRNA linked to distant metastasis, with its expression in breast carcinoma associated with aggressive cancer phenotypes, serving as a strong prognostic factor (35). In this research, silencing Twist1 gene expression resulted in a 4.47-fold increase in miR-1-1 expression levels. Using the TargetScan platform (http://www.targetscan.org/vert_72/) for target prediction, it was found that CXC chemokine receptor 4 (CXCR4), a metastasis-associated gene, may represent a common signaling pathway. It was hypothesized that Twist1 gene inhibition could upregulate miR-1-1 via this shared pathway (36).

The data obtained by silencing the Twist1 gene in this study showed that miR-1-1, previously identified as a tumor suppressor, was upregulated. It is hypothesized that Twist1 gene silencing inhibits metastasis, proliferation, motility, and apoptosis in cancer cell lines.

miR1-1 is primarily expressed in heart and skeletal muscle, where it is regulated by muscle differentiation factors during heart development. It functions within serum response factor-myocardin-dependent pathways in cardiac progenitor cells and is controlled by key muscle differentiation factors such as serum response factor, myoblast determination protein 1, and myocyte enhancer factor-2 (37). miR-1 regulates several critical genes involved in muscle and heart function, including kruppel-like factor 4, heat shock protein 60, heart and neural crest derivatives expressed 2 (a transcription factor essential for cardiomyocyte development), stanniocalcin 2, and components of the Transforming Growth Factor-beta (TGF- β) signaling pathway (38).

Dysregulation of miR-1-1 has been linked to various cancers, including liver cancer, lung cancer, BC, colon cancer, medulloblastoma, glioblastoma, and pancreatic cancer. In particular, downregulation of miR-1 is common in TNBC and is associated with poor prognosis and lower survival rates in BC. Additionally, miR-1 has been implicated in chemotherapy-induced cardiotoxicity, particularly in BC patients treated with anthracyclines, including epirubicin (38).

Functionally, overexpression of miR-1-1 in BC cells decreases cell proliferation and invasion while promoting apoptosis through the downregulation of B-cell lymphoma 2 (BCL2), Slug, and metastasis-associated lung adenocarcinoma transcript 1 (MALAT1), ultimately reducing tumor growth (38). The expression of miR-1-1, which has been shown to play a tumor-suppressive role, increases upon the suppression of Twist1. Therefore, Twist1 may be considered a key regulator of miR-1-1 in TNBC progression.

miR-193b-3p is recognized as a tumor suppressor in BC and various cancer cell lines, playing a critical role in regulating metastatic processes. miR-193b-3p has been shown to be significantly downregulated in MDA-MB-231 and MCF-7 cells. Silencing of miR-193b-3p in BC abrogates the inhibition of several proteins associated with metastatic genes, potentially conferring metastatic properties to the cells. These findings are

supported by pathway analyses using KEGG (Kyoto Encyclopedia of Genes and Genomes) and IPA (Ingenuity Pathway Analysis) tools, which identify key signaling pathways linked to poor prognosis in patients (39).

In our study, miR-193b-3p expression levels decreased by 1.52-fold. Given the data, this unexpected reduction in tumor suppressor miRNA aligns with previous findings suggesting that miRNA expression levels can exhibit oncogenic or tumor-suppressive behavior depending on their mechanisms of action. The results from this study further support the hypothesis that miR-193b-3p can induce diverse behaviors in cancer cells.

miR-193b targets estrogen receptor-alpha to inhibit estrogen-induced growth in BC cells, with its target genes involved in cell signaling and steroid hormone production. This suggests that miR-193b plays a role in inhibiting steroid-dependent growth in BC (40). Additionally, miR-193b reduces lipid accumulation and adipogenic marker expression in cultured cells, though its knockdown after differentiation has minimal impact. miR-193b expression also inhibits the differentiation of mouse C2C12 myoblasts into multinucleated myotubes and serves as a key regulator of brown fat differentiation, partially by repressing myogenesis (41). Based on these results, Twist1 may potentially regulate miR-193b-mediated myogenic differentiation in BC cells.

miR-181 is aberrantly expressed in tumor tissues and plays a significant role in cancer progression. The overexpression of miR-181b-5p downregulates E-cadherin by interacting with various transcription factors, thereby promoting invasion and metastasis. These findings indicate that miR-181b-5p modulates TGF- β 1-induced EMT by directly targeting E-cadherin (42, 43). In this study, a marked decrease in miR-181b-5p expression was observed following the suppression of Twist1 gene expression. Mechanistic analysis revealed that the interleukin 6 (IL-6) pathway and NF- κ B activity were particularly prominent. The signal transducer and activator of transcription 3 (STAT3), along with miR-21-5p and miR-181b-5p, has been shown to directly influence IL-6 expression (44). The absence of a significant change in miR-21-5p expression levels in this study suggests that Twist1 affects miR-181b-5p through a pathway other than IL-6.

Previous research has demonstrated that miR-181b-5p, which exhibits epigenetic oncogenic behavior, can inhibit NF- κ B activity, potentially mediating the epigenetic link between inflammation and cancer. It is hypothesized that a shared pathway exists between the epigenetic mechanisms of Twist1 and the regulation

of NF- κ B activity by miR-181b-5p. This shared pathway indicates that the inhibition of Twist1 may downregulate miR-181b-5p expression.

miR-181b is a critical regulator of the phosphatidylinositol 3-kinase (PI3K) pathway, playing a key role in cellular metabolic adaptations that support high proliferation rates during development. It modulates the expression of phosphatase and tensin homolog (PTEN) to regulate PI3K signaling. Mice deficient in miR-181b exhibit severe defects in lymphoid development and T-cell homeostasis, which are linked to impaired PI3K signaling (45). Based on this literature, we propose that the Twist1 transcription factor could regulate the PI3K pathway through miR-181b by modulating PTEN expression in TNBC cells.

miR-148a-3p can function as either an oncogene or a tumor suppressor, depending on the context (46, 47). In our study, a significant decrease in miR-148a-3p expression was observed following the suppression of Twist1. The miR-148a/152 family has been identified as a key regulator of DNA methyltransferase 1 (DNMT1), playing a crucial role in epigenetic modifications and gene expression control (48). Our findings suggest that DNMT1 expression may be influenced by the epigenetic mechanisms of Twist1, potentially affecting the regulation of miR-148a-3p expression. This aligns with Xu et al.'s (2013) findings, which demonstrate DNMT1's role in epigenetic modifications and gene expression control (40). Inhibition of the Twist1 gene may impact cancer cell differentiation and survival by altering the expression of key regulatory miRNAs, including miR-148a-3p.

miR-148a acts as a negative regulator of the innate immune response and the antigen-presenting capacity of mouse dendritic cells (DCs). Its expression is upregulated in mouse DCs during maturation and activation induced by agonists of Toll-like receptor (TLR) 3, TLR4, and TLR9. Overexpression of miR-148a inhibits the production of cytokines, including IL-6, IL-12, tumor necrosis factor (TNF), and interferon- β . It also suppresses the upregulation of major histocompatibility complex class II (MHC II) expression and DC-initiated, antigen-specific T-cell proliferation. This inhibition occurs through the targeting of Camk2a expression. Liu et al. (2010) proposed that miR-148a fine-tunes the innate immune response (49). In light of these findings, further analyses are warranted to investigate the potential roles of Twist1 in the innate immune system and its implications for breast cancer progression.

miR-210-3p may have an effect on cancer cell survival and metastasis (50). In this research, suppression of the Twist1 gene led to a significant increase in the expression level of miR-210-3p. Based on previous studies, this increase in miR-210-3p expression may be mediated by the fibroblast growth factor receptor through the RAS signaling pathway, which modulates the RAS-mitogen-activated protein kinase signaling cascade (51, 52). It is proposed that the inhibition of Twist1 through this common signaling pathway may elevate miR-210-3p expression. Notably, miR-210-3p has previously been classified as a tumor suppressor. Therefore, suppression of the Twist1 gene may hinder cancer cell survival and metastasis by upregulating miR-210-3p.

miR-210 expression progressively increases in human umbilical vein endothelial cells (HUVECs) upon exposure to hypoxia. Overexpression of miR-210 in normoxic endothelial cells stimulates the formation of capillary-like structures in a 3D gel and enhances vascular endothelial growth factor (VEGF)-induced cell migration. Conversely, miR-210 inhibition via anti-miRNA transfection suppresses hypoxia-induced capillary-like structure formation and reduces cell migration in response to VEGF. While miR-210 overexpression does not affect endothelial cell growth, anti-miR-210 transfection inhibits cell growth and induces apoptosis under both normoxic and hypoxic conditions (53).

miR-210 downregulates ephrin-A3 expression, and the expression of an miR-210-resistant ephrin-A3 allele prevents miR-210-mediated stimulation of tubulogenesis and chemotaxis. Fasanaro et al. (2008) concluded that miR-210 plays a key role in the endothelial cell response to hypoxia (53). Antisense-mediated downregulation of miR-210 has been reported to suppress cell viability, induce G0/G1 phase arrest, increase the apoptotic rate, and enhance radiosensitivity in hypoxic human hepatoma cells. Reporter assays indicate that miR-210 targets the 3' UTR of apoptosis-inducing factor, mitochondrion-associated 3 (AIFM3), leading to the downregulation of AIFM3 expression. Human hepatoma cells expressing antisense miR-210 and AIFM3 small interfering RNA exhibit reduced apoptosis following irradiation compared to control cells, suggesting that miR-210 typically downregulates AIFM3-mediated apoptosis (54).

Based on this information, a detailed investigation into the hypoxia-related angiogenesis and cancer development processes regulated by miR-210, modulated by Twist1 in TNBC cells, could elucidate the precise role of Twist1 in miR-210-mediated pathways.

CONCLUSION

In summary, the findings of this research provide novel insights into the regulatory role of Twist1 in modulating miRNA expression patterns within TNBC cells. The miRNAs identified in connection with Twist1 signaling pathways represent potential candidates for the development of new therapeutic strategies targeting TNBC. Further investigation is required to elucidate the underlying molecular mechanisms and to validate the clinical relevance of these findings in patients with TNBC.

Acknowledgments

We would like to thank Selçuk University Scientific Research Projects Coordination Office.

Authorship contributions

BO and SP contributed to the study conception and design. AK, BO and SP conducted the cells experiments. FSB drafted the first manuscript. BO and SP revised the manuscript. All authors contributed to the data interpretation, critically reviewed each draft of the manuscript, and approved the final version for submission.

Data availability statement

The data that support the findings of this study are available on request from the corresponding author.

Declaration of competing interest

The authors declare that they have no known competing financial interests or personal relationships that could have appeared to influence the work reported in this paper.

Ethics

This study protocol was reviewed and approved by Selçuk University Faculty of Medicine Ethics Committee, approval number 2024/113.

Funding

Funding for this study was provided by Selçuk University Scientific Research Projects Coordination Office, grant number 17202072.

REFERENCES

1. Sung H, Ferlay J, Siegel RL, Laversanne M, Soerjomataram I, Jemal A, Bray F. Global cancer statistics 2020: GLOBOCAN estimates of incidence and mortality worldwide for 36 cancers in 185 countries. *CA: a cancer journal for clinicians*. 2021;71(3):209-49.

2. McCarthy AM, Friebel-Klingner T, Ehsan S, He W, Welch M, Chen J, et al. Relationship of established risk factors with breast cancer subtypes. *Cancer Med.* 2021;10(18):6456-67.
3. Yao H, He G, Yan S, Chen C, Song L, Rosol TJ, Deng X. Triple-negative breast cancer: is there a treatment on the horizon? *Oncotarget.* 2017;8(1):1913-24.
4. Zhang B, Shetti D, Fan C, Wei K. miR-29b-3p promotes progression of MDA-MB-231 triple-negative breast cancer cells through downregulating TRAF3. *Biol Res.* 2019;52(1):38.
5. Dziechciowska I, Dąbrowska M, Mizielska A, Pyra N, Lisiak N, Kopczyński P, et al. miRNA Expression Profiling in Human Breast Cancer Diagnostics and Therapy. *Current Issues in Molecular Biology.* 2023;45(12):9500-25.
6. Hussen BM, Abdullah ST, Rasul MF, Salihi A, Ghafouri-Fard S, Hidayat HJ, Taheri M. MicroRNAs: Important Players in Breast Cancer Angiogenesis and Therapeutic Targets. *Front Mol Biosci.* 2021;8:764025.
7. O'Brien J, Hayder H, Zayed Y, Peng C. Overview of microRNA biogenesis, mechanisms of actions, and circulation. *Frontiers in endocrinology.* 2018;9:402.
8. Annese T, Tamma R, De Giorgis M, Ribatti D. microRNAs Biogenesis, Functions and Role in Tumor Angiogenesis. *Front Oncol.* 2020;10:581007.
9. Vidigal JA, Ventura A. The biological functions of miRNAs: lessons from in vivo studies. *Trends in cell biology.* 2015;25(3):137-47.
10. Muñoz JP, Pérez-Moreno P, Pérez Y, Calaf GM. The Role of MicroRNAs in Breast Cancer and the Challenges of Their Clinical Application. *Diagnostics (Basel).* 2023;13(19).
11. Ji W, Sun B, Su C. Targeting MicroRNAs in Cancer Gene Therapy. *Genes (Basel).* 2017;8(1).
12. Zhang X, Wei C, Li J, Liu J, Qu J. MicroRNA-361-5p inhibits epithelial-to-mesenchymal transition of glioma cells through targeting Twist1. *Oncol Rep.* 2017;37(3):1849-56.
13. Xu Y, Qin L, Sun T, Wu H, He T, Yang Z, et al. Twist1 promotes breast cancer invasion and metastasis by silencing Foxa1 expression. *Oncogene.* 2017;36(8):1157-66.
14. Rao X, Huang X, Zhou Z, Lin X. An improvement of the $2^{-(\Delta\Delta CT)}$ method for quantitative real-time polymerase chain reaction data analysis. *Biostat Bioinforma Biomath.* 2013;3(3):71-85.
15. Dang K, Myers KA. The Role of Hypoxia-Induced miR-210 in Cancer Progression. *International Journal of Molecular Sciences.* 2015;16(3):6353-72.
16. Han C, Yu Z, Duan Z, Kan Q. Role of microRNA-1 in human cancer and its therapeutic potentials. *Biomed Res Int.* 2014;2014:428371.
17. Khordadmehr M, Shahbazi R, Sadreddini S, Baradaran B. miR-193: a new weapon against cancer. *Journal of cellular physiology.* 2019;234(10):16861-72.
18. Jordan-Alejandro E, Campos-Parra AD, Castro-López DL, Silva-Cázares MB. Potential miRNA Use as a Biomarker: From Breast Cancer Diagnosis to Metastasis. *Cells.* 2023;12(4).
19. Yu X, He T, Tong Z, Liao L, Huang S, Fakhouri WD, et al. Molecular mechanisms of TWIST1-regulated transcription in EMT and cancer metastasis. *EMBO Rep.* 2023;24(11):e56902.
20. Qin Q, Xu Y, He T, Qin C, Xu J. Normal and disease-related biological functions of Twist1 and underlying molecular mechanisms. *Cell Res.* 2012;22(1):90-106.
21. Beck B, Lapouge G, Rorive S, Drogat B, Desaedelaere K, Delafaille S, et al. Different levels of Twist1 regulate skin tumor initiation, stemness, and progression. *Cell Stem Cell.* 2015;16(1):67-79.
22. Jiang X, Guo D, Li W, Yu T, Zhou J, Gong J. Combination Twist1 and CA15-3 in axillary lymph nodes for breast cancer prognosis. *Mol Med Rep.* 2017;15(3):1123-34.
23. Zhao Z, Rahman MA, Chen ZG, Shin DM. Multiple biological functions of Twist1 in various cancers. *Oncotarget.* 2017;8(12):20380-93.
24. Fattahi F, Saeednejad Zanjani L, Vafaei S, Habibi Shams Z, Kiani J, Naseri M, et al. Expressions of TWIST1 and CD105 markers in colorectal cancer patients and their association with metastatic potential and prognosis. *Diagnostic Pathology.* 2021;16(1):26.
25. Liang Y, Hu J, Li J, Liu Y, Yu J, Zhuang X, et al. Epigenetic Activation of TWIST1 by MTDH Promotes Cancer Stem-like Cell Traits in Breast Cancer. *Cancer Res.* 2015;75(17):3672-80.
26. Li X, Xu F, Chang C, Byon J, Papayannopoulou T, Deeg HJ, Marcondes AM. Transcriptional regulation of miR-10a/b by TWIST-1 in myelodysplastic syndromes. *haematologica.* 2013;98(3):414.
27. Yu Y, Zhao Y, Sun X-H, Ge J, Zhang B, Wang X, Cao X-C. Down-regulation of miR-129-5p via the Twist1-Snail feedback loop stimulates the epithelial-mesenchymal transition and is associated with poor prognosis in breast cancer. *Oncotarget.* 2015;6(33):34423.
28. Li Q, Chen Z, Cao X, Xu J, Xu J, Chen Y, et al. Involvement of NF- κ B/miR-448 regulatory feedback loop in chemotherapy-induced epithelial-mesenchymal transition of breast cancer cells. *Cell Death & Differentiation.* 2011;18(1):16-25.
29. Nairismägi M-L, Füchtbauer A, Labouriau R, Bramsen JB, Füchtbauer E-M. The proto-oncogene TWIST1 is regulated by microRNAs. *PLoS One.* 2013;8(5):e66070.
30. Yeh TC, Huang TT, Yeh TS, Chen YR, Hsu KW, Yin PH, et al. miR-151-3p Targets TWIST1 to Repress Migration of Human Breast Cancer Cells. *PLoS One.* 2016;11(12):e0168171.
31. Yu J, Xie F, Bao X, Chen W, Xu Q. miR-300 inhibits epithelial to mesenchymal transition and metastasis by targeting Twist in human epithelial cancer. *Molecular cancer.* 2014;13:1-12.
32. Li L-Z, Zhang CZ, Liu L-L, Yi C, Lu S-X, Zhou X, et al. miR-720 inhibits tumor invasion and migration in breast cancer by targeting TWIST1. *Carcinogenesis.* 2014;35(2):469-78.

33. Yamasaki T, Yoshino H, Enokida H, Hidaka H, Chiyomaru T, Nohata N, et al. Novel molecular targets regulated by tumor suppressors microRNA-1 and microRNA-133a in bladder cancer. *International Journal of Oncology*. 2012;40(6):1821-30.
34. Liu R, Li J, Lai Y, Liao Y, Liu R, Qiu W. Hsa-miR-1 suppresses breast cancer development by down-regulating K-ras and long non-coding RNA MALAT1. *International journal of biological macromolecules*. 2015;81:491-7.
35. Minemura H, Takagi K, Miki Y, Shibahara Y, Nakagawa S, Ebata A, et al. Abnormal expression of miR-1 in breast carcinoma as a potent prognostic factor. *Cancer Sci*. 2015;106(11):1642-50.
36. Leone V, D'Angelo D, Rubio I, de Freitas PM, Federico A, Colamaio M, et al. MiR-1 is a tumor suppressor in thyroid carcinogenesis targeting CCND2, CXCR4, and SDF-1 α . *The Journal of Clinical Endocrinology & Metabolism*. 2011;96(9):E1388-E98.
37. Zhao Y, Samal E, Srivastava D. Serum response factor regulates a muscle-specific microRNA that targets Hand2 during cardiogenesis. *Nature*. 2005;436(7048):214-20.
38. Khan P, Ebenezer NS, Siddiqui JA, Maurya SK, Lakshmanan I, Salgia R, et al. MicroRNA-1: Diverse role of a small player in multiple cancers. *Seminars in Cell & Developmental Biology*. 2022;124:114-26.
39. Yang Z, He M, Wang K, Sun G, Tang L, Xu Z. Tumor suppressive microRNA-193b promotes breast cancer progression via targeting DNJC13 and RAB22A. *International journal of clinical and experimental pathology*. 2014;7(11):7563.
40. Leivonen S-K, Rokka A, Östling P, Kohonen P, Corthals GL, Kallioniemi O, Perälä M. Identification of miR-193b targets in breast cancer cells and systems biological analysis of their functional impact. *Molecular & Cellular Proteomics*. 2011;10(7).
41. Sun L, Xie H, Mori MA, Alexander R, Yuan B, Hattangadi SM, et al. Mir193b-365 is essential for brown fat differentiation. *Nature cell biology*. 2011;13(8):958-65.
42. Pan D, Fujimoto M, Lopes A, Wang YX. Twist-1 is a PPAR δ -inducible, negative-feedback regulator of PGC-1 α in brown fat metabolism. *Cell*. 2009;137(1):73-86.
43. Hernandez YG, Lucas AL. MicroRNA in pancreatic ductal adenocarcinoma and its precursor lesions. *World journal of gastrointestinal oncology*. 2016;8(1):18.
44. Iliopoulos D, Jaeger SA, Hirsch HA, Bulyk ML, Struhl K. STAT3 activation of miR-21 and miR-181b-1 via PTEN and CYLD are part of the epigenetic switch linking inflammation to cancer. *Molecular cell*. 2010;39(4):493-506.
45. Henao-Mejia J, Williams A, Goff LA, Staron M, Licona-Limón P, Kaech SM, et al. The microRNA miR-181 is a critical cellular metabolic rheostat essential for NKT cell ontogenesis and lymphocyte development and homeostasis. *Immunity*. 2013;38(5):984-97.
46. Cuk K, Zucknick M, Heil J, Madhavan D, Schott S, Turchinovich A, et al. Circulating microRNAs in plasma as early detection markers for breast cancer. *International journal of cancer*. 2013;132(7):1602-12.
47. Yuan K, Lian Z, Sun B, Clayton MM, Ng IO, Feitelson MA. Role of miR-148a in hepatitis B associated hepatocellular carcinoma. *PloS one*. 2012;7(4):e35331.
48. Xu Q, Jiang Y, Yin Y, Li Q, He J, Jing Y, et al. A regulatory circuit of miR-148a/152 and DNMT1 in modulating cell transformation and tumor angiogenesis through IGF-IR and IRS1. *Journal of molecular cell biology*. 2013;5(1):3-13.
49. Liu X, Zhan Z, Xu L, Ma F, Li D, Guo Z, et al. MicroRNA-148/152 impair innate response and antigen presentation of TLR-triggered dendritic cells by targeting CaMKII α . *The Journal of Immunology*. 2010;185(12):7244-51.
50. Samaan S, Khella HW, Girgis A, Scorilas A, Lianidou E, Gabril M, et al. miR-210 is a prognostic marker in clear cell renal cell carcinoma. *The Journal of Molecular Diagnostics*. 2015;17(2):136-44.
51. Schild C, Trueb B. Aberrant expression of FGFR1, a novel FGF receptor, in ovarian tumors. *International journal of molecular medicine*. 2005;16(6):1169-73.
52. Tsuchiya S, Fujiwara T, Sato F, Shimada Y, Tanaka E, Sakai Y, et al. MicroRNA-210 regulates cancer cell proliferation through targeting fibroblast growth factor receptor-like 1 (FGFR1). *Journal of Biological Chemistry*. 2011;286(1):420-8.
53. Fasanaro P, D'Alessandra Y, Di Stefano V, Melchionna R, Romani S, Pompilio G, et al. MicroRNA-210 modulates endothelial cell response to hypoxia and inhibits the receptor tyrosine kinase ligand Ephrin-A3. *Journal of biological chemistry*. 2008;283(23):15878-83.
54. Yang W, Sun T, Cao J, Liu F, Tian Y, Zhu W. Downregulation of miR-210 expression inhibits proliferation, induces apoptosis and enhances radiosensitivity in hypoxic human hepatoma cells in vitro. *Experimental cell research*. 2012;318(8):944-54.

Research Article

COMPARATIVE ASSESSMENT OF AUDITORY AND VESTIBULAR FUNCTIONS IN MULTIPLE SCLEROSIS PATIENTS USING AUDIOLOGICAL DIAGNOSTIC TOOLS

 Serap UÇAR ^{1,2*},  Özgür SÜRMEİOĞLU ¹,  Halime DANA ³

¹Çukurova University Faculty of Medicine, Department of Ear, Nose and Throat, ADANA, TURKIYE

²Erciyes University, Halil Bayraktar Vocational School of Health Services, KAYSERİ, TURKIYE

³Erciyes University Faculty of Medicine, Department of Medical Biology, KAYSERİ, TURKIYE

*Correspondence: serapucar@erciyes.edu.tr

ABSTRACT

Objective: As a demyelinating disease of the central nervous system, multiple sclerosis (MS) can be marked by tiredness, ataxia, sensory complaints, attention, and motor speech, as well as weakness in the arms and legs. Cortical symptoms, cognitive decline, hearing loss and epileptic seizures are typical symptoms. The aim of this study is to determine the impact of MS on the auditory and vestibular pathways.

Materials and Methods: MS patients mental abilities were assessed in this study, accounting for vestibular and auditory function. Fifteen MS patients and fifteen healthy controls were recruited. The experimental and patient groups underwent vestibular and audiological testing and the results from these two groups were compared. The patients underwent simultaneous impedance audiometry.

Results: The data from our study showed significant results for the right and left ears of MS patients when we used pure tone audiometry. In the Auditory Brainstem Response (ABR) test, unilateral sensorineural hearing loss was observed in seven patients. On the Video Head Impulse Test (VHIT), the vestibulo-ocular reflex (VOR) gains of 9 MS patients were outside normal limits, while the VOR gains of one patient were low in the left lateral canal. On the Vestibular evoked myogenic potentials test, wave latencies were delayed in 12 of the patients and the left P1 and N1 waveforms were not observed in two patients.

Conclusion: Based on the findings of our study, we can say that auditory and vestibular functions are significantly impaired in MS patients. We can recommend that studies with larger patient populations should be developed.

Keywords: ABR, MS, psychosocial problems, vestibular function tests, pure tone audiometry.

Received: 30 September 2024

Revised: 03 December 2024

Accepted: 04 December 2024

Published: 22 December 2024



Copyright: © 2024 by the authors. Published Aydın Adnan Menderes University, Faculty of Medicine and Faculty of Dentistry. This is an open access article under the Creative Commons Attribution Non Commercial 4.0 International (CC BY-NC 4.0) License.

INTRODUCTION

Multiple Sclerosis (MS) is a chronic, inflammatory, demyelinating disease that is usually seen in young adults and causes neurological and cognitive function loss (1). It has been shown that gray matter and white matter are affected. Genetic and various environmental factors influence the disease's development (2). Movement issues, migraines, epileptic seizures, hearing loss, cognitive decline, and cortical symptoms are typical symptoms (3). MS symptoms may occur as prodromal or acute episodes. Although the disease's first findings are mostly in remission, remission or partial attacks are seen or not seen in later ataxias (4, 5). Evoked potential (EP) examinations are most frequently applied in the clinic to diseases that cause demyelinating lesions in the central nervous system, especially MS (6). The electrical potentials are recorded by applying sensory stimuli to MS patients through the scalp, and their formation times are evaluated with evoked potentials. Visual Evoked Potentials (VEP) and Somatosensory Evoked Potentials (SEP) applications applied to MS patients are essential for both diagnosis and patient follow-up (7, 8). Demyelinating plaques can also form in the vestibular and central pathways, resulting in hearing and balance disorders. For example, these plaques can also develop in the brainstem, where the auditory and vestibular pathways are located (9). In addition, it has been suggested that the vestibular nuclei and root vestibule of the 8th cranial nerve are one of the most common anatomical sites for inflammation (10). Peripheral nerve connections within the cochlea may be affected by demyelination, resulting in peripheral auditory and vestibular involvement in people with MS (11, 12). This study hypothesizes that MS patients will exhibit significant auditory and vestibular dysfunction compared to healthy controls. While previous studies have explored auditory and vestibular dysfunctions in MS, few have systematically compared these functions using comprehensive diagnostic tests such as ABR, Vestibular evoked myogenic potentials (VEMP), and Video Head Impulse Test (VHIT) in a controlled setting. This study, which compared hearing and balance levels between MS patients and healthy controls, has the potential to significantly enhance our understanding of MS's impact on auditory and vestibular functions. The findings could provide valuable insights into the fields of neurology, audiology, and otolaryngology, sparking further research and discussion in these areas.

MATERIALS AND METHODS

The methodology of the study was comprehensive. All stages of the study are summarized in Figure 1. A total of 15 MS patients aged between 27 and 55 years, with or without hearing and balance problems, who were diagnosed with definite MS at the Neurology Department from the Adana MS Patients and Relatives Association, and who had not had an attack for at least two months were included in the study. The control group we included in the study consisted of 15 individuals and the age range was between 27 and 55, as in MS patients.

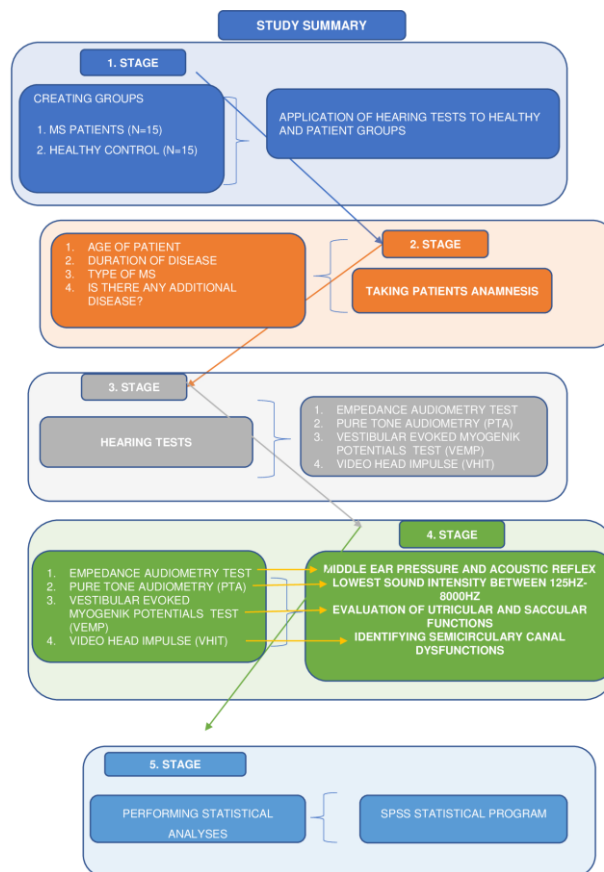


Figure 1. Experimental Design

The number of patients and controls to be used in the study was determined based on the reference article by performing a power analysis. The α value was taken as 0.05 and the beta value as 0.95. As a result of these calculations, the effect size was found to be 1.2456822. As a result, the total number was determined

as 30, with 15 people per group (13). The control group consisted of individuals who were examined at the ENT Department and who had no hearing or balance problems. Participants who had previously been diagnosed with hearing loss, had a history of vestibular disorder or had an attack in less than two months, had a lower extremity fracture within two months before inclusion in the study and/or had other medical conditions that would affect the study procedures were not included in the study. The audiologic and vestibular function tests of the study were performed at the Audiology Unit of the ENT Department of the Çukurova University Faculty of Medicine, ensuring the reliability and validity of the results. The first immittance measurements (Interacoustics brand AT-235 model device) were made on the study participants. Thus, it was determined that the patients did not have a middle ear pathology that prevented hearing, and pure tone signals with decreasing intensity were sent to them at random rhythmic intervals via pure tone audiometer (Interacoustics brand AC-40 model). In this way, the right and left hearing thresholds recorded on the pure tone audiometer were marked on the audiogram. Then, speech tests were performed, and the patient's speech discrimination scores (SD = speech discrimination) were determined. Then, brainstem auditory response audiometry (with GSI-Audera model device) was performed on the patients while resting and in their natural sleep using insert headphones (TDH-39 model). Responses obtained from the brainstem were recorded by sending click stimuli via a computer and electrodes. In the recording, an average was made by giving approximately 1500-2000 stimuli. ABR testing included variations in click stimulus frequency to evaluate its effects on auditory brainstem responses in MS patients. Then, a VEMP test was performed on the patients via ABR equipment. In the cVEMP test, the responses recorded from the SCM muscle were obtained via surface electrodes attached to 1/3 or 1/2 of the patient's SCM muscle, the middle of the forehead and the sternum. signals were sent via insert earphones (TDH 39 model) attached to both ears of the patient, and positive waves (P1) and negative waves (N1) were obtained with the ABR device (GSI-Audera model device) via electrodes placed on the SCM muscle. In response to the high-intensity sound stimulus, the SCM muscle contracted using various methods, and the latencies of the biphasic waves obtained in the electromyographic recording were evaluated. The functions of the saccule, inferior vestibular nerve, and lower brainstem were assessed in the cVEMP test. Measurements were made using 30 msec AC sound stimuli at 100 dB SPL. In the

VHIT test, patients were made to look at a previously determined fixed point; their heads were tilted forward by 30 degrees, and the lateral semicircular canals were made parallel to the ground plane. The patients were turned forward, backwards, right, and left with sudden, small, rapid movements. The movement was sudden (>3000 degrees/s²), unexpected by the patient and at angles less than 20-30 degrees. To obtain high-resolution and fast recordings, VOR gains were calculated numerically with the help of a computer to determine saccades that were not seen and detected with the naked eye. In the VHIT device used in this study, eye movements were recorded with a camera placed on the glasses. Measurements were made with the EyeSeeCam VHIT (Interacoustics, A/S DK-5610) device and evaluated with the OtoAccess™ computer program. Before starting the test, the device was calibrated. Participants were asked to read the informed consent form at the beginning of the study and their approval was obtained. The Çukurova University Faculty of Medicine Non-Interventional Clinical Research Ethics Committee evaluated the study's compliance with ethical principles and obtained ethical approval (31.08.2018/5).

Statistical analysis

Sample T-test was used to compare the left and right high-frequency hearing and balance thresholds of MS and control groups according to age range at a 5% significance level. In examining the factors affecting MS disease, the data were checked for normal distribution, and the patient and healthy groups were compared by applying sample T-test to those with normal distribution. The significance level between the variables was accepted as statistically significant for $p < 0.05$. The dependent variables in this study were the balance and hearing thresholds of the right and left ears, and the independent variables were age, gender, marital status, disease duration, etc. The results were analyzed in the IBM SPSS 22.0 statistical program.

RESULTS

The socio-demographic characteristics of the patient and control groups participating in the study are shown in tables as supplement data. The mean age of the healthy control group participating in the study was 39.26 ± 6.75 , and the mean age of MS patients was 38.80 ± 9.14 .

Results of pure tone hearing thresholds test

Pure tone hearing thresholds of the patient group were found to be statistically significant in the right ear ($p=0.001$) and left ear ($p=0.002$) compared to the control group (Table 1). According to these results, hearing thresholds were significantly increased in MS patients compared to healthy controls, indicating hearing loss. In our study, according to the pure tone audiometry results applied to MS patients, a higher degree of hearing loss was observed in the right ear compared to the left ear.

Table 1: Analysis Results of Pure Tone Audiometry Test Applied to Groups

Parameters	Control Group (n=15)	Patient Group (n=15)	F	p
Pure Tone R	6.53 ± 3.29 dB	21.8 ± 14.45 dB	21.84 dB	0.001
Pure Tone L	8.8 ± 3.74 dB	17.4 ± 12.81 dB	11.61 dB	0.002

The data were represented as mean ± standard error of mean. Differences in means were compared by sample t-test. Statistical significance was defined as p-values of 0.05 or less. In the patient group, right (R) ($p=0.001$) and left (L) ($p=0.002$) ear hearing thresholds were found to be statistically significant compared to the control group.

Results of ABR test

Hearing thresholds in the ABR test were found to be statistically significant in the right ($p=0.001$) and left ($p=0.002$) ears in the patient group compared to the control group (Table 2). According to these results, ABR thresholds were significantly increased in MS patients compared to healthy controls, indicating hearing loss. Looking at the ABR results we applied to MS patients, we obtained higher thresholds in the right ear compared to the left ear, indicating a greater degree of hearing loss in the left ear.

Table 2: Analysis results of ABR test applied to groups

Parameters	Control Group (n=15)	Patient Group (n=15)	F	p
R	20.0 ± 0.001 dB HL	27.14 ± 14.23 dB HL	12.8 dB	0.001
L	20.66 ± 2.58 dB HL	30.0 ± 13.0 dB HL	11.89 dB	0.002

The data were represented as mean ± standard error of mean. Differences in means were compared by sample t-test. Statistical significance was defined as p-values of 0.05 or less. It was observed that the right (R) ($p=0.001$) and left (L) ($p=0.002$) ear hearing thresholds in the patient group were statistically significant compared to the control group.

Results of VEMP test

VEMP score enables better evaluation of brainstem involvement; while also correlating well with disability and disease duration. In the VEMP test records applied to the participants, the latencies of the electrical waves (P1 and N1) obtained from the sternocleidomastoid (SCM muscle) were measured. The SCM muscle is a large muscle pair located in the neck region. The SCM muscle provides neck movements and facilitates head rotation. The right ear P1 (RP1), right ear N1 (RN1), left ear P1 (LP1) and left ear N1 (LN1) latencies of the patient and control groups were measured. It was observed that the right P1 ($p=0.05$), right N1 ($p=0.05$) and left P1 ($p=0.01$), left N1 ($p=0.002$) wave latencies in the patient group were statistically significant compared to the control group (Table 3). In the VEMP test, it was determined that 40% of the patients ($n=12$) had delayed latency values of the P1 and N1 waves. The values of the participants in the control group were within normal limits.

Multiple sclerosis (MS) lesions may impair VEMP responses affecting the vestibular fascicles, vestibular nuclei and their efferents, and cerebellum all of which are all involved in relaying and processing of the vestibular signals. These delays in the latency values of the patient waves indicate brainstem involvement, and more delay was observed in the left ear of the patients than in the right ear.

Table 3: Analysis results of left ear vemp test applied to groups

Parameters	Control Group (n=15)	Patient Group (n=12)	F	p
LP1	14.16 ± 1.70 ms	15.86 ± 5.85 ms	6.45 ms	0.01
LN1	22.94 ± 1.39 ms	23.75 ± 4.62 ms	12.16 ms	0.002
RP1	13.66 ± 1.88 ms	16.90 ± 5.56 ms	4.15 ms	0.05
RN1	23.6 ± 1.97 ms	25.60 ± 2.83 ms	3.95 ms	0.05

The data were represented as mean ± standard error of mean. Differences in means were compared by sample t-test. Statistical significance was defined as p-values of 0.05 or less. It was observed that the right P1 (RP1) ($p=0.05$), right N1 (RN1) ($p=0.05$) and left P1 (LP1) ($p=0.01$), left N1 (LN1) ($p=0.002$) latencies of wave in the patient group were statistically significant compared to the control group.

Results of VHIT test

In VHIT recordings, right anterior semicircular canal (RA), right lateral semicircular canal (RL), right posterior semicircular canal (RP) ($p<0,004$), left anterior semicircular canal thresholds (LA) ($n=15$), left lateral canal gains (LL), and left posterior semicircular canal gains (LP) ($p<0.01$) were measured. According to the

results of the VHIT test, 27% of the patients (n=8) were seen to have gain values outside the normal range compared to the control group (Table 4). According to VHIT test results, low channel gains in MS patients indicate that the functions in the vestibular channels are impaired.

Table 4: Analysis Results of Right Ear VHIT Test (Anterior, Posterior, Lateral Canals)

Parameters	Control Group (n=15)	Patient Group (n=14)	F	p
RA	0.90 ± 0.17	0.73 ± 0.21	0.74	0.39
RL	0.91 ± 0.19	0.89 ± 0.21	0.55	0.46
RP	1.02 ± 0.23	0.86 ± 0.35	0.10	0.004
LA	0.98 ± 0.14	0.81 ± 0.28	0.67	0.41
LL	0.90 ± 0.14	0.90 ± 0.10	3.92	0.05
LP	1.03 ± 0.10	0.80 ± 0.21	6.24	0.01

The data were represented as mean ± standard error of mean. Differences in means were compared by sample t-test. Statistical significance was defined as p-values of 0.05 or less. In VHIT recordings, the mean Right Anterior (RA) values in the experimental group were 0.73±0.21 (p=0.39), Right Lateral (RL) values were 0.89±0.21 (p=0.46), and Right Posterior (RP) values were 0.86±0.35 (p=0.004); Left Anterior (LA) values were found to be 0.81±0.28 (p=0.41), Left Lateral (LL) values were found to be 0.90±0.10 (p=0.05) and Left Posterior (LP) values were found to be 0.80±0.21 (p=0.01). In our study, in the VHIT test, 27% of the patients (n=8) were found to have gain values outside the normal range.

DISCUSSION

MS is a chronic inflammatory disease affecting the central nervous system, and its etiology is unknown (14). It is essential to equalize the variables in case-control type studies. The variables in this study were age, gender, marital status, disease duration, hearing, and balance thresholds. These variables affect the social lives of the patients (15). Hearing loss due to demyelination in MS patients may be of peripheral or central origin (16). PTA was measured with a dual-channel Interacoustics AC40 Clinical Audiometer calibrated at frequencies of 250, 500, 1000, 2000, 4000 and 6000 Hz according to the modified Hughson-Westlake ascending method (Jerger et al., 1959) in a soundproof booth. Hearing loss was calculated separately for each pure tone frequency stimulus, and the amount of threshold shift above the standard audiometric zero (dB HL) was also calculated. In our study, sensorineural hearing loss was detected in 27% of the patients in the pure tone audiometry test applied to the patients. Bilateral hearing loss was present in 23% (n=7) of 8 patients, while unilateral sensorineural hearing loss was observed in 4%. Middle ear pressures were Type A tympanogram in 100% of patients, and acoustic reflex was obtained in all patients. In a study, according to the results of pure

tone audiometry test and acoustic reflex test applied to 30 MS patients and 23 healthy volunteer participants, no significant results were obtained in MS patients compared to healthy volunteers (17). In another study, case history assessment, otoscopic examination, pure tone audiometry, and ABR testing were performed on 45 MS patients, and it was predicted that the results could be a valid and useful measure in the evaluation of brainstem functions and prediction of disability in MS (18). In a prospective study, ABR testing was performed on 40 participants, and a total of 160 BERA recordings obtained from 80 ears of 40 participants were examined. 20 of these were MS patients and 20 were healthy volunteers in the control group. Significant prolongation of wave latencies was observed in the right and left ears of patients in the MS group (19). In our study, when the click stimulus frequency was 20 per second in the ABR applied to 30 participants in all groups, the right and left ear thresholds were observed as 20 dB HL, and in the patient group, the hearing threshold of the right ear was observed as 20 dB HL and the left ear as 30 dB HL. However, when we increased the click stimulus frequency, the wave morphology in the ABR was distorted in all groups and even artifactual waveforms were observed. cVEMP results allow assessment of brainstem involvement. VEMP are feedforward, low-latency electromyographic responses induced by acoustic stimuli. cVEMP test activates an inhibition reflex (the vestibulocollic reflex) that is recorded from the tonically contracted ipsilateral SCM muscle, reflecting vestibulospinal pathway activity. This reflex arc consists of neuroreceptors of the saccular macula, inferior vestibular nerve, lateral vestibular nucleus, medial vestibulospinal tract, and spinal cord motor neurons supplying muscles in the neck. While the VEMP test has used for the assessment of acoustic neuroma and peripheral vestibular disorders such as Meniere disease and vestibular neuritis, it can provide a stream of information about brainstem function as most of the vestibulocollic reflex arc is centered in the brainstem (20).

In 2008, Zeigelboim et al. conducted a study to define vestibular abnormalities in 30 MS patients. The study group included patients without psychological or oculomotor paresis, internuclear ophthalmoplegia or severe visual impairment. The evaluation phase of vestibular function tests consisted of labyrinth function and ocular tests—the results of the electronystagmography test provided information about changes in corneoretinal potentials. Vestibular changes were observed in 86% of the patients evaluated. Bilateral

peripheral vestibulopathy was detected in 20% of the patients, and left peripheral vestibulopathy was detected in 17% (21).

In a study conducted with the participation of 35 adult patients, VEMP test was applied to patient and control groups and then the results of the groups were compared. There was no significant difference between the groups in terms of c-VEMP results, there was no significant difference between the o-VEMP results except for N1-P1 amplitudes. When N1-P1 amplitudes were compared with controls, it was observed that they were significantly lower (22).

vHIT can be used as a diagnostic test for brainstem lesions, so any decrease in vHIT results may predict the onset of brainstem involvement in MS patients. Therefore, it seems necessary to include a VOR function test during the clinical practice of MS patients (23). Our study aims to evaluate the vestibular semicircular canal function in MS using vHIT to determine the angular vestibular reflex associated with stimulation of the six semicircular canals. Our findings revealed that there may be VOR dysfunction in MS and that there was a significant correlation between the VOR gains of the vertical canals and balance clinical scales.

The limitations of our study are the small number of patients, being a single-center study, and the inability to make gender-based comparisons due to gender inequality in patient numbers.

CONCLUSION

As a result of the literature review and the data obtained from our study, significant results were obtained for the right and left ears of MS patients to whom we applied the pure tone audiometry test. There was evidence that it impacted these patients' high frequency hearing sensitivity. In the ABR test, unilateral hearing loss was observed in seven patients when the click stimulus frequency was 20 per second. When the click stimulus frequency was 70 per second, no waveform was observed in any patient. In the VHIT test, while the VOR gains of 9 MS patients were outside the normal limits, the VOR gains of one patient in the left lateral canal were low. The gain values obtained in the anterior and lateral canals in the right and left ears were statistically insignificant.

In contrast, the posterior canal gains in the right and left ears were statistically significant. In the VEMP test, the P1 and N1 wave latencies of 14 patients in the control group were close to normal limits, and the wave latencies of patients were outside the normal limits. The wave latencies of 12 patients in the patient group were delayed, and the two patients' left-side P1 and N1 waveforms were not observed. The VEMP test showed that the left P1 and N1 waves showed statistically significant results, while the right P1 and N1 waves showed statistically insignificant values. While the average EDSS score of the patients in the control group according to the BDI scale was 1.13 points, the average of the patients with MS was 4.23. More patients and more research are needed to obtain reliable results.

Acknowledgments

We/I would like to thank the Proofreading & Editing Office of the Dean for Research at Erciyes University for copyediting and proofreading service for this manuscript.

Authorship contributions

S.U.; Design, Data Collection, Analysis and Interpretation, Literature Search, Writing-Original Draft. Ö.S.; Concept, Design. H.D.; Design, Analysis, Writing-Original Draft.

Data availability statement

The data that support the findings of this study are available from the corresponding author upon reasonable request.

Declaration of competing interest

No conflict of interest was declared by the authors

Ethics

The Çukurova University Faculty of Medicine Non-Interventional Clinical Research Ethics Committee evaluated the study's compliance with ethical principles and obtained ethical approval (31.08.2018/5).

Funding

This work has not received any funding support.

REFERENCES

1. Hauser, S. L., & Cree, B. A. Treatment of multiple sclerosis: a review. *The American journal of medicine*, 2020;133(12), 1380-1390.
2. Tunalı G. Epidemiyoloji. Tunalı G editör. *Türkiye Klinikleri Nöroloji Dergisi Multipl skleroz Özel Sayısı*. 2004;161-5.
3. Brown TR, Kraft GH. Exercise and rehabilitation for individuals with multiple sclero. *Phys Med Rehabil Clin N Am*, 2005;16:513-55.
4. Thompson AJ, Banwell BL, Barkhof F, Carroll WM, Coetzee T, Comi G, et al. Diagnosis of multiple sclerosis: 2017 revisions of the McDonald criteria. *Lancet Neurol*. 2018;17(2):162-173.
5. Freedman MS, Devonshire V, Duquette P, et al. Treatment Optimization in Multiple Sclerosis: Canadian MS Working Group Recommendations. *Canadian Journal of Neurological Sciences / Journal Canadien des Sciences Neurologiques*. 2020;47(4):437-455.
6. Rishiq D, Harkrider A, Springer C, Hedrick M. Click-evoked and speech-evoked auditory brainstem responses from individuals with multiple sclerosis. *Neurosci Lett*. 2021; Jan 1;740:135460.
7. Kallmann BA, Fackelmann S, Toyka KV, Rieckmann P, Reiners K. Early abnormalities of evoked potentials and future disability in patients with multiple sclerosis. *Mult Scler* 2006; 12: 58- 65.
8. Idiman F. Multipl sklerozda uyarılmış potansiyeller. Tunalı G editör. *Türkiye Klinikleri Nöroloji Dergisi Multipl skleroz Özel Sayısı*. 2004: 197- 202.
9. Coelho A, Ceranić B, Prasher D, Miller DH, Luxon LM. Auditory efferent function is affected in multiple sclerosis. *Ear Hear*. 2007 Sep;28(5):593-604.
10. Corrêa DG, Hygino da Cruz LC Jr, Freddi TAL. The Vestibulocochlear Nerve: Anatomy and Pathology. *Semin Ultrasound CT MR*. 2023 Apr;44(2):81-94.
11. Bogie JFJ, Stinissen P, Hendriks JJA. Macrophage subsets and microglia in multiple sclerosis. *Acta Neuropathol* 2014; 128:191–213.
12. Di Stadio A, Ralli M. Inner ear involvement in multiple sclerosis: an underestimated condition? *Mult Scler* 2018; 24:1264–5.
13. Parsa MS, Mohammadkhani G, Hajabolhassani F, Jalae S, Zakeri H. Cervical and ocular vestibular evoked myogenic potentials in multiple sclerosis participants. *Med J Islam Repub Iran*. 2015 Jan 26; 29:164.
14. Gür E, Binkhamis G, Kluk K. Effects of multiple sclerosis on the auditory-vestibular system: a systematic review. *BMJ Open*. 2022 Aug;12(8): e060540.
15. Sharifi N, Kohpeima Jahromi V, Zahedi R, Aram S, Ahmadi M. Social stigma and its relationship with quality of life in multiple sclerosis patients. *BMC Neurol*. 2023 Nov 17;23(1):408.
16. Ralli M, Di Stadio A, Visconti IC, Russo FY, Orlando MP, Balla MP. Otolaryngologic symptoms in multiple sclerosis: a review. *Int Tinnitus J*. 2018;22(2):160-169.
17. Bozhöyük MS, Kutlu S, Ocağ E, Özaydın Aksun Z, Tokgöz Yılmaz S, Yücesan C, Yorulmaz İ. Efferent işitsel sistemin multipl sklerozlu hastalarda elektrofizyolojik yöntemlerle değerlendirilmesi. *J Ear Nose Throat Head Neck Surg*. 2024;32(3).
18. Srinivasan VS, Krishna R, Munirathinam BR. Effectiveness of Brainstem Auditory Evoked Potentials Scoring in Evaluating Brainstem Dysfunction and Disability Among Individuals with Multiple Sclerosis. *Am J Audiol*. 2021 Jun 14;30(2):255-265.
19. Kaytancı E, Ozdamar OI, Acar GO, Tekin M. Evaluation of transiently evoked otoacoustic emissions and auditory brainstem responses in patients with multiple sclerosis. *Ear Nose Throat J*. 2016 Oct-Nov;95(10-11).
20. Güven H, Bayır O, Aytaç E, Ozdek A, Comoğlu SS, Korkmaz H. Vestibular-evoked myogenic potentials, clinical evaluation, and imaging findings in multiple sclerosis. *Neurol Sci*. 2014 Feb;35(2):221-6.
21. Zeigelboim BS, Arruda WO, Mangabeira-Albernaz PL, Iório MCM, Jurkiewicz AL, Martins-Bassetto J, Klagenberg KF. Vestibular Findings in Relapsing, Remitting Multiple Sclerosis: A Study of thirty patients. *International Tinnitus Journal*, 2008; 14(2): 139-144.
22. Aydın Cantürk İ, Mutlu BÖ, Yılmaz O, Bayazıt YA. Peripheral Vestibular System Involvement in Multiple Sclerosis and Associations with the Disease Severity. *ORL J Otorhinolaryngol Relat Spec*. 2023;85(3):150-155.
23. Pavlović I, Ruška B, Pavičić T, Krbot Skorić M, Crnošija L, Adamec I, Habek M. Video head impulse test can detect brainstem dysfunction in multiple sclerosis. *Mult Scler Relat Disord*. 2017 May; 14:68-71.

Research Article

THE UTILITY OF HEMATOLOGICAL INDICES AT THE INITIAL ADMISSION TO THE NEUROSURGERY CLINIC IN CERVICAL DISC HERNIATION

 Havva Yasemin ÇİNPOLAT ^{1*},  Ali AKAR ²,  Ümit Ali MALÇOK ²,  Sevil ALKAN ³

¹Çanakkale Onsekiz Mart University Faculty of Medicine Department of Medical Biochemistry, Çanakkale, TURKIYE

²Çanakkale Onsekiz Mart University Faculty of Medicine Department of Neurosurgery, Çanakkale, TURKIYE

³Çanakkale Onsekiz Mart University Faculty of Medicine Department of Infectious Diseases and Clinical Microbiology, Çanakkale, TURKIYE

*Correspondence: yaseminarattan@gmail.com

ABSTRACT

Objective: This study aimed to investigate hematological indices to predict spontaneous regression in patients with cervical disc herniation (CDH) during the initial visit to outpatient clinics.

Materials and Methods: This retrospective study was carried out at a single center by reviewing laboratory parameters to assess the outcomes of CDH patients. The cohort consisted of patients with CDH who had undergone surgery, those who had undergone conservative treatment and achieved spontaneous regression, and a control group without CDH. The laboratory data consisted of the neutrophil-to-lymphocyte ratio (NLR), monocyte-to-lymphocyte ratio (MLR), and systemic immune-inflammatory index (SIII).

Results: Differences in the NLR, MLR, and SIII were statistically significant across groups ($p < 0.001$). Compared with the spontaneous regression and control groups, the surgical intervention group presented significantly greater NLR, MLR, and SIII values. According to the comparison of the patients with CDH in terms of the level of herniation, there were no significant differences at the C4-C5 and upper levels, whereas there was a statistically significant increase in the NLR, MLR, and SIII in the surgical intervention group compared with the spontaneous regression group at the C6-C7 level ($p = 0.015$, $p < 0.001$, and $p = 0.003$, respectively).

Conclusion: This study provides valuable insights into the use of hematological indices to predict the need for surgical intervention in CDH patients. The observed associations emphasize their practical use, providing a way for further research and their inclusion in routine diagnostic protocols for CDH management.

Keywords: cervical disc herniation, inflammation, systemic immune-inflammatory index, neutrophil-to-lymphocyte ratio, monocyte-to-lymphocyte ratio

Received: 01 October 2024
Revised: 09 November 2024
Accepted: 11 November 2024
Published: 22 December 2024



Copyright: © 2024 by the authors. Published Aydın Adnan Menderes University, Faculty of Medicine and Faculty of Dentistry. This is an open access article under the Creative Commons Attribution Non Commercial 4.0 International (CC BY-NC 4.0) License.

INTRODUCTION

Cervical radiculopathy refers to functional impairment in a specific area of the upper extremity caused by irritation or compression of the cervical spinal nerve root. Cervical disc herniation (CDH), or cervical disc disease, is the disturbance and displacement of the gel-like disc structure located between the cervical vertebrae, causing compression in the spinal canal and foramina. There are 85 cases of cervical radiculopathy per 100,000 people worldwide, and 20–25% of these cases are caused by CDH (1). Cervical radiculopathy is more commonly observed in males, peaking between 50 and 54 years of age. Patients who have chronic pain that is resistant to medical treatment for longer than six weeks and who also experience weakness in their arms and legs as a result of the involvement of arm-extending nerves necessitate surgery (2). Although spontaneous regression is a common occurrence in the lumbar area, it has also been noted to occur in the cervical region, with a rate of approximately 40% for improving CDH (3, 4). Three mechanisms for spontaneous regression have been described in the literature. First, the herniated portion progressively loses water content, contracts, and withdraws into the intervertebral space. Second, the herniation is helped to retract by the posterior longitudinal ligament, which is situated between the cartilaginous tissue and the spinal canal. Third, when the herniation advances into the epidural region, an inflammatory reaction results in enzymatic breakdown and phagocytosis, which slow cartilaginous tissue absorption and encourage neovascularization. According to several recent articles, the third mechanism is more likely to be the dominant process (5-8). The intriguing interaction of inflammatory responses resulting in enzymatic breakdown and neovascularization are some of the proposed mechanisms that hold great promise for further investigation in the field of spinal health research. Understanding the intricate underpinnings of these systems may provide new insights into therapeutic targets and treatment approaches for people with such diseases.

The subparameters of the hemogram, such as the neutrophil, lymphocyte, monocyte, and platelet counts, can be used to determine a variety of different ratios that can be used to assess inflammation and the immune response. Hematologically calculated indices depict a wide range of immune pathways and cell functions (9, 10). These calculated indices offer important information about the inflammatory and immunological conditions of patients. These ratios may help with the diagnosis, prognosis, and follow-up of

various diseases and conditions marked by altered immune responses and inflammation by revealing the balance and interactions between various immune cell populations. As a result, the hemogram and the ratios derived from it are extremely important in clinical practice, helping medical professionals make wise decisions and provide individualized patient care (11, 12). The neutrophil-to-lymphocyte ratio (NLR), monocyte-to-lymphocyte ratio (MLR), platelet-to-lymphocyte ratio (PLR), and systemic immune-inflammatory index (SII) are all signs of systemic inflammation in a number of diseases (13, 14).

The goal of this study was to ascertain whether the NLR, MLR, PLR, and SII parameters might be used to predict spontaneous regression in patients with CDH at the time of their initial admission to the neurosurgical clinic.

MATERIALS AND METHODS

This study was designed retrospectively and conducted in a single center at Çanakkale Onsekiz Mart University Hospital. The scientific ethics committee of Çanakkale Onsekiz Mart University approved the study with a decision dated May 4, 2023, and numbered 06/16, and it was then carried out under the principles of the Helsinki Declaration.

Patient selection

Patients with CDH who attended the neurosurgery outpatient clinics at Çanakkale Onsekiz Mart University Hospital between April 1, 2020, and April 1, 2023, made up all of the study participants over the age of 18. Three groups of patients were formed by scanning hospital archive records. The first group consisted of patients who underwent single-level anterior microdiscectomy due to CDH. Patients with CDH who were eligible for single-level surgery but were unable to undergo surgery were included in the second group. During normal follow-up, however, they exhibited spontaneous regression with medical treatment. The control group included patients who complained of neck pain at the time of admission, had routine blood tests, and had no evidence of CDH on cervical magnetic resonance imaging (MRI). The exclusion criteria for

the study included those with cervical spondylosis, those with a history of previous spinal surgery, multilevel CDH, diabetes mellitus, active infections, rheumatological conditions, cervical spondylotic myelopathy, chronic obstructive pulmonary disease, osteoporosis, malignancy, hypertension, and cardiovascular disease. The control group was subjected to the same exclusion criteria. The demographic details of the patients, including age, sex, clinical findings, cause of surgery, type of surgery, and hemogram parameters, were retrieved from the hospital's medical records.

Laboratory analysis

For the surgical intervention, spontaneous regression, and control groups, laboratory data were gathered at the time of the patient's initial admission to the outpatient clinic without the use of any analgesics, anti-inflammatory medications, or muscle relaxants for the management and treatment of pain. The complete blood cells were analyzed on a Mindray BC6200 automated hematology analyzer (Mindray Biomedical Electronics, Shenzhen, China). To determine the NLR, MLR, and PLR, the absolute neutrophil count was divided by the absolute lymphocyte count. The same was done for the absolute monocyte cell counts by the absolute lymphocyte cell counts, and so on for the absolute platelet cell counts by the absolute lymphocyte cell counts. The SIII was calculated with the following formula: $\text{platelet count} \times \text{neutrophil count} / \text{lymphocyte count}$.

Statistical analysis

The total sample size needed to reach 80% power with a 95% confidence interval and a 0.25 effect size was 159 cases, according to the G*Power program (v3.1.9.7). SPSS v17.0 (SPSS for Windows, Chicago, IL, USA) and Jamovi Project v2.3 (2022) were used to carry out the statistical analyses. The Shapiro–Wilk test was used to check whether the data distribution was normal. The median (1st quartile–3rd quartile) was used to represent continuous data without a normal distribution, and the mean \pm standard deviation (SD) was used to represent data with a normal distribution. Numbers (percentages) were used to summarize categorical variables, and the chi-square test or Fischer's exact test was used to compare them. One-way analysis of

variance for parametric data was used to compare the differences between groups. The homogeneity of variances was tested with Levene's test. Tukey's test or the Games-Howell test was used for post hoc analysis. Kruskal-Wallis and Dwass-Steel-Critchlow-Fligner pairwise comparisons were used for nonparametric data. Independent sample t tests or Mann-Whitney U tests were used to compare the surgical intervention and spontaneous regression groups according to the level of herniation. The cutoff values of the NLR, MLR, and SIII were detected via receiver operating characteristic (ROC) analysis, and the area under the curve (AUC) values were calculated. The effect size was calculated for the identified differences in the analyses and interpreted according to Cohen's (1988) classification. A p value of less than 0.05 was used to indicate statistical significance.

RESULTS

Table 1. Demographic results of participants

Variable	Surgical intervention (n=64)	Spontaneous regression (n=64)	Control (n=65)	p-value*
Age, years	47 (42-57)	44 (39-50)	43 (38-52)	0.054
Gender				0.851
Female, n (%)	31 (48.4%)	34 (53.1%)	32 (49.2%)	
Male, n (%)	33 (51.6%)	30 (46.9%)	33 (50.8%)	
Level of herniation				0.741
C3-C5**, n (%)	11 (17.2%)	12 (18.8%)		
C5-C6, n (%)	32 (50.0%)	35 (54.7%)		
C6-C7, n (%)	21 (32.8%)	17 (26.6%)		

*p<0.05 was considered significant. **C3-C5 represents C3-C4 and C4-C5 levels of herniation. Continuous data was expressed as the median (1st quartile-3rd quartile). Categorical data was expressed as number (percentage).

There were 64 (33.2%) patients who underwent surgery for CDH in the surgical intervention group, and the same quantity was true in the spontaneous regression group. The control group consisted of 65 (33.6%) patients. Among the participants, 96 (49.7%) were male. Among the males, 33 (51.6%) were in the surgical intervention group, 30 (46.9%) were in the spontaneous regression group, and 33 (50.8%) were in the control group. All the patients with CDH presented with single-level herniation. Tables 1 and 2 present participant demographics along with laboratory findings.

Table 2. Test results of participants in surgical treatment, spontaneous regression, and control groups

Parameters	Surgical intervention (n=64)	Spontaneous regression (n=64)	Control (n=65)	p value*	Effect size**
NLR	2.42±0.79	1.95±0.57	1.93±0.44	<0.001	0.120
MLR	0.27 (0.21-0.34)	0.20 (0.17-0.23)	0.19 (0.17-0.22)	<0.001	0.274
PLR	126 (103-159)	123 (105-148)	130 (106-157)	0.574	0.009
SIII	630±156	541±193	522±159	<0.001	0.073

*p<0.05 was considered significant. ** η^2 was used for effect size. η^2 results represented 0.14 large, 0.06 medium and 0.01 small effects. Normally distributed data was expressed as the mean ± standard deviation. Non-normally distributed data were expressed as the median (1st quartile-3rd quartile). NLR, neutrophil-to-lymphocyte ratio; MLR, monocyte-to-lymphocyte ratio; PLR, platelet-to-lymphocyte ratio; SIII, systemic immune-inflammatory index

The NLR, MLR, and SIII were significantly different ($p<0.001$) between the groups, whereas the PLR did not differ between the groups ($p=0.574$). A moderate effect size was observed for the NLR and SIII, whereas a large effect size was observed for the MLR. The differences in the NLR, MLR, and SIII between the spontaneous regression group and the control group were not statistically significant ($p=0.971$, $p=0.831$, and $p=0.804$, respectively). Compared with those in the spontaneous regression group, the NLR, MLR, and SIII in the surgical intervention group were significantly greater ($p<0.001$, $p<0.001$, and $p=0.009$, respectively). The NLR, MLR, and SIII were significantly greater in the surgical intervention group than in the control group ($p<0.001$) (Figure 1a-c).

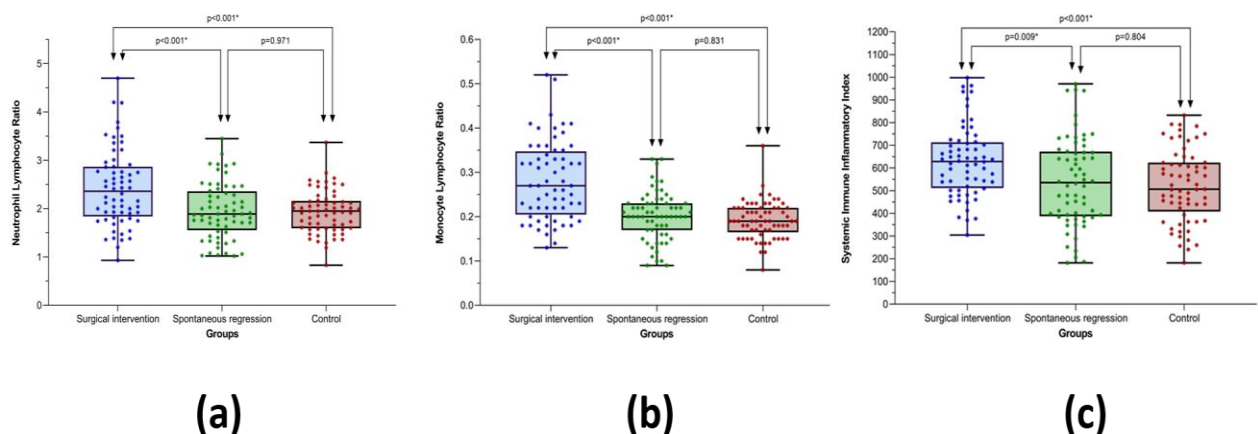


Figure 1. (a) Neutrophil-to-lymphocyte ratios in the surgical treatment, spontaneous regression and control groups, (b) Monocyte-to-lymphocyte ratios in the surgical treatment, spontaneous regression and control groups, (c) Systemic immune inflammatory index in the surgical treatment, spontaneous regression and control groups

When the surgical intervention and spontaneous regression groups were compared according to the level of herniation, no statistically significant difference was observed in any parameter at the C4-C5 and upper levels ($p < 0.05$). When the two groups were compared at the C5-C6 level, the surgical intervention group had significantly greater NLRs and MLRs ($p = 0.002$, and $p < 0.001$, respectively). At the C6-C7 level, compared with those in the spontaneous regression group, the NLR, MLR, and SIII in the surgical intervention group were significantly greater ($p = 0.015$, $p < 0.001$, and $p = 0.003$, respectively) (Table 3). The ROC analysis revealed that the NLR cutoff value for predicting surgery was 2.51, with an AUC of 0.683 (95% CI 0.600–0.767) and values of 43.8% for sensitivity, 87.6% for specificity, 63.6% for positive predictive value (PPV), and 75.8% for negative predictive value (NPV). The MLR had a cutoff value of 0.25 and an AUC of 0.778 (95% CI 0.704- 0.852), with a sensitivity of 57.8%, a specificity of 89.9%, a PPV of 74%, and an NPV of 81.1%. A cutoff value of 447 with a sensitivity of 92.2%, a specificity of 35.7%, a PPV of 41.5%, and an NPV of 90.2% was found for SIII (AUC=0.658, 95% CI 0.581- 0.736). The findings of the ROC curve analysis are summarized in Table 4, and Figure 1(c) illustrates the ROC curve analysis of the NLR, MLR and SIII for predicting surgical intervention.

Table 3. Test results of the patients in surgical treatment and spontaneous regression groups according to herniation level

Parameters	Herniation level	Surgical intervention	Spontaneous regression	p value*
NLR	C3-C5**	2.05 (1.79-2.30)	2.09 (1.80-2.31)	1.000
	C5-C6	2.40±0.59	1.97±0.54	0.002
	C6-C7	2.52 (1.75-3.48)	1.76 (1.33-2.15)	0.015
MLR	C3-C5**	0.22 (0.19-0.25)	0.22 (0.17-0.26)	1.000
	C5-C6	0.28±0.08	0.19±0.05	<0.001
	C6-C7	0.32 (0.22-0.36)	0.21 (0.20-0.23)	<0.001
PLR	C3-C5**	124 (108-136)	111 (105-136)	0.712
	C5-C6	121 (103-150)	122 (103-145)	0.821
	C6-C7	138 (109-169)	126 (107-156)	0.411
SIII	C3-C5**	615 (511-685)	595 (516-668)	0.880
	C5-C6	628±162	551±199	0.087
	C6-C7	647 (552-720)	453 (346-672)	0.003

* $p < 0.05$ was considered significant. **C3-C5 represents C3-C4 and C4-C5 levels of herniation. Normally distributed data was expressed as the mean ± standard deviation. Non-normally distributed data were expressed as the median (1st quartile-3rd quartile). NLR, neutrophil-to-lymphocyte ratio; MLR, monocyte-to-lymphocyte ratio; PLR, platelet-to-lymphocyte ratio; SIII, systemic immune-inflammatory index

Table 4. ROC analysis of NLR, MLR and SIII to predict the surgery indication at first admission

Parameters	Cutoff	AUC	95% CI	Sensitivity	Specificity	PPV	NPV	p value
NLR	2.51	0.683	0.600-0.767	43.8%	87.6%	63.6%	75.8%	<0.001
MLR	0.25	0.778	0.704-0.852	57.8%	89.9%	74.0%	81.1%	<0.001
SIII	447	0.658	0.581-0.736	92.2%	35.7%	41.5%	90.2%	<0.001

ROC, receiver operating characteristics; NLR, neutrophil-to-lymphocyte ratio; MLR, monocyte-to-lymphocyte ratio; SIII, systemic immune-inflammatory index; AUC, area under curve; CI, confidence intervals; PPV, positive predictive value; NPV, negative predictive value

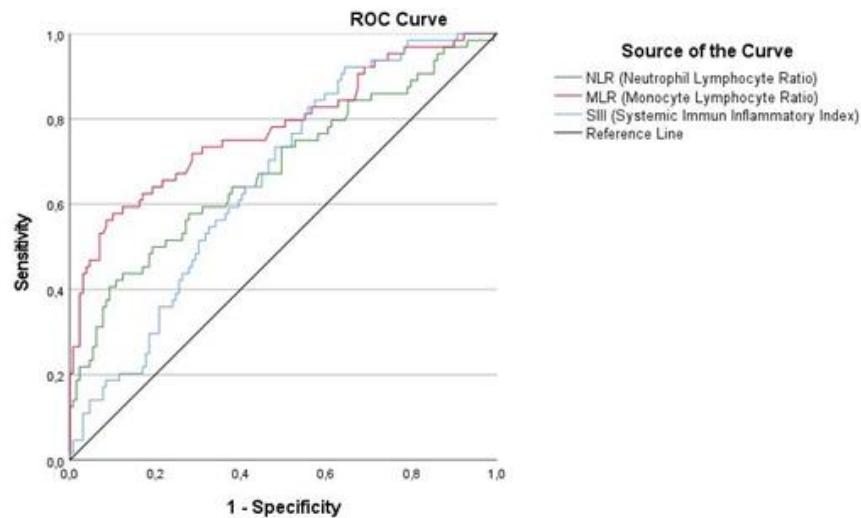


Figure 2 Receiver operating characteristic curves of the neutrophil-to-lymphocyte ratio, monocyte-to-lymphocyte ratio, and systemic immune-inflammatory index

DISCUSSION

This study provides valuable insights into the potential clinical usefulness of inflammatory markers, particularly the NLR, MLR, and SIII, in determining the most suitable treatment approach for CDH. This study aimed to investigate noninvasive and easily accessible biomarkers that could assist in predicting the clinical outcomes of CDH, particularly in determining the necessity of surgical intervention or the option of medical follow-up. In accordance with the currently available literature, this study is the first to investigate hematological indices to predict spontaneous regression in CDH patients.

The pathogenesis of numerous spinal disorders involves inflammation to varying degrees. Although previously believed to be primarily mechanical or degenerative, inflammation is also present in conditions

such as disc herniation (15). Although inflammation has historically been thought of predominantly as detrimental and linked to the evolution of the disease, it is still unclear whether it is a cause or an effect of intervertebral disc degeneration and herniation. As recently proposed for other tissues, restoring intervertebral disc degeneration function may necessitate a balanced inflammatory response (16, 17). Induced degenerative discs release proinflammatory chemokines, chemokine ligand 5, and chemokine ligand 6. Chemokine ligand 5 has been associated with discogenic back pain (18). Xue et al. compared 34 patients with lumbar disc herniation (LDH) and 20 healthy controls and reported that LDH patients had significantly elevated serum levels of interleukin (IL)-21 and IL-17 compared with healthy controls. Disc tissues from individuals with LDH exhibited elevated expression levels of IL-21, IL-17, and cyclooxygenase-2 (19). Kang et al. revealed that the levels of nitric oxide, IL-1, IL-6, and tumor necrosis factor alpha were significantly greater in the cervical disc tissues of patients suffering from discogenic neck pain than in those of symptomatic and healthy controls (20).

However, the process of testing these markers is more complex, costly, and uncommon for use daily. In contrast, we used SIII, NLR, and MLR values calculated from hemogram tests in our study to measure inflammation in CDH patients. The distinct patient groups presented significant differences in the NLR, MLR, and SIII, indicating the potential value of these inflammatory markers in identifying CDH-related variations. The effect size analyses, which range from moderate to high, highlight the robustness of these associations and emphasize their clinical importance. Group comparisons between surgical intervention and spontaneous regression, as well as between surgical intervention and control groups, revealed specific patterns in these inflammatory markers. In contrast to the spontaneous regression and control groups, the surgical intervention group presented notable increases in the NLR, MLR, and SIII. Upon eliminating potential inflammatory diseases, the NLR and MLR had specificities of over 87% for both indices at the optimal cutoff values for predicting surgical intervention, as determined by ROC analysis. Despite the low specificity of SIII, it exhibited a sensitivity of 92.2%. These results imply that these markers may serve as indicators necessitating surgical intervention, offering clinical decision-makers useful information at initial patient admission.

Several studies have investigated the relationships between inflammatory biomarkers and LDH in the literature. Yilmaz et al. recently reported that the NLR was a standalone predictor in patients with LDH and low back pain (21). Similarly, a study by Bozkurt et al. revealed that patients with LDH had more pain before and after surgery, especially when their NLRs were higher, which is a known sign of inflammation (22). In contrast to controls, Sugimori et al. reported that patients with LDH had significantly higher mean levels of high-sensitivity CRP. Notably, they reported no discernible association between the level of herniation in question and high-sensitivity CRP levels (23).

Studies examining CDH and inflammation, however, are relatively uncommon. Previously, 126 individuals with neck pain were examined, and particular characteristics were identified in patients with CDH. The CDH group presented significantly greater leucocyte counts, neutrophil counts, NLRs, and C-reactive protein (CRP) levels than did the normal cervical MRI patients with neck pain and healthy controls. Notably, multilevel CDH patients had a significantly greater NLR than controls did. These results suggest a link between the development of CDH and the inflammatory response. Higher NLRs and CRP levels may act as warning signs and prompt early protective measures against disc degeneration and CDH. The importance of these inflammatory markers in understanding and perhaps lowering the risk of CDH is emphasized by the few comparable studies that have been carried out (24). Our study differs from other previously published studies in that it makes comparisons on the basis of the CDH level. The lack of significant differences at the C4-C5 and upper levels and the distinct variations at the C5-C6 and C6-C7 levels highlight the importance of considering specific anatomical locations in the assessment of CDH. These results suggest that herniation at C4-C5 and upper levels is most likely related to a mechanical or degenerative etiology, whereas herniation at lower levels is likely to have an inflammatory etiology.

The study's limited sample size and retrospective approach were the primary limitations. Even though we excluded patients with acute and chronic inflammatory diseases from the study during the patient selection process, the study's findings might have been impacted by an inflammatory condition that the patient may have had but did not disclose in the archived records. Another drawback of this study was the lack of

access to postoperative follow-up tests to examine the status of systemic inflammatory responses in CDH patients in the surgical intervention and spontaneous regression groups.

CONCLUSION

This study offers critical new understanding of the diagnostic potential of inflammatory markers, particularly the NLR, MLR, and SIII, in determining whether surgical intervention in CDH patients is likely. These markers are candidates to become helpful parameters in clinical decision-making and provide clinicians with more tools to customize patient care in the context of CDH. Although more research is necessary to validate and improve these findings, the observed associations highlight their clinical relevance and suggest potential integration into routine diagnostic protocols for CDH management.

Acknowledgments

The authors thank Assoc. Prof. Dr. Çetin Toraman contributed to the statistical analyses.

Authorship contributions

Surgical and medical practices: AA, ÜAM; Concept: HYÇ, AA; Design: HYÇ, AA; Data collection and processing: HYÇ, ÜAM, SA; Analysis and interpretation: HYÇ; Literature search: AA, ÜAM, SA; Writing: HYÇ, SA, AA

Data availability statement

The data of the study will be provided by the corresponding author upon request.

Declaration of competing interest

The authors have no conflicts of interest to declare.

Ethics

The scientific ethics committee of Çanakkale Onsekiz Mart University approved the study, with the decision dated 04.05.2023 and numbered 06/16.

Funding

There was no organization funding for this study.

REFERENCES

1. Bhaganagare AS, Nagesh SA, Shrihari BG, Naik V, Nagarjun MN, Pai BS. Management of cervical monoradiculopathy due to prolapsed intervertebral disc, an institutional experience. *J Craniovertebr Junction Spine* 2017;8(2):132-5.
2. Woods BI, Hilibrand AS. Cervical radiculopathy: epidemiology, etiology, diagnosis, and treatment. *J Spinal Disord Tech* 2015;28(5):E251-9.
3. Yoon WW, Koch J. Herniated discs: when is surgery necessary? *EFORT Open Rev* 2021;6(6):526-30.
4. Orief T, Orz Y, Attia W, Almusrea K. Spontaneous resorption of sequestered intervertebral disc herniation. *World Neurosurg* 2012;77(1):146-52.
5. Henmi T, Sairyo K, Nakano S, Kanematsu Y, Kajikawa T, Katoh S, et al. Natural history of extruded lumbar intervertebral disc herniation. *J Med Investig* 2002;49(1-2):40-3.
6. Turk O, Yaldiz C. Spontaneous regression of cervical discs: Retrospective analysis of 14 cases. *Medicine (Baltimore)* 2019;98(7):e14521.
7. Saal JS, Saal JA, Yurth EF. Nonoperative management of herniated cervical intervertebral disc with radiculopathy. *Spine (Phila Pa 1976)* 1996;21(16):1877-83.
8. Aljohani S, Alshantiti M, Alzahrani M. Unexpected Recovery: A Report on the Spontaneous Regression of a Herniated Cervical Disc. *Cureus* 2023;15(7):e41429.
9. Han LH, Jia YB, Song QX, Wang JB, Wang NN, Cheng YF. Prognostic significance of preoperative lymphocyte-monocyte ratio in patients with resectable esophageal squamous cell carcinoma. *Asian Pac J Cancer Prev* 2015;16(6):2245-50.
10. Ustundag Y, Demir C, Demir M, Huysal K, Yesil MR, Karaca MS. The relationship between serum vitamin D levels and hematological inflammatory indices in patients with heart failure. *Int J Med Biochem* 2024;7(1):1-5.
11. Fan Z, Ji H, Li Y, Jian X, Li L, Liu T. Relationship between monocyte-to-lymphocyte ratio and coronary plaque vulnerability in patients with stable angina. *Biomark Med* 2017;11(11):979-90.
12. Geng Y, Zhu D, Wu C, Wu J, Wang Q, Li R, et al. A novel systemic inflammation response index (SIRI) for predicting postoperative survival of patients with esophageal squamous cell carcinoma. *Int Immunopharmacol* 2018;65:503-10.
13. Xie QK, Chen P, Hu WM, Sun P, He WZ, Jiang C, et al. The systemic immune-inflammation index is an independent predictor of survival for metastatic colorectal cancer and its association with the lymphocytic response to the tumor. *J Transl Med* 2018;16(1):273.
14. Fu H, Qin B, Hu Z, Ma N, Yang M, Wei T, et al. Neutrophil-and platelet-to-lymphocyte ratio are correlated with disease activity in rheumatoid arthritis. *Clin Lab* 2015;61(3-4):269-73.
15. Roberts S, Butler RC. Inflammatory mediators as potential therapeutic targets in the spine. *Curr Drug Targets Inflamm Allergy* 2005;4(2):257-66.
16. Sun Z, Zhang M, Zhao XH, Liu ZH, Gao Y, Samartzis D, et al. Immune cascades in human intervertebral disc: the pros and cons. *Int J Clin Exp Pathol* 2013;6(6):1009-14.
17. Santos SG, Lamghari M, Almeida CR, Oliveira MI, Neves N, Ribeiro AC, et al. Adsorbed fibrinogen leads to improved bone regeneration and correlates with differences in the systemic immune response. *Acta Biomater* 2013;9(7):7209-17.
18. Grad S, Bow C, Karppinen J, Luk KD, Cheung KM, Alini M, et al. Systemic blood plasma CCL5 and CXCL6: Potential biomarkers for human lumbar disc degeneration. *Eur Cell Mater* 2016;31:1-10.
19. Xue H, Yao Y, Wang X, Zhang F, Jiang X, Liu J, et al. Interleukin-21 Is Associated with the Pathogenesis of Lumbar Disc Herniation. *Iran J Allergy Asthma Immunol* 2015;14(5):509-18.
20. Kang X, Qian M, Qin T, Liu M, Xu H, Xu B. Increased Expression of Inflammatory Cytokines and Discogenic Neck Pain. *Orthop Surg*. 2024 Jan;16(1):227-233.
21. Yılmaz A, Altaş H, Yıldırım T, Kaygısız Ş, Işık HS. The clinical predictive value of the neutrophil to lymphocyte ratio as a biomarker in lumbar disc herniation. *Middle Black Sea J Health Sci* 2019;5(2):145-50.
22. Bozkurt H, Arac D, Cigdem B. Effect of Preoperative Uric Acid Level and Neutrophil/Lymphocyte Ratio on Preoperative and Postoperative Visual Analog Pain Scores in Patients with Lumbar Disc Herniation: A Cross-Sectional Study. *Turk Neurosurg* 2019;29(5):705-9.
23. Sugimori K, Kawaguchi Y, Morita M, Kitajima I, Kimura T. High-sensitivity analysis of serum C-reactive protein in young patients with lumbar disc herniation. *J Bone Joint Surg Br* 2003;85(8):1151-4.
24. Ethemoglu KB, Erkoç YS. Is There Any Relationship between Cervical Disc Herniation and the Blood Inflammatory Response? *Cureus* 2020;12(8):e10161.

Research Article

HIGH PREVALENCE OF TRANSFERABLE INTEGRON-ASSOCIATED DRUG RESISTANCE IN *Escherichia coli* STRAINS ISOLATED FROM BLOOD CULTURES IN A UNIVERSITY HOSPITAL IN TRABZON, TURKEY

 Ahu REİS ¹,  Osman Birol ÖZGÜMÜŞ ²,  Erva RAKICI ²,  İnci DURUKAN ¹,
 Celal Kurtuluş BURUK ¹,  Gülçin BAYRAMOĞLU ¹,  Ali Osman KILIÇ ¹

¹ Department of Medical Microbiology, Faculty of Medicine, Karadeniz Technical University, Trabzon, TURKIYE

² Department of Medical Microbiology, Faculty of Medicine, Recep Tayyip Erdogan University, Rize, TURKIYE

*Correspondence: akilic@ktu.edu.tr

ABSTRACT

Objective: This study aimed to determine the carriage of transferable integron-associated drug resistance in *Escherichia coli* (*E. coli*) strains isolated from blood cultures.

Materials and Methods: A total of 111 *E. coli* isolates were included in this study. Antimicrobial susceptibility testing of the isolates against 17 antibiotics was performed using an automated microbiology system. Integron-specific polymerase chain reactions (PCR) were used to detect the presence of integrons. The antibiotic resistance gene cassettes in the variable regions of integrons were analyzed by DNA sequencing. Plasmid transfer assays were performed using the broth mating method. The clonal relationships among integron-carrying strains were evaluated by pulsed-field gel electrophoresis (PFGE).

Results: Resistance rates to antibiotics ranged from 0.9% to 63%. Thirty-eight strains carried gene cassettes encoding *dfrA7*, *dfr17-aadA5*, *dfrV*, *dfrA1-aadA1*, and *dfrA12-aadA2*. Seven strains possessed class 2 integrons with gene arrays *dfrA1-sat2-aadA1* and *dfrA1-sat2-aadA30*. Twenty-two integron-carrying isolates harbored conjugative resistance plasmids, three of which were identified as belonging to the IncN group. Two strains with class 1 integrons, isolated from different clinics, exhibited similar patterns in the PFGE analysis.

Conclusion: Approximately 50% of *E. coli* isolates from blood cultures at our hospital were found to carry integron-associated transferable drug resistance, suggesting their potential role in the horizontal dissemination of resistance genes. Further research is needed to understand the prevalence of *E. coli* strains of blood origin and the role of integrons and gene cassette arrays in the spread of resistance.

Keywords: *Escherichia coli*, Gene Cassette, Integron, Conjugation, Plasmid

Received: 01 October 2024
Revised: 02 December 2024
Accepted: 04 December 2024
Published: 22 December 2024



Copyright: © 2024 by the authors. Published Aydın Adnan Menderes University, Faculty of Medicine and Faculty of Dentistry. This is an open access article under the Creative Commons Attribution Non-Commercial 4.0 International (CC BY-NC 4.0) License.

INTRODUCTION

Bloodstream infections (BSIs) are among the most significant nosocomial infections, contributing to increased mortality and morbidity due to rising antimicrobial resistance (1). *Escherichia coli*, an opportunistic pathogen, is capable of causing a wide range of infections, from those in the gastrointestinal tract to extraintestinal infections, such as those affecting the central nervous system, urinary tract, and bloodstream. Globally, it is a leading cause of bloodstream infections and exhibits resistance to many drugs (2). While most bacterial infections are treatable with antibiotics, *E. coli* and other pathogens can rapidly develop antibiotic resistance, making infections more difficult to manage and potentially life-threatening (3). The excessive and inappropriate use of antimicrobials accelerates the emergence and spread of resistance. Therefore, the timely and effective use of antimicrobial drugs is essential in preventing resistance (4). Bacteria can develop resistance to antibiotics through genetic mechanisms involving mobile genetic elements (MGEs), such as plasmids, transposons (Tn), insertion sequences (IS), and integrons. Integrons, especially those located on plasmids or transposons, play a critical role in disseminating antimicrobial resistance genes, particularly in gram-negative bacteria. These integrons carry drug-resistant genes and facilitate the exchange of genetic elements. They are classified based on the sequence of *intI* gene, with classes 1 and 2 being the most prevalent (5).

The class 1 integrons consist of two conserved regions namely 5' (5'CS) and 3' (3'CS), and a variable region (VR) containing gene cassettes. The 5'CS includes the integrase gene (*intI*), which encodes the tyrosine recombinase enzyme, the recombination site (*attI*), and a promoter (P) region involved in the expression of inserted genes or gene cassettes. The 3'CS contains the defective quaternary ammonium resistance gene (*qacEΔ1*) and the *sulI* gene, which mediates resistance to sulfonamides. The variable region, located between these two conserved regions, contains the *attC* site, where various antibiotic resistance cassettes are integrated via recombination. Unlike class 1 integrons, class 2 integrons lack *sul* genes and typically include resistance gene cassettes such as *dfra1*, *sat2*, and *aadA1*, which confer resistance to aminoglycosides and sulfamethoxazole (6).

Although several studies in Turkey have investigated integron-associated drug resistance in *E. coli* isolates from urine samples (7, 11), very few reports are available (12) on the *E. coli* isolates from blood samples.

This study aimed to identify transferable integron-associated drug resistance in *E. coli* strains isolated from patients in various clinics.

MATERIALS AND METHODS

Sampling, isolation and identification of bacterial strains

A total of 111 *E. coli* strains were isolated from hospitalized patients at Karadeniz Technical University's Medical Microbiology Laboratory between January and December 2014. The bacterial strains were cultured using 5% sheep blood agar and EMB agar. Conventional biochemical methods and MALDI-TOF MS (Microflex™, Bruker, Germany) were employed to confirm species-level identification.

Antimicrobial susceptibility testing

Antimicrobial susceptibility testing was performed using the Phoenix ID/AST automated microbiology system (Becton Dickinson Diagnostic Instrument Systems, Sparks, MD, USA), following the manufacturer's instructions. Antibiotic susceptibility test results were interpreted according to Clinical and Laboratory Standards Institute (CLSI) criteria. The isolates were tested for the following antibiotics: amikacin (AK), ampicillin/sulbactam (SAM), aztreonam (ATM), cefazolin (CZ), cefepime (FEP), cefoperazone/sulbactam (CES), cefoksitin (FOX), ceftazidime (CAZ), ceftriaxone (CRO), ciprofloxacin (CIP), ertapenem (ERT), gentamicin (CN), imipenem (IPM), levofloxacin (LEV), meropenem (MEM), piperacillin tazobactam (TZP) and trimethoprim/sulfamethoxazole (SXT). The susceptibility of isolates containing class 1 and class 2 integrons was determined using the disc diffusion method in accordance with CLSI criteria (13). Antibiotic discs (Oxoid, UK) containing ampicillin (10 µg), streptomycin (10 µg), tetracycline (30 µg), nalidixic acid (30 µg), and chloramphenicol (30 µg) were used for this purpose.

DNA isolation

DNA templates for polymerase chain reaction (PCR) were prepared using a modified boiling method based on the protocol by Perez et al (14). After washing, the supernatant was used as the DNA template for PCR analyses.

Detection of integron gene cassettes and integrase genes

To detect integron gene cassettes in *E. coli* isolates, specific primers were used: For class 1 integrons: *intI*-1F (GGTCAAGGATCTGGATTTGG) and *intI*-1R (ACATGCGTGTAATCATCGTC). For class 2 integrons: *intI*-2F (CACGGATATGCGACAAAAGGT) and *intI*-2R (GTAGCAAACGAGTGACGAAATG). To amplify the variable regions of the integrons, the following primers were used: For class 1 integrons: 5'-CS (GGCATCCAAGCAGCAAG) and 3'-CS (AAGCAGACTTGACCTGA). For class 2 integrons: hep51 (GATGCCATCGCAAGTACGAG) and hep74 (CGGGATCCCGGACGGATGCACGATTTGTA). PCR reaction conditions and compositions followed previously described methods (15).

DNA sequencing and data analysis

PCR products from class 1 and class 2 integrons were purified using the High Pure PCR Clean-up Micro Kit (Roche, Germany). Cloning was performed with the pGEM-T Easy Vector System (Promega, USA) and T4 DNA Ligase enzyme, following the manufacturer's guidelines as described by Sambrook et al. (16). After incubation, blue-white colony screening was used for selection. Plasmid DNA from selected white colonies was isolated using the alkaline lysis method (17). Recombinant plasmids carrying amplicons of class 1 and class 2 integrons were sequenced on an ABI 3130 Genetic Analyzer (Applied Biosystems, USA) using SP6 and T7 promoter primers. DNA sequence data were analyzed using BLAST (<http://www.ncbi.nlm.nih.gov/BLAST>) and CLUSTALW2 (<http://www.ebi.ac.uk/Tools/msa/clustalw2>) for sequence alignment and comparisons (18).

Conjugation experiment

Transfer experiments of plasmids from integron-containing isolates were performed based on the broth mating principle, which was previously described (19). *Escherichia coli* isolates containing integrons were used as donors, and *E. coli* J53-2 (met pro Rif^R) as the recipient cells. Broth cultures of both donor and recipient were mixed in equal volumes (1:1) and incubated for 20 hours at 37°C without shaking. Transconjugants were selected on LB agar supplemented with rifampicin (300 µg/mL), to which the recipient cells are resistant, and either trimethoprim (25 µg/mL) or streptomycin (100 µg/mL) to which the donor cells are resistant.

Isolation of plasmid DNA

A colony was picked from transconjugant plates and sub-cultured in 3 mL of LB broth at 150 rpm shaking at 37°C for 16-18 hours. A 1.5-ml aliquot of the overnight culture was centrifuged at 12,000 rpm to pellet the bacteria. The cells were lysed, and plasmid DNA was isolated using the standard alkali-lysis method. Finally, the pellet was dried at 37°C and resuspended in 30-40 µl of 1X TE buffer containing 0.5-1 µg/mL of RNase. Plasmid DNA was analyzed by electrophoresis, and visualized under a UV transilluminator (20).

PCR-based replicon typing

To identify the incompatibility (Inc) groups that contribute significantly to the dissemination of resistance genes, plasmids isolated from transconjugants were subjected to replicon typing using specific primers as described by Götz et al. (21).

Pulsed-field gel electrophoresis (PFGE)

Clonal relationship among 58 *E. coli* isolates containing integrase genes (*intI-1* and *intI-2*) belonging to class 1 and class 2 integrons were determined using the PFGE method, with modifications based on the studies of Durmaz et al. (22). PFGE was performed with the CHEF DR-III (Bio-Rad, USA) system using a 1% ultrapure agarose gel in 2L of 0.5X TBE. The gel was stained in a solution containing 10 mg/mL ethidium bromide for 30

minutes. Gel visualization and photography were conducted using the VersaDoc™ system, and images were analyzed with GelJ software, version 2.

Statistical analysis

Statistical analyses were performed using Pearson's Chi-square test and Fisher's Exact test with the Statistical Package for the Social Sciences (SPSS) version 23 for Windows. A p-value of < 0.05 was considered statistically significant.

RESULTS

Antimicrobial resistance phenotypes of *E. coli* isolates

Antimicrobial susceptibility tests for 111 *E. coli* isolates from blood cultures were performed using the Phoenix™ 100 device. The resistance rates of the isolates to 17 antibiotics are shown in Figure 1.

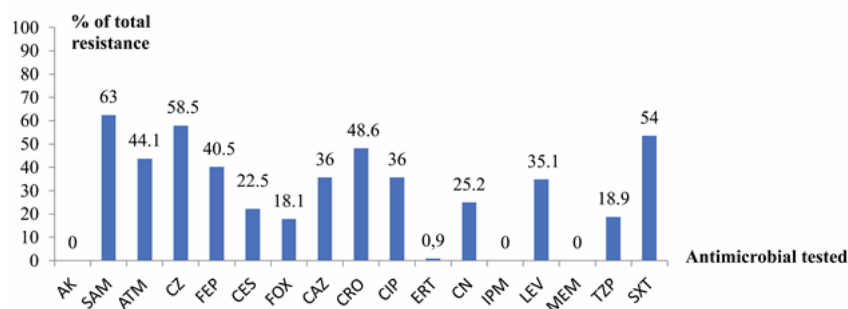


Figure 1. Total antimicrobial resistance rates of 111 clinical *Escherichia coli* isolates.

The highest resistance percentage was observed for SAM 63% (n=70), while the lowest was for ERT 0.9% (n=1). Resistance rates to other antibiotics were as follows: ATM 44.1% (n=49), CZ 58.5% (n=65), FEP 40.5% (n=45), CES 22.5% (n=25), FOX 18.1% (n=20), CAZ 36% (n=40), CRO 48.6% (n=54), CIP 36% (n=40), CN 25.2% (n=28), LEV 35.1% (n=39), TZP 18.9% (n=21), and SXT 54% (n=60). None of the isolates was resistant to AK, IPM, and MEM (Fig. 1). In a subset of 45 *E. coli* isolates with class 1 and class 2 integron gene cassettes, tested using the

disc diffusion method, resistance to ampicillin, streptomycin, and tetracycline was found to be 66.6% (n=30), while resistance to nalidixic acid was 64.4% (n=29). The lowest resistance rate was 26.6% (n=12) for chloramphenicol (Figure 2).

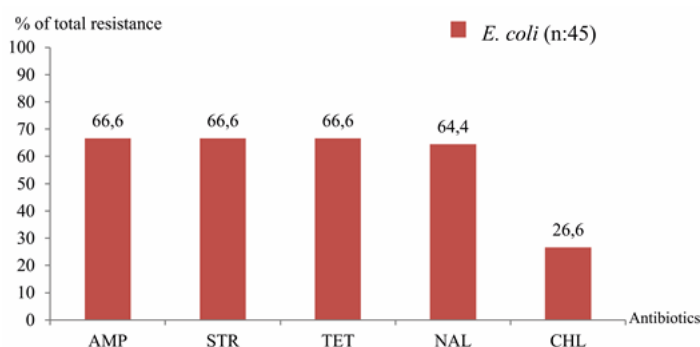


Figure 2. Total antimicrobial resistance rates of *E. coli* isolates containing class 1 and class 2 integrons.

Statistical analysis revealed significant differences in antimicrobial resistance between strains with and without class 1 and class 2 integrase genes for SAM, ATM, CZ, FEP, CAZ, CRO, CIP, and SXT ($p < 0.05$). However, no significant differences were observed for CES, FOX, ERT, CN, LEV, and TZP antibiotics ($p > 0.05$). Statistical analysis could not be conducted for AK, IPM, and MEM, as no resistant strains were found in either group.

PCR for integrons

A total of 111 *E. coli* isolates were screened for the presence of class 1 and class 2 integrase genes. Of these, 51 isolates (46%) were positive for class 1 integrase, and seven isolates (6%) were positive for class 2 integrase. PCR analysis of the variable region of class 1 integrons showed that 38 isolates (34%) contained class 1 integrons, while 13 isolates (11.7%) carried empty integrons. Class 2 integrons were detected in 7 isolates (6%) (Supplementary Table 1). Gene cassette arrays of 45 *E. coli* isolates with integrons were determined by DNA sequencing. Among 27 of the 38 isolates with class 1 integrons, five gene cassette arrays were identified: *dfrA7*, *dfr17-aadA5*, *dfrV*, *dfrA1-aadA1* ve *dfrA12-aadA2*, associated with trimethoprim and streptomycin-

spectinomycin resistances. These arrays ranged from 800-1800 bp in length. Gene cassette arrays could not be sequenced for 11 class 1 integrons due to technical difficulties of the unknown nature (TEC002, TEC005, TEC010, TEC015, TEC020, TEC043, TEC055, TEC057, TEC072, TEC078 and TEC091). For the seven isolates with class 2 integrons, two gene cassette arrays were identified: *dfrA1-sat2-aadA1* and *dfrA1-sat2-aadA30*, approximately 2500 bp in length. Sequencing was unsuccessful for three class 2 integrons (TEC012, TEC033, TEC081) (Supplementary Table 1).

Conjugation experiments

Plasmid transfer studies were executed on 45 *E. coli* isolates with integrons. Among these, 22 isolates (48.8%) carried conjugative plasmids larger than 100 kb. Conjugation frequency ranged from 10^{-9} to 10^{-8} . Transconjugants were validated genotypically using previously established PCR methods. PCR assays revealed that three plasmids (pTEC010, pTEC015 and pTEC075) belonged to the IncN group. No Inc P, IncQ, or IncW group plasmids were detected in any of the transconjugants (Supplementary Table 1).

Pulsed-field gel electrophoresis analysis

PFGE dendrogram analysis of 50 *E. coli* strains with integrons, their antibiotic resistance patterns, and sources shown in Figure 3. These strains were divided into 39 distinct groups, some of which were further subdivided into subgroups (A, B, C). Eleven subgroups (4, 7, 9, 10, 12, 13, 14, 16, 25, 35, 37) showed similarity rates above 80%. Subgroups 13 showed similarity rates exceeding 90%. Notably, strains TEC010 and TEC015 all carrying class 1 integrons, demonstrated high clonal similarity despite significant differences in their clinical origins and antibiotic resistance patterns. Eight strains were excluded from the analysis because the DNA pattern quality obtained as a result of PFGE experiments was not sufficient for dendrogram analysis.

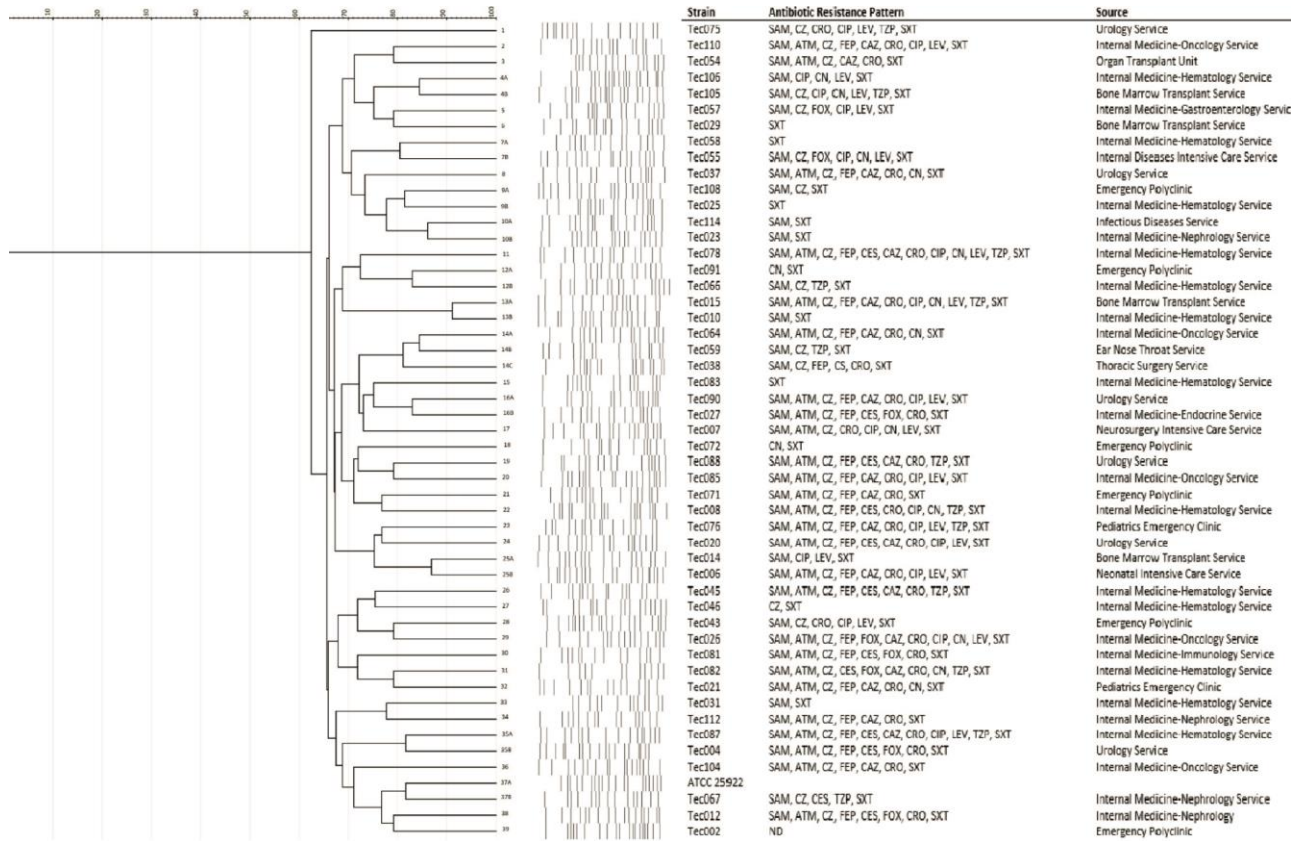


Figure 3. Dendrogram analysis of *E. coli* isolates containing class 1 and class 2 integrons

DISCUSSION

Infections caused by Gram-negative bacteria, such as septicemia, are significant contributors to mortality and morbidity. The isolation of bacteria, particularly from blood cultures, often indicates a severe invasive infection requiring immediate antimicrobial therapy. Among these, *E. coli* is one of the most commonly isolated pathogens from blood cultures. The World Health Organization (WHO) has identified *E. coli* as a priority pathogen of concern due to its role in the global development of antimicrobial resistance, especially infections affecting the blood and urinary tract. Antibiotic resistance presents a considerable challenge to public health. Accurate detection of resistant bacteria and determination of antimicrobial resistance, particularly in clinical laboratories, are therefore essential for enabling clinicians to administer effective antibiotic treatments (23, 24).

In our study, the antibiotic resistance patterns of *E. coli* from blood cultures were analyzed against 17 different antibiotics. Resistance rates were highest against SAM, CZ, CRO, and SXT, as also reported in the previous studies (25, 26). As a matter of fact, these antibiotics have historically been used extensively in the empirical treatment of sepsis and other infections (23). Our findings align with those of Kreidl et al. (27), who reported resistance rates of 71.8% against aminopenicillins and 37.5% against CIP. Furthermore, all *E. coli* isolates in our study were sensitive to AK and carbapenems (IPM and MEM), consistent with findings by Anvarinejad et al. (28).

Timely and accurate diagnosis and treatment are essential for mitigating the severe effects of sepsis and reducing mortality. Identifying common bacterial pathogens and their resistance patterns is crucial for guiding appropriate antimicrobial therapy. Ampicillin, nalidixic acid, SXT, and tetracyclines, widely used in both clinical and veterinary medicine (28), showed significant resistance in this study. Notably, strains with class 1 and class 2 integrons exhibited the highest resistance rates. These classes of integrons contain genes conferring resistance to trimethoprim and streptomycin. Class 1 integrons, in particular, harbor the *sul1* gene encoding sulfonamide resistance adjacent to the 3'-conserved region (29). Integrons are genetic elements that facilitate the capture, insertion, and exchange of antibiotic resistance gene cassettes, thereby playing a significant role in the dissemination of resistance genes, particularly among Gram-negative bacteria (30). The high prevalence of trimethoprim and streptomycin resistance in this study are thought to be resulted in the integrons containing various antibiotic gene cassette arrays.

Multidrug resistance in Enterobacterales is often associated with antimicrobial resistance genes carried by integrons (31). In Türkiye, numerous studies have focused on integrons in bacteria from clinical (32), animal (33), and aquatic (34) sources. Although there are some epidemiological studies in clinical bacteria, especially in urine samples (9), research on the molecular characterization of *E. coli* strains from blood samples remains limited. In this study, 46% (111/51) of isolates carried the *intI1* gene, with 38 isolates (34%) containing class 1 integrons, and 13 isolates (11.7%) having empty integrons. Additionally, 6% (111/7) of isolates carried the *intI2* gene, and all of these belong to class 2 integrons.

The frequency of the *intI1* gene (34%) observed in this study is comparable to findings by Liu et al. (35) (41.33%) but lower than results reported by Abdel-Rhman et al. (36) (98.33%) and Liu et al. (35) (67.39 %). The lower prevalence of class 1 integrons may be attributed to alternative resistance mechanisms, such as of beta-lactamase enzyme production, efflux pumps overexpression, reduced bacterial outer membrane permeability, and intrinsic resistance factors (37). Class 2 integrons were identified at a rate of 6%, consistent with Ahumado-Santos et al. (38), who reported a low prevalence (1.4%).

The predominance of class 1 integrons over class 2 integrons in our isolates is consistent with another study (11). Empty integrons found in 13 isolates may represent bacteria containing empty integrons are probably due to the presence of a very large gene cassette and the inability to amplify these gene cassettes (39, 40). We believe that the presence of empty integrons in bacteria could make these isolates have the potential to become multi-drug resistant by capturing antibiotic resistance genes from other bacteria in the hospital environment and spreading to the other bacteria of both commensal and clinical origin.

The presence of *dfrA* genes encoding trimethoprim resistance and *aad/aac* genes encoding aminoglycoside resistance has been widely reported (41, 42). Gene cassette arrays such as *dfrA1*, *dfrA5*, *aadA1*, and *aadA5* are common in clinical bacteria, as reported by Cicek et al. (8) and Sandalli et al. (7). The *dfrA17/aadA5* gene array, which confers resistance to trimethoprim and streptomycin, is often plasmid-mediated and associated with the proliferation of resistant bacterial isolates in clinical settings (43). In our study, 22 isolates (48.8%) containing class 1 and class 2 integrons harbored conjugative plasmids (>100 kb) confirmed through mating assays. These plasmids, particularly of the IncP and IncN groups, are known for their broad host range and role in spreading multidrug resistance in clinical settings (44).

The clonal relationships of integron-containing *E. coli* isolates were evaluated using PFGE. While PFGE effectively differentiated subgroups, it showed limited correlation with antibiotic resistance profiles, suggesting the influence of other genetic factors. Notably, isolates from different clinical origins and resistance profiles exhibited over 90% similarity in PFGE analyses, while clonally unrelated isolates from the same source displayed similar resistance profiles (Fig. 3). Also, TEC078 and TEC087 isolates, which were isolated from the same clinical source and had almost the same antibiotic resistance profiles, were determined as clonally

unrelated in different branches. As a result, PFGE patterns determined in *E. coli* isolates containing integrons and similar gene cassettes showed little clonal association.

CONCLUSION

This study is among the few to investigate the prevalence of integrons in *E. coli* isolates from blood samples in Türkiye. The transfer of antibiotic resistance genes via integrons and plasmids poses significant challenges for managing infectious diseases. Continuous surveillance of antimicrobial resistance in invasive *E. coli* isolates is essential to monitor trends and guide effective treatment strategies. Understanding the mechanisms of resistance, including the role of integrons, can inform the development of targeted antimicrobial therapies. Further research is needed to explore the interplay between integrons, gene cassette arrays, and resistance mechanisms in bloodstream infections.

Acknowledgments

We sincerely thank the Scientific Research Project Unit of Karadeniz Technical University for their support of this study (Grant number: 5335/2015).

Authorship contributions

AR, OBÖ and AOK designed the study; AR, CKB and GB collected *E. coli* isolates and carried out phenotypic identification; AR, ER and İD performed the molecular assay; AR, OBÖ, ER and AOK prepared and revised the manuscript. All authors gave the final approval of the version to be published.

Data availability statement

The authors state that the data supporting the study's results can be found in the article. Additionally, the raw data can be obtained from the corresponding author upon a reasonable request.

Declaration of competing interest

The authors declare that they have no conflict of interest.

Ethics

This study was approved by Karadeniz Technical University Faculty of Medicine Scientific Research Ethics Committee (Date: 12.10.2015, Decision no:3, Reference number 2015/117).

Funding

The present study was supported by the Scientific Research Project Unit of Karadeniz Technical University (Grant number: 5335/2015).

REFERENCES

1. Delle RD, Pezzotti P, Fontana C, Altieri A, Minelli S, Mariotti B, Cerretti R, Leoni D, Andreoni M, Sarmati L. An in-depth analysis of nosocomial bloodstream infections due to Gram-negative bacilli: clinical features, microbiological characteristics and predictors of mortality in a 1 year, prospective study in a large tertiary care Italian hospital. *Infectious Diseases* 2019; 51(1): 12-22.
2. Hastak P, Cummins ML, Gottlieb T, Cheong E, Merlino J, Myers GS, Chowdhury PR. Genomic profiling of *Escherichia coli* isolates from bacteraemia patients: a 3-year cohort study of isolates collected at a Sydney teaching hospital. *Microbial genomics* 2020; 6(5).
3. Lipworth S, Vihta KD, Chau K, Barker L, George S, Kavanagh J, Davies T, Vaughan A, Andersson M, Jeffery K, Oakley S, Morgan M, Hopkins S, Peto T, Crook DW, Walker AS, Stoesser N. Ten-year longitudinal molecular epidemiology study of *Escherichia coli* and *Klebsiella* species bloodstream infections in Oxfordshire, UK. *Genome Medicine*; 13(1): 1-13.
4. Aricò MO, Valletta E, Caselli D. Appropriate Use of Antibiotic and Principles of Antimicrobial Stewardship in Children. *Children* 2023; 10(4): 740.
5. Boucher Y, Labbate M, Koenig JE, Stokes HW. Integrons: mobilizable platforms that promote genetic diversity in bacteria. *Trends Microbiol.* 2007; 15:301-9.
6. Barlow RS, Gobius KS. Diverse class 2 integrons in bacteria from beef cattle sources. *Journal of Antimicrobial Chemotherapy* 2006; 58: 1133-1138.
7. Sandalli C, Buruk CK, Sancaktar M, Ozgumus OB. Prevalence of integrons and a new *dfrA17* variant in Gram-negative bacilli which cause community-acquired infections. *Microbiol Immunol* 2010; 54: 164-169. <https://doi.org/10.1111/j.1348-0421.2010.00197.x>
8. Cicek CA, Ozgumus OB, Saral A, Sandalli C. Antimicrobial resistance patterns and integron carriage of *Escherichia coli* isolates causing community-acquired infections in Turkey. *Annals of laboratory medicine* 2014; 34(2): 139-44.
9. Cicek CA, Sandalli C, Budak EE, Yağmur G, Çizmeçi Z, Ak S, Balcı PÖ, Şay Coşkun SU, Ay Altıntop Y, Fırat M, Sarı F, Çalışkan A, Yıldız N Sancaktar M, Özgümüş OB. İdrar Kültürlerinden İzole Edilen *Escherichia coli* Suşlarında Sınıf 1 ve Sınıf 2 İntegron Gen Kasetlerinin Karakterizasyonu: Çok Merkezli Bir Çalışma. *Mikrobiyol Bul* 2016; 50(2): 175-185.
10. Düzgün AÖ, Okumuş F, Saral A, Çiçek AÇ, Cinemre S. Determination of antibiotic resistance genes and virulence factors in *Escherichia coli* isolated from Turkish patients with urinary tract infection. *Revista da Sociedade Brasileira de Medicina Tropical* 2019; 52, e20180499.
11. Cicek CA, Şemen V, Ejder NA, Gündoğdu DZU, Kalcan SK, Köse FT, Özgümüş OB. Molecular epidemiological analysis of integron gene cassettes and tetA/tetB/tetD gene associations in *Escherichia coli* strains producing extended-spectrum β-lactamase (ESBL) in urine cultures. *Advances in Clinical and Experimental Medicine* 2022; 31(1): 71-79.
12. Öner SZ, Karaday E, Çalışkan A, Demir M, Şenol H, Kaleli İ. Integron distribution and relationship to antimicrobial resistance in *E. coli* isolated from blood culture. *Indian Journal of Medical Microbiology* 2024; 48, 100554.
13. Wayne, PA. National Committee for Clinical Laboratory Standards. Performance standards for antimicrobial susceptibility testing. Tenth Informational supplement, M100-S10 (M2): National Committee for Clinical Laboratory Standards, 2000.
14. Perez-Perez FJ, Hanson ND. Detection of plasmid-mediated AmpC beta-lactamase genes in clinical isolates by using multiplex PCR. *J Clin Microbiol* 2002; 40(6): 2153-62.
15. Machado E, Canto'n R, Baquero F, Gala'n JC, Rolla'n A, Peixe L, Coque TM. Integron Content of Extended-Spectrum-Lactamase-Producing *Escherichia coli* Strains over 12 Years in a Single Hospital in Madrid, Spain. *Antimicrobial Agents and Chemotherapy* 2005; 49(5): 1823-1829.
16. Sambrook J, Fritsch EF, Maniatis T (1989) *Molecular cloning: a laboratory manual* (No. Ed. 2). Cold spring harbor laboratory press
17. Kado CI, Liu ST. Rapid procedure for detection and isolation of large and small plasmids. *J Bacteriol* 1981; 145(3): 1365-73.

18. Rohlf FJ (1993). NSYS-PC: Numerical Taxonomy and Multivariate Analysis System. New York: Exeter Software.
19. Mokracka J, Koczura R, Pawłowski K, Kaznowski A. Resistance patterns and integron cassette arrays of Enterobacter cloacae complex strains of human origin. Journal of Medical Microbiology 2011; 60: 737-743.
20. Majumdar S, Chatterjee A. Ammonium acetate induced isolation of plasmid DNA (2014) Online International Interdisciplinary Research Journal ISSN2249-9598, Volume-IV
21. Götz A, Pukall R, Smit E, Tietze E, Prager R, Tschäpe H, Van Elsas JD, Smalla K. Detection and characterization of broad-host-range plasmids in environmental bacteria by PCR. Applied and environmental microbiology 1996; 62(7): 2621-2628.
22. Durmaz R, Otlu B, Koksall F. The optimization of a rapid pulsed-field gel electrophoresis protocol for the typing of *Acinetobacter baumannii*, *Escherichia coli* and *Klebsiella* spp. Jpn J Infect Dis 2009; 62: 372-377.
23. Ibrahim DR, Dodd CE, Stekel DJ, Meshioye RT, Diggle M, Lister M, Hobman JL. Multidrug-Resistant ESBL-Producing *E. coli* in Clinical Samples from the UK. Antibiotics 2023; 12(1): 169.
24. Birru M, Woldemariam M, Manilal A, Aklilu A, Tsalla T, Mitiku A, Gezmu T. Bacterial profile, antimicrobial susceptibility patterns, and associated factors among bloodstream infection suspected patients attending Arba Minch General Hospital, Ethiopia. Scientific reports 2021; 11(1): 1-13.
25. Duran H, Çeken N, Atik B. *Escherichia coli* ve *Klebsiella pneumoniae* Türlerinde Antibiyotik Direnci ne Durumda? Yoğun Bakım Ünitesinden Beş Yıllık Analiz. Fırat Tıp Dergisi/Firat Med J 2022; 27(2): 116-120
26. Son T, Manh ND, Trung NT, Quyen DT, Meyer CG, Phuong NTK, Hoan PQ, Sang VV, Nurjadi D, Velavan T, Bang MH, Song LH. Molecular detection of blaCTX-M gene to predict phenotypic cephalosporin resistance and clinical outcome of *Escherichia coli* bloodstream infections in Vietnam. Annals of clinical microbiology and antimicrobials 2021; 20(1): 1-9.
27. Kreidl P, Kirchner T, Fille M, Heller I, Lass-Flörl C, Orth-Höller D. Antibiotic resistance of blood cultures in regional and tertiary hospital settings of Tyrol, Austria (2006-2015): Impacts & trends. PloS one 2019; 14(10): e0223467.
28. Anvarinejad M, Khalifeh M, Mardaneh J, Pouladfar G, Dehyadegari MA. Bloodstream infections in the south of Iran: microbiological profile and antibiotic-resistance patterns of isolated bacteria. Crescent J Med Biol Sci 2021; 8(4): 312-318.
29. Hu LF, Chang X, Ye Y, Wang ZX, Shao YB, Shi W, Li X, Li JB. *Stenotrophomonas maltophilia* resistance to trimethoprim/sulfamethoxazole mediated by acquisition of sul and dfrA genes in a plasmid-mediated class 1 integron. Int J Antimicrob Agents 2011; 37(3): 230-4.
30. Sacristán C, Esperón F, Herrera-León S, Iglesias I, Neves E, Nogal V, Muñoz MJ, de la Torre A. Virulence genes, antibiotic resistance and integrons in *Escherichia coli* strains isolated from synanthropic birds from Spain. Avian Pathol 2014; 43(2): 172-5.
31. Zhu W, Wang T, Zhu Y, Xiao L, Liu W, Wei Q. Two-dimensional PCR for detecting class 1, 2 and 3 integrons. Heliyon 2022; 8(11): e11844.
32. Başkan C, Sırıken B, Tüfekci EF, Kılınç Ç, Ertürk Ö, Erol İ (2022) Presence of quorum sensing system, virulence genes, biofilm formation and relationship among them and class 1 integron in carbapenem-resistant clinical *Pseudomonas aeruginosa* isolates. Archives of Microbiology 2022; 204(8): 464.
33. Rakici E, Altunisik A, Sahin K, Ozgumus OB. Determination and molecular analysis of antibiotic resistance in Gram-negative enteric bacteria isolated from *Pelophylax* sp. in the Eastern Black Sea Region. Acta Veterinaria Hungarica 2021; 69(3): 223-233.
34. Sivri N, Sandalli C, Ozgumus OB, Colakoglu F, Dogan D. Antibiotic resistance profiles of enteric bacteria isolated from Kucukcekmece Lagoon (Istanbul-Turkey). Turkish Journal of Fisheries and Aquatic Sciences 2012; 12(3).
35. Liu W, Zhao F, Chen J. Analysis of drug resistance genes of integrons in clinical isolates of *Escherichia coli* from elderly bloodstream infections. Cellular and Molecular Biology 2022; 68(6): 67-72.
36. Abdel-Rhman SH, Elbargisy RM, Rizk DE. Characterization of integrons and quinolone resistance in clinical *Escherichia coli* isolates in Mansoura City, Egypt. International Journal of Microbiology 2021.
37. Dehkordi MK, Halaji M, Nouri S. Prevalence of class 1 integron in *Escherichia coli* isolated from animal sources in Iran: a systematic review and meta-analysis. Tropical Medicine and Health 2020; 48:16.
38. Ahumada-Santos YP, Báez-Flores ME, Díaz-Camacho SP, de Jesús Uribe-Beltrán M, Eslava-Campos CA, Parra-Unda JR, Delgado-Vargas F. Association of phylogenetic distribution and presence of integrons with multidrug resistance in *Escherichia coli* clinical isolates from children with diarrhoea. Journal of Infection and Public Health 2020; 13(5): 767-772.
39. Partridge SR, Tsafnat G, Coiera E, Iredell JR. Gene cassettes and cassette arrays in mobile resistance integrons. FEMS Microbiol Rev 2009; 33(4): 757-784.

-
40. Ndi OL, Barton MD. Incidence of class 1 integron and other antibiotic resistance determinants in *Aeromonas* spp. from rainbow trout farms in Australia. *J Fish Dis* 2011; 34(8): 589-99.
 41. Szmolka A, Nagy B. Multi drug resistant commensal *Escherichia coli* in animals and its impact for public health. *Frontier in microbiology* 2013; 4: 258. <https://doi.org/10.3389/fmicb.2013.00258>
 42. Düzgün AÖ, Saral A (2018) Investigation of Antibiotic Resistance Genes and Class 1 Integron in Multi-Drug Resistant *P. aeruginosa* and *E. coli* Strains. *Cumhuriyet Sci. J.* 2018; Vol. 39-4: 1063-1068.
 43. Chen J, Su Z, Liu Y, Wang S, Dai X, Li Y, Peng S, Shao Q, Zhang H, Wen P, Yu J, Huang X, Xu H. Identification and characterization of class 1 integrons among *Pseudomonas aeruginosa* isolates from patients in Zhenjiang, China. *International Journal of Infectious Diseases* 2009; 13(6): 717-721.
 44. Schlüter A, Szczepanowski R, Pühler A, Top EM. Genomics of IncP-1antibiotic resistance plasmids isolated from wastewater treatment plants provides evidence for a widely accessible drug resistance gene pool. *FEMS Microbiol Rev* 2007; 31: 449-477.

Research Article

THIOL/DISULPHIDE HOMEOSTASIS AND VASCULAR ENDOTHELIAL GROWTH FACTOR LEVELS IN SALIVA OF TYPE 1 DIABETIC CHILDREN WITH GINGIVITIS

 **Sultan KELEŞ**¹,  **Burçin İrem ABAS**²,  **Ahmet ANIK**³,  **Ayşe ANIK**⁴,  **Özge ÇEVİK**²

¹ Department of Pediatric Dentistry, Faculty of Dentistry, Aydın Adnan Menderes University, Aydın, TURKIYE

² Department of Biochemistry, Faculty of Medicine, Aydın Adnan Menderes University Aydın, TURKIYE

³ Department of Pediatric Endocrinology, Faculty of Medicine, Aydın Adnan Menderes University Aydın, TURKIYE

⁴ Department of Pediatrics, Faculty of Medicine, Aydın Adnan Menderes University Aydın, TURKIYE

*Correspondence: dtsultank@gmail.com

ABSTRACT

Objective: To evaluate the thiol/disulphide homeostasis and level of vascular endothelial growth factor (VEGF) in saliva of patients with type 1 diabetes mellitus and gingivitis.

Materials and Methods: Forty children with type 1 diabetes mellitus (DM) and 40 systemically healthy (H) children were included the study. Based on children' periodontal and systemic health status, they were divided into four subgroups: 1) systemically and periodontally healthy subjects (Hh), 2) systemically healthy subjects with gingivitis (Hg), 3) diabetic subjects with periodontal health (DMh), 4) diabetic subjects with gingivitis (DMg). Probing depth (PD), gingival index (GI) and plaque index (PI) were recorded. An automated technique was used to measure the thiol/disulphide homeostasis parameters, and ELISA was used to measure the VEGF concentrations in unstimulated whole saliva.

Results: DM and H groups had comparable clinical periodontal parameters and salivary VEGF levels ($p>0.05$). GI, PI, PD, and disulphide amounts were significantly higher in the gingivitis subgroups (Hg and DMg) than in the periodontally healthy subgroups (Hh and DMh) ($p<0.001$). The gingivitis subgroups (Hg and DMg) had significantly higher amounts of VEGF compared to the periodontally healthy subgroups (Hh and DMh) ($p<0.001$).

Conclusions: Thiol/disulphide homeostasis shifts towards disulphide direction in diabetic children with gingivitis. Thiol/disulphide homeostasis and VEGF levels in saliva may be diagnostic markers of gingival inflammation.

Keywords: Saliva, gingivitis, diabetes mellitus, oxidative stress

Received: 04 December 2024

Revised: 14 December 2024

Accepted: 17 December 2024

Published: 22 December 2024



Copyright: © 2024 by the authors. Published by Aydın Adnan Menderes University, Faculty of Medicine and Faculty of Dentistry. This is an open access article under the Creative Commons Attribution Non Commercial 4.0 International (CC BY-NC 4.0) License.

INTRODUCTION

Type 1 diabetes mellitus (T1DM) occurs from autoimmune destruction of pancreatic beta cells, resulting to the loss of insulin production and hyperglycemia, and it is frequently recognized in children and young adults (1). An increase in cytokine release, impaired antioxidation and damage caused by reactive oxygen species (ROS) in beta cells act in its pathogenesis (2).

Thiols are organic compounds that take part in the elimination of ROS via nonenzymatic pathways. They contain succinyl groups, which are made up of a sulfur atom and a hydrogen atom bonded to a carbon atom. An increase in ROS induces oxidation of sulfur atoms and the constitution of covalent bonds between sulfur atoms, resulting in disulfide conversion. The generated disulphide linkages can be reduced to thiol groups, hence preserving thiol/disulphide homeostasis (3,4). Thiol/disulphide homeostasis is required for detoxification and includes the following parameters: native and total thiol; disulphide; and disulphide/native thiol, disulphide/total thiol, and native thiol/total thiol ratios (3,4). These parameters have been investigated as oxidative stress markers in a variety of degenerative disorders, including obesity, coronary heart disease, respiratory diseases, Alzheimer's disease, slow coronary flow, type 1 diabetes mellitus, and periodontal pathologies (5-7). Durmus et al. (8) found that oxidative damage in pancreatic β -cells caused a shift in thiol/disulphide balance in diabetic children, favoring disulphide.

Gingivitis is a common inflammatory disease that affects solely the soft tissues around the teeth during childhood and adolescence (9). The early detection and treatment of gingivitis are crucial because the degradation of periodontal tissues can result in tooth loss if treatment is not received (10). The inflammatory response and oxidant/antioxidant balance is a critical factor in the development of diabetes and periodontal disease, which are both chronic pathological situations that are related by numerous underlying biological mechanisms (11). Increased production of ROS in periodontal tissues of diabetic individuals leads to development of insulin resistance that inhibits cell proliferation and angiogenesis in the periodontal tissues. There are many studies showed that the diabetic children are more prone to have periodontal diseases compared to healthy controls (12,13).

Vascular endothelial growth factor (VEGF) is a multifunctional biomarker that stimulates microvascular permeability and acts as an endothelial cell mitogen (14). It has been shown to act as an serious role in the pathogenesis of growth of tumors, rheumatoid arthritis, atherosclerosis of coronary arteries, Kawasaki disease, T1DM, and periodontal disease (14-16). There are many oxidative stress indicators such as total antioxidant capacity, nitric oxide, glutathione peroxidase, malondialdehyde, total oxidative status, and 8-hydroxydeoxyguanosine detected in the biological fluids of the individuals with T1DM and/or gingivitis (17). Studies concluded that hyperglycemia related to T1DM and the presence of oxidative stress may induce the expression of VEGF (13). Since thiol/disulfide homeostasis is thought to be a marker of oxidative stress, it can be hypothesized that it may be related to VEGF levels in saliva. Therefore, the objective of the study was to evaluate thiol/disulphide homeostasis parameters and VEGF in saliva of type 1 diabetic children with gingivitis.

MATERIALS AND METHODS

Subjects and Clinical Examinations

40 with type 1 diabetes mellitus (DM) and 40 systemically healthy (H) individuals; aged 9–13 years were consecutively included in this research at the Department of Pediatric Dentistry, Faculty of Dentistry, Aydin Adnan Menderes University, Aydin, Türkiye, between July and October 2020. Ethical approval was obtained from the ethics committee of the University (protocol number 2020/114). The trial was carried out in compliance with the Declaration of Helsinki's rules of 1975, as revised in 2013. The study design was explained to the parents of the children and they signed informed consent before the participation. The study was recorded at <http://www.clinicaltrial.gov> (Protocol Registration Receipt NCT04470635).

After obtaining each participant's medical and dental history, oral examinations were conducted. Depending on their periodontal condition, the children were split up into four subgroups: 1) systemically and periodontally healthy participants (Hh, n = 20), 2) systemically healthy participants with gingivitis (Hg) (n =

20), 3) diabetic participants with periodontal health (DMh, n = 20), and 4) diabetic participants with gingivitis (DMg, n = 20).

Inclusion criteria were as follows: 1) aged 9–13 years, 2) the patients confirmed as T1DM with a HbA1c value of $<7.5\%$ by a pediatric endocrinologist at least twelve months before the trial (18), and not having any other systemic illnesses 3) not having any disease for systemically healthy children (parental reporting) 4) presence of first molars and maxillary and mandibular incisors that are fully erupted and free of cavities.

Exclusion criteria were as follows: 1) uncontrolled diabetic mellitus, 2) periodontitis or periodontal intervention including antibacterial or anti-inflammatory medications within the preceding six months, 3) needing restorative and endodontic treatment, 4) using immunosuppressive medications within the previous 6 months, 5) using orthodontic appliances, and 6) presence of clinical attachment loss.

Periodontal measurements

Gingival index (GI), plaque index (PI), and probing depth (PD) were among the periodontal measurements that were employed (19). First molars and completely erupted, caries-free permanent maxillary and mandibular incisors were used for clinical measurements, and they were thought to represent the entire mouth (19,20).

Data were collected from buccal, lingual/palatinal, mesial, and distal sites of the teeth. The probing depth was noted as the distance from the gingival margin to the bottom of the probed pocket. Participants were confirmed as gingivitis when $GI \geq 1$ and $PD \leq 3$ mm at all measured sites for 12 teeth. Children were diagnosed as periodontal health if they had $GI < 1$ and $PD < 3$ mm (19,20).

A pediatric dentist (SK) conducted all clinical periodontal measurements with a manual periodontal probe (Williams, Hu-Friedy, Chicago, IL). Prior the study, calibration of the researcher was conducted on ten children with gingivitis for PD. The intra-examiner agreement coefficient was 0.97 for PD.

Gathering of saliva samples

Samples were gathered in the morning from 9:00 am to 10:00 am to reduce the impact of circadian rhythm on biomarker levels. Unstimulated saliva samples were gathered one day after periodontal clinical measurements. The subjects were told not to engage in oral care activities like flossing, brushing, and mouth rinsing, and to abstain from eating and drinking for 2 hours before providing samples. Before collecting saliva, each patient was instructed to irrigate their mouth with water for 2 minutes, wait 10 minutes, and then spit into sterile 50 - mL polypropylene tubes for 5 minutes. Saliva samples were stored at a temperature of -80° C, until further examination.

Measurement of thiol/disulphide homeostasis parameters

Erel and Neselioglu developed an automated analysis method that had been used in many studies, to assess salivary thiol/disulphide homeostasis (3,4). In the first step, the reducible disulphide bonds were decreased to create available functional thiol groups. Formaldehyde was utilized to eliminate the unreacted and spent sodium borohydride, and following the interaction with DTNB, all sulfhydryl groups, comprising both reduced and original groups, were quantified. The level of dynamic disulphide was calculated by subtracting half of the total thiol groups from the native thiol groups. After determining the levels of native thiols, total thiols, and disulphide in $\mu\text{mol/L}$, the ratios of Disulphide/total thiol, native thiol/total thiol, and disulphide/native thiol percentages were determined (21).

Measurement of VEGF level in saliva

Thawed saliva samples were warmed to 37°C and thoroughly mixed before being analyzed. VEGF level in saliva were measured by the enzyme-linked immunosorbent assay (ELISA) using commercial kits (Human Vascular endothelial growth factor level ELISA kit, Sunred Biotechnology, Shanghai) consistent with the manufacturer's guidelines. The minimum determination level for VEGF level was 20 pg/ml. Plates were quantified at 450 nm with 650 nm as a reference wavelength via an ELISA reader (DTX 880 Multimode Reader,

Beckman Coulter, Miami, FL). VEGF concentrations were calculated from the standard curve and presented in pg/ml.

Statistical Analysis

Based on a prior study (22), the number of participants required was determined using a power analysis software (G*Power version 3.0.8, Heinrich Heine University, Düsseldorf) with a 95% power, 0.83 effect size, and α set at 0.05. According to these criteria, each group needed a minimum of 39 patients. The sample size was changed to 80 in order to account for the possibility of missing samples or data. The statistical software program SPSS version 22.0 (IBM Inc., Chicago, IL) was used to analyze descriptive statistics and the normality of subgroup data. The Kolmogorov-Smirnov normality test was used to validate the distribution of the biochemical and clinical data. The study parameters were analyzed using the Kruskal Wallis test and the Mann-Whitney U test. The Spearman's Rank Correlation tests was used to assess whether the association between the clinical and biochemical parameters were linear, with a significance level of $\alpha = 0.05$.

RESULTS

Subjects sand salivary samples characteristics

For children in systemic health, the mean age (years \pm SD) was 11.25 ± 1.89 , while for children with type 1 diabetes, it was 10.95 ± 1.83 . For children with diabetes and those in systemic health, the gender distributions were 21/19 and 22/18, respectively. For both gender and age, there were no statistically significant differences between the diabetic children and the systemically healthy group ($p > 0.05$).

Periodontal clinical parameters

Table 1 displays the periodontal clinical indicators for children with DM and systemically healthy children. For the 12 permanent teeth, children with DM had PD, GI, and PI numbers that were comparable to those of

children in systemically healthy group ($p > 0.05$). Compared to the periodontally healthy subgroups, the Hg and DMg subgroups had significantly higher PD, GI, and PI values ($p < 0.001$) (Table 2).

Evaluation of thiol/disulphide homeostasis data of the groups and subgroups

Total thiol and disulphide levels were determined higher in systemically healthy children compared to diabetic children in Table 1 ($p < 0.001$). Native thiol levels were lower in diabetic children compared to healthy controls, but the difference between the groups was not statistically significant ($p > 0.05$).

Table 1. Periodontal clinical parameters, HbA1c values, thiol/disulphide homeostasis parameters and VEGF levels in saliva of the study groups and their comparisons.

Parameters	H (n= 40)	DM (n= 40)	P*
Age (year)	11.0(10.0-12.8)	10.0(10.0-12.0)	0.461
Gender			0.499**
Female (%)	24(60)	21(53)	
Male (%)	16(40)	19(47)	
HbA1c (%)	5.30(5.20-5.70)	7.30(5.60-7.40)	<0.001
PI	0.80 (0.30-2.00)	0.70 (0.30-2.00)	0.778
GI	1.20 (0.51-2.00)	1.20 (0.43-2.45)	0.729
PD (mm)	1.45 (0.91-2.02)	1.50 (0.96-2.39)	0.491
VEGF (pg/ml)	41.4 (34.8-55.9)	44.0 (33.0-58.4)	0.722
Native thiol ($\mu\text{mol/L}$)	12.9 (9.3-23.9)	11.2 (4.80-23.9)	0.405
Total thiol ($\mu\text{mol/L}$)	98.1(61.9-162.3)	51.4 (21.8-90.4)	0.001
Disulphide ($\mu\text{mol/L}$)	101.6 (64.4-177.3)	52.8 (23.6-85.6)	<0.001
Disulphide /native thiol(%)	7.58 (4.73-16.39)	3.94 (1.89-9.32)	0.015
Disulphide /total thiol (%)	1.10 (1.03-1.23)	1.07 (0.70-1.26)	0.227
Native thiol/total thiol (%)	0.14 (0.07-0.27)	0.27 (0.11-0.55)	0.023

*Mann-Whitney U test, **Chi-square test. Data were given as n (%), median (25p-75p).

Native thiol/total thiol ratio was statistically higher in diabetic children compared to systemically healthy controls. Disulphide/native thiol ratio was statistically significantly higher in systemically healthy children. There was no statistically significant difference in terms of disulphide/total thiol ratio between the groups ($p > 0.05$). Native thiol levels were higher in DMh subgroup compared to DMg subgroup. Total thiol level was higher in Hh subgroup compared to DMh subgroup. Disulphide levels were higher in gingivitis subgroups

compared to periodontally healthy subgroups. DM subgroup presented the highest native thiol/total thiol ratio and the lowest disulphide/native thiol ratio compared to other subgroups (Table 2).

Comparison of salivary VEGF level among groups and subgroups

VEGF were measured in all specimens. There was no significant difference in the VEGF levels in saliva between individuals with DM and systemically healthy individuals ($p > 0.05$) (Table 1). The Hg subgroup had significantly higher VEGF amount compared to the Hh subgroup ($p < 0.001$) (Table 2).

Table 2. Anthropometric data and periodontal clinical parameters of the children in the subgroups.

Parameters	Hh (n=20)	Hg (n=20)	DMh(n=20)	DMg (n=20)	P*
Age (year)	11.0(10.0-12.0)	11.0(10.0-13.8)	12.0(10.0-13.0)	10.0(9.0-12.0)	0.323
Female (%)	14(70)	10(50)	11(55)	10(50)	0.535**
Male (%)	6(30)	10(50)	9(45)	10(50)	
HbA1c (%)	5.30(5.20-5.70)	5.50(5.32-5.70)	7.35(5.71-7.40)	7.30(6.20-7.40)	<0.001 ^a
PI	0.30 (0.20-0.34)	2.00 (1.43-2.00)	0.30 (0.20-0.40)	2.00 (1.40-2.00)	<0.001 ^b
GI	0.53 (0.38-0.68)	2.00 (1.74-2.50)	0.45 (0.39-0.69)	2.40 (1.90-2.62)	<0.001 ^b
PD (mm)	0.92(0.77-1.20)	2.02(1.80-2.36)	0.97(0.76-1.20)	2.39(1.88-2.67)	<0.001 ^b
VEGF (pg/ml)	35.42 (30.50-39.38)	55.11 (44.72-64.72)	45.59 (29.46-62.05)	42.49 (34.73-58.32)	<0.001 ^c
NT(μmol/L)	12.36 (8.99-18.83)	15.74 (11.24-24.73)	20.23 (11.24-31.19)	6.74 (3.65-14.61)	0.013 ^d
TT (μmol/L)	90.89 (46.47-126.83)	112.46 (64.70-183.06)	28.76 (15.15-86.27)	62.65 (45.70-91.15)	0.004 ^e
D (μmol/L)	95.50 (55.00-134.57)	112.40 (72.08-208.63)	44.18 (17.28-77.70)	60.75 (40.01-92.95)	<0.001 ^e
D/NT(%)	7.15 (4.73-13.75)	7.58 (4.78-18.17)	2.15 (1.20-5.01)	9.23 (3.17-15.68)	<0.001 ^f
D/TT(%)	1.10 (0.98-1.21)	1.11 (1.06-1.27)	1.15 (0.66-1.67)	1.06 (0.78-1.12)	0.326
NT/TT(%)	0.14 (0.08-0.27)	0.14 (0.06-0.27)	0.52 (0.19-0.99)	0.11 (0.07-0.31)	<0.001 ^g

*Kruskal-Wallis test **chi-square test, Data were given as n (%), median (25p-75p), n^a Group DMh & Group Hh; Group DMh & Group Hg; Group DMg & Group Hg; Group DMg & Group Hh, $p < 0.001$. ^b Group DMh & Group DMg, Group DMh & Group Hg, Group DMg & Group Hh, Group Hg & Group Hh, $p < 0.001$, ^c Group Hg & Group Hh, $p < 0.001$, ^d Group DMh & Group DMg, $p < 0.001$, ^e Group DMh & Group Hg, $p < 0.001$, ^f Group DMh & Group DMg, $p = 0.003$; Group DMh & Group Hg, $p = 0.001$; Group DMh & Group Hh, $p = 0.007$, ^g Group DMh & Group DMg, $p = 0.001$; Group DMh & Group Hg, $p = 0.002$; Group DMh & Group Hh, $p = 0.005$ **Abbreviations:** NT, Native thiol; TT, Total thiol; D, Disulphide; D/NT, Disulphide/native thiol ; D/TT, Disulphide/ total thiol; NT/TT, Native thiol/ total thiol.

Correlation between thiol/disulphide homeostasis parameters, VEGF level and clinical parameters

Table 3 displays the correlations between biochemical data and clinical periodontal markers. Significant correlations were found between salivary VEGF levels and PI, GI, and PD ($r = 0.425$, $p < 0.01$; $r = 0.337$, $p < 0.01$; $r = 0.228$, $p < 0.05$, respectively). Furthermore, the total thiol and disulphide and the VEGF level were positively correlated ($r = 0.281$, $p < 0.05$; $r = 0.273$, $p < 0.05$).

Table 3. Correlations between clinical parameters and biochemical findings of all study groups.

Parameters	HbA1c	PD	GI	PI	VEGF	NT	TT	D	D/NT	D/TT	NT/TT
HbA1c	1,000	0,128	0,065	0,057	-0,026	-0,059	-,386**	-,419**	-,276*	-0,033	,278*
PD	0,128	1,000	,735**	,667**	,228*	-0,136	0,174	0,204	,272*	0,051	-,257*
GI	0,065	,735**	1,000	,777**	,337**	-0,104	0,130	0,118	0,201	-0,023	-0,214
PI	0,057	,667**	,777**	1,000	,425**	-0,120	0,185	0,182	,239*	-0,043	-,255*
VEGF	-0,026	,228*	,337**	,425**	1,000	0,167	,281*	,273*	0,007	-0,104	-0,021
NT	-0,059	-0,136	-0,104	-0,120	0,167	1,000	0,181	0,170	-,679**	0,113	,671**
TT	-,386**	0,174	0,130	0,185	,281*	0,181	1,000	,932**	,494**	-,241*	-,540**
D	-,419**	0,204	0,118	0,182	,273*	0,170	,932**	1,000	,537**	0,079	-,514**
D/NT	-,276*	,272*	0,201	,239*	0,007	-,679**	,494**	,537**	1,000	-0,067	-,976**
D/TT	-0,033	0,051	-0,023	-0,043	-0,104	0,113	-,241*	0,079	-0,067	1,000	,265*
NT/TT	,278*	-,257*	-0,214	-,255*	-0,021	,671**	-,540**	-,514**	-,976**	,265*	1,000

**Correlation is significant at the 0.01 level (2-tailed), *Correlation is significant at the 0.05 level (2-tailed).

Abbreviations: NT, Native thiol; TT, Total thiol; D, Disulphide; D/NT, Disulphide/native thiol ; D/TT, Disulphide/ total thiol; NT/TT, Native thiol/ total thiol.

There was no association between total thiol, native thiol and disulphide levels and periodontal clinical parameters. There was negative association between native thiol/total thiol ratio and PI and PD ($r = -0.255$, $p < 0.05$; $r = -0.257$, $p < 0.05$, respectively). There was positive relationship between disulphide/native thiol ratio and PI and PD ($r = 0.239$, $p < 0.05$; $r = 0.272$, $p < 0.05$, respectively).

DISCUSSION

This study revealed the shift of dynamic thiol/disulphide homeostasis toward disulphide form in individuals with T1DM and gingivitis by evaluating saliva samples for the first time. VEGF levels in saliva

was similar in children with T1DM and healthy controls. However, the salivary VEGF levels were increased in systemically healthy children with gingivitis.

Hyperglycemia can trigger pathways that increase inflammation, apoptosis, and oxidative stress, and T1DM is linked to increased levels of systemic indicators of inflammation that lead to microvascular and macrovascular problems (23). The imbalance between ROS and antioxidant molecules leads to oxidative stress. Redox modification of radical-based cysteine residues or oxidation between two electrons occurs when ROS levels rise above the physiological threshold. The sulfur atom in the cysteine side chain is oxidized in this redox reaction to produce disulphide (24). Thus, when the cellular level starts, oxidant radicals are linked to the initial stage of oxidative damage, and dynamic thiol/ disulphide homeostasis progresses toward disulphide form. Although underlying mechanisms are unclear, pancreatic β -cell failure is a critical event in the onset of T1DM. Because of their low capacity to withstand oxidative stress, β -cells are more vulnerable to it. ROS are linked to proinflammatory conditions at the onset of T1DM (25). Studies on both adults and children have demonstrated that diabetics have higher levels of thiol oxidation than healthy controls (8,21). In this study, total thiol level was significantly higher in healthy controls compared to diabetic children. This data confirmed that the diabetic children might had higher levels of thiol oxidation.

Gingivitis is commonly seen periodontal disease in children and adolescents and it may be induced by plaque, steroid hormone-related gingivitis, and drug-influenced gingival enlargement. Plaque microorganisms can initiate periodontal diseases and gingivitis is considered as the earliest stage of periodontitis, the development of which occurs in only long-term untreated gingivitis (25). There are many studies revealed that diabetic children were more prone to periodontal diseases compared to their healthy counterparts (26-28). There are many mechanisms to connect periodontal disease with T1DM. Both T1DM and periodontal disease are categorized as inflammatory disorders that share similar pathogenic mechanisms, including the action of pro-inflammatory mediators. Studies revealed that diabetic patients exhibit heightened levels of pro-inflammatory mediators in their gingival tissues, including IL-1 β (interleukin-1beta), tumor necrosis factor-alpha (TNF- α), IL-6, matrix metalloproteinases (MMPs), prostaglandins (PGs), the association between

receptor activator of nuclear factor kappa-B ligand and osteoprotegerin (RANKL/OPG), VEGF, and oxidative stress, all of which significantly contribute to the onset and advancement of periodontal disease (29,30).

VEGF is an angiogenic biomarker of importance in inflammation and wound healing (31). VEGF has been determined in human periodontal tissue, gingival crevicular fluid (GCF) and saliva in various periodontal diseases (32,33). Pradeep et al. (34) determined that the GCF VEGF amounts had an increasing pattern from health to plaque-induced gingivitis in systemically healthy adults. Moreover, studies evaluated serum levels of VEGF showed that the serum VEGF level significantly increased in participants with diabetes compared to healthy controls (35). In the present study, salivary VEGF level was higher in diabetic children compared to healthy controls without a statistically significant difference. These data suggests that the the similarity in the salivary VEGF levels from diabetic and systemically healthy children in the present study is due to the good glycemic control in the diabetic individuals included to trial. In subgroups, healthy children with gingivitis showed the highest salivary VEGF levels compared to other groups. Additionally, periodontal clinical parameters were significantly correlated with salivary VEGF levels. In accordance with the present study, Padma et al. (36) determined that VEGF levels in GCF increased progressively from healthy to gingivitis in adults. Studies revealed that, T1DM was a more declared significant risk factor for periodontal disease and vascular complications, and there was an important association between HbA1c and oxidative stress (37). Seçkin et al. (35) stated that It may be appropriate to evaluate the levels of VEGF and oxidative stress markers in diabetic children.

Thiol/disulfide homeostasis has recently been used to evaluate the free radical status in an organism both at physiological and pathological conditions, therefore determination of this homeostasis can provide valuable information related to normal or pathological biochemical processes in many disease in children. In this study we used saliva samples to evaluate the thiol/disulfide homeostasis. Hasan et al. (38) performed a study to evaluate the possibility of using saliva, as an alternative biological fluid instead of blood serum to detect thiol homeostasis, and they concluded that saliva might be an alternative sample that is easy to collect from children (39). Tayman et al. (40) found a significant positive correlation between the severity of periodontal disease and serum total thiol and disulphide levels. As far as we know, there is no study evaluate

the thiol/disulfide homeostasis in diabetic children with gingivitis. Therefore, we could not compare our results to the literature. In the present study, total thiol and native thiol levels were lower in diabetic children compared to healthy individuals. Additionally, Tayman et al. (40) reported that the disulfide level was higher in gingivitis subgroup similar to adult studies. This indicates that antioxidant balance is impaired in diabetic patients and systemically healthy children with gingivitis. In this study, disulfide/native thiol ratios were higher in diabetic children with gingivitis. It may be resulted by more reduction of native thiol level compared to disulfide levels. Taken together, it may be suggested that thiol/disulfide homeostasis has potential to act as a diagnostic tool in detecting periodontal diseases in diabetic children.

Studies have shown that serum and tissue VEGF levels are high in diabetic children (35,41). VEGF expression is induced by hyperglycemia, advanced glycation end products, and oxidative stress (42,43). In this study, the positive correlation between disulfide and VEGF levels in saliva may support the relationship between VEGF and ROS-induced oxidative stress response in T1DM.

This study has some limitations. A study group that includes children who had uncontrolled diabetes mellitus should be added the study design. Children's systemic situation for systemically healthy group were recorded on the basis of their parents's reports. Therefore, it is not certain whether they have no any other systemic diseases. Additionally, the cross-sectional design of present study could not allow to establish causal association between thiol disulfide homeostasis parameters, level of VEGF and periodontal status. Prospective longitudinal studies with larger sample sizes should be performed to explore the potential effects of the thiol/disulfide homeostasis.

CONCLUSION

Based on the limitations of this research, it can be inferred that the balance of thiol/disulfide homeostasis shifts toward the disulfide direction in diabetic children suffering from gingivitis. The elevated levels of VEGF in the saliva among the gingivitis subgroups and their positive association with periodontal clinical measurements indicate that VEGF might serve as a valuable marker for diagnosing gingivitis in

children. This study findings need to be confirmed with longitudinal studies with the aim of determining the effect of thiol/disulphide homeostasis and salivary VEGF levels in children with T1DM and gingivitis.

Acknowledgments

We thank our patients and their families for their cooperation.

Authorship contributions

Concept: SK, AA ; Design: SK, OC, AA ; Data Collection or Processing: SK, AA, BIA; Analysis or Interpretation: SK, OC, AA, BIA, Literature Search: SK, OC, AA, BIA; Writing: SK, OC, AA, BIA.

Data availability statement

Data can be requested from the authors.

Declaration of competing interest

No conflict of interest was declared by the authors.

Ethics

This study was approved by the ethics committee of the Aydin Adnan Menderes University Faculty of Medicine (protocol number 2020/114).

Funding

This work has not received any funding support.

REFERENCES

1. Katsarou A, Gudbjörnsdottir S, Rawshani A, Dabelea D, Bonifacio E, Anderson BJ et al. Type 1 diabetes mellitus. *Nat Rev Dis Primer.* 2017;3(1):1-17.
2. Neyestani TR, Ghandchi Z, Eshraghian MR, Kalayi A, Shariatzadeh N, Houshiarrad A. Evidence for augmented oxidative stress in the subjects with type 1 diabetes and their siblings: A possible preventive role for antioxidants. *Eur J Clin Nutr.* 2012;66(9):1054-58.
3. Erel O, Neselioglu S. A novel and automated assay for thiol/disulphide homeostasis. *Clin Biochem.* 2014;47(18):326-32.
4. Kırzioğlu FY, Demirci S, Varol Ç, Ünlü MD, Calapoğlu M, Orhan H. Periodontal Health and Salivary Thiol-Disulphide Homeostasis in Multiple Sclerosis Patients. *Med J SDU* 2024;31(2):125-34.
5. Mengen E, Uçaktürk SA, Kocaay P, Kaymaz O, Neşelioğlu S, Erel O. The significance of thiol/disulfide homeostasis and ischemia-modified albumin levels in assessing oxidative stress in obese children and adolescents. *J Clin Res Pediatr Endocrinol.* 2020;12(1):45-54.
6. Ünal K, Erzin G, Yüksel RN, Alisik M, Erel O. Thiol/disulphide homeostasis in schizophrenia patients with positive symptoms. *Nord J Psychiatry.* 2018;72(4):281-84.
7. Arslan B, Arslan GA, Tuncer A, Karabudak R, Dinçel AS. Evaluation of thiol homeostasis in multiple sclerosis and neuromyelitis optica spectrum disorders. *Front Neurol.* 2021;12:716195.
8. Durmuş SY, Sahin NM, Ergin M, Neselioglu S, Aycan Z, Erel Ö. How does thiol/disulfide homeostasis change in children with type 1 diabetes mellitus?. *Diabetes Res Clin Pract.* 2019;149:64-8.
9. Kulkarni VK, Dixit M, Balasubramanian S, Jetpurwala A. Gingival and periodontal diseases in children. *Illustrated pediatric dentistry-part* 2023;2:264.

10. Blufstein A, Pejčić N, Spettel K, Hausmann B, Seki D, Ertekin T, et al. Salivary microbiome and MRP-8/14 levels in children with gingivitis, healthy children, and their mothers. *J Periodontol* 2024; 1:13 <https://doi.org/10.1002/JPER.23-0632>
11. Buranasin P, Kominato H, Mizutani K, Mikami R, Saito N, Takeda K, et al. Influence of reactive oxygen species on wound healing and tissue regeneration in periodontal and peri-implant tissues in diabetic patients. *Antioxidants* 2023;12(9):1787.
12. Gunasekaran S, Silva M, O'Connell MA, Manton DJ, Hallett KB. Caries experience and gingival health in children and adolescents with type 1 diabetes mellitus—A cross-sectional study. *Pediatr Diabetes* 2022;23(4):499-506.
13. Selway CA, Jensen ED, Pena AS, Smart G, Weyrich LS. Type 1 diabetes, periodontal health, and a familial history of hyperlipidaemia is associated with oral microbiota in children: a cross-sectional study. *BMC Oral Health* 2023;23(1):15.
14. Chiarelli F, Spagnoli A, Basciani FA, Tumini S, Mezzetti A, Cipollone F, et al. Vascular endothelial growth factor (VEGF) in children, adolescents and young adults with type 1 diabetes mellitus: relation to glycaemic control and microvascular complications. *Diabetic Medicine*. 2000;17(9):650-56.
15. Sakalioğlu EE, Aliyev E, Lütfioğlu M, Yavuz Ü, Açıkgöz G. Vascular endothelial growth factor (VEGF) levels of gingiva and gingival crevicular fluid in diabetic and systemically healthy periodontitis patients. *Clin Oral Investig*. 2007;115:120.
16. Afacan B, Öztürk VÖ, Paşalı Ç, Bozkurt E, Köse T, Emingil, G. Gingival crevicular fluid and salivary HIF-1 α , VEGF, and TNF- α levels in periodontal health and disease. *J Periodontol*. 2019;90(7):788-97.
17. Varvařovská J, Racek J, Štětina R, Sýkora J, Pomahačová R, Rušavý Z, et al. Aspects of oxidative stress in children with type 1 diabetes mellitus. *Biomed Pharmacother*. 2004;58(10): 539-45.
18. American Diabetes Association; 13. Children and Adolescents: Standards of Medical Care in Diabetes—2019. *Diabetes Care*, 42: S148–S164.
19. Keles S, Anik A, Cevik O, Abas BI, Anik A. Gingival crevicular fluid levels of interleukin-18 and tumor necrosis factor-alpha in type 1 diabetic children with gingivitis. *Clin Oral Investig*. 2020; 24(10):3623-31.
20. Doğusal G, Afacan B, Bozkurt E, Sönmez I. Gingival crevicular fluid and salivary resistin and tumor necrosis factor-alpha levels in obese children with gingivitis. *J Periodontol*. 2018;89(8):973-82.
21. Ates I, Kaplan M, Inan B, Alısk M, Erel O, Yılmaz N, et al. How does thiol/disulfide homeostasis change in prediabetic patients? *Diabetes Res Clin Pract*. 2015;110(2):166-71.
22. Ates I, Kaplan M, Yuksel M, Mese D, Alısk M, Erel Ö, et al. Determination of thiol/disulphide homeostasis in type 1 diabetes mellitus and the factors associated with thiol oxidation *Endocr*. 2016;51(1):47-51.
23. Preshaw PM, Alba AL, Herrera D, Jepsen S, Konstantinidis A, Makrilakis K, et al. Periodontitis and diabetes: a two-way relationship. *Diabetologia* 2012;55(1):21-31.
24. Leenders F, Groen N, de Graaf N, Engelse MA, Rabelink TJ, de Koning EJP, et al. Oxidative Stress Leads to β -Cell Dysfunction Through Loss of β -Cell Identity . *Front Immunol* . 2021;12:690379.
25. Liu X, Xu J, Li S, Wang X, Liu J, Li X. The prevalence of gingivitis and related risk factors in schoolchildren aged 6–12 years old. *BMC Oral Health* 2022;22(1):623.
26. Babatzia A, Papaioannou W, Stavropoulou A, Pandis N, Kanaka-Gantenbein C, Papagiannoulis L, et al. Clinical and microbial oral health status in children and adolescents with type 1 diabetes mellitus†. *Int Dent J*. 2020;70(2):136-44.
27. Ferizi L, Bimbashi V, Kelmendi J. Association between metabolic control and oral health in children with type 1 diabetes mellitus. *BMC Oral Health*. 2022;22(1):502.
28. Ismail AF, McGrath CP, Yiu CKY. Oral health status of children with type 1 diabetes: a comparative study. *J Pediatr Endocrinol Metab*. 2017; 30(11):1155-59.
29. Costa R, Ríos-Carrasco B, Monteiro L, López-Jarana P, Carneiro F, Relvas M. Association between Type 1 Diabetes Mellitus and Periodontal Diseases. *J Clin Med*. 2023;12(3):1147.
30. Santamaria-Jr M, Bagne L, Zaniboni E, Santamaria MP, Jardini MAN, Felonato M, et al. Diabetes mellitus and periodontitis: Inflammatory response in orthodontic tooth movement. *Orthod Craniofac Res*. 2020;23(1):27-34.
31. Prapulla DV, Sujatha PB, Pradeep AR (2007) Gingival Crevicular Fluid VEGF Levels in Periodontal Health and Disease. *J Periodontol*. 2007;78(9):1783-7.
32. Patil PB, Patil BR. Saliva: A diagnostic biomarker of periodontal diseases. *J Indian Soc Periodontol*. 2011;15(4):310-7.
33. Belstrøm D, Damgaard C, Könönen E, Gürsoy M, Holmstrup P, Gürsoy UK. Salivary cytokine levels in early gingival inflammation *J Oral Microbiol*. 2017; 9(1):1364101.
34. Pradeep AR, Prapulla DV, Sharma A, Sujatha PB. Gingival crevicular fluid and serum vascular endothelial growth factor: Their relationship in periodontal health, disease and after treatment. *Cytokine*. 2011;54(2):200-4.
35. Seckin D, İlhan N, İlhan N, Ertugrul S. Glycaemic control, markers of endothelial cell activation and oxidative stress in children with type 1 diabetes mellitus. *Diabetes Res Clin Pract*. 2006;73(2):191-7.
36. Padma R, Sreedhara A, Indeever P, Sarkar I, Kumar CS (2014). Vascular Endothelial Growth Factor Levels in Gingival Crevicular Fluid Before and after Periodontal Therapy. *J Clin Diagn Res J*. 2014; 8(11):ZC75-9.
37. Hertiš Petek T, Petek T, Močnik M, Marčun Varda N. Systemic Inflammation, Oxidative Stress and Cardiovascular Health in Children and Adolescents: A Systematic Review. *Antioxidants*. 2022; 11(5):894.
38. Hasan HR, Abdel Rasul RJ. Impact of psoriasis disease and its treatment with Etanercept on serum and saliva thiol-disulfide homeostasis. *Egypt J Chem*. 2023;66(9):37-46.

-
39. Tvarijonaviciute A, Martinez-Lozano N, Rios R, Marcilla de Teruel MC, Garaulet M, Cerón JJ. Saliva as a non-invasive tool for assessment of metabolic and inflammatory biomarkers in children. *Clin Nutr.* 2020;39(8):2471-8.
40. Tayman MA, Bal C, Nural C, Günhan M (2021) Evaluation of Dynamic Thiol/Disulphide Homeostasis in Patients with Periodontitis. *Meandros Med Dental J.* 2021;22:41-9.
41. Kallinikou D, Soldatou A, Tsentidis C, Louraki M, Kanaka-Gantenbein C, Kanavakis, E et al. Diabetic neuropathy in children and adolescents with type 1 diabetes mellitus: diagnosis, pathogenesis, and associated genetic markers. *Diabetes Metab Res Rev.* 2019;35(7), e3178.
42. Rossino MG, Lulli M, Amato R, Cammalleri M, Dal Monte M, Casini G. Oxidative stress induces a VEGF autocrine loop in the retina: relevance for diabetic retinopathy. *Cells* 2020; 9(6):1452
43. Domingueti, CP, Dusse LMSA, das Graças Carvalho M, de Sousa LP, Gomes KB, Fernandes AP. Diabetes mellitus: The linkage between oxidative stress, inflammation, hypercoagulability and vascular complications. *J Diabetes Complications.* 2016;30(4):738-45.

Research Article

EVALUATION OF FRACTAL ANALYSES OF THE TRABECULAR BONE REGION IN LESIONED AND HEALTHY MANDIBULAR FIRST PERMANENT MOLARS ACCORDING TO AGE AND GENDER ON PANORAMIC RADIOGRAPHS

 Elif BİLGİN^{1*} and  Emin Caner TÜMEN¹

¹ Department of Pediatric Dentistry, Dicle University Faculty of Dentistry, Diyarbakır, TURKIYE

*Correspondence: elf.bars@gmail.com

ABSTRACT

Objective: This study aimed to investigate the fractal dimension values of trabecular bone in periapical lesions and healthy mandibular first permanent molars, based on age and gender, using panoramic radiographs.

Material and Methods: The panoramic radiographs of a total of 216 patients aged 6-16 years who applied to Dicle University Faculty of Dentistry Department of Pedodontics in 2022 were retrospectively examined. The patients were equally distributed by gender into three age groups: 6-9, 10-12, and 13-16 years. Fractal analysis was applied using the ImageJ program to the regions of interest (ROI's) of 25x25 pixels determined from two different regions on each digital panoramic radiograph, and fractal dimension calculations were performed. The data were analyzed using the Shapiro-Wilk and/or Kolmogorov-Smirnov tests, as well as the Mann-Whitney U and Kruskal-Wallis H tests. The confidence interval for all statistical tests was set at 95%, and the significance level was accepted as $p < 0.05$.

Results: According to the results of the study, the average fractal dimension value of the lesioned region was 1.106, while the average fractal dimension value of the healthy region was 1.116. No statistically significant difference was found in the fractal dimension values between both the lesioned and healthy groups, as well as between the age and gender groups ($p > 0.05$).

Conclusion: Fractal dimension (FD) calculation is a reliable method for detecting early-stage periapical lesions. However, to achieve more comprehensive evaluations, future studies should integrate histological and clinical parameters and compare 2D and 3D imaging techniques with larger sample sizes.

Keywords: Periapical Lesion, Panoramic Radiography, Fractal Analysis, ImageJ, ROI

Received: 18 November 2024
Revised: 17 December 2024
Accepted: 18 December 2024
Published: 22 December 2024



Copyright: © 2024 by the authors. Published Aydın Adnan Menderes University, Faculty of Medicine and Faculty of Dentistry. This is an open access article under the Creative Commons Attribution Non Commercial 4.0 International (CC BY-NC 4.0) License.

INTRODUCTION

The radiographic diagnosis of periapical pathologies is the first step in determining the treatment strategy. For periapical pathologies to be diagnosed using conventional radiographs, there must be approximately %30-50 mineral loss in the bone (1). This can lead to the inability to detect lesion formation in the early stages with conventional radiographs. Trabecular bone is often preferred for evaluating bone health because it is metabolically more active than cortical bone and has a significantly higher renewal rate (2). Considering these factors, the combined examination of the bone structure of the jaws using radiographs and analyses has gained importance in dentistry in recent years. For this purpose, the "Fractal Analysis" method, which is a non-invasive diagnostic tool capable of detecting bone loss at an early stage and providing objective data, has been developed (3). The word "fractal" is derived from the Latin word "fractus," meaning "broken" or "fragmented" (4). Fractal Analysis (FA) is a mathematical method that allows for the quantitative description of complex structures and shapes that cannot be expressed by integral dimensions. It is numerically expressed as fractal dimension (FD). FD describes the complexity of a structure. Generally, a high FD indicates a more complex structure, while a low FD indicates a simpler internal order (5). Fractal analysis is used in medicine for the detection and monitoring of diseases and has gradually found a wide range of applications in dentistry (6).

This study aims to evaluate the fractal dimensions of trabecular bone in the apical regions of both lesioned and healthy mandibular first permanent molars using panoramic radiographs, with the goal of exploring the potential of fractal analysis for radiographic diagnosis and investigating the relationship between fractal dimension and factors such as gender and age.

MATERIALS AND METHODS

Power Analysis of the Study

The patients were equally distributed by gender into three age groups: 6-9, 10-12, and 13-16 years. A theoretical power value of 81% was calculated with a 5% margin of error and a 95% confidence level, based

on gender distinction and an effect size of 0.25. The study aimed to include at least 216 observations. The power calculation was performed using the GPower 3.1 software package.

Study Sample

The panoramic radiographs of a total of 216 patients aged 6-16 years who applied to Dicle University Faculty of Dentistry Department of Pedodontics in 2022 were retrospectively examined. This is a monocentric, cross-sectional study aimed at evaluating and comparing fractal dimension analyses of trabecular bone in specific regions of the lesioned and healthy lower permanent first molars, based on age and gender. The analysis was performed using ImageJ software on panoramic radiographs saved in TIFF format. Inclusion criteria for the panoramic radiographs involved ensuring the clear visibility of the mandibular anterior, premolar, molar, ramus, angle, TMJ region, and inferior mandibular cortex, the absence of ghost images, and the use of the same device and consistent exposure parameters for capturing the radiographs.

Study groups were formed for three different age groups: 6-9 years, 10-12 years, and 13-16 years, considering gender distribution. A total of 72 patients, 36 boys and 36 girls from each age group, were selected to meet the inclusion criteria, totaling 216 patients (Table 1).

Table 1. Inclusion and exclusion criterias.

Inclusion	Being in the mixed and/or permanent dentition period.
	Having erupted mandibular first permanent molars.
	Having a lesion at the apex of either the 36 or 46 tooth.
	Having either the 36 or 46 tooth without decay.
	No extraction performed on the 36 and 46 teeth.
	Patients with diagnostic panoramic radiographs without various artifacts or positioning errors.
Exclusion	Presence of cysts and tumors involving the 36 and/or 46 teeth.
	Prior restorative treatment and/or root canal treatment on the 36 and/or 46 teeth.
	Presence of a fracture in the relevant bone region.

Data Collection

All panoramic radiographs were taken with a Progeny (Midmark Company, USA) X-ray device using the following exposure parameters: 0.5 mm focal spot, 3.2 mm filtration, 70 kVp, 10 mA, and 15.9 seconds.

Application of Fractal Analysis

In our study, the ImageJ 1.54d image analysis program, which can be downloaded for free from "https://imagej.nih.gov," was used for FD measurement. The analysis was conducted by E.B. using the box counting method by White and Rudolph (7). High-resolution images of patients included in the study were obtained in Tagged Image File Format (TIFF) from the database for processing panoramic images. Using the ImageJ 1.54d program, the images belonging to the patients were opened and the relevant regions (ROI - Region of Interest) were selected (Figure 1). On each panoramic radiograph, one ROI was determined from the apical region of the healthy mandibular first permanent molar (caries-free and without a lesion at the apex) and its symmetric mandibular first permanent molar with a lesion at the apex. The selected ROI's were 25x25 pixels in size, with a total of 2 ROI's per patient (Figure 1).

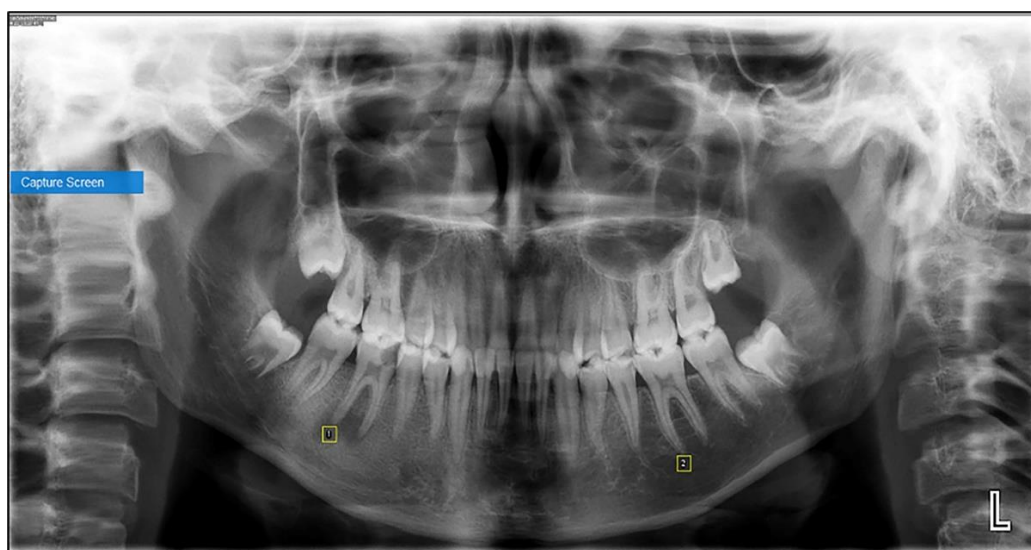


Figure 1. Selected regions of interest (ROI's) on panoramic radiograph; ROI 1 is determined at the apex of the lesioned right mandibular first permanent molar, and ROI 2 is determined at the apex of the healthy left mandibular first permanent molar.

The steps followed in the method designed by White and Rudolph for fractal dimension analysis were used (7) (Figure 2).

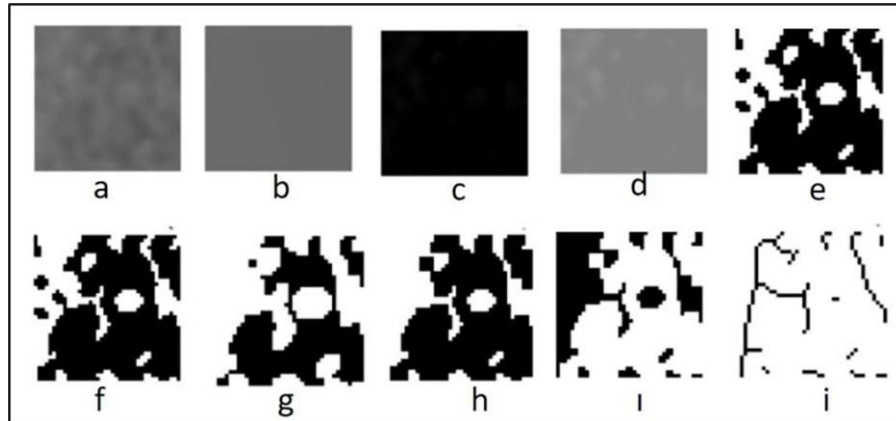


Figure 2. Steps of the box counting method; a. Cropped image of the relevant region, b. Duplicated image, c. Application of Gaussian filter, d. Image subtracted from the original, e. Addition of gray tones, f. Creation of a binary (two-color) image, g. Erosion, h. Dilation, i. Inversion of colors, i. Skeletonization.

Initially, panoramic radiographic images saved in TIFF format were transferred to the ImageJ program, and the square-shaped relevant region (ROI) of 25x25 pixels selected on the radiograph (Figure 1) was cropped using the "crop" feature. The cropped ROI was duplicated using the "duplicate" feature. The duplicated image was blurred using the "Gaussian Blur" filter with a sigma value of 35 pixels. The purpose of this step is to remove density differences on the image caused by soft tissue covering the bone surface and changes in bone thickness, making sharper differences more pronounced. Next, the blurred image was subtracted from the original image using the "Subtract" feature, and 128 gray tones were added to each pixel using the "Add" feature. The various brightness areas in the resulting image distinguish the trabecular structure from the bone marrow. The "Binary" process was applied to convert the image to black and white, creating a two-color image, making the outlines of the trabecular structure and bone marrow clearly visible. The noise in the image was eroded and reduced using the "Erode" feature, and the existing areas were enlarged and clarified using the "Dilate" feature. The image was inverted using the "Invert" feature, making the black areas white and the white areas black, revealing the outlines of the trabecular bone. The outlines of the trabecular bone were converted into a skeletal structure with lines using the "Skeletonize" feature, making them ready for fractal analysis. As the final step, the fractal dimension calculation for the trabecular outlines was performed using the "Analyze" feature. The image was divided into squares of 2, 3, 4, 6, 8, 12, 16, 32, and 64 pixels in size using the "Fractal Box Count" option (Figure 3).

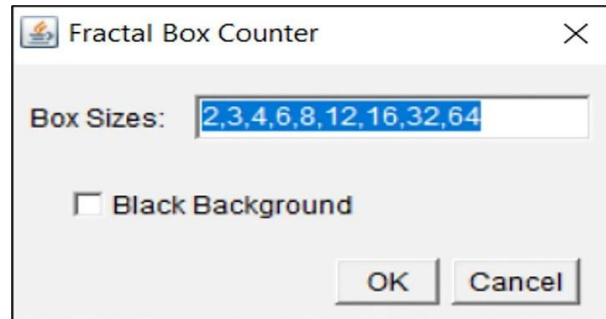


Figure 3. Box counting algorithm in fractal analysis.

The number of squares containing trabeculae and the total number of squares in the image were calculated for each pixel of various sizes. A logarithmic scale graph of the obtained values was plotted. The slope of the line obtained by connecting the points on the graph provided the fractal dimension value, indicating the complexity of the structure (7) (Figure 4).

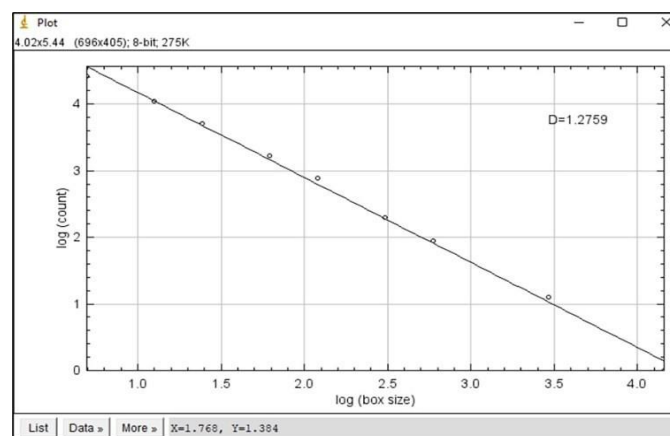


Figure 4. Plotting of values on a logarithmic scale. The slope of the line represents the fractal dimension value and is indicated by "D" in the figure. $FD = D$

Statistical Analysis

The data obtained in this study were analyzed using the licensed IBM SPSS V 21 software package. The Shapiro-Wilk and/or Kolmogorov-Smirnov tests were performed to assess the normality of the variables, considering the number of units. Since the variables did not follow a normal distribution, the Mann-Whitney U and Kruskal-Wallis H tests were employed to examine the differences between groups. In cases where significant differences were observed in the Kruskal-Wallis H test, the Post-Hoc Multiple Comparison Test was applied to identify the groups exhibiting differences. The confidence interval for all statistical tests was set at 95%, and the significance level was accepted as $p < 0.05$.

RESULTS

A total of 216 patients, comprising 108 girls and 108 boys aged 6-16 years, who met the inclusion criteria for this retrospective study, were selected as the sample. Fractal dimension measurements of the trabecular bone in the apical region of lesioned and healthy right or left mandibular first permanent molars were performed using panoramic radiographs. The measurement results were then compared based on gender and age.

Demographic Results

Of the participants included in the study, 50% were girls and 50% were boys. The participants were divided into three equal age groups: 6-9 years, 10-12 years, and 13-16 years (Table 2).

Table 2. Demographic data.

		Sample Size	%
Gender	Boy	108	50
	Girl	108	50
	Total	216	100
Age	6-9 years	72	33.33
	10-12 years	72	33.33
	13-16 years	72	33.33
	Total	216	100

FD Measurements

The average fractal dimension (FD) measurement value of the lesioned group among the participants is 1.106, while the average FD measurement value of the healthy group is 1.116 (Table 3).

Table 3. Distributions of measurement values.

	n	Mean	Median	Min	Max	Sd
Lesioned fractal analysis measurement value	216	1.106	1.139	0.051	1.346	0.156
Healthy fractal analysis measurement value	216	1.116	1.154	0.104	1.314	0.182

n: Sample size; *Sd*: Standard deviation.

Although no statistically significant difference was found between the groups in terms of fractal dimension measurements for lesioned and healthy areas, the FD value measured from the radiographs of the lesioned group was found to be lower ($p>0.05$) (Table 4).

Table 4. Analysis results regarding the difference between groups in terms of lesioned and healthy fractal analysis measurement values.

Group								Mann Whitney U Test		
		n	Mean	Median	Min	Max	Sd	Mean Rank	z	p
Fractal Analysis Measurement Value	Lesioned	216	1.106	1.139	0.051	1.346	0.156	205.16	-1.887	0.059
	Healthy	216	1.116	1.154	0.104	1.314	0.182	227.84		
	Total	432	1.111	1.144	0.051	1.346	0.17			

Although no statistically significant difference was found between genders in terms of fractal dimension measurements for lesioned and healthy areas, the FD values measured from the radiographs of boys were found to be higher ($p>0.05$) (Table 5).

Table 5. Analysis results regarding the difference between genders in terms of lesioned and healthy fractal analysis measurement values.

Gender								Mann Whitney U Test		
		n	Mean	Median	Min	Max	Sd	Mean Rank	z	p
Lesioned fractal analysis measurement value	Boy	108	1.11	1.131	0.563	1.346	0.136	107.65	-0.2	0.841
	Girl	108	1.102	1.14	0.051	1.305	0.174	109.35		
	Total	216	1.106	1.139	0.051	1.346	0.156			
Healthy fractal analysis measurement value	Boy	108	1.136	1.152	0.384	1.312	0.13	110.39	-0.444	0.657
	Girl	108	1.096	1.154	0.104	1.314	0.222	106.61		
	Total	216	1.116	1.154	0.104	1.314	0.182			

n: Sample size; Significant at $p \leq 0.05$; Sd: Standard deviation; z: Mann Whitney U Test Statistic.

No statistically significant difference was found between the age groups regarding the fractal dimension measurement values for both lesioned and healthy areas ($p>0.05$) (Table 6).

Table 6. Analysis results regarding the difference between age groups in terms of lesioned and healthy fractal analysis measurement values.

	Age							Kruskal Wallis H Test		
	Years	n	Mean	Median	Min	Max	Sd	Mean Rank	H	p
Lesioned fractal analysis measurement value	6-9	72	1.116	1.15	0.673	1.305	0.138	113.79	1.393	0.498
	10-12	72	1.079	1.132	0.051	1.326	0.201	101.76		
	13-16	72	1.122	1.126	0.834	1.346	0.114	109.95		
	Total	216	1.106	1.139	0.051	1.346	0.156			
Healthy fractal analysis measurement value	6-9	72	1.132	1.147	0.538	1.312	0.131	108.65	0.299	0.861
	10-12	72	1.126	1.148	0.538	1.314	0.131	105.58		
	13-16	72	1.089	1.172	0.104	1.305	0.256	111.27		
	Total	216	1.116	1.154	0.104	1.314	0.182			

n: Sample size; Significant at $p \leq 0.05$; *Sd*: Standard deviation; *H*: Kruskal Wallis H Test Statistic.

DISCUSSION

Periapical pathologies provide general information about the need for endodontic treatment. Additionally, in the pediatric patient group, tooth extraction may be preferred over endodontic treatments in the presence of periapical lesions, especially in teeth with open apices. The diagnosis of periapical pathologies is the first step in determining the treatment strategy to be applied (8).

It is not possible to monitor early-stage bone destruction with radiographic examination. It has been reported that mineral loss in the bone must be between %30-50 to be diagnosed with conventional radiographs (9). This situation poses the risk of failing to detect lesion formation at an early stage with conventional radiographs. Changes in the trabecular and cortical structure of the bone can be an early indication of certain pathologies, local or systemic diseases; therefore, the combined examination of the bone structure of the jaws using radiographs and analyses has become quite important in dentistry (3).

In recent years, "fractal analysis," a radiographic analysis method that can detect bone loss at an early stage, is not affected by adversities that can hinder the accurate evaluation of radiographs, and provides completely objective data by eliminating practitioner-dependent factors, has been frequently used (10). It is a mathematical analysis method that can evaluate irregular and complex body structures. Some researchers

have shown that the complex structure of trabecular bone can be examined on radiographs using this method (7, 11). When applied to trabecular bone images on radiographs, this method is considered a reflection of the trabecular bone microarchitecture and provides information about changes in mineral content and density in the alveolar bone over time (12, 13). It is thought that the fractal analysis method will contribute to radiographic examination by examining details in the bone structure that are not visible to the naked eye (14, 15).

Considering this information, the use of fractal analysis as a non-invasive diagnostic tool based on objective and quantitative data was preferred in our study for diagnosing periapical pathologies. This method was selected due to its superior ability to reflect the metabolic activity of trabecular bone and its potential to offer valuable diagnostic insights in detecting changes in bone structure.

Since it is free to use and easily accessible, fractal analysis in our study was performed using the box counting method with the ImageJ 1.54d (ImageJ®, National Institute of Mental Health, Bethesda, MD, US) software.

In a study by Demirbaş et al., where they examined the trabecular structure of the mandible using fractal analysis on panoramic radiographs of patients with sickle cell anemia, they found lower FD values compared to healthy individuals. The FD values were lower in the anemia group (1.68 ± 0.08) compared to the control group (1.71 ± 0.04) (16). These findings support the results of Gümüşsoy et al., who found lower FD values in patients with chronic kidney failure compared to healthy individuals (17). Demiralp et al. found the average FD values in patients using bisphosphonates (1.39 ± 0.14) to be higher than those of the healthy control group (1.38 ± 0.07). They suggested that this result might be related to the reduced bone resorption in patients using bisphosphonates (18). Southard et al., in a study conducted on 10 cadaver maxillae, created artificial bone lesions and found that the average FD value decreased from 1.26 to 1.1 with ongoing mineral loss in the calculations they performed on the periapical radiographs they obtained (12). Chen et al., in a study where they measured FD in periapical radiographs taken for follow-up at 3, 6, and 12 months after root canal treatments of premolar and molar teeth with periapical lesions larger than 2 mm, observed a significant increase in fractal dimension 3 months after the root canal treatment ($p < 0.05$). They concluded that fractal analysis could be used to detect changes in periapical trabecular bone at an early stage after root canal

treatment (19). In a study by Aktuna Belgin et al., where they evaluated the mesial and distal interdental regions of mandibular first molars in periodontitis and healthy individuals using fractal analysis on periapical radiographs, the average FD value was found to be 1.04 in the healthy group and 0.97 in the periodontitis group. The average FD value was significantly lower in the periodontitis group compared to the healthy group ($p < 0.05$) (20).

In a study by ShROUT et al., cadaver mandibles were divided sagittally into two halves, and trabecular bone was gradually removed in 4 stages. Fractal analysis was applied to the periapical radiographs taken after each stage. They reported an increase in fractal dimension over time as the stages progressed (21). In a study by Ruttiman et al., trabecular bone decalcification was performed on cadaver mandibles using 10% formic acid, and fractal analysis was then performed on the periapical radiographs taken afterward. They reported that the FD values calculated after decalcification were greater than the FD values calculated before decalcification (22).

According to the literature, there is no consensus on the relationship between FD and the complexity of trabecular bone. In some cases, a decrease in FD value can be observed in radiographs due to reduced bone density. In one study, this was explained by the fact that demineralization makes the bone more porous and simple, increasing the spaces within the bone due to the decreased complexity of the trabecular structure (23). In some cases, despite a decrease in bone density in radiographs, an increase in FD value can be observed. In one study, it was stated that the loss of thin trabecular structure due to demineralization could cause abrupt density changes in radiographic images, leading to changes in fractal dimension. In other words, the increase in FD was expressed as a reflection of the increase in image roughness due to the architectural irregularity of the trabecular network through demineralization (24). These results regarding the observation of FD increase are similar to the studies by ShROUT et al. (21) and Ruttiman et al. (22).

In our study, the average FD value of healthy teeth was found to be 1.116, and the average FD value of lesioned teeth was found to be 1.106. No statistically significant difference was found between the FD values ($p > 0.05$). Our findings are consistent with the studies of Demirbař et al. (16), Gümüřsoy et al. (17), Chen et al. (19), Southard et al. (12), and Aktuna Belgin et al. (20), which report that the FD value in the diseased or lesioned group is lower compared to the healthy group.

In some studies examining the effect of gender on FD, it has been reported that women have lower FD values than men. In a study by Güleç et al., which investigated the effect of gender on FD in systemically healthy individuals, a significant difference was found between the FD values of the right angulus and left condyle according to gender, and it was reported that FD values were generally lower in women (25). In a study by Alman et al. examining FD values in patients with osteopenia according to gender, it was found that women had lower FD values than men (26). Higher FD values in men are associated with a higher and more complex trabecular structure. In contrast, the trabecular structure in women is more porous and contains fewer trabeculae (27).

There are also studies in the literature that report no relationship between gender and FD. In a study by Updike et al., which examined the effect of chronic periodontitis on FD, no relationship was found between gender and FD (3). In a study by Gümüşsoy et al., which used fractal analysis to examine changes in the trabecular structure of the mandible caused by chronic kidney failure, no relationship was found between gender and FD (17).

In this study, the sample consisted of an equal number of boys and girls, with 36 boys and 36 girls in each age group (6-9, 10-12, and 13-16 years), totaling 216 individuals. No statistically significant difference was found between the fractal dimension (FD) values of lesioned and healthy teeth according to gender ($p>0.05$). The observation that boys had higher FD values, although not statistically significant, is consistent with the findings of Güleç et al. (25) and Alman et al. (26). Our results also align with the studies by Updike et al. (3) and Gümüşsoy et al. (17), which report no association between gender and FD. We suggest that the variability in results from studies investigating the relationship between gender and FD may be attributed to differences in sample sizes and gender distribution inequalities.

In a study by Demirbaş et al. examining the relationship between changes in the trabecular structure of the mandible and fractal dimension (FD) on panoramic radiographs of patients with sickle cell anemia, it was found that the average FD values of patients under 20 years old were significantly lower than those of patients over 20 years old (16). In a study by Demiralp et al. involving patients using bisphosphonates, no significant relationship was found between FD values and age (18). Similarly, in a study by Güleç et al. measuring FD

values on panoramic radiographs of children aged 5-11 years with sleep bruxism, no significant relationship was observed between age and FD values. The researchers attributed these findings in children to developmental changes occurring with age (28).

In our study, no statistically significant difference was found between the fractal dimension (FD) values of lesioned and healthy teeth based on age ($p>0.05$). Our findings are consistent with those of Demiralp et al. (18) and Güleç et al. (28), who also reported no relationship between age and FD in the literature.

Factors such as anatomical variations, the variety of radiographic methods used to obtain 2D bone images, radiographic errors such as artifacts, lack of calibration in radiographic devices, differences in sample sizes, the profiles of patients included in the samples, the techniques used for FD measurement, and the varied selection of regions of interest (ROIs) in terms of size, location, and shape are believed to contribute to the inability to standardize the results found in the literature (29).

Due to the retrospective nature of this study, potential effects of systemic diseases present in the sample group on FD values, as well as challenges in maintaining consistent panoramic radiograph standards in pediatric patients, can be considered limitations of our study.

CONCLUSION

Based on the findings and insights from our study, FD calculation can be recommended as a quantitative and objective method for detecting early-stage periapical lesions that are clinically suspected but not visible to the naked eye. Although fractal analysis is a reliable technique, it is crucial to incorporate histological and clinical parameters in future studies to reach consensus among researchers. While 2D imaging methods are frequently employed in evaluating fractal dimension, further comprehensive studies comparing these methods with 3D imaging techniques and including larger sample sizes are needed.

Acknowledgments

This study was produced by the specialization thesis published under the supervision of E.C.T.

Authorship contributions

E.B. and E.C.T. designed the research study; performed the research; analyzed the data; wrote the manuscript. All authors contributed to editorial changes in the manuscript. All authors read and approved the final manuscript.

Data availability statement

The data that support the findings of this study are available from the corresponding author upon reasonable request.

Declaration of competing interest

The authors have no conflicts of interest to declare.

Ethics

This study, approved by the Local Ethics Committee of the Faculty of Dentistry, Dicle University, under protocol number 2022-45 on December 28, 2022, was conducted in accordance with the ethical principles of the World Medical Association's Declaration of Helsinki.

Funding

No financial support was received from any institution or organisation for this study.

REFERENCES

1. Bender I, Seltzer S. Roentgenographic and direct observation of experimental lesions in bone:II. *Journal of endodontics*. 2003;29(11):707-12.
2. Frost HM. Dynamics of bone remodeling. *Bone biodynamics*. 1964;315-34.
3. Updike SX, Nowzari H. Fractal analysis of dental radiographs to detect periodontitis-induced trabecular changes. *Journal of periodontal research*. 2008;43(6):658-64.
4. Geraets W, Van Der Stelt P. Fractal properties of bone. *Dentomaxillofacial Radiology*. 2000;29(3):144-53.
5. Mandelbrot BB, Mandelbrot BB. *The fractal geometry of nature: WH freeman New York*; 1982.
6. Kurşun-Çakmak EŞ, Bayrak S. Comparison of fractal dimension analysis and panoramic-based radiomorphometric indices in the assessment of mandibular bone changes in patients with type 1 and type 2 diabetes mellitus. *Oral surgery, oral medicine, oral pathology and oral radiology*. 2018;126(2):184-91.
7. White SC, Rudolph DJ. Alterations of the trabecular pattern of the jaws in patients with osteoporosis. *Oral Surgery, Oral Medicine, Oral Pathology, Oral Radiology, and Endodontology*. 1999;88(5):628-35.
8. Kantor ML, Zeichner SJ, Valachovic RW, Reiskin AB. Efficacy of dental radiographic practices: options for image receptors, examination selection, and patient selection. *The Journal of the American Dental Association*. 1989;119(2):259-68.
9. Jeffcoat MK. Radiographic methods for the detection of progressive alveolar bone loss. *Journal of periodontology*. 1992;63:367-72.
10. Sener E, Cinarcik S, Baksi BG. Use of fractal analysis for the discrimination of trabecular changes between individuals with healthy gingiva or moderate periodontitis. *Journal of periodontology*. 2015;86(12):1364-9.
11. Kato CN, Barra SG, Tavares NP, Amaral TM, Brasileiro CB, Mesquita RA, et al. Use of fractal analysis in dental images: a systematic review. *Dentomaxillofacial Radiology*. 2020;49(2):20180457.
12. Southard TE, Southard KA, Jakobsen JR, Hillis SL, Najim CA. Fractal dimension in radiographic analysis of alveolar process bone. *Oral Surgery, Oral Medicine, Oral Pathology, Oral Radiology, and Endodontology*. 1996;82(5):569-76.
13. Bollen A, Taguchi A, Hujoel P, Hollender L. Fractal dimension on dental radiographs. *Dentomaxillofacial Radiology*. 2014.

14. Jolley L, Majumdar S, Kapila S. Technical factors in fractal analysis of periapical radiographs. *Dentomaxillofacial Radiology*. 2006;35(6):393-7.
15. Amer ME, Heo M-S, Brooks SL, Benavides E. Anatomical variations of trabecular bone structure in intraoral radiographs using fractal and particles count analyses. *Imaging science in dentistry*. 2012;42(1):5.
16. Demirbaş AK, Ergün S, Güneri P, Aktener BO, Boyacıoğlu H. Mandibular bone changes in sickle cell anemia: fractal analysis. *Oral Surgery, Oral Medicine, Oral Pathology, Oral Radiology, and Endodontology*. 2008;106(1):e41-e8.
17. Gumussoy I, Miloglu O, Cankaya E, Bayrakdar IS. Fractal properties of the trabecular pattern of the mandible in chronic renal failure. *Dentomaxillofacial Radiology*. 2016;45(5):20150389.
18. Demiralp KÖ, Kurşun-Çakmak EŞ, Bayrak S, Akbulut N, Atakan C, Orhan K. Trabecular structure designation using fractal analysis technique on panoramic radiographs of patients with bisphosphonate intake: a preliminary study. *Oral Radiology*. 2019;35:23-8.
19. Chen S-K, Oviir T, Lin C-H, Leu L-J, Cho B-H, Hollender L. Digital imaging analysis with mathematical morphology and fractal dimension for evaluation of periapical lesions following endodontic treatment. *Oral Surgery, Oral Medicine, Oral Pathology, Oral Radiology, and Endodontology*. 2005;100(4):467-72.
20. Aktuna Belgin C, Serindere G. Evaluation of trabecular bone changes in patients with periodontitis using fractal analysis: A periapical radiography study. *Journal of Periodontology*. 2020;91(7):933-7.
21. Shrout MK, Jett S, Mailhot JM, Potter BJ, Borke JL, Hildebolt CF. Digital image analysis of cadaver mandibular trabecular bone patterns. *Journal of periodontology*. 2003;74(9):1342-7.
22. Ruttimann UE, Webber RL, Hazelrig JB. Fractal dimension from radiographs of peridental alveolar bone: a possible diagnostic indicator of osteoporosis. *Oral surgery, oral medicine, oral pathology*. 1992;74(1):98-110.
23. Sanchez-Molina D, Velazquez-Ameijide J, Quintana V, Arregui-Dalmases C, Crandall JR, Subit D, et al. Fractal dimension and mechanical properties of human cortical bone. *Medical engineering & physics*. 2013;35(5):576-82.
24. Saeed SS, Ibraheem UM, Alnema MM. Quantitative analysis by pixel intensity and fractal dimensions for imaging diagnosis of periapical lesions. *International Journal of Enhanced Research in Science Technology & Engineering*. 2014;3(5):138-44.
25. Güleç M, Taşöker M, Özcan S. Mandibular trabeküler kemiğin fraktal boyutu: Yaş, cinsiyet ve ilgi alanı seçiminin önemi nedir? *Selcuk Dental Journal*. 2019;6(4):15-9.
26. Alman A, Johnson L, Calverley D, Grunwald G, Lezotte D, Hokanson J. Diagnostic capabilities of fractal dimension and mandibular cortical width to identify men and women with decreased bone mineral density. *Osteoporosis International*. 2012;23:1631-6.
27. Podsiadlo P, Dahl L, Englund M, Lohmander L, Stachowiak G. Differences in trabecular bone texture between knees with and without radiographic osteoarthritis detected by fractal methods. *Osteoarthritis and Cartilage*. 2008;16(3):323-9.
28. Gulec M, Tassoker M, Ozcan S, Orhan K. Evaluation of the mandibular trabecular bone in patients with bruxism using fractal analysis. *Oral radiology*. 2021;37:36-45.
29. Pornprasertsuk S, Ludlow J, Webber R, Tyndall D, Yamauchi M. Analysis of fractal dimensions of rat bones from film and digital images. *Dentomaxillofacial Radiology*. 2001;30(3):179-83.

Research Article

HOW RELIABLE IS THE AMOUNT OF INTERPROXIMAL REDUCTION CLINCHECK SOFTWARE RECOMMENDS?

 Yasemin TUNCA¹,  Nihal FAHRZADEH²,  Murat TUNCA¹

¹ Department of Orthodontics, Faculty of Dentistry, Kutahya Health Sciences University, Kutahya, TURKIYE

² Department of Orthodontics, Faculty of Dentistry, Van Yuzuncu Yil University, Van, TURKIYE

*Correspondence: dtmurattunca@gmail.com

ABSTRACT

Objective: This study was conducted to evaluate the reliability of Bolton analysis results obtained with ClinCheck software and the interproximal reduction (IPR) ratios the software recommends.

Materials and Methods: From the Invisalign® clear aligner system database, 120 individuals were divided into three groups according to Angle classification: dental class I (n=43), dental class II (n=49), and dental class III (n=28) malocclusions. The Bolton analysis data and the IPR amounts determined by Align Technology's digital treatment planning interface, ClinCheck, were evaluated separately for the maxilla and mandible for each individual. A discrepancy was defined as the condition in which the Bolton ratio the software determined and the suggested IPR amount for the anterior ratio and the overall ratio exceeded 2 mm. The average anterior Bolton ratio and suggested anterior Bolton ratio, along with the total Bolton ratio and suggested total Bolton ratio for all individuals, were compared using Cronbach's alpha.

Results: It was determined that the average suggested anterior Bolton ratio for individuals with class I malocclusion was higher than that for individuals with other malocclusions ($p=0.008$). Cronbach's alpha for the anterior Bolton ratio and the suggested anterior Bolton ratio was 0.131 whereas the overall ratio and the suggested overall Bolton ratio value were determined to be 0.41. Both values are defined as indicating weak reliability.

Conclusion: A weak reliability relationship was detected between the Bolton values obtained with the ClinCheck software and the IPR suggestions provided in treatment planning.

Keywords: Invisalign, clincheck software, interproximal reduction, bolton

Received: 13 November 2024

Accepted: 18 December 2024

Published: 22 December 2024



Copyright: © 2024 by the authors. Published Aydın Adnan Menderes University, Faculty of Medicine and Faculty of Dentistry. This is an open access article under the Creative Commons Attribution Non Commercial 4.0 International (CC BY-NC 4.0) License.

INTRODUCTION

In clear aligner treatments, software that facilitates digital treatment planning for diagnosis and treatment purposes is utilized (1). Each clear aligner manufacturer employs its own software under various names (2). Currently, the widely preferred company Invisalign® (Align Technology, San Jose, Calif) uses ClinCheck™ (Align Technology) (1,2). This software offers clinicians model analyses used for diagnostic purposes before treatment planning, such as tooth movement charts, space analysis, initial and final overjet, overbite, and Bolton analysis (3).

Three-dimensional models obtained with scanners give near-real results in linear measurements or analyses and are reliably used (4–6). Meade et al. (7) stated that the initial overjet and overbite values in ClinCheck can be reliably used. However, Martin et al. (8) mentioned that although the mesiodistal widths of teeth, excluding the molars, are acceptable, the results of the Bolton analysis are not accurate and acceptable, especially for individuals with excess material in the mandibular teeth. Shailendran et al. (9) also indicated that the mesiodistal widths of teeth obtained with ClinCheck are recorded as smaller, and attention should be paid to this issue in Bolton analysis ratios and treatment planning.

In the studies, it was reported that gender had no effect on the bolton ratio, while significant differences were found in the bolton ratios of individuals with different dental malocclusions (10,11). Differences in Bolton analysis can lead the clinician to consider different treatment plans. This particularly includes unnecessary or insufficient interproximal reduction (IPR) from the enamel surface, which might result in the planned tooth movement not occurring as well as complications, such as diastema and black triangles after treatment. Fiori et al. (12) stated that in ClinCheck, the IPR process presents the least accurate data, 49% in the maxilla and 42% in the mandible.

In clear aligner treatments, the software used offers the clinician a treatment plan based on the results of the Bolton analysis. This treatment plan may include options such as leaving a diastema or performing an IPR procedure. The initial prescription the clinician requests in their software preferences is also important. Our study was conducted to evaluate the reliability of Bolton analysis results obtained with ClinCheck and the recommended IPR rates for individuals who will undergo treatment planning with the Invisalign system

(Align Technology, San Jose, Calif). Our study's null hypothesis (H0) is "There is no reliability between the results of the Bolton analysis obtained with digital treatment planning and the treatment plans."

MATERIALS AND METHODS

This retrospective study commenced with the approval of the Non-Invasive Clinical Research Ethics Committee of Van Yüzüncü Yıl University (2023/13-11). All individuals or parents of individuals under 18 who applied to the Orthodontics Department of Van Yüzüncü Yıl University for treatment were informed about the study, and written consent forms were obtained. G*power software (ver. 3.1.9.7; Heinrich-Heine-Universität Düsseldorf, Düsseldorf, Germany) was used to determine the sample size. The total sample size was calculated as minimum 84, based on an effect size (d) of 0.4, a Type I error ($\alpha = 0.05$), and a power value of 90% for the three main groups.

The study included individuals aged 15-35 with permanent dentition and no missing, impacted, or atypically erupted teeth. Excluded were cases with prosthetic restorations, such as crowns or implants affecting mesiodistal width; decay; fillings; enamel defects; more than 6 mm of crowding or polydiastema, crown angulations over 45 degrees; indications for orthognathic surgery; cleft lip and palate or other craniofacial anomalies; and those with incomplete three-dimensional model images in screening scans.

All data used in this study were collected from the database registered with the Invisalign® clear aligner system. Participants were divided into three groups based on Angle's classification: dental class I (n=43), dental class II (n=49), and dental class III (n=28) malocclusion.

For the participants' scans, the iTero Element® (iTero Element 5D, Align Technologies Inc, San Jose, CA, USA) three-dimensional intraoral scanner device by Align Technology was used. Following the sequence in the manufacturer's scanning guide, occlusal, lingual, and buccal surfaces and finally, rotating tooth surfaces were scanned. After patients were scanned with the intraoral scanner device, the created tooth-jaw models, along with a detailed treatment plan, were virtually sent to the Invisalign® laboratory. Each patient's prescription in all three groups was checked to ensure the doctor had given no IPR instructions and that the "as needed" option was selected in the IPR section. Additionally, the clinician determined the necessary treatment package

from Align Technology's Comprehensive (unlimited aligners), Moderate (up to 20 aligners), and Lite packages (up to 14 aligners) based on the type of malocclusion.

As a result of these procedures, the Invisalign® company, using software (Treat) that simulates tooth movements, sent back to the clinician a virtual treatment plan and the Bolton analysis results of individuals and the proposed IPR amounts through the ClinCheck™ program as the initial treatment plan (Figure 1). All data were collected from the initial treatment plan in ClinCheck™, with Bolton analysis data for each individual noted in millimeters separately for the maxilla and mandible in an Excel sheet. Then, the proposed IPR data for the same individual in the tools section of ClinCheck™ program were calculated separately for the maxilla and mandible and added to the Excel sheet. Inconsistencies were noted if the discrepancy between the Bolton analysis determined by the software and the suggested amount of IPR exceeded 2 mm in either the anterior or total ratio (13). All data for this study were used from a single clinician's (..) system, and the same clinician noted necessary calculations in the Excel sheet.

Statistical analysis

Descriptive statistics for the focused attributes were expressed as count, mean, and standard deviation. An ANOVA analysis was conducted to evaluate differences between groups regarding the variables, and the Duncan test was applied for multiple comparisons. The reliability of the anterior Bolton ratio and total Bolton ratio values was tested using Cronbach's alpha reliability scale. The Cronbach's alpha range was considered as follows: excellent reliability for $0.90 \leq \alpha \leq 1$, high reliability for $0.70 \leq \alpha < 0.90$, moderate reliability for $0.50 \leq \alpha < 0.70$, and low reliability for $\alpha < 0.50$. (14) The level of statistical significance was set at 5%, and the SPSS (IBM Corp. Armonk, NY, version 21) statistical software package was used for the calculations.

RESULTS

Table 1 presented demographic data according to classes, including gender, average age, and treatment package. Table 2 showed the data of individuals with consistent and inconsistent anterior and total Bolton ratios across the classes. In the anterior Bolton ratio, 5, 10, and 7 individuals were found to have

inconsistent recommended Bolton ratios in Class I, II, and III, respectively. For the total Bolton ratio, 6, 5, and 5 individuals in Class I, II, and III, respectively, were identified with inconsistent recommended Bolton ratios.

Table 1. Distribution of demographic characteristics by classes and packages.

		Class I	Class II	Class III	Total
Gender	Female	32	30	19	120
	Male	11	19	9	
Age (M ± SD)		28.4 ± 8.63	27.14 ± 9.18	27.36 ± 7.88	27.64 ± 8.64
Package	Lite	6	3	2	120
	Moderate	4	1	1	
	Comprehensive	33	45	25	

Table 3 displays the statistical comparisons of the anterior Bolton ratio, total Bolton ratio, recommended anterior Bolton ratio, and recommended total Bolton ratios among the classes. It was found that only the mean of the recommended anterior Bolton ratio in individuals with Class I malocclusion was significantly higher than in individuals with other malocclusions ($p=0.008$).

Table 2. Data of compliant and non-compliant individuals in the overall bolton ratio and anterior bolton ratio within classes.

	Class	Compliant (n)	Non compliant (n)
Anterior Bolton Ratio	I	38	5
	II	39	10
	III	21	7
Overall Bolton Ratio	I	37	6
	II	44	5
	III	23	5

Table 3. Comparisons of anterior bolton ratio, overall bolton ratio, recommended anterior bolton ratio and recommended overall bolton ratio between classes.

	Class	n	Mean	SD	Min	Max	p
Anterior Bolton Ratio	I	43	.1307	.37990	.00	1.89	.728
	II	49	.1963	.61617	.00	3.75	
	III	28	.1107	.46222	.00	2.42	
Overall Bolton Ratio	I	43	.4612	.89087	.00	3.38	.448
	II	48	.2627	.55102	.00	2.38	
	III	28	.4221	.92357	.00	3,49	
Recommended Anterior Bolton Ratio	I	43	.1814 ^a	.49917	.00	2,50	.008
	II	49	.0000 ^b	.00000	.00	.00	
	III	28	.0000 ^b	.00000	.00	.00	
Recommended Overall Bolton Ratio	I	43	.1558	.44040	.00	2.10	.245
	II	49	.2306	.64395	.00	3.00	
	III	28	.0321	.17008	.00	.90	

ANOVA test, SD : Standart Deviation, Min: Minimum, Max: Maximum, n: number of individuals, a-b: No difference between classes with the same letter, $p < 0.05$

Table 4 presents the comparison of Cronbach's alpha between the anterior Bolton ratio and recommended anterior Bolton ratio and between the total Bolton ratio and recommended total Bolton ratio for all individuals. Cronbach's alpha for the anterior Bolton ratio and recommended anterior Bolton ratio was 0.131, and for the total Bolton ratio and recommended total Bolton ratio, it was 0.41. Both values indicate low reliability.

Table 4. Comparison of the Cronbach's Alpha value of the mean of the anterior bolton ratio and the mean of the recommended anterior bolton ratio, and the Cronbach's Alpha value of the mean of the overall bolton ratio and the recommended overall bolton ratio in all individuals.

	n	Mean	SD	Min	Max	α
Anterior Bolton Ratio	120	.1528	.50391	.00	3.75	0.131
Recommended Anterior Bolton Ratio	120	.0650	.30915	.00	2.50	
Overall Bolton Ratio	120	.3719	.77907	.00	3.49	0.41
Recommended Overall Bolton Ratio	120	.1575	.49818	.00	3.00	

Cronbach's Alpha Reliability, SD : Standart Deviation, Min: Minimum, Max: Maximum, n: number of individuals

DISCUSSION

Digital models can accurately obtain linear distances (15,16). Clear aligner software also provides data for some ratios derived from linear measurements, such as the Bolton analysis (8,9). However, there seems to be a gap in the literature regarding the interpretation of these data in treatment options such as leaving a diastema after treatment or IPR during treatment. Studies comparing real mesiodistal measurements of teeth with software-generated Bolton analyses exist (8,9). Current study, however, was conducted to determine the reliability of IPR planning corresponding to Bolton ratios the software identified. In our study, inconsistencies in the recommended IPR amount were found in 22 individuals for the anterior Bolton ratio and in 16 individuals for the total ratio. Furthermore, Cronbach's alpha for the anterior Bolton ratio and recommended anterior Bolton ratio as well as the total Bolton ratio and recommended total ratio were determined to be of low reliability. Therefore, our study's null hypothesis, H_0 , was accepted.

What is ClinCheck's working principle? This is not fully known (17). It is stated that the software used in clear aligner treatments provides outputs based on specific algorithms and inputs (18). Invisalign's website also mentions that it is a cloud-based software supported by data from over 16 million smiles (19). The fact that the software decides where to place optimized attachments without clinician intervention and the limited information about the software suggests it may offer similar treatments to those used in previous malocclusion cases. This seems akin to the system in which numerous images of certain diseases are input into an artificial intelligence database, which then provides preliminary diagnoses when it recognizes similar patterns (20). Nevertheless, many factors affect an individual's orthodontic treatment, including malocclusion type, crowding degree, age, gender, and cooperation (21). Therefore, each orthodontic problem requires a patient-specific orthodontic treatment plan. Even though Invisalign claims to provide treatment plans within minutes without technician involvement, the clinician's role remains crucial for accurate and realistic treatment planning despite all the technological infrastructure.

The recent literature on orthodontics confirms the clinical applicability and validity of the accuracy and reliability of linear measurements, such as space analysis and mesiodistal lengths of teeth, calculated using three-dimensional scanners and software (22–29). However, the treatment plans these software programs offer

do not seem as consistent as linear measurements. Different software can suggest different treatment plans for the same malocclusion (18). Based on Bolton analysis results, a clinician can choose to leave space after treatment or apply IPR during treatment (30). In this context, Andrews' six keys to occlusion, including factors such as molar relationship, crown angulation, crown inclination, absence of rotations, absence of spaces, and the Spee curve, are essential for a correct occlusal relationship (31). Here, even if there is no mesiodistal discrepancy in maxillary and mandibular teeth, the position and inclinations of the incisors are important for proper alignment.

Variability in 1-NA and 1-NB angles and positions can lead to excess space or crowding on the arch. Therefore, in addition to photos and scan images, it is suggested that individuals' cephalometric values should also be reported in the treatment planning software. Additionally, the software should define limits for incisor position and angle. A recent application mentioned the possibility of importing CBCT images into the program (3). However, the lack of indication for every patient and still not providing cephalometric values highlights the importance of clinician vigilance regarding the software.

What is the threshold value of the Bolton discrepancy? Proffit (32) suggested that significant anterior Bolton ratio discrepancies are likely when the upper lateral incisor is not larger than the lower lateral incisor. Additionally, he reported that for posterior Bolton ratio consistency, the second upper and lower premolars should be equal. He also mentioned that Bolton discrepancies under 1.5 mm are not clinically significant. Many studies have typically defined a Bolton discrepancy as 1.5 mm (33–37). Othman and Harradine (13), however, suggested a threshold value of 2 mm for this discrepancy. In the current study, a 2-mm threshold value was accepted, thus considering discrepancies exceeding 2 mm between the Bolton discrepancy identified by ClinCheck software and its recommended IPR amounts as inconsistent.

Martin et al. (8) indicated that although ClinCheck Pro 6.0's results show a positive bias, its measurements for tooth widths, excluding molars, are acceptable. However, they also noted that the software does not use the original Bolton formula and especially in cases of mandibular excess, the anterior Bolton ratio and total Bolton ratio values are not accurate and clinically unacceptable. Shailendran et al. (9) reported that although optical profilometer and caliper measurements are reliable, ClinCheck Pro systematically

underestimates the mesiodistal widths of teeth, with this systematic error increasing toward the posterior of the arch. They found the software moderately reliable for Bolton values.

Zhang et al. (38) evaluated the incidence of open gingival embrasure formations following clear aligner treatment in a large sample. In their study of 2500 individuals, they reported encountering open gingival embrasures in 25.7% of cases between maxillary incisors and 40.3% between mandibular incisors posttreatment. They also emphasized that the IPR process did not prevent this problem. This high incidence rate is concerning. Although their study seems different in subject from ours, it suggests that ClinCheck does not account for the inclination and position of incisors. This supports the need for clinical evaluation of linear and proportional deviations in treatment plans, reinforcing the results of our study. Hariharan et al.(39) stated that the amounts of IPR ClinCheck determines often surpass the actual need. Additionally, our study was conducted to compare the values the software program detected and suggested, revealing weak reliability between the identified anterior Bolton ratio and the suggested anterior Bolton ratio and between the total Bolton ratio and the suggested total Bolton ratio.

The lack of knowledge about how the software calculates the Bolton ratio and the exclusion of software besides ClinCheck from the study are limitations. Further research is needed with a larger sample size and modifications in the software to incorporate incisor position and inclination values.

CONCLUSION

A weak reliability relationship was identified between Bolton values obtained with ClinCheck software and the IPR proposals in the treatment planning. This finding highlights the potential benefits of developing versions of the software that can integrate cephalometric values, such as incisor positions and inclinations.

Acknowledgments

Authors of this study thank to Prof. Dr. Sıddık KESKİN (Department of Biostatistics, Faculty of Medicine, Van Yüzüncü Yıl University)

Authorship contributions

Concept: Yasemin Tunca, Design: Murat Tunca, Supervision: Yasemin Tunca, Resources: Nihal Fahrzadeh, Materials: Nihal Fahrzadeh, Data collection and/or processing: Yasemin Tunca, Analysis and/or interpretation: Murat Tunca, Literature search: Murat Tunca, Nihal Fahrzadeh, Yasemin Tunca, Writing manuscript: Murat Tunca, Yasemin Tunca, Nihal Fahrzadeh, Critical review: Yasemin Tunca

Data availability statement

Not applicable.

Declaration of competing interest

The authors have stated explicitly that there are no conflicts of interest in connection with this article.

Ethics

This study commenced with the approval of the Non-Invasive Clinical Research Ethics Committee of Van Yüzüncü Yıl University (2023/13-11).

Funding

This study was not financially supported.

REFERENCES

1. Hartshorne J, Wertheimer MB. Emerging insights and new developments in clear aligner therapy: A review of the literature. *AJO-DO Clinical Companion* 2022;2:311–324.
2. Dhingra A, Palomo JM, Stefanovic N, et al. Comparing 3D Tooth Movement When Implementing the Same Virtual Setup on Different Software Packages. *J Clin Med* 2022;11:5351.
3. Invisalign. *ClinCheck® Evaluation Guide*.
4. Wiranto MG, Engelbrecht WP, Tutein Nolthenius HE, et al. Validity, reliability, and reproducibility of linear measurements on digital models obtained from intraoral and cone-beam computed tomography scans of alginate impressions. *Am J Orthod Dentofacial Orthop* 2013;143:140–147.
5. Naidu D, Freer TJ. Validity, reliability, and reproducibility of the iOC intraoral scanner: a comparison of tooth widths and Bolton ratios. *Am J Orthod Dentofacial Orthop* 2013;144:304–310.
6. Aragón MLC, Pontes LF, Bichara LM, et al. Validity and reliability of intraoral scanners compared to conventional gypsum models measurements: a systematic review. *Eur J Orthod* 2016;38:429–434.
7. Meade MJ, Blundell H, Weir T. Predicted overbite and overjet changes with the Invisalign appliance: a validation study. *Angle Orthod*. Epub ahead of print September 1, 2023. DOI: 10.2319/041323-269.1.
8. Adobes Martin M, Lipani E, Bernes Martinez L, et al. Reliability of Tooth Width Measurements Delivered by the Clin-Check Pro 6.0 Software on Digital Casts: A Cross-Sectional Study. *Int J Environ Res Public Health* 2022;19:3581.
9. Shailendran A, Weir T, Freer E, et al. Accuracy and reliability of tooth widths and Bolton ratios measured by ClinCheck Pro. *Am J Orthod Dentofacial Orthop* 2022;161:65–73.
10. Alqahtani H. A study to estimate tooth size discrepancy values specific to Saudi orthodontic patients: A systematic review and meta-analysis. *Saudi Dent J* 2023;35:498–507.
11. Machado V, Botelho J, Mascarenhas P, et al. A systematic review and meta-analysis on Bolton's ratios: Normal occlusion and malocclusion. *J Orthod* 2020;47:7–29.
12. Fiori A, Minervini G, Nucci L, et al. Predictability of crowding resolution in clear aligner treatment. *Prog Orthod* 2022;23:43.
13. Othman S, Harradine N. Tooth size discrepancies in an orthodontic population. *Angle Orthod* 2007;77:668–674.
14. Cronbach LJ. Coefficient alpha and the internal structure of tests. *Psychometrika* 1951;16:297–334.
15. Fleming PS, Marinho V, Johal A. Orthodontic measurements on digital study models compared with plaster models: a systematic review. *Orthod Craniofac Res* 2011;14:1–16.
16. Leifert MF, Leifert MM, Efstratiadis SS, et al. Comparison of space analysis evaluations with digital models and plaster dental casts. *Am J Orthod Dentofacial Orthop* 2009;136:16.e1–4; discussion 16.

17. Laganà G, Malara A, Lione R, et al. Enamel interproximal reduction during treatment with clear aligners: digital planning versus OrthoCAD analysis. *BMC Oral Health* 2021;21:199.
18. Eliliwi M, ElShebiny T, de Menezes LM, et al. Comparing virtual setup software programs for clear aligner treatment. *J World Fed Orthod* 2023;12:50–55.
19. <https://www.invisalign.com/provider/ccpro6.0>. ClinCheck 6.0 | Invisalign Provider Available from: <https://www.invisalign.com/provider/ccpro6.0>. Accessed December 24, 2023.
20. Pinto-Coelho L. How Artificial Intelligence Is Shaping Medical Imaging Technology: A Survey of Innovations and Applications. *Bioengineering (Basel)* 2023;10:1435.
21. Skidmore KJ, Brook KJ, Thomson WM, et al. Factors influencing treatment time in orthodontic patients. *Am J Orthod Dentofacial Orthop* 2006;129:230–238.
22. Choi W-J, Lee S-J, Moon C-H. Evaluation of accuracy of 3-dimensional printed dental models in reproducing intermaxillary relational measurements: Based on inter-operator differences. *Korean J Orthod* 2022;52:20–28.
23. Brown GB, Currier GF, Kadioglu O, et al. Accuracy of 3-dimensional printed dental models reconstructed from digital intraoral impressions. *Am J Orthod Dentofacial Orthop* 2018;154:733–739.
24. Mack S, Bonilla T, English JD, et al. Accuracy of 3-dimensional curvilinear measurements on digital models with intraoral scanners. *Am J Orthod Dentofacial Orthop* 2017;152:420–425.
25. Sousa MVS, Vasconcelos EC, Janson G, et al. Accuracy and reproducibility of 3-dimensional digital model measurements. *Am J Orthod Dentofacial Orthop* 2012;142:269–273.
26. Kumar AA, Phillip A, Kumar S, et al. Digital model as an alternative to plaster model in assessment of space analysis. *J Pharm Bioallied Sci* 2015;7:S465-469.
27. Brandão MM, Sobral MC, Vogel CJ. Reliability of Bolton analysis evaluation in tridimensional virtual models. *Dental Press J Orthod* 2015;20:72–77.
28. Porto BG, Porto TS, Silva MB, et al. Comparison of linear measurements and analyses taken from plaster models and three-dimensional images. *J Contemp Dent Pract* 2014;15:681–687.
29. Al-Mashraqi AA, Alhammadi MS, Gadi AA, et al. Accuracy and reproducibility of permanent dentitions and dental arch measurements: comparing three different digital models with a plaster study cast. *Int J Comput Dent* 2021;24:353–362.
30. Wise RJ, Nevins M. Anterior tooth site analysis (Bolton Index): how to determine anterior diastema closure. *Int J Periodontics Restorative Dent* 1988;8:8–23.
31. Andrews LF. The six keys to normal occlusion. *Am J Orthod* 1972;62:296–309.
32. William Proffit, Henry Fields, Brent Larson, et al. *Contemporary Orthodontics*. 6 th. Elsevier, 2018.
33. Freeman JE, Maskeroni AJ, Lorton L. Frequency of Bolton tooth-size discrepancies among orthodontic patients. *Am J Orthod Dentofacial Orthop* 1996;110:24–27.
34. Crosby DR, Alexander CG. The occurrence of tooth size discrepancies among different malocclusion groups. *Am J Orthod Dentofacial Orthop* 1989;95:457–461.
35. Bernabé E, Major PW, Flores-Mir C. Tooth-width ratio discrepancies in a sample of Peruvian adolescents. *Am J Orthod Dentofacial Orthop* 2004;125:361–365.
36. Santoro M, Ayoub ME, Pardi VA, et al. Mesiodistal crown dimensions and tooth size discrepancy of the permanent dentition of Dominican Americans. *Angle Orthod* 2000;70:303–307.
37. Araujo E, Souki M. Bolton anterior tooth size discrepancies among different malocclusion groups. *Angle Orthod* 2003;73:307–313.
38. Zhang Y, Wang X, Wang J, et al. IPR treatment and attachments design in clear aligner therapy and risk of open gingival embrasures in adults. *Prog Orthod* 2023;24:1.
39. Hariharan A, Arqub SA, Gandhi V, et al. Evaluation of interproximal reduction in individual teeth, and full arch assessment in clear aligner therapy: digital planning versus 3D model analysis after reduction. *Prog Orthod* 2022;23:9.

Research Article

FACTORS THAT ARE DETERMINANT IN THE PREPARATION OF EFFECTIVE AND RELIABLE COLONOSCOPY: A PROSPECTIVE CLINICAL STUDY FROM A SINGLE CENTER

İSümevra İŞİK^{1*}, İAltay KANDEMİR², İYaşar Barış TURGUT¹, İİsmail TAŞKIRAN², İMehmet Hadi YAŞA²

¹Internal Medicine Clinic, Aydın State Hospital, Efeler, Aydın, TURKIYE

²Department of Internal Medicine, Aydın Adnan Menderes University Faculty of Medicine, Aydın, TURKIYE

*Correspondence: dr.sumeyrazncr@gmail.com

ABSTRACT

Objective: Adequate bowel preparation is crucial for the effective diagnosis and treatment of colorectal diseases prior to undergoing a colonoscopy. This study aims to assess the significance of preparation for colonoscopy and to identify factors that influence its effectiveness positively or negatively.

Materials and Methods: The study included all patients who underwent colonoscopy at the Endoscopy Unit of the Gastroenterology Clinic at Aydın Adnan Menderes University Hospital from January 2021 to January 2022.

Results: A total of 303 patients participated in the study, comprised of 155 females and 148 males. It was found that Laxeno/Sennozid A+B Calcium (Ca)-based preparations were the most commonly used (55.4%) for bowel cleansing. Evaluation of drug-related side effects revealed that nausea and vomiting were the most frequently reported issues, occurring in 45.6% of patients. The Boston bowel readiness scale assessment indicated that patients most often received scores of 2 and 3 across all colon segments. Statistically significant differences were observed in the parameters of creatinine and phosphorus between pre- and post-procedure assessments for those using Lax phosphosode/sodium phosphate. Similar differences were noted for the Ca parameter in patients using pegdine/polyethylene glycol (PEG).

Conclusion: This study concluded that neither age nor gender significantly influenced the quality of bowel cleansing. Furthermore, when comparing the cleaning efficacy and side effects of various agents, no particular agent demonstrated superiority. Additionally, the potential for renal damage and electrolyte imbalances resulting from these agents was examined; post-usage evaluations indicated no impact following PEG use, while elevated phosphate levels were noted after sodium phosphate and senna usage, with creatinine levels rising after senna administration.

Key words: Bowel cleansing efficacy, Boston bowel preparation scale, Renal impairment

Received: 31 October 2024
Revised: 05 December 2024
Accepted: 09 December 2024
Published: 22 December 2024



Copyright: © 2024 by the authors. Published Aydın Adnan Menderes University, Faculty of Medicine and Faculty of Dentistry. This is an open access article under the Creative Commons Attribution-NonCommercial 4.0 International (CC BY-NC 4.0) License.

INTRODUCTION

Colonoscopy is one of the endoscopic procedures performed for screening, diagnosis, and interventional purposes today. The purpose of colonoscopy is to visualize the colon up to the terminal ileum. For the diagnosis and treatment of colorectal diseases, it is very important that bowel preparation is sufficient before the colonoscopy procedure. Complete cleanliness of the intestine during the procedure increases the success of the examination and prevents the procedure from being performed again. If bowel preparation is not sufficient, this situation causes overlooking pathological lesions, if any, repetition of the procedure, loss of labor and time, cost increase and decrease in patient satisfaction (1).

Today, there are proven standard practices for adequate colon cleansing. Despite standard practices, adequate colon cleansing cannot be achieved in some patients. In studies investigating the reasons for this; A significant correlation was found between the time of initiation of the procedure, compliance with the preparation instructions, hospitalization, presence of constipation, male gender, history of comorbid diseases, and inadequate bowel preparation (2). In general, a low-fiber diet that avoids foods containing grains and other hard-to-digest substances is recommended for a few days before the procedure day, and this diet has been shown to be at least as effective as the clear liquid diet and has been associated with an increase in patient satisfaction (3). Nowadays, drugs used in bowel preparation include:

Polyethylene glycol (PEG), an isosmotic preparation containing a balanced electrolyte solution, is a high-molecular-weight polymer that is not absorbed in the intestinal mucosa. It minimizes fluid exchange in the colon membrane, helping to retain the electrolytes present in the solution and preventing their absorption. This prevents the development of systemic electrolyte imbalance. The patient is instructed to start PEG administration the evening before the procedure. A total of 4 liters of PEG solution should be consumed in divided doses. The first 2 liters should be consumed the night before, and the remaining 2 liters on the morning of the procedure, finishing at least 4 hours before the colonoscopy. Patients should also avoid solid food for at least 24 hours prior to the procedure (4).

Sodium phosphates are hyperosmotic preparations based on PEG and they are similar to intestinal preparations with magnesium citrate (5). It is generally well tolerated in healthy individuals (6). However, its

use is limited due to the potential for renal damage, even in patients with normal renal function. Acute phosphate nephropathy has been reported (7). Patients with heart failure, kidney damage, liver failure, electrolyte imbalance, or those taking diuretics are advised against using sodium phosphate. The recommended dose for sodium phosphate is two 45 mL doses. The first dose is taken the evening before the procedure, and the second dose is taken 4-6 hours before the procedure. Patients should drink plenty of water following each dose and remain hydrated throughout the preparation (8, 9).

Senna laxatives are containing anthraquinone derivatives, senna increases colonic motility and transit by acting on the intestinal mucosa. It also inhibits water and electrolyte secretion. Senna is often combined with PEG to enhance its effectiveness and reduce the amount of PEG used (10). Patients are instructed to take 2 tablets of Senna (15 mg) the evening before the procedure, followed by at least 2 liters of clear liquids. Additional hydration is recommended, and patients are advised to drink water or clear fluids up to 2 hours before the procedure (11).

Recording the quality of bowel preparation in colonoscopy reports is essential. The U.S. Colorectal Cancer Task Group describes a thorough examination as one in which residual colonic contents do not obscure lesions, except for small polyps (5 mm or less) (12). Various scoring systems have been developed to assess the quality of clinical colonoscopy preparations. The Aronchick Scale, Ottawa Bowel Preparation Scale, and Boston Bowel Preparation Scale (BBPS) are commonly used to evaluate bowel cleansing quality. The BBPS is a 10-point scoring system (ranging from 0 to 9) that assesses bowel preparation quality across three segments of the colon following all cleansing steps during colonoscopy and has been validated for both reliability and accuracy (13).

This study aimed to assess the significance of colonoscopy preparation and to identify factors that positively or negatively impact its effectiveness. With the results to be obtained in this study, we believe that identifying an optimal colonoscopy preparation method tailored to each patient can reduce the number of unnecessary procedures, enhance the procedure's success rate, and ultimately yield positive outcomes for both patient satisfaction and cost-effectiveness.

MATERIALS AND METHODS

This study was approved by Aydın Adnan Menderes University Faculty of Medicine Non-Interventional Clinical Research Ethics Committee's decision dated 24.03.2022, number 12 and protocol number 2022/30, and was carried out in Aydın Adnan Menderes University Practice and Research Hospital Gastroenterology Clinic Endoscopy Unit. It is a descriptive and analytical-cross-sectional type research. The research was conducted between January 2021 and January 2022. All patients who underwent colonoscopy between January 2021 and January 2022 were included in the study.

All colonoscopies in this study were performed by the same experienced endoscopist to ensure consistency in the procedure and minimize variability in outcomes.

As data collection tools, a survey form prepared by the researcher, developed in line with the relevant literature, and the Boston colonoscopy preparation evaluation scale will be used. Data will be obtained by scanning patient files. Patients' age, gender, height, weight, body mass index (BMI), comorbid disease history (diabetes mellitus, coronary artery disease, Parkinson's disease, cerebrovascular accident, Alzheimer disease, etc.), number of medications used, indication for colonoscopy, family history, side effects due to medications (nausea, vomiting, abdominal pain/bloating, weakness, dizziness/lightheadedness), enema use status and the colonoscopy preparation method they used will be recorded. Changes in the balance of urea, creatinine, sodium, potassium, calcium, and phosphorus will be evaluated in patients before and after colonoscopy. After the colonoscopy procedure, colonoscopy reports will be examined and the adequacy of colonoscopy cleaning will be recorded using the Boston colonoscopy preparation evaluation scale. In the study, the relationship between colonoscopy preparation and age, gender, height, weight, BMI, comorbid disease history, number of medications used, and preparation method applied will be evaluated. In addition, changes in electrolyte, renal functions, and phosphorus balance after colonoscopy will be evaluated and their relationship with age, gender, height, weight, BMI, comorbid disease history, number of medications used, and preparation method applied will be examined.

Research data were analyzed using the SPSS 21.0 statistical software. The normality of continuous variables was assessed through visual methods (histograms and probability plots) as well as analytical tests (Kolmogorov-Smirnov and Shapiro-Wilk). For the descriptive statistics, the mean and standard deviation were used for data following a normal distribution, while the median and range (minimum-maximum) were applied to data that did not follow a normal distribution. The Chi-square test was employed to examine differences between categorical variables. The Student's t-test or One-Way ANOVA was used to compare continuous variables with parametric properties across independent groups, while the Mann-Whitney U test or Kruskal-Wallis ANOVA was used for non-parametric continuous variables. Pearson's test was applied for correlations involving parametric continuous variables, and Spearman's test was used for non-parametric continuous variables. A p-value of less than 0.05 was considered statistically significant.

Scoring in the BBPS score is as follows: 0 (inadequate), unprepared colon segment where the mucosa cannot be evaluated due to solid stool that cannot be cleared; 1 (poor), some of the mucosa in the colon segment is visible, but other areas of the colon segment are poorly visible due to staining, residual stool, and/or opaque fluid; 2 (good), good visualization of the colonic mucosa but few debris, small pieces of stool and/or opaque fluid; and 3 (excellent), good visualization of the entire mucosa of the colon segment, no debris, small pieces of stool or opaque fluid (Fig. 1).

RESULTS

A total of 303 patients, 155 women and 148 men, were included in this study. The average age of the patients was 59.5 ± 14.7 years and the average BMI was 27.6 ± 4.5 . When the education and income status was evaluated, the rate of those with high school education or higher was found to be 37.0%, and the rate of those whose income was less than the expenses was 29.7%. It was determined that 70.3% of the patients used medication constantly, 70.3% had a comorbid disease, and 10.2% had a family history of colon cancer (Table 1).

Table 1. Demographic and Clinical Characteristics of the Patients

		n	Mean ± SD
Age (min=21.0, max=97.0)		303	59.5±14.7
BMI (min=10.7, max=45.7)		303	27.6±4.5
		n	%
Gender	Female	155	51.2
	Male	148	48.8
Education level	Below high school level education	191	63.0
	High school and above education level	112	37.0
Income level	Income less than expenses	90	29.7
	Income equal to or greater than expenses	213	70.3

History of colonoscopy was evaluated in the patients. It was determined that 41.3% of the patients had previously undergone colonoscopy. The medications administered to patients for intestinal cleansing were evaluated. It was determined that laxeno/sennozid A+B calcium-containing preparations, pegdin/PEG (23.1%) and lax phosphosoda/sodium phosphate (21.5%) were most frequently used for intestinal cleansing (55.4%).

Table 2. Bowel Cleansing Medications and Associated Side Effects

		Bowel cleansing medication						p
		Lax Phosphosoda/Sodium Phosphate		Laxeno/Sennozid A+B Calcium		Pegdin/PEG		
		n	%	n	%	n	%	
Drug side effect	No	23	35.4	76	45.2	32	45.7	0.353
	Yes	42	64.6	92	54.8	38	54.3	
Side effects associated with bowel cleansing medication	Abdominal pain	18	42.9	38	41.3	11	28.9	0.334
	Nausea and vomiting	18	42.9	43	46.7	18	47.4	
	Dizziness	3	7.1	5	5.4	7	18.4	
	Other	3	7.1	6	6.5	2	5.3	

PEG: Polyethylene glycol

When drug-related side effects were evaluated, it was observed that the patients most frequently experienced nausea and vomiting (45.6%). Side effects were detected at a rate of 64.6% in those using lax phosphosoda/sodium phosphate for bowel cleansing, in 54.8% in those using laxeno/sennozid A+B calcium drug, and in 54.3% in those using pegdin/PEG drug. However, no statistical significance was found between the groups. Among the side effects, nausea and vomiting were observed to be the most common side effects in all three drugs (Table 2).

Table 3. Biochemistry Changes Before and After Colonoscopy

		Before the procedure				After the procedure				p	
		n	Avarage	SS	Min	Max	Avarage	SS	Min		Max
Lax Phosphosoda/Sodium Phosphate	Urea	28	30.33	14.64	7.00	71.00	30.57	18.33	8.00	110.00	0.799
	Creatinine	28	0.87	0.32	0.47	1.99	0.94	0.42	0.57	2.60	0.389
	Sodium	27	139.66	1.96	135.00	143.00	138.81	2.90	133.00	143.00	0.072
	Potassium	27	4.35	0.55	3.40	5.20	4.12	0.54	2.90	5.10	0.086
	Phosphorus	7	3.41	0.64	2.50	4.50	4.98	2.22	3.80	10.00	0.027
	Calcium	20	9.27	0.39	8.20	9.90	9.16	0.65	7.60	10.30	0.344
	Magnesium	12	1.87	0.14	1.49	2.03	2.23	0.86	1.73	4.70	0.450
Laxeno/Sennozid A+B Calcium	Urea	56	30.17	13.09	8.90	59.00	29.14	14.54	9.00	107.00	0.658
	Creatinine	63	0.84	0.19	0.53	1.50	0.89	0.26	0.58	2.05	0.013
	Sodium	56	138.85	2.52	133.00	144.00	138.17	2.87	125.00	143.00	0.081
	Potassium	56	4.36	0.51	1.97	5.10	4.33	0.50	3.10	5.80	0.310
	Phosphorus	26	3.36	0.85	1.20	4.70	4.16	1.44	2.00	10.00	0.008
	Calcium	46	9.18	0.52	8.00	10.90	9.31	0.52	8.30	10.40	0.069
	Magnesium	28	1.86	0.22	1.47	2.28	1.88	0.20	1.47	2.20	0.493
Pegdin/PEG	Urea	25	36.56	21.97	7.00	107.00	41.00	44.66	10.00	227.00	0.819
	Creatinine	28	0.96	0.40	0.44	1.83	0.99	0.44	0.56	2.23	0.316
	Sodium	25	139.92	2.88	132.00	144.00	139.68	4.32	130.00	148.00	0.635
	Potassium	25	4.50	0.47	3.70	5.80	4.42	0.50	3.50	5.50	0.240
	Phosphorus	12	3.72	1.27	2.00	6.30	3.55	0.71	2.10	4.50	0.666
	Calcium	21	8.85	0.72	6.70	9.80	9.15	0.72	7.10	10.20	0.016
	Magnesium	8	1.96	0.13	1.78	2.18	1.85	0.36	1.06	2.24	0.362

PEG: Polyethylene glycol

The BBPS applied to the patients was evaluated. It was observed that patients most frequently received scores of 2 and 3 from all colon segments. Additionally, biochemistry parameters were evaluated before and after the colonoscopy procedure. A statistically significant difference was detected between before and after the procedure in terms of creatinine, Na, K, P and Ca parameters. Biochemistry parameters were evaluated before and after colonoscopy according to the drugs used for bowel cleansing. There was a statistically

significant difference in terms of P parameter between before and after the procedure in those using the drug Lax phosphosoda/sodium phosphate, creatinine and P parameters between before and after the procedure in those using the calcium drug laxeno/sennozidA+B, and Ca parameter between before and after the procedure in those using the drug pegdin/PEG. A difference was detected (Table 3).

Table 4. BBPS Scores and Associated Factors

		n	%
Left colon	A part of the intestine cannot be visualized in the colonoscopy due to solid stool (0 point).	15	5.0
	Presence of liquid or semi-solid stool in a part of the intestine (1 point).	62	20.5
	The inner surface of the intestine (mucosa) is clearly visible and there is a small amount of stool (2 points).	133	43.9
	The inner surface of the intestine (mucosa) is excellently visualized and there is no liquid (3 points)	93	30.7
Transverse colon	A part of the intestine cannot be visualized in the colonoscopy due to solid stool (0 point).	8	2.6
	Presence of liquid or semi-solid stool in a part of the intestine (1 point).	58	19.1
	The inner surface of the intestine (mucosa) is clearly visible and there is a small amount of stool (2 points).	140	46.2
	The inner surface of the intestine (mucosa) is excellently visualized and there is no liquid (3 points)	97	32.0
Right colon	A part of the intestine cannot be visualized in the colonoscopy due to solid stool (0 point).	22	7.3
	Presence of liquid or semi-solid stool in a part of the intestine (1 point).	81	26.7
	The inner surface of the intestine (mucosa) is clearly visible and there is a small amount of stool (2 points).	118	38.9
	The inner surface of the intestine (mucosa) is excellently visualized and there is no liquid (3 points)	82	27.1

According to age; BBPS scores were evaluated according to body mass index (over or below 65 years of age), according to education level, income level, presence of comorbid diseases, family history of colon cancer, and colonoscopy history. No statistically significant difference was detected in terms of BBPS scores of these parameters. BBPS scores were evaluated according to the medications used for bowel cleansing. No statistically significant difference was detected in terms of BBPS scores between those using lax

phosphosoda/sodium phosphate, laxeno/sennozide A+B calcium and pegdin/PEG drugs for bowel cleansing. Demographic data, presence of comorbid disease, family history of colon cancer, and colonoscopy history were evaluated among those with adequate and inadequate bowel cleansing according to BBPS. There was no statistically significant difference between those with adequate and inadequate bowel cleansing in terms of demographic data, presence of comorbid diseases, family history of colon cancer and colonoscopy history (Table 4).

DISCUSSION

Colonoscopy is the gold standard method in the diagnosis and treatment of the lower gastrointestinal system. Intestinal preparation has an important place to increase the success of the procedure and prevent repeat procedures. In this study, we evaluated the factors affecting the effectiveness and reliability of bowel preparation and investigated what needs to be done for optimal preparation. The goals of ideal bowel preparation are: the fecal content should be safely evacuated from the colon, the appearance and histology of the colon mucosa should not be affected, cleaning should be achieved in a short period of time, cleaning should be comfortable, and cleaning should not cause significant changes in the fluid and electrolyte balance (14).

It has been shown in the literature that the success of the colonoscopy procedure is affected by many factors such as age, gender, comorbid disease, the agent used in preparation, and the patient's compliance with the procedure (15). Due to insufficient cleaning during the colonoscopy procedure, the procedure cannot be performed optimally and the procedure may need to be repeated. In the study conducted by Ness et al., an inadequate colon cleansing was reported in 21.7% of colonoscopies (16). In their study, Kaplan et al. reported that among all colonoscopy procedures, the excellent cleaning rate was 38%, the good cleaning rate was 17%, the average cleaning rate was 26%, and the poor cleaning rate was 19% (17). When the colonoscopy procedures in our study were evaluated, it was found that there was inadequate bowel cleansing at a rate of 25.4%. In different studies, it has been found that the rates of bowel cleansing in procedures are different. We think that this difference in the literature may depend on the sociocultural and socioeconomic characteristics of the society in the regions where the studies were conducted, as well as the difference in the agents used before the

procedure in the center where the procedure was performed, and the experience of the team following the procedures.

It is thought that age and gender differences of the patients may also be factors in inadequate bowel cleansing. Özkan et al. reported in their study that they found that bowel preparation worsened as age increased (18). In their study evaluating gastrointestinal endoscopic interventions in elderly patients, Kandemir et al. reported that bowel preparation worsened with age, and that this deterioration was especially significant in individuals over the age of 80 (19). Unlike these studies, there are also studies in the literature reporting that there is no relationship between age and bowel cleansing (20). Regarding the relationship between gender and bowel cleansing; there are also studies reporting that there is no difference between genders, while there are studies stating that male gender is significant in insufficient bowel cleansing (21). In our study, we found that there was no statistically significant difference when bowel cleansing rates were compared between age and gender groups. When the effect of education level on bowel cleansing was evaluated, Karayel et al. reported that they did not detect a statistically significant difference (22). In our study, consistent with the literature, no statistically significant difference was detected between bowel cleansing quality and educational status.

When comorbidities in patients undergoing the procedure were evaluated, no statistically significant relationship was found between the presence of comorbidities and the quality of bowel cleansing. Görücü et al. (20) reported that there was no statistically significant difference between the presence of comorbid disease and the quality of bowel cleansing. Unlike other studies, Karayel et al. only evaluated the relationship between the presence of diabetes mellitus (DM) and the quality of bowel cleansing and reported that the presence of DM negatively affected the quality of bowel cleansing, regardless of the agent used (21). In our study, no statistically significant difference was found between the presence of comorbid disease and the quality of bowel cleansing.

It is thought that the agents used for bowel cleansing may affect the quality. The aim of the studies is to reveal the advantages and disadvantages of the agents used. In their study comparing the quality of intestinal cleansing with the use of sodium phosphate and sennozide, Sücüllü et al. reported that adequate cleansing

quality was achieved with both agents and that sodium phosphate was more easily tolerated by patients (15). In another study comparing sodium phosphate, sennoside and PEG, it was reported that all three were similar in terms of effectiveness and reliability (22). In our study, consistent with the literature, no statistically significant difference was detected between the agents in terms of bowel cleansing quality.

When the side effects in the patients were evaluated in our study, an average of 56.8% side effects was found. The most common side effects were nausea and vomiting in 45.9% and abdominal pain in 39%. When they compared the sodium phosphate and sennoside groups in terms of side effects, Sücüllü et al. reported that the sodium phosphate group was more easily tolerated (15). In our study, it was determined that there was no statistically significant difference when the side effects recorded and the agents used were compared.

There are many studies on the effects of agents used in colonoscopy preparation on fluid electrolyte balance. The advantages of PEG solutions are that they do not damage the colon mucosa and do not cause electrolyte imbalance. There are studies reporting that PEG can be used safely in patients with a history of heart failure, renal disease, decompensated cirrhosis and electrolyte imbalance (23). There are publications and case reports indicating that sodium phosphate application may cause renal parenchymal damage, which may progress to renal function decline, acute kidney injury and even end-stage renal failure, in addition to electrolyte disturbances, although the mechanism is not fully understood, and this situation is called "phosphate nephropathy" (24). There is no evidence that senna group agents cause electrolyte imbalance. Due to the high sugar content it contains, careful use is recommended in patients with impaired blood sugar regulation (12). In our study, there were sodium phosphate, PEG and sennozide usage groups, and kidney function values and electrolytes were evaluated. In the sodium phosphate group, phosphorus was found to increase significantly ($p=0.02$) in the post-procedure period. On the other hand, no significant change was detected in urea-creatinine values. These data support the view that nephrotoxicity may be associated with an increase in the dose used. In the group that underwent bowel cleansing with senna, a statistically significant increase in creatinine and phosphorus values was detected after the procedure. In the PEG group, no statistically significant changes were detected in kidney function tests and electrolytes.

CONCLUSION

Colonoscopy is a gold standard method in diagnostic and therapeutic fields, and a successful intervention is possible with optimal colonoscopy preparation. For this reason, the endoscopy team's detailed evaluation of the patient's condition and choosing the most appropriate colonoscopy preparation method for the patient will increase the success rate of the procedure and reduce the rate of unnecessary repeat procedures. As a result, in this study, we found that age and gender have no effect on the quality of bowel cleansing. We found that there was no correlation between the increase in educational status and the quality of bowel cleansing. When the effects of the presence of comorbidities in patients were examined, we found that it had no effect on the preparation quality. However, in our study, no additional evaluation was made regarding specific comorbidities and whether these comorbid conditions were under control. When the difference in cleaning quality and the presence of side effects were evaluated between the agents used, no superiority over each other was determined. When renal damage and electrolyte imbalance that may develop due to the agents used were evaluated, it was determined that there was no effect after the use of PEG, phosphate was high after the use of sodium phosphate and senna, and creatinine was high after the use of senna. However, how long this imbalance that developed after the use of sodium phosphate and senna continued and the status of permanent damage were not evaluated. And the dose of the agents was not adjusted according to the characteristics of the patient group. We believe that clearer data on this subject can be obtained through studies with longer follow-up and different dosage adjustments.

Acknowledgments

Authorship contributions

SI, AK and MHY designed the study; SI, YBT and İT collected the data and carried out statistical analysis; YBT performed the literature search; AK and MHY supervised the study; SI, YBT, İT and AK prepared and revised the manuscript. All authors gave the final approval of the version to be published.

Data availability statement

Data availability statement here

Declaration of competing interest

The data that support the findings of this study are available from the corresponding author upon reasonable request.

Ethics

This study received ethics committee approval from the non-invasive clinical research ethics committee of Aydın Adnan Menderes University Faculty of Medicine with protocol number 2022/30.

Funding

This work has not received any funding support

REFERENCES

1. Rex DK, Imperiale TF, Latinovich DR, Bratcher LL. Impact of bowel preparation on efficiency and cost of colonoscopy. *Am J Gastroenterol.* 2002;97(7):1696-700.
2. Ness RM, Manam R, Hoen H, Chalasani N. Predictors of inadequate bowel preparation for colonoscopy. *Am J Gastroenterol.* 2001;96(6):1797-802.
3. Bal K. Gastroenterolojide tanısal işlemler. Yazıcı H, Hamuryudan V, Sonsuz A, editörler. *Cerrahpaşa İç Hastalıkları. Medikal Yayıncılık.* 2007:717-741.
4. ASGE Standards of Practice Committee, Anderson MA, Ben-Menachem T, Gan SI, Appalaneni V, Banerjee S, Cash BD, Fisher L, Harrison ME, Fanelli RD, Fukami N, Ikenberry SO, Jain R, Khan K, Krinsky ML, Lichtenstein DR, Maple JT, Shen B, Strohmeyer L, Baron T, Dominitz JA. Management of antithrombotic agents for endoscopic procedures. *Gastrointest Endosc.* 2009; 70:1060.
5. Diab FH, Marshall JB. The palatability of five colonic lavage solutions. *Aliment Pharmacol Ther.* 1996;10(5):815-9.
6. Kontani M, Hara A, Ohta S, Ikeda T. Hypermagnesemia induced by massive cathartic ingestion in an elderly woman without pre-existing renal dysfunction. *Intern Med.* 2005;44(5):448-52.
7. Heher EC, Thier SO, Rennke H, Humphreys BD. Adverse renal and metabolic effects associated with oral sodium phosphate bowel preparation. *Clin J Am Soc Nephrol.* 2008;3(5):1494-503.
8. Desmeules S, Bergeron MJ, Isenring P. Acute phosphate nephropathy and renal failure. *N Engl J Med.* 2003;349(10):1006-7.
9. Keeffe EB. Colonoscopy preps: what's best? *Gastrointest Endosc.* 1996;43(5):524-8. (Cotton PB, W.C.P.g.e., 3rd edition, Blackwell Scientific Publications, Oxford, London 1990. p.160.
10. Ziegenhagen DJ, Zehnter E, Tacke W, Kruis W. Addition of senna improves colonoscopy preparation with lavage: a prospective randomized trial. *Gastrointest Endosc.* 1991;37(5):547-9.
11. Günay E, Abuoğlu H. Kolonoskopi öncesi barsak hazırlığında polietilen glikol, sennozid ve sodyum fosfatın etkinliğinin karşılaştırılması. *Turk J Colorectal Dis.* 2018;28:177-181.
12. Rex DK, Bond JH, Winawer S, Levin TR, Burt RW, Johnson DA, et al. Quality in the technical performance of colonoscopy and the continuous quality improvement process for colonoscopy: recommendations of the U.S. Multi-Society Task Force on Colorectal Cancer. *Am J Gastroenterol.* 2002;97: 1296- 308.
13. Parmar R, Martel M, Rostom A, Barkun AN. Validated scales for colon cleansing: A systematic review. *Am J Gastroenterol.* 2016;111:197-204.
14. Calderwood AH, Jacobson BC. Comprehensive validation of the Boston Bowel Preparation Scale. *Gastrointest Endosc.* 2010;72:686-692.
15. Sücüllü İ, Filiz Aİ, Okul O, Yücel E, Kurt Y, Akın ML. Kolonoskopi öncesi barsak temizliğinde sodyum fosfat ve sennosid'in karşılaştırılması: prospektif randomize çalışma. *Kolon Rektum Hast Derg.* 2008;18(3):133-137.
16. Ness RM, Manam R, Hoen H, Chalasani N. Predictors of inadequate bowel preparation for colonoscopy. *Am J Gastroenterol* 2001;96:1797- 1802.
17. Kaplan M. Kolonoskopi hazırlığı için polietilen glikol, sodyum fosfat ve sennosid kullanımının karşılaştırılması. *Endoskopi Gastrointestinal,* 2018;26(3):74-77.

18. Özkan ZK, Ünver S, Fındık ÜY, Fidan Ş, Albayrak D. Kolonoskopi yapılan hastalarda retrospektif analizle yetersiz bağırsak hazırlığı nedeniyle tamamlanamayan kolonoskopi işlemlerinin sıklığının belirlenmesi. *Endoskopi Gastrointestinal*, 2016;24(3):78-82.
19. Kandemir A, Arabul M, Çelik M, Alper E, Vatansever S, Ünsal B. Assessment of gastrointestinal endoscopic procedures in aged patients. *Turkish Journal of Geriatrics* 2013;16:43-7.
20. Görücü KY, Uslan İ, Acartürk G. Yatan hastalarda kolonoskopi öncesi barsak hazırlığı talimatlarına hastaların uyumu ve tolerans düzeyi. *Sakarya Tıp Dergisi*, 2011;1(4):135-139
21. Karayel TH. Kolonoskopi hazırlığının etkinliği ve güvenilirliği üzerinde etkili olan faktörler. *Tıpta Uzmanlık Tezi*. Denizli: T.C. Pamukkale Üniversitesi Tıp Fakültesi İç Hastalıkları Anabilim Dalı, 2018.
22. Bektaş H, Balık E, Bilsel Y, Yamaner S, Bulut T, Bugra D, Buyukuncu Y, Akyuz A, Sokucu N. Comparison of sodium phosphate, polyethylene glycol, and senna solutions in bowel preparation: A prospective, randomized controlled clinical study. *Digestive Endoscopy* 2005;17:290-96.
23. Fernandez-Juarez G, Parejo L, Villacorta J, Tato A, Cazar R, Guerrero C, Marin IM, Ocaña J, Mendez-Abreu A, López K, Gruss E, Gallego E. Kidney injury after sodium phosphate solution beyond the acute renal failure. *Nefrologia*, 2016. 36(3): p. 243-8.
24. Yağcı MF. Kolonoskopi hazırlığında rektal sodyum fosfat solüsyonu kullanımının fosfat nefropatisiyle ilişkisi. *Tıpta Uzmanlık Tezi*, Sivas: T.C. Cumhuriyet Üniversitesi Tıp Fakültesi İç Hastalıkları Anabilim Dalı, 2017.

Research Article

UNVEILING PREOPERATIVE CLINICAL PROFILES IN PEDIATRIC AORTIC COARCTATION: INSIGHTS INTO SURGICAL INTERVENTIONS AND INSTITUTIONAL ANESTHESIA PRACTICES

 Canan SALMAN ÖNEMLİ ¹ *,  Kübra EVREN ŞAHİN ²,  Ömer Faruk GÜLAŞTI ³,
 Mustafa KARAÇELİK ³,  Çağatay BİLEN ⁴

¹ Department of Anesthesiology and Reanimation, İzmir City Hospital, İzmir, TURKIYE.

² Department of Anesthesiology, Dr. Behçet Uz Child Disease and Pediatric Surgery Training and Research Hospital, İzmir, TURKIYE

³ Department of Pediatric Cardiovascular Surgery Dr. Behçet Uz Child Disease and Pediatric Surgery Training and Research Hospital, İzmir, TURKIYE

⁴ Department of Pediatric Cardiovascular Surgery, Aydın Adnan Menderes University Faculty of Medicine, Aydın, TURKIYE

*Correspondence: canan_ege_35@hotmail.com

ABSTRACT

Objective: The study seeks to provide valuable insights into the outcomes of anesthesia and surgical practices employed in our institution, addressing the challenges posed by preoperative conditions such as heart failure, inotropic support requirements, and mechanical ventilation needs, particularly in the delicate population of newborns.

Materials and Methods: Our investigation conducted a retrospective analysis encompassing all patients who underwent surgery for aortic coarctation at the Pediatric Cardiac Surgery Clinic of the 350-bed Dr. Behçet Uz Child Disease and Pediatric Surgery Training and Research Hospital between 2012 and 2021.

Results: The study encompassed a cohort of 97 patients spanning from newborns to adolescents, with 61 males and 36 females, revealing a 19.5% incidence of genetic anomalies. Intraoperatively, 4.1% of patients required vasodilators, and 13.4% had a triple inotropic requirement. Postoperatively, monitoring distribution included 59 patients in the cardiac surgery intensive care unit, 36 in the neonatal intensive care unit, and 2 in the pediatric intensive care unit. Early extubation within the first 24 hours was achieved in 57.7% of patients.

Conclusion: This research contributes critical insights aimed at refining treatment strategies and enhancing overall outcomes, with particular attention to addressing challenges related to delayed extubation and postoperative vasodilator requirements.

Keywords: Aortic coarctation, surgery, anesthesia, postoperative complications, risk factors.

Received: 13 August 2024
Revised: 16 December 2024
Accepted: 20 December 2024
Published: 22 December 2024



Copyright: © 2024 by the authors. Published Aydın Adnan Menderes University, Faculty of Medicine and Faculty of Dentistry. This is an open access article under the Creative Commons Attribution Non Commercial 4.0 International (CC BY-NC 4.0) License.

INTRODUCTION

The prevalence of congenital heart disease has demonstrated a marked increase over the past three decades, particularly in developed countries, while maintaining relative stability globally. Noteworthy rises have been particularly prominent in Western European nations such as Germany, Austria, and France (1). Serving as a cultural and geographic bridge between Western and Eastern regions, Turkey experiences an annual incidence of approximately 11,000 to 17,000 newborns with congenital heart disease, necessitating intervention or surgery in 5,000 to 6,000 cases due to critical congenital heart disease (2). Among these conditions, aortic coarctation ranks among the twelve most prevalent critical congenital heart diseases, boasting a prevalence of 5.8 per 10,000 live births and emerging as the most prevalent within this group (3,4).

In the pediatric population, aortic coarctation manifests as a cardiac anomaly characterized by a congenital obstruction in the aortic lumen, potentially accompanied by aortic arch lesions. Clinical presentations range from heart failure and cardiovascular collapse to organ failure, acidosis, shock, and, in severe cases, even death, contingent on the degree of left-sided heart obstruction (5). Aortic coarctation may manifest in isolation or concomitantly with genetic anomalies, cardiac anomalies, respiratory system anomalies, abdominal wall anomalies, and brain anomalies (6). Intracardiac defects associated with aortic coarctation encompass ventricular septal defect (VSD), atrial septal defect (ASD), atrioventricular septal defect (AVSD), left ventricular out-flow tract obstruction, left ventricular hypoplasia, aortic arch hypoplasia, patent ductus arteriosus (PDA), the double outlet of the right ventricle (DORV), and total anomalous pulmonary venous connection (TAPVC) (7-9). Approximately 20-30% of pediatric patients with coarctation exhibit a bicuspid aortic valve (8-10).

The urgency of surgical treatment for aortic coarctation hinges on the preoperative clinical situation, presenting challenges such as preoperative heart failure, the requirement for inotropic support, and the need for mechanical ventilation, particularly in newborns. This study aims to offer a comprehensive understanding of the preoperative clinical characteristics associated with pediatric aortic coarctation cases subjected to surgical intervention. Additionally, the study seeks to provide valuable insights into the outcomes of anesthesia and surgical practices employed in our institution, addressing the challenges posed by preoperative

conditions such as heart failure, inotropic support requirements, and mechanical ventilation needs, particularly in the delicate population of newborns.

MATERIALS AND METHODS

Our investigation conducted a retrospective analysis encompassing all patients who underwent surgery for aortic coarctation at the Pediatric Cardiac Surgery Clinic of the 350-bed Dr. Behçet Uz Child Disease and Pediatric Surgery Training and Research Hospital between 2012 and 2021. The approval was obtained from the ethics committee of the Dr. Behçet Uz Child Disease and Pediatric Surgery Training and Research Hospital on 19/11/2020 with protocol number 2020/16-08. Informed consent was secured from the parents of all patients.

Data collection

Patient information, including age, gender, weight, height, body surface area (BSA), blood type, American Society of Anesthesiologists (ASA) score, RACHS (Risk adjustment for congenital heart surgery) score, genetic anomalies, accompanying cardiac defects, history of non-cardiac surgery, history of cardiopulmonary resuscitation (CPR), preoperative investigations (echocardiography findings, trans-fontanel ultrasonography findings, laboratory results), and preoperative clinical findings (heart failure, inotropic requirements, mechanical ventilation requirements, renal insufficiency), was extracted from medical records and hospital automation system records.

Intraoperative data were systematically collected, encompassing the type of operation, surgical technique, additional cardiac surgeries performed, intraoperative complications, anesthesia duration, intraoperative inotropic requirements, and postoperative lactate levels.

Postoperative data recorded included vasodilator infusion, complications, duration of mechanical ventilation, intensive care, hospital stay, VVR score, need for additional surgeries and anesthesia, and mortality.

Anesthesia management

Upon admission to the operating room, patients received intravenous midazolam at a dose of 0.05 mg/kg. Subsequently, warming procedures were initiated, and monitoring was conducted, encompassing electrocardiogram (ECG), non-invasive blood pressure, peripheral oxygen saturation, Bispectral Index (Medtronic, Minneapolis, MN, USA), and Near-infrared Spectroscopy (INVOS; Medtronic, Minneapolis, Minnesota, USA).

Anesthesia induction involved midazolam (0.1 mg/kg), ketamine (2 mg/kg), fentanyl (1 mcg/kg), and low-dose sevoflurane inhalation, followed by intravenous rocuronium (1 mg/kg) administration and endotracheal intubation. Tidal volume was maintained at 8-10 ml/kg with end-tidal carbon dioxide (etCO₂) monitoring. Positive end-expiratory pressure (PEEP) was applied as 5cmH₂O in all patients. If the airway pressure was not high after intubation, the volume-controlled mode was preferred; if it was high, the pressure-controlled mode was preferred. Respiratory rate was adjusted according to the patient's age and metabolic status to maintain arterial carbon dioxide (PaCO₂) levels of 35-45 mmHg. The lowest effective FiO₂ level was used to keep oxygen saturation within the range of 92-98.

The left arm was not used because the subclavian artery was usually clamped or tied, and arterial monitoring was performed from the right radial artery. Acid-base balance was regularly monitored through blood gas analysis and ventilator settings were adjusted according to these values when necessary. Prostaglandin E1 infusion, which was started to allow postductal flow in infants, was continued. Central venous catheterization was executed via the left internal jugular vein, initiating intravenous fluid resuscitation at a rate of 10 ml/kg. The fluid infusion was adjusted based on central venous pressure monitoring.

Proximal and distal blood pressure differences were monitored during aortic clamping. When the aorta is cross-clamped, proximal aortic pressure increases while distal aortic pressure decreases. No attempt was made to reduce this pressure to normal values using a vasodilator, as this would lead to inadequate perfusion of the spinal cord. However, uncontrolled hypertension was not allowed. Since vasodilation and temporary hypotension may occur when the aortic clamp is removed, inotropic support was available to prevent

hemodynamic fluctuation. Inotrope infusion selection and dose adjustment were made according to the patient's clinical condition and weight.

To prevent acidosis due to increased lactic acid and PaCO₂, especially before removing the aortic clamp, mild hyperventilation was performed by increasing the respiratory rate. Post-repair, clamps were removed, hemostasis was achieved. Pressurized ventilation was applied to eliminate atelectasis that occurred before the thorax was closed. Closure procedures were applied with attention to lung expansion, and postoperative pain was managed with pethidine and paracetamol. If the patient's hemodynamics were stable, blood gases were normal, and temperature was appropriate, he was extubated under operating room conditions. Patients were closely monitored in the intensive care unit for the initial 24 hours post-surgery.

Statistical analysis

Statistical analyses were conducted using SPSS 27.0 (IBM SPSS Corp.; Armonk, NY, USA). Descriptive statistics were presented in tabular form, representing continuous variables as mean \pm standard deviation or median, minimum, and maximum, based on distribution. Categorical variables were summarized as numbers and percentages. The normal distribution characteristics of variables were analyzed with Kolmogorov-Smirnov and Shapiro-Wilk tests.

RESULTS

The study encompassed a cohort of 97 patients spanning from newborns to adolescents, with 61 males and 36 females, revealing a 19.5% incidence of genetic anomalies. Isolated aortic coarctation was identified in 26 patients, while additional cardiac anomalies were observed in others (Table 1). Notably, balloon angioplasty had been previously performed in 14.4% of patients, and 4.1% underwent non-cardiac surgery during the preoperative period. The preoperative assessment indicated an ASA V score in 3.1% of patients. During this period, 27 patients required inotropic support for heart failure, 22 patients needed mechanical ventilation, four experienced kidney failure due to perfusion impairment, and six presented with cerebral pathology (Table 1).

The predominant surgical approach was left thoracotomy, and various surgical techniques were applied to patients, as detailed in Table 3 and Figure 1(a). Difficult intubation emerged as the most common anesthesia complication in patients with genetic anomalies. Intraoperatively, 4.1% of patients required vasodilators, and 13.4% had a triple inotropic requirement (Table 2).

Table 1. Demographic and Preoperative data

Demographic data		Preoperative data	
	n (%)		n (%)
Age			
Newborn	41 (42.3 %)	RACHS score, mean	8.15 (6-16)
Infant	37 (38.1 %)	ASA score	
Toddler	8 (8.2 %)	III	72 (74.2 %)
Preschool	2 (2.1 %)	IV	22 (22.7 %)
School	41 (42.3 %)	V	3 (3.1 %)
Adolescent	37 (38.1 %)	Preoperative non-cardiac surgery	4 (4.1 %)
Gender		Tracheoesophageal fistula	2 (2.1 %)
Male	61 (62.9 %)	Hirschsprung	1 (1 %)
Female	36 (37.1 %)	Intestinal perforation	1 (1 %)
Weight, mean (min-max)	3.8 (1.8-63)	History of Preoperative CPR	2 (2.1 %)
Height, mean (min-max)	52 (43-170)	History of preoperative COVID-19	1 (1 %)
BSA, mean (min-max)	0.34 (0.15-1.72)	Arrhythmia	
Genetic abnormality	19 (19.5 %)	Long QT syndrome	1 (1 %)
Hypoplastic aortic arch	47 (48.4 %)	Pulmonary hypertension	22 (22.6 %)
Other cardiac defects		Valve anomaly	
VSD	28 (28.8 %)	Mitral regurgitation	2 (2.1 %)
ASD	19 (19.5 %)	Tricuspid regurgitation	10 (10.3 %)
Pulmonary stenosis	6 (6.2 %)	Aortic stenosis	3 (3.1 %)
AVSD	3 (3.1 %)	Left ventricular concentric hypertrophy	11 (11.3 %)
Heterotaxy syndrome	3 (3.1 %)	Pericardial effusion	2 (2.1 %)
DORV	2 (2.1 %)	Preoperative mechanical ventilation	22 (22.6 %)
Shone complex	2(2.1%)	Preoperative heart failure	31 (31.9 %)
Tetralogy of Fallot	1 (1%)	Preoperative need for medication	
TAPVC	1 (1 %)	Positive Inotropes	27 (27.8 %)
Bicuspid aortic valve	22 (22.6 %)	Milrinone	7 (7.2 %)
Coarctation type		Prostaglandin E1	14 (14.4 %)
Discrete	76 (78.4 %)	Preoperative renal failure	4 (4.1 %)
Tubular	21 (21.6 %)	Preoperative trans fontanel ultrasonogra-phy	
Localization of coarctation		Normal	62 (91.1 %)
Juxtaductal	89 (91.7 %)	Germinal matrix hemorrhage	5 (7.4 %)
Preductal	8 (8.3 %)	Hydrocephaly	1 (1.5 %)
Preoperative peak gradient, mean (min-max)	45 (30-100)		
History of balloon angioplasty intervention	14 (14.4 %)		

* BSA: body surface area , #VSD: ventricular septal defect , † ASD: atrial septal defect , ‡ AVSD: atrioventricular septal defect , § DORV: the double outlet of the right ventricle, ** TAPVC: total anomalous pulmonary venous connection. * RACHS: Risk adjustment for congenital heart surgery, #ASA: American Society of Anesthesiologists, † CPR: cardiopulmonary resuscitation

Postoperatively, monitoring distribution included 59 patients in the cardiac surgery intensive care unit, 36 in the neonatal intensive care unit, and 2 in the pediatric intensive care unit. Early extubation within the first 24 hours was achieved in 57.7% of patients (Figure 1 b).

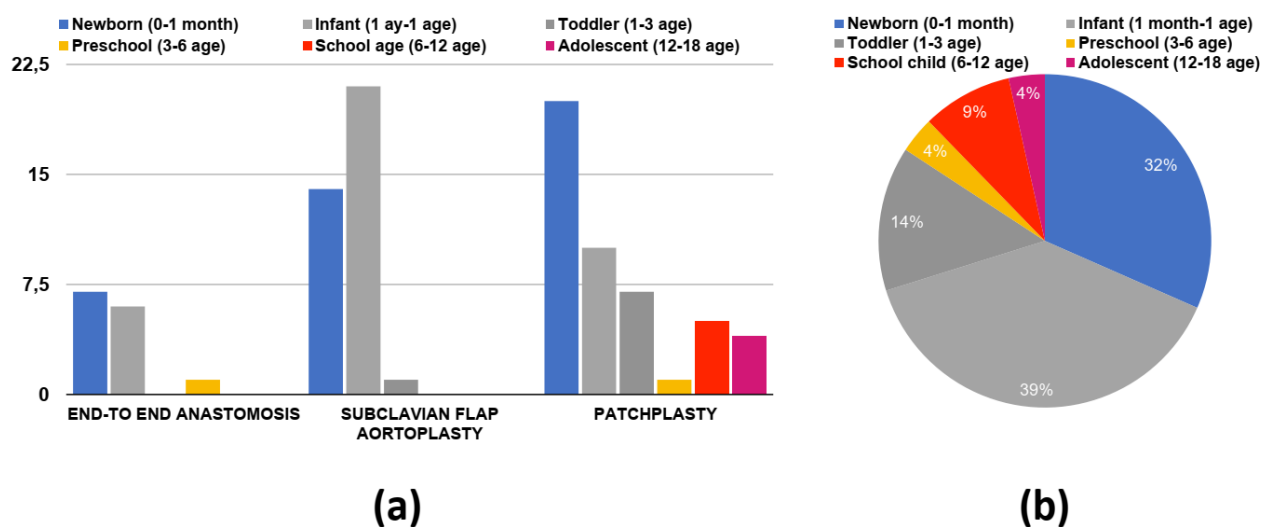


Figure 1. (a) Distribution of operation types according to pediatric age, (b) Distribution of extubations performed in the first 24 hours postoperatively

The prevalent cardiac-related complication in the postoperative period was identified as low cardiac output syndrome (LCOS). Five patients required non-cardiac surgical interventions during this period, necessitating general anesthesia. The overall mortality rate stood at 9.3%, with an early mortality rate of 5.2% attributed to cardiac reasons and the remaining 4.1% linked to prolonged hospitalization leading to sepsis in the neonatal and pediatric intensive care units (Table 2).

Table 2. Intraoperative and Postoperative data

Intraoperative data		Postoperative data		
	n (%)		n (%)	Mean (min-max)
Operation type		Vasodilators infusion	7 (7.2 %)	
Thoracotomy	95(97.9 %)	VIS score		13.7 (0-143,7)
Sternotomy	2 (2.1 %)	VVR score		21.0 (0-186.5)
Surgical technique		Extubation time		
End-to-end anastomosis	15(15.4 %)	0-24 hours	56 (57.7 %)	
Subclavian flap aortoplasty	35(36.1 %)	25-48 hours	9 (9.2 %)	
Patchplasty	47(48.4 %)	49-72 hours	4 (4.1 %)	
Simultaneous cardiac surgery		73-96 hours	8 (8.2 %)	
Pulmonary artery banding	15(15.4 %)	> 97 hours	20 (20.6 %)	
Modified Blalock-Taussig shunt	1 (1 %)	ICU stay (days)		18.9 (1-111)
Thromboendarterectomy	1 (1 %)	Neonatal ICU		38.2 (1-111)
Complications		Cardiovascular surgery ICU		5.8 (1-18)
Difficult intubation	4 (4.1 %)	Pediatric ICU		57.5 (20-95)
Bradycardia	2 (2.1 %)	Postoperative complications		
Intraoperative need for vasodilators	4 (4.1 %)	Re-intubation	3 (3.1 %)	
Intraoperative need for inotropes		Bradyarrhythmia	3 (3.1 %)	
One	35(36.1 %)	LCOS	5 (5.2 %)	
Two	25(25.7 %)	Seizure	2 (2.1 %)	
Three	13(13.4 %)	Sepsis	4 (4.1 %)	
	Mean (min-max)	Postoperative need for surgery or anesthesia		
Lactate value at the end of the operation (mmol/l)	2 (0.8-6.4)	Re-coarctation	4 (4.1 %)	
Anesthesia time (minute)	217.8 (80-400)	VSD and pulmonary artery debanding	5 (5.2 %)	
		Pulmonary venous return anomaly	1 (1 %)	
		Supravalvular aort stenosis	1 (1 %)	
		Vena cava superior candida vegetation	1 (1 %)	
		Subdural hematoma draining	1 (1 %)	
		Bronchoscopy	2 (2.1 %)	
		Tracheostomy	2 (2.1 %)	
		Mortality	9 (9.3 %)	
		Early (LCOS)	5 (5.2 %)	
		Late (Sepsis)	4 (4.1 %)	

* VIS: vasoactive inotropic score, #VVR: Vasoactive-Ventilation-Renal, † ICU: intensive care unit ‡ LCOS: low cardiac output syndrome, § VSD: ventricular septal defect

DISCUSSION

This study delves into the surgical management of pediatric patients undergoing aortic coarctation surgery, with an emphasis on anatomical classification and clinical implications. Anatomically, aortic coarctation is predominantly classified based on the location of the obstructed area in the ductus arteriosus, with juxta ductal stenosis being the most common, alongside the preductal and postductal stenosis (5).

Clinical manifestations of aortic coarctation, often asymptomatic in the neonatal period before ductus arteriosus closure, can progress to respiratory failure and various symptoms, including left ventricular hypertrophy, cardiomegaly, heart failure, and pulmonary edema if diagnosed late (5). Our study identified

heart failure in 31.9% of patients, with 27.8% requiring inotropic infusion, aligning with literature reporting preoperative heart failure rates ranging from 11.2% to 32% (11-12).

Preoperative renal failure, observed in 12% of aortic coarctation cases in previous studies, adds to the complexity (11). Mechanical ventilation, especially in critically ill pediatric patients, may extend hospital stays after congenital heart surgery. Additionally, aortic arch hypoplasia is prevalent in 31% of infants, often accompanied by other intracardiac pathologies (13).

Pediatric anesthesia management for aortic coarctation necessitates meticulous monitoring, slow induction, and successful intubation. Airway abnormalities and difficult intubation risks are higher, particularly in patients with genetic syndromes and congenital heart disease, underscoring the importance of preoperative identification to prevent complications (14).

Blood pressure must be carefully managed during aortic coarctation surgery. Hemodynamic fluctuations can adversely affect organ perfusion. Therefore, invasive blood pressure monitoring will help evaluate the effectiveness and safety of the applied treatment. Inotropic support may be required to balance hemodynamic fluctuations that may occur during anesthesia induction and maintenance. In addition, sudden hemodynamic changes may occur during the clamping and unclamping of the aorta in the intraoperative period and the use of inotropes may be required (15,16). After the cross-clamp is removed, infants generally do not have hypertension, but older children experience paradoxical blood pressure elevations that need to be controlled aggressively. Uncontrolled hypertension may pose a risk of cerebral hemorrhage. Adequate pain control and early extubation may help prevent postoperative hypertension (16).

Each patient should be evaluated individually and ventilator parameters should be adjusted according to the specific needs of the patient. Appropriate tidal volume adjustment under general anesthesia helps prevent over ventilation and lung damage. The respiratory rate should be adjusted according to the patient's age and metabolic status to maintain target (PaCO₂) levels. Application of PEEP supports alveolar stability and reduces the risk of atelectasis. However, excessive PEEP application should be avoided because this may negatively affect cardiac output by reducing venous return. Since prolonged application of high FiO₂ levels can lead to oxygen toxicity, it is preferable to keep them as low as possible. Pressure-controlled ventilation

modes may be preferred to avoid excessive airway pressures. This helps protect lung tissue and reduces the risk of barotrauma. The effect of positive pressure ventilation on hemodynamic parameters should be considered. Adjustments should be made to take into account the potential effects of ventilation settings on cardiac output and blood pressure, especially during aortic clamping. Atelectasis may occur due to long surgical procedures and inadequate ventilation. Pulmonary edema may develop due to fluid accumulation in the lungs as a result of deterioration of fluid balance and heart failure.

Acid-base balance should be monitored regularly by blood gas analysis and ventilator settings should be adjusted according to these values when necessary. In particular, PaCO₂ and pH levels are important in evaluating the effectiveness of ventilation strategies. Ventilation and perfusion disorders can lead to acidosis or alkalosis. In particular, changes in calcium and potassium levels can affect cardiac and neuromuscular functions.

Postoperative complications encompass a spectrum, including persistent hypertension, low cardiac output syndrome (LCOS), chylothorax, recoarctation, renal failure, necrotizing enterocolitis (NEC), neurological complications, diaphragm paralysis, bronchial compression, and left recurrent laryngeal nerve injury (5,8,10,13). Our study identified a postoperative complication rate of 17.6%, including sepsis and reintubation, with a direct complication rate of 8.3%.

Infants operated for aortic coarctation face increased mortality risks associated with prematurity, low birth weight, genetic anomalies, mechanical ventilation, renal failure, sepsis, and necrotizing enterocolitis (6). Complex cardiac lesions further elevate hospital stay and mortality rates (11). Despite including patients with severe heart failure, our study had no intraoperative mortality, with an early mortality rate within the first 30 days at 5.1%.

In Turkey, where approximately one-third of congenital heart diseases are critical and require early intervention, risk factors for prolonged postoperative hospital stay in pediatric patients undergoing isolated aortic coarctation surgery include prematurity, genetic abnormalities, congenital anomalies, non-cardiac surgeries, and a Vasoactive-Ventilation-Renal (VVR) score exceeding 25 for 12 hours postoperatively (2,6,17).

The VVR score emerges as a valuable predictor for outcomes in pediatric cardiac surgery, aiding in anticipating prolonged intensive care and hospital stay, ventilation duration, and mortality (18,19). Maller newborns and those receiving higher opioid amounts pose risks for delayed extubation, necessitating careful consideration in pediatric patients with aortic coarctation (20). In pediatric patients with extubation in the operating room after aortic coarctation, it has been noted that postoperative intensive care stay does not decrease, and there is a longer need for vasodilators due to high blood pressure (21). Repair of aortic coarctation surgery under cardiopulmonary bypass (CPB) in conjunction with other heart malformations highlights prolonged operation duration as an independent risk factor for perioperative brain injury in children under two years old (22).

CONCLUSION

In summary, this study contributes essential insights into the complexities of aortic coarctation surgery in the pediatric population, enhancing our understanding of the clinical landscape and offering valuable guidance for treatment strategies and outcomes improvement. The findings underscore the multifaceted nature of aortic coarctation, emphasizing the significance of risk factor identification for tailored postoperative care. The VVR score emerges as a robust predictor, facilitating outcome anticipation in pediatric cardiac surgery. Addressing challenges related to delayed extubation and post-extubation vasodilator needs is crucial for optimizing patient management. Anesthesia management plays a central role in preventing complications during and after surgery. Continuous monitoring of hemodynamic parameters, appropriate adjustment of ventilator parameters, appropriate fluid and drug management, pain control and keeping the patient's physiological condition stable reduce the risk of complications. Optimal management of these factors is essential in increasing surgical success and ensuring patient safety. In addition, it is important for the anesthesia team to work in coordination with the surgical team for early detection and intervention of possible problems.

Acknowledgments

None

Authorship contributions

All authors contributed equally to the writing of this paper.

Data availability statement

Data availability statement here

Declaration of competing interest

All the authors declare no conflict of interest.

Ethics

The approval was obtained from the ethics committee of the Dr. Behçet Uz Child Disease and Pediatric Surgery Training and Research Hospital on 19/11/2020 with protocol number 2020/16-08.

Funding

The authors declare that this study has received no financial support.

REFERENCES

1. Wu W, He J, Shao X. Incidence and mortality trend of congenital heart disease at the global, regional, and national level, 1990-2017. *Medicine* 2020; 99:23.
2. Dilli D, Varan B, Tasoglu, Oguz SS, Caylan N, Tezel B. Neonatal Critical Congenital Heart Diseases Screening Guide. Turkish Ministry of Health, General Directorate of Public Health, Ankara 2021, page 1-13.
3. Mai CT, Isenburg JL, Canfield MA, Meyer RE, Correa A, Alverson CJ et al. National population-based estimates for major birth defect, 2010-2014. *Birth Defects Research* 2019; 111(18):1420-35.
4. Stallings EB, Isenburg JL, Aggarwal D, Lupo PJ, Oster ME, Shephard H et al. Prevalence of critical congenital heart defects and selected co-occurring congenital anomalies, 2014-2018: A U.S. population-based study. *Birth Defects Research* 2022; 114(2):45-56.
5. Raza S, Aggarwal S, Jenkins P, Kharabish A, Anwer S, Cullington D et al. Coarctation of the aorta: Diagnosis and Management. *Diagnostics* 2023; 13:2189.
6. Schoenberg L, Prodhan P, Spray B, Akmyradov C, Zakaria D. Risk factors for increased post-operative length of stay in children with coarctation of aorta. *Pediatric Cardiology* 2021;42(7):1567-74.
7. Wu Y, Li J, Wu C, Zhu J, He L, Feng C et al. Diagnosis and surgical repair for coarctation of the aorta with intracardiac defects: A single center experience based on 93 infants. *Frontiers in Pediatrics* 2020; 8:49.
8. Padalino MA, Bagatin C, Bordin G, Tua L, Francescato A, Pradegan N et al. Surgical repair of aortic coarctation in pediatric age: A single center two decades experience. *Journal of Cardiac Surgery* 2019; 1-10.
9. Fox EB, Latham GJ, Ross FJ, Joffe D. Perioperative and anesthetic management of coarctation of the aorta. *Seminars in Cardiothoracic and Vascular Anesthesia* 2019; 1-13.
10. Minotti C, Scioni M, Castaldi B, Guariento A, Biffanti R, Di Salvo G et al. Effectiveness of repair of aortic coarctation in neonates: A long-term experience. *Pediatric Cardiology* 2022; 43:17-26.
11. Heremans L, Henkens A, Beco G, Carbonez K, Moniotte S, Rubay JE et al. Results of coarctation repair by thoracotomy in pediatric patients: A single institution experience. *World Journal of Pediatric and Congenital Heart Surgery* 2021; 12(4):492-99.
12. McFarland CA, Truong DT, Pinto NM, Minich LL, Burch PT, Eckhauser AW. Implications of left ventricular dysfunction at presentation for infants with coarctation of the aorta. *Pediatric Cardiology* 2021; 42:72-7.
13. Brown JW, Rodefeld MD, Ruzmetov M. Transverse Aortic Arch Obstruction: When to Go from the Front. *Semin Thorac Cardiovasc Surg Pediatr Card Surg Ann* 2009; 12:66-9.
14. Foz C, Peyton J, Staffa SJ, Kovatsis P, Park, R, DiNardo JA et al. Airway abnormalities in patients with congenital heart disease: Incidence and associated factors. *Journal of Cardiothoracic and Vascular Anesthesia* 2021;35(1):139-44.

15. Mageed NA, Abd El Baser II, Taman HI. Anesthetic management of surgical repair of coarctation of aorta in neonates and infants. *Anesthesia & Surgery* 2020;1(5):1-5.
16. Hensley FA, Martin DE, Gravlee GP. A practical approach to cardiac anesthesia. In: Çiğdem Evren Denker editor. Chapter 14: Anesthetic management for patients with congenital heart disease: The pediatric population. Ankara: Güneş Tıp Kitabevleri, 2015: 389-451.
17. Kaipa S, Yabrodi M, Benneyworth BD, Ebenroth ES, Mastropietro CW. Analysis of factors associated with prolonged postoperative course after surgical repair of aortic coarctation. *Cardiology in Young* 2021; 31(2):191-98.
18. Alam S, Akunuri S, Jain A, Mazahir R, Hegde R. Vasoactive-ventilation-renal score in predicting outcome postcardiac surgery in children. *International Journal of Critical Illness & Injury Science* 2018; 8(3):143-48.
19. Abnay P, Sharma R, Bhan A, Raina M, Vadhera A, Akole R. Vasoactive-ventilation-renal score and outcomes in infants and children after cardiac surgery. *Frontiers in Pediatrics* 2023; 11:1086626. doi: 10.3389/fped.2023.1086626
20. Gil D, Aljiffry A, Dryer R, Rao N, Figueroa J, Downey L et al. Extubation delays and the associated prostaglandin and opiate dose following coarctation of the aorta repair. *Progress in Pediatric Cardiology* 2022; 67:101574.
21. Mohammed AK, Hassanien HM, Sobhy R. Coarctation of the aorta: to extubate early or to extubate late. *Pediatric Anesthesia and Critical Care Journal* 2016; 4(1):35-42.
22. Cheng M, Xu HZ, Zhang KJ, Peng XL, Pan ZX, Hu Y. Risk factors of perioperative brain injury in children under two years undergoing coarctation repair. *Pediatric Neurology* 2023; 141:109-17.

2024 Refree Index

Ahmet Cem Esmer	Gökmen Akkaya	Nasibe Aycan Yılmaz
Ahmet Koçak	Gülay Ok	Nazire Nurdan Çakır
Ahu Soyocak	Güliz Uyar Güleç	Nihal Şimşek Özek
Alp Ergör	Gülnur Emingil	Nilgün Yersal
Alper Tabaru	Hamdi Oğuzman	Nuray Ercan
Armagan Akkuş	Hasan Murat Aydoğdu	Nurhan Özalp
Atilla Yılmaz	Hicran DönmezÖzkan	Onur Doğan Dağ
Aycan Aşık	Hüseyin Şeker	Onur Elmas
Aylin Altay Koçak	İbrahim Tekeoğlu	Özlem Bozkurt Girit
Bertan Kesim	İlknur Çağlar	Rüya Sessiz
Burak Özşeker	İsmail Sarı	Salih Doğan
Burcu Yormaz	Kerim Esenboğa	Sanaz Sandry
Bülent Bozdoğan	Kivanç Karaman	Seda Baştürk
Cemre Koç	Mehmet Akdağ	Seda Sabah Özcan
Cesareddin Dikmetaş	Mehmet Kış	Sedef Zeliha Öner
Ceyda Akın	Mehmet Sinan Doğan	Seher Polat
Damla Güneş Ünlü	Mehmet Turgut	Sema Nur Sevinç Gül
Deniz Tazeoğlu	Melike Metin	Sera Derelioğlu
Devrim Saribal	Merve Erkmén	Sibel Acar
Dilek Yonar	Merve Kırşan	Sibel Seçkin Pehlivan
Ekim Sağlam Gürmen	Metin Çalışkan	Soner Sertan Kara
Elif Funda Şener	Mine Geçgelen Cesur	Soukrie Sekertzi
Emine Şen Tunç	Muhammed Ulvi Yalcin	Şeyho Cem Yücetaş
Esra Baltacıoğlu	Murat Toprak	Şükran Acıpınar
Esra Bolat Gümüş	Mustafa Çelik	Tuğba Bezgin
Esra Talay Çevlik	Mustafa Emin Çanakçı	Tuğrul Aslan
Ezgi Akan	Mustafa Tunalı	Ufuk Ok
Feyza Otan Özden	Mustafa Umut Somuncu	Uğur Köktürk
Filiz Yağcı	Mustafa Zortuk	Yakup Üstün
Fusun Eroğlu	Müge Gülcihan Önal	Yazgı Ay Ünüvar
Gökhan Özkan	Münir Tolga Yücel	Yiğit Kılıç
Gökhan Sargın	Mürteza Çakır	Yunus Emre Özlüer
		Zekeriya Düzgün

2024 Author Index

Altay Kandemir.....	492	Fahinur Ertuğrul.....	70
Abdulhalim Aysel.....	70	Fatıma Kübra Altınay Karaca.....	337
Abdullah Tunçez.....	365	Fatih Durur.....	63
Adem Keskin.....	244	Fatih Öznurhan.....	337
Ahmad Yahyazadeh.....	12	Fatma Şengül Bağ.....	396
Ahmet Anık.....	451	Ferhat Şirinyıldız.....	244
Ahu Reis.....	436	Fezan Mutlu.....	253
Akın Kol.....	396	Filiz Adana.....	36
Ali Akar.....	43, 424	Funda Demirtaş Korkmaz.....	209
Ali Osman Kılıç.....	436	Funda Seher Özalp Ateş.....	145
Anıl Özgün Karatekin.....	78	Gamze Kutlu.....	63
Arzu Yetkiner.....	70	Gamze Solakoğlu.....	119
Aslıhan Merve Toprak.....	365	Gizem Yücesoy.....	195
Asuman Deveci Özkan.....	209	Göknil Alkan Demetoğlu.....	51,109
Ayça Doğan Mollaoğlu.....	233	Gül Taşlı Yeşilçayır.....	85
Ayça Tuzcu.....	154	Gülcan Coşkun Akar.....	70
Aylin Sönmez.....	19	Gülcan Güleç.....	253
Ayşe Ege Selman.....	169	Gülçin Bayramoğlu.....	436
Ayşe Anık.....	451	Gürler Akpınar.....	222
Ayşe Tuğba Eminsoy Avcı.....	379	Halime Dana.....	412
Ayşegül Gülyeryüz.....	92	Handan Çelik.....	70
Bahadır Öztürk.....	365,396	Hatice Feray Arı.....	5
Behlül Bülent Altunkeser.....	365	Hatice Fulya Yılmaz.....	317
Berke Can Erel.....	1	Havva Yasemin Çinpolat.....	424
Burcu Karaduman.....	169	Hüseyin Şeker.....	51
Burçin İrem Abas.....	451	Hüseyin Tezcan.....	365
Canan Salman Önemli.....	506	Işıl Sönmez.....	57
Cansu Yıkıcı Çöl.....	262	İbrahim Uğur Çalış.....	253, 351
Cem Gunaltay.....	279	İnci Durukan.....	436
Çağatay Bilen.....	506	İpek Okutan.....	244
Çimen Güran.....	154	İsmail Taşkıran.....	492
Damla Ünlü.....	97	İyimser Üre.....	253
Didem Turgut Coşan.....	253, 351	Kader Yıldız.....	195
Duygu Yeşilfidan.....	36	Kenan Demir.....	365
Ebru Olgun.....	119, 195	Kurtuluş Buruk.....	436
Ekim Sağlam Gürmen.....	145	Kübra Evren Şahin.....	506
Elif Bilgin.....	466	Lale Cerrahoğlu.....	19
Emin Caner Tümen.....	466	Mehmet Akın.....	28
Emir Esim.....	379	Mehmet Ali Kılıçarslan.....	262
Erkan Gümüş.....	85	Mehmet Gökhan Kaya.....	305
Erva Rakıcı.....	36	Mehmet Hadi Yaşa.....	492
Esin Alpöz.....	70	Melis Danişman Sonkurt.....	253
Esra Talay Çevlik.....	109	Meltem Hendek.....	119
Esra Ulusoy Mutluol.....	28	Merve Başol Göksuluk.....	195
Ethem Acar.....	305	Merve Gülsen Bal Albayrak.....	222

2024 Author Index

Merve Özkan.....	36	Tuğba Çiçek.....	182
Mine Geçgelen Cesur.....	154,279	Turgay Şimşek.....	222
Muhammed Ulvi Yalçın.....	365	Ümit Ali Malçok.....	424
Muhammet Salih Ateş.....	365	Ümüt Altuğ.....	5
Murat Arı.....	5	Varlık K Erel.....	1
Murat Kasap.....	222	Yakup Üstün.....	379
Murat Tunca.....	133,481	Yasemin Akbulut.....	63
Mustafa Gündoğar.....	78	Yasemin Özkan.....	19
Mustafa Karaçelik.....	506	Yasemin Tunca.....	481
Mustafa Yorgancıoğlu.....	145	Yasemin Turan.....	19
Mürteza Çakır.....	43	Yaşar Barış Turgut.....	492
Nazan Ersin.....	70	Yener Okutan.....	51
Nazif Aygöl.....	365	Yunus Emre Özlüer.....	85
Nazire Esra Özer.....	262	Zafer Cantürk.....	222
Nazire Nurdan Çakır.....	97	Zekeriya Düzgün.....	209
Nazlı Ezer Özer.....	233	Zekiye Eroğlu.....	292
Nihal Fahrzadeh.....	481	Zeynep Şahin.....	262
Nimet Gençoğlu.....	78	Zülal Çoban.....	57
Onur Can Polat.....	365		
Osman Birol Özgümüş.....	436		
Ömer Faruk Gülaştı.....	506		
Özge Çevik.....	85,451		
Özgür Er.....	379		
Özgür Sürmelioglu.....	412		
Özlem Arık.....	262		
Özlem Bozkurt Girit.....	317		
Özlem Çölgeçen.....	292		
Özlem Sezer.....	244		
Özüm Daşdemir Özkan.....	70		
Pelin Dilsiz Eker.....	1		
Pınar Okyay.....	19		
Pınar Yıldız.....	97,109		
Recai Acı.....	244		
Samet Semiz.....	244		
Sema Kaya.....	133		
Sena Aykut.....	169		
Sencar Öztürk.....	19		
Serap Uçar.....	412		
Sercan Göde.....	70		
Sevil Alkan.....	424		
Sevinç Yanar.....	222		
Sultan Keleş.....	451		
Suray Pehlivanoglu.....	396		
Sümeyra Işık.....	492		
Taner Karakaya.....	244		

2024 Subject Index

3D printing.....	262	Complicated appendicitis.....	305
3D technology.....	1	Compomer.....	337
6-Mercaptopurine.....	12	Composite.....	337
ABR.....	412	Composite Resins.....	262
Acute appendicitis.....	305	Conjugation.....	436
Agmatine.....	317	Continuous wave of condensation.....	379
Air-abrasion.....	51	Deep Brain Stimulation.....	43
Airway management.....	1	Demineralization.....	28
Alvarado score.....	305	Dental implant.....	119
Anesthesia.....	518	Dental students.....	169
Ankylosing Spondylitis.....	244	Dentist.....	63
Antibiotic.....	5	Dentistry.....	169
Aortic coarctation.....	518	Denture base resins.....	109
Appendicitis inflammatory response score.....	305	Denture liners.....	109
Articular eminence inclination.....	133	Diabetes mellitus.....	451
Artificial aging.....	97	DNase I.....	351
Artificial intelligence.....	169	Elderly Myocardial Infarction.....	365
Assessment scale.....	19	Electroforming.....	292
Attitudes.....	169	Emergency department.....	305
Backfill obturation.....	379	Epidemiology.....	57
Beliefs.....	169	Er,Cr:YSGG laser.....	97
Bibliometric analysis.....	43	Er:YAG laser.....	51
Bibliometrics.....	182	Escherichia coli.....	436
Bolton.....	481	Flexural strength.....	97
Bone.....	154	Fractal analysis.....	466
Boston bowel preparation scale.....	492	Free gingival graft.....	119
Bowel cleaning quality.....	492	FTIR.....	233
Breast cancer.....	396	Galvanoceramic.....	292
CAD/CAM milling.....	262	Gene cassette.....	436
Cancer.....	351	Gene polymorphism.....	253
Caries.....	57	Gingival crevicular fluid.....	154
Carrier-based obturation.....	379	Gingival thickness.....	279
Cerebral Ischemia.....	85	Gingivitis.....	451
Cervical disc herniation.....	424	Graft shrinkage.....	119
cf-DNA.....	351	Gram negative bacterias.....	5
Citations.....	182	Hard relining material.....	51
Claudin-5.....	85	Hardness.....	28
Clincheck.....	481	Health.....	36
Collaborations.....	182	Health literacy.....	36
Collagenase.....	222	Health policy.....	63
		High-carbohydrate diet.....	233

2024 Subject Index

High-fat diet.....	233	Oral health.....	63
Hs-CRP.....	365	OVCAR-3.....	351
Human leukocyte antigen b27.....	244	Overdenture attachment system.....	51
ImageJ.....	466	Oxidative stress.....	451
Inflammation.....	424	Panoramic radiography.....	466
Inlay.....	292	Pediatrics.....	5
Integron.....	436	Perceptions.....	169
Intensive care unit.....	5	Periapical lesion.....	466
Interproximal reduction.....	481	Periodontal ligament.....	379
Invisalign.....	481	Periodontitis.....	195
Junctional Adhesion Molecule-A.....	85	Peripheral neuropathy.....	317
Keratinized mucosa width.....	119	PIV.....	244
Levofloxacin.....	5	Planning.....	63
Lithium disilicate.....	97	Plasmid.....	436
Lymphoedema.....	19	Postoperative complications.....	518
Male Rat.....	12	Premature Ejaculation.....	253
Mandibula.....	279	Primary cells.....	222
Marginal Discrepancy.....	292	Primary dentition.....	57
Maxilla.....	279	Propolis.....	12
MCF-10A.....	351	Protein secondary structure.....	233
MDA-MB-231.....	396	Proteomics.....	222
Medical education.....	145	Psychosocial problems.....	412
Medical students.....	145	Pulmonary embolism.....	182
Metal housing.....	51	Pure tone audiometry.....	412
Methotrexate.....	317	Push-out bond strength.....	51
Methylation.....	351	Rapid maxillary expansion.....	154
MicroRNA.....	396	Rats.....	85
Microsurgery.....	119	Reliability and validity.....	19
Monocyte to lymphocyte ratio.....	424	Renal injury.....	492
MS.....	412	Resistant.....	5
Myofunctional treatment.....	28	Retention.....	154
NeoMTA.....	337	Risk factors.....	518
NeoPutty.....	337	ROI.....	466
Neurosurgery.....	43	S1P.....	253
Neutrophil Extracellular Trap.....	195	S1P receptors.....	253
Neutrophil to lymphocyte ratio.....	424	Saliva.....	451
Non-complicated appendicitis.....	305	Sciatic nerve.....	317
Nurse.....	36	Shear bond.....	337
Obesity.....	233	SII.....	244
Occludin.....	85	Skeletal anomaly.....	133
Occlusal features.....	57	Smoking.....	195

2024 Subject Index

Social media.....	145
Spectroscopy.....	233
Student.....	36
Sublingual Gland.....	12
suPAR.....	365
Surgery.....	518
Systemic immune-inflammatory index.....	424
Temperature rise.....	379
Temporomandibular joint space.....	133
Tensile bond strength.....	109
TheraCal PT.....	337
Thiostrepton.....	209
Thrombolytic therapy.....	182
TLR4 receptor.....	209
Toll like receptors.....	209
Training.....	36
Treatment duration.....	222
Triple-negative breast cancer.....	209
Twin-block.....	28
Twist1.....	396
Vestibular function tests.....	412
Videolaryngoscope.....	1
Young Myocardial Infarction.....	365